**TU**Delft

Delft University of Technology

Solar home systems for improving electricity access
An off-grid solar perspective towards achieving universal electrification

Narayan, Nishant

**DOI**
[10.4233/uuid:aa29b04f-4cd7-41fa-b48b-5edc75fef104](10.4233/uuid:aa29b04f-4cd7-41fa-b48b-5edc75fef104)

**Publication date**
2019

**Document Version**
Final published version

**Important note**
To cite this publication, please use the final published version (if applicable).
Please check the document version above.

# Solar Home Systems for improving electricity access

## An off-grid solar perspective towards achieving universal electrification

## Dissertation

for the purpose of obtaining the degree of doctor
at Delft University of Technology
by the authority of the Rector Magnificus, Prof. dr. ir. T. H. J. J. van der Hagen,
chair of the Board for Doctorates
to be defended publicly on Wednesday, 20 November 2019 at 10:00 am

by

## Nishant Shankar Narayan

Master of Science in Sustainable Energy Technology,
Delft University of Technology, The Netherlands,
born in Dombivli, India.

An e-version of this dissertation is available at http://repository.tudelft.nl/

To *Appa*, who always gave back to others. Wish you were here.

To *Mathe*. I wish I could be as selfless as you. I try.

To *Sanaa*, my love. I know you are happier than me as I finish this book. You've endured through this more than I could ever have asked for. On the bright side, now there's one less PhD project standing between me and the chores.

# Contents

# SUMMARY

*To achieve great things, two things are needed:*
*a plan, and not quite enough time*

Leonard Bernstein

More than a billion people globally lacked access to electricity in 2016. For various reasons, national grid extension is not an economically viable solution for the un(der-)electrified regions. As most of these electricity-starved regions lie in tropical latitudes with abundant sunshine, the use of off-grid, solar-based solutions like solar home systems (SHS) is a logical approach, especially when considering the falling costs of photovoltaic (PV) module and battery storage in recent times. However, state-of-the-art SHS is limited in its power levels and availability. Moreover, sub-optimal system sizing of SHS leads to either over-utilization — and therefore, faster battery degradation — or under-utilization of the SHS battery, leading to higher system costs. Additionally, off-grid SHS designs suffer from a lack of reliable load profile data needed as the first step for an off-grid PV system (e.g., SHS) design. The work undertaken in this dissertation aims to analyze the technological limits and opportunities of using SHS in terms of power level, availability, and battery size, lifetime for striving towards universal electrification.

### ELECTRIFICATION PATHWAYS

In **Chapter 2**, the three main electrification pathways, viz., grid extension, centralized microgrids, and standalone solar-based solutions like pico-solar and SHS are analyzed for their relative merits and demerits. Grid extension can provide broad-scale electricity and high power levels; however, it needs a certain level of population density and electricity demand to be an economically viable pathway. Centralized microgrids also require a minimum electricity demand threshold and good knowledge of the expected electricity demand before they are setup. Standalone systems like solar lanterns and SHS have, despite having the highest per Wp system costs, the highest adoption rates at the household level, despite their limitation in power levels. The requirements from an ideal pathway are also discussed, which must not only allow the use of higher power appliances, but also enable the inevitable climb up the energy ladder for the consumer.

### LOAD PROFILE CONSTRUCTION

Load profiles are often the first step for the technical design of an off-grid energy system like SHS, while reliable load profiles are often unavailable. In **Chapter 3**, a methodology is presented to quantify the electricity demand of the households in the form of load profiles for the various tiers of the multi-tier framework (MTF) for measuring household electricity access. The so-called super-efficient off-grid DC appliances are considered in this study. The described methodology is scalable, and the resulting load profiles can be made more accurate with complementary field surveys for the target communities.

### Battery and SHS

Battery is a critical component of the SHS; it is the most expensive SHS component while also the component with lowest lifetime. In **Chapter 4**, a non-empirical battery lifetime estimation methodology is presented that can be used at the design phase of SHS for comparing the performance of candidate battery choices at hand in terms of battery lifetime. An SHS case-study simulation for a tier-3 load is carried out and the battery activity is analyzed. Comparison of this proposed dynamic model with an experimentally derived empirical model of $LiFePO_4$ battery yielded very close results, with the state of health (SOH) values over time being within less than 3% of each other.

An optimal standalone system size is calculated for each tier of energy consumption in **Chapter 5**, taking into account the battery lifetime, temperature impact on SHS performance, power supply availability in terms of the loss of load probability (LLP), and excess PV energy. A genetic algorithm-based multi-objective optimization is performed, giving insights on the delicate interdependencies of the various system metrics like LLP, excess PV energy, and battery lifetime on the SHS sizing. This exercise concludes that meeting the electricity requirements of tiers 4 and 5 level of electrification is untenable through SHS alone.

### SHS-based microgrids

Consequently, a bottom-up DC microgrid born out of the interconnection of SHS is explored in **Chapter 6**. A modular and scalable architecture for such a bottom-up, interconnected SHS-based architecture is introduced, and the benefits of the microgrid over standalone SHS are quantified in terms of lower battery sizes and the defined system metrics. On modeling the energy sharing between the SHS, it is shown that battery sizing gains of more than 40% and 30% could be achieved with SHS interconnectivity at tier 5 and tier 4 levels, respectively, as compared to standalone SHS to meet the same power availability threshold.

Finally, a Geo-Information System (GIS)-based methodology is presented in **Chapter 7** that takes into account the spatial spread of the households while utilizing graph theory-based approaches to arrive at the optimal microgrid topology in terms of network length. A total of 42 different remote sites around the world are considered in the study. Graph theory-based layouts (minimum spanning trees) are seen to outperform conventional topologies like ring, spider, bus in terms of average network length, highlighting the usefulness of this study.

The research carried out in this dissertation underlines the technological limitations of SHS in aiming towards universal electrification, while highlighting the benefits of moving towards a bottom-up approach in building DC microgrids through interconnected SHS, which can enable the climb up the so-called electrification ladder.

# SAMENVATTING

In 2016 hadden ruim miljard mensen wereldwijd geen toegang tot elektriciteit. Om meerdere redenen is uitbreiding van het landelijke elektriciteitsnet voor deze contexten meestal geen economisch verantwoorde oplossing. De elektriciteit-arme regio's liggen voornamelijk in de tropische gebieden, met veel zon, hierdoor zijn de off-grid, zonne-energie oplossingen, zoals solar home systems (SHS) een logische keuze, des te meer gezien de exponentieel dalende kosten van PV en batterijopslag in de laatste jaren. Echter heeft de state-of-the-art SHS belangrijke beperkingen, zoals relatief lage vermogens die ze kunnen leveren en de beperkte beschikbaarheid van elektriciteit. Verder heeft suboptimale dimensionering van SHS negatieve gevolgen, in de vorm van of over-utilisatie oftewel snelle batterij degradatie, of onder-utilisatie oftewel een te dure systeem. Ten slotte is er gebrek aan betrouwbare energieverbruiksprofiel data een belangrijke beperking in een optimaal ontwerp van een SHS. Dit proefschrift streeft ernaar om technische limieten en mogelijkheden van SHS, vooral vermogensniveau, beschikbaarheid, batterijcapaciteit dimensionering en levensduur te onderzoeken.

### ELEKTRIFICATIE ROUTES

In Hoofdstuk 2 zijn de drie belangrijkste elektrificatie routes geëvalueerd: het landelijke elektriciteitsnet, gecentraliseerde microgrids en standalone zonne-energie oplossingen zoals pico-solar en SHS. Uitbreiding van het elektriciteitsnet biedt toegang tot elektriciteit op schaal en hoge vermogenniveaus. Aan de andere kant zijn er bepaalde bevolkingsdichtheid en elektriciteitsverbruik nodig om deze oplossing economisch rendabel te maken. Voor een economisch verantwoord ontwerp van gecentraliseerde microgrids is eveneens een bepaald elektriciteitsverbruik vereist. Standalone oplossingen, zoals zonne-energie lantaarns en SHS, hebben een brede grote marktadoptie laten zien, al zijn ze relatief duurder en beperkt in vermogen die ze kunnen leveren. De eisen van een ideale elektrificatie route zijn ook uitgestippeld, die zowel het klimmen van de zogenaamde elektrificatieladder als gebruik van hoog-vermogen huishoudelijke apparaten mogelijk maakt.

### CREËREN VAN HET ENERGIEVERBRUIKSPROFIEL VAN HUISHOUDENS

Om tot een passend ontwerp van een off-grid zonne-energie systeem te komen, is het van groot belang om het verbruikspatroon van een huishouden te kennen, welke apparaten van elektriciteit voorzien moeten zijn en op welke tijden gedurende de dag ze in gebruik zijn. Echter zijn betrouwbare energieverbruiksprofielen in doelregio's vaak niet beschikbaar. In Hoofdstuk 3 is een methodologie ontwikkeld om de elektriciteitsvraag van huishoudens te kwantificeren in de vorm van energieverbruiksprofiel behorend tot verschillende rangen van de multi-tier framework (MTF). MTF is geïntroduceerd om verschillende niveaus van huishoudelijk elektriciteitstoegang te duiden. Dit onderzoek

gebruikt zogenaamde super-efficiente off-grid DC huishoudelijke apparaten. De ontwikkelde methodologie is schaalbaar en de nauwkeurigheid van de energieverbruiksprofielen kan met aanvullende veldonderzoeken verbeterd worden.

### BATTERIJ EN SHS

Batterij is een kritische schakel in een SHS, het is de duurste en de kortste levensduur component in het systeem. In Hoofdstuk 4 is een methodologie geïntroduceerd om op een non-empirische manier de levensduur van de batterij te berekenen. De methodologie kan in het SHS ontwerp gebruikt worden om de levensduur van verschillende batterijkeuzes met elkaar te vergelijken.

Een simulatie voor een representatieve SHS voor MTF Tier 3 is uitgevoerd om de batterijactiviteit te analyseren. De dynamische model en de experimentele empirische model van de LiFePO4 batterij leveren goede resultaten overeenkomst, het verschil tussen de state-of-health (SOH) van de batterij tussen de twee modellen is minder dan 3

Hoofdstuk 5 presenteert optimale dimensionering van een SHS voor elke MTF Tier. Daarbij is rekening gehouden met de levensduur van de batterij, de invloed van de temperatuur op de SHS, elektriciteit beschikbaarheid, loss of load probability (LLP), en zonne-energie overschot. Met behulp van op genetisch algoritmes gebaseerde multi-objective optimalisatie is inzicht gekregen in hoe de verschillende afwegingen tussen de LLP, zonne-energieoverschot en batterijlevensduur effect hebben op dimensionering van SHS. Ten slotte is aangetoond dat de hoogste niveaus van MTF, Tiers 4 en 5, met SHS alleen niet haalbaar zijn.

### SHS-GEBASEERDE MICROGRIDS

Aansluitend op de inzichten van Hoofdstuk 5, is een bottom-up DC microgrid bestaand uit meerdere, onderling verbonden SHS in Hoofdstuk 6 verder onderzocht. De voordelen van deze modulaire, schaalbare, SHS-gebaseerde microgrids vergeleken met standalone SHS wat betreft de batterijcapaciteiten en andere systeemindicatoren zijn gekwantificeerd. Het is aangetoond dat doordat elektriciteit tussen huishoudens gedeeld kan worden, voor dezelfde elektriciteitsbeschikbaarheid voor MTF Tier 4 en Tier 5, respectievelijk 30% en 40% minder batterijcapaciteit gebruikt kunnen worden. Tenslotte wordt in Hoofdstuk 7 een op Geo-informatie systeem (GIS) gebaseerde methodologie geïntroduceerd die rekening houdt met de ruimtelijke verspreiding van de huishoudens en de grafentheorie gebruikt om tot — vanuit het oogpunt van netwerklengte — optimale microgrid topologie te komen. In totaal zijn 42 verschillende afgelegen locaties in de wereld gebruikt als case-studies. De lay-outs die uit de grafentheorie (minimale opspannende bomen) voortkomen blijken vanuit het oogpunt van de netwerklengte betere resultaten op te leveren dan de conventionele topologieën zoals ring, spider, bus.

Het onderzoek uitgevoerd in dit proefschrift brengt de beperkingen van het SHS-concept in het bereiken van universele elektriciteitstoegang naar voren. Tegelijkertijd wordt de nadruk gelegd op de voordelen van een bottom-up benadering van het bouwen van DC-microgrids door het verbinden van individuele SHS. Daardoor kan de elektrificatieladder sneller en beter beklommen worden.

<div align="right">

# 1

</div>

<div align="right">

## INTRODUCTION

</div>

<div align="right">

*We are the first generation that can put an end to poverty
and we are the last generation that can put an end to climate change*

Ban Ki-moon

</div>

## 1.1. MOTIVATION

### 1.1.1. ENERGY ACCESS

In 2016, the 17 Sustainable Development Goals (SDGs) of the 2030 Agenda for Sustainable Development came into force. In the same year, an estimated 1.1 billion people globally lacked access to electricity [1].
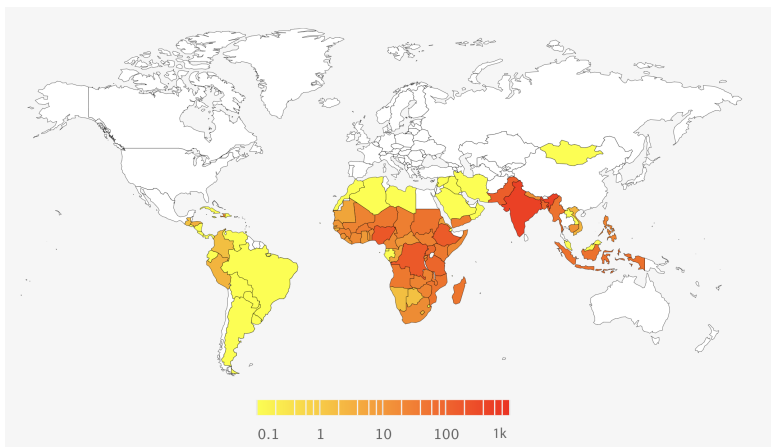


Figure 1.1: Map showing the global population in millions without electricity access in 2016. (Obtained from the electricity access database of the IEA [2].)

**1**

It is no wonder then that the United Nations defines SDG 7 as "Ensure access to affordable, reliable, sustainable and modern energy for all" [3]. Specifically, SDG 7-1 targets universal access to reliable, affordable, and modern energy services by 2030, for which increasing the global access to electricity is crucial [3]. Figure 1.1 shows the global distribution of the population lacking electricity access as of 2016. Majority of this population lives in sub-Saharan Africa and South/South-East Asia.

Figure 1.2 depicts the 17 SDGs of the 2030 Agenda for Sustainable Development adopted at the United Nations. SDG 7 deals with energy, which will be the focus of the work described in this dissertation.



Figure 1.2: The 17 Sustainable Development Goals adopted in September 2015, set to be achieved by 2030 (Image source: [3]). Focus of this dissertation will be on SDG 7.

### BENEFITS OF ELECTRIFICATION

There is ample evidence reported in the literature on the many benefits electrification brings about across geographies. For example, health benefits can be reaped from electrification when incumbent household fuel such as wood, coal, and kerosene are replaced, as evidenced from a study in South Africa [4]. Clean energy sources like solar photovoltaic (PV), which is a technology that converts incident radiation into electricity, can provide a viable alternative instead of dirty fuels like coal and kerosene. Switching over from kerosene lamp to solar PV-based lighting has shown to have improved the health and increased the human development index (HDI) in studies conducted in India [5]. In general, studies have shown a high degree of correlation between HDI and access to electricity [6, 7]. Other health benefits come in the form of better nutrition and well-being; when moving from dirty fuels to solar-based lighting, savings from light expenditures are reportedly spent on better-balanced diet [8]. Even the advent of basic lighting services improves not only the productivity at home, but also creates more opportunities for

**1**

women and improves the study hours of children [8]. The most direct and immediate benefits are in the form of the technological leap and associated cost savings while going from fossil-fuel-based indoor energy consumption to electricity. For instance, for a given amount of light output, kerosene costs 325 times the cost of electrically lighting an incandescent bulb, 1625 times that of a compact fluorescent lamp, let alone the more efficient option like the LED lights [9, 10].

Thus, it can be seen how SDG 7 is inseparably interlinked to other SDGs, like SDG 3 (good health), 4 (quality education), 5 (gender equality), 13 (climate action), among others (Figure 1.2).

### THE ILL-EFFECTS OF ENERGY POVERTY

Contrasting the benefits of electrification are the ill-effects of lack of electricity and energy, also sometimes referred to as energy poverty. Energy poverty is inseparably linked to economic poverty. The most affected victims of energy poverty are usually the economically marginalized population of any country [1]. Energy poverty necessitates the reliance on dirty fuels and often a high percentage of the household income expenditure on inefficient energy sources [9, 11]. Energy poverty can lead to serious health concerns (indoor air pollution, lack of efficient medical care), and also further fuel economic poverty while impacting gender roles and educational opportunities. Additionally, there are other environmental effects like greenhouse gas (GHG) emissions, which are usually not associated with smaller, economically poorer countries because they use relatively little commercial energy. However, almost 80% of total energy use in Africa is in the form of burning wood and other biomass fuels [12].
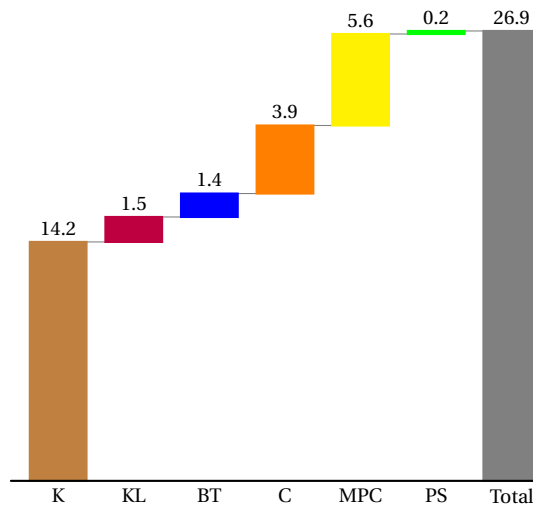


Figure 1.3: Estimated annual spending in $ billion on off-grid lighting and phone charging in Asia and Africa in 2014. K=Kerosene, KL=Kerosene Lamps, BT=Battery Torches, C=Candles, MPC=Mobile Phone Charging, PS=Pico solar (small solar products like solar lanterns). Data sourced and adapted from [13].

---

[1] also known as Base-of-Pyramid (BoP), which has been defined in the past as a demographic representation of the inequality of income or wealth

**1**

The irony of energy poverty is that the economically poor tend to pay more for the same energy service as compared to the same energy services in the richer parts of the world. A case in point is mobile phone charging. The estimated annual spending on phone charging and off-grid lighting per source in 2014 is shown in Figure 1.3. In 2014, the 240 million strong mobile phone subscriber base (living off-grid in Asia and Africa) were estimated to have spent almost $0.15 to $0.25 per phone charge [2], leading to an incredible per kWh equivalent cost of $30 to $50 [13]. Therefore, energy poverty can even be seen as one of the factors in keeping the energy-poor locked into the cycle of poverty and marginalization.

### ENERGY ACCESS AND ELECTRICITY ACCESS

It should be noted that electricity access is a part of the broader category of energy access that additionally includes, e.g., energy for heating and cooking. As electrification is already a crippling global problem that needs urgent attention, the work described in this dissertation pertains to electrification only. Furthermore, cooking has an additional factor of strong cultural dimension, which prevents the applicability of a universal solution. On the other hand, for electricity access, the benefit of scale could be potentially reached. Therefore, the term electricity access and energy access may have been used interchangeably in this dissertation while referring to household-level electrification.

### 1.1.2. ILLUMINATED BUT NOT ELECTRIFIED

Figure 1.4 shows the global horizontal irradiance for different regions around the world. A quick comparison with Figure 1.1 reveals the paradoxical nature of the regions in South/South-East Asia and sub-Saharan Africa: these are places amply illuminated by the sun, but un(der)-electrified. That is, despite lacking sufficient electricity infrastructure, these regions are blessed with abundant sunshine, making solar PV power the perfect candidate source of electricity.
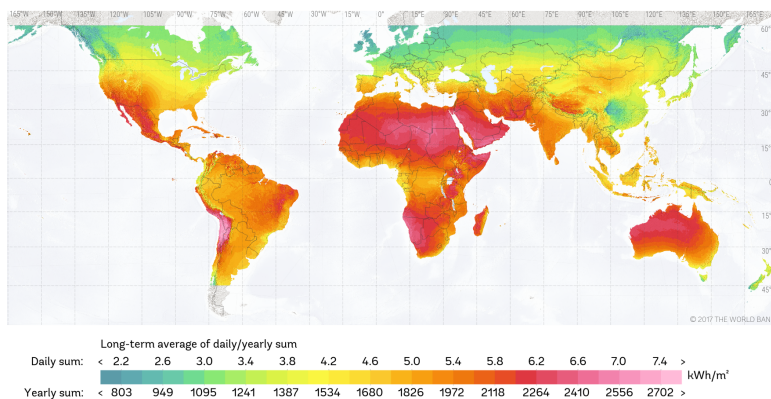


Figure 1.4: Map showing the global horizontal irradiance around the world in terms of daily and yearly sums. (Obtained from the Global Solar Atlas, owned by the World Bank Group and provided by Solargis.)

---

[2] this can amount to up to 10% of the daily household income for a BoP household!

**FALLING SOLAR PV COSTS**

The technology costs of the so-called exponential technologies like solar PV, LED and batteries have been declining. The global average levelized cost of electricity (LCOE) for utility-scale PV in 2017 reduced to $0.1/kWh, representing a 73% fall between 2010 and 2017 [14]. Figure 1.5 shows the LCOE range for utility-scale PV from 2010-2017. Solar PV is increasingly competing neck-and-neck with conventional fossil fuel-based power sources, and that too without any subsidies; by 2020, the average LCOE for solar PV is poised to fall below $0.06/kWh [15]. These trends not only make solar PV the candidate renewable energy technology of choice but also make it the opportune moment to accelerate solar PV-based electrification efforts, in line with the idea of "clean energy" of SDG 7.
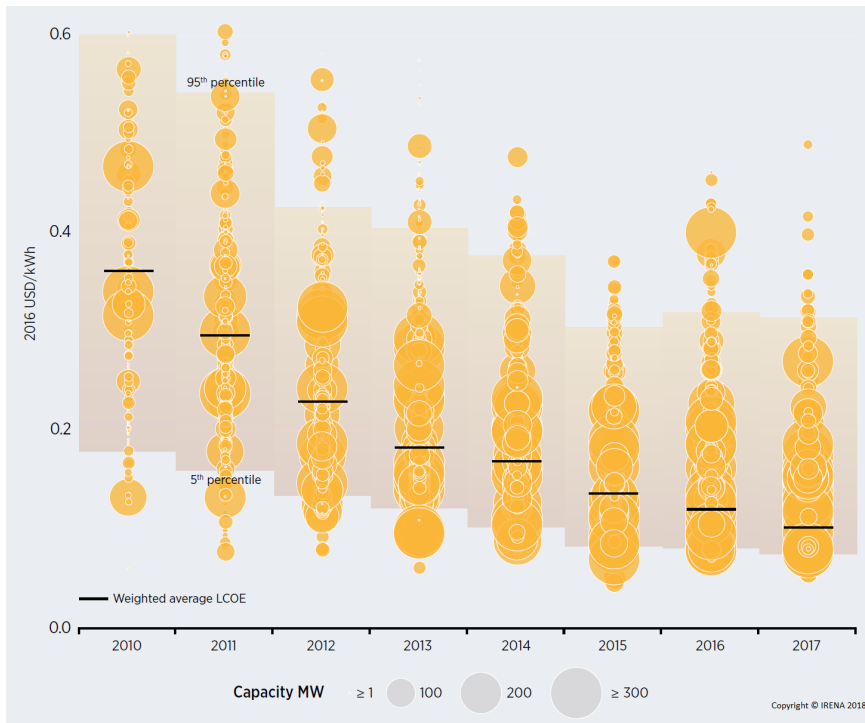


Figure 1.5: Global weighted average and range of LCOE from utility-scale solar PV projects from 2010-2016 (Source: [15]. Data from IRENA Renewable Cost Database [15]).

## 1.1.3. CHALLENGES WITH GRID-BASED ELECTRIFICATION

Figure 1.6 shows the distribution of the global population without electricity across regions. A vast majority (nearly 85%) of the global population without electricity access lives in rural areas.

Due to the remote location of the unelectrified villages and unstable electricity-grid in many of these regions, grid-based electrification is certainly not an immediate solution to eradicate energy poverty. Despite accelerated efforts towards increasing energy access,

the current rate is still deemed insufficient to meet SDG 7 by 2030 [16]. Moreover, there
are many factors why grid-based electrification has not reached uniformly across the
whole country for several nations. Examples of these factors include inefficient policies,
corruption, technological inefficiency, among others [17, 18, 19].

Grid-based electrification for remote rural areas is in general fraught with financial
risks. For example, 55% of Kenya Power and Lighting Corporation (KLPC)'s customers,
who are situated mainly in rural areas, spend roughly $3 a month on electricity [20]. Even
for higher power consuming customers, it has been shown that the payback period on
a typical KPLC rural grid connection is over 44 years [21]. Thus, in many areas, as more
rural customers are added to African utilities, the utilities tend to lose more money.

The other problem plaguing the grid-based electricity in the un(der-)electrified re-
gions of the world is the reliability of power supply. It was observed in 2018 that the grid
connection in urban and peri-urban areas in the Africa cities of Dar es Salaam and Nairobi
supplied reliable power within the standard usable voltage range for only 47 percent of
the time [21].

Transmission and connection costs are also bottlenecks for grid-based electricity.
Up to 40% of all grid-based electricity costs can be attributed to transmission costs
[10]. Economically viable grid extension demands a certain population density and per
connection electricity consumption, which are both factors that are almost certain to be
worse for the least grid-connected areas of any country. Moreover, average grid extension
costs can be high, estimated to be at around $500 per connection [10].
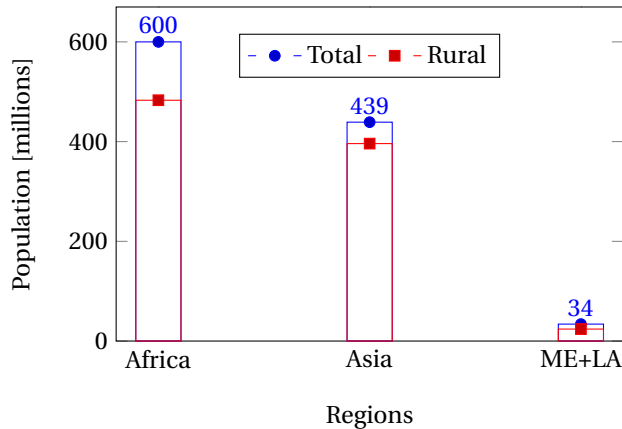


Figure 1.6: Distribution of globally unelectrified population as of 2016 (data sourced from IEA [22]). ME:
Middle-East; LA: Latin America.

Finally, a grid-based electricity paradigm is still fossil-fuel-based in many countries,
leading to worsening effects on climate change while exhibiting technology-inertia in
terms of switching to or integrating a higher proportion of renewables.

In the presence of these challenges facing grid-based electrification, the other alter-
native is off-grid electrification. The biggest advantage of off-grid electrification is that
access to basic energy needs can be accelerated in comparison with grid-based electrifi-
cation. Additionally, it is far easier to integrate renewables in off-grid systems due to the

opportunity to design the systems from scratch as well as their relatively smaller sizes. Moreover, for last mile connectivity and reaching low population density areas with low electricity demand, off-grid solutions are the most viable options.

Note: A detailed review of the challenges of grid-based electrification in comparison with off-grid electrification can be found in Chapter 2.

### 1.1.4. SOLAR HOME SYSTEMS

Solar PV-based off-grid rural electrification seems to complement, as well as compensate for, the grid extension efforts in most of the target regions in need of accelerated electrification. Solar Home Systems (SHS) are the perfect examples of solar PV products providing off-grid electrification. An SHS is usually defined as a solar PV-based generator rated 11 Wp to more than 100 Wp with a suitable battery storage [23]. The maximum PV module rating in an SHS kit is expected not to exceed 350 Wp as per the current standards [24]. Figure 1.7 shows an example of an SHS from the company BBOXX active in East Africa; the SHS contains a PV module, battery storage with power electronics, and DC loads. The SHS is by definition standalone, i.e., it is not connected to the grid. The term solar home systems may be used interchangeably with a standalone PV system, although the term SHS has largely come to be used in the context of off-grid electrification.



Figure 1.7: Example of an SHS consisting of PV panel, battery storage and DC loads (model bPower50; image courtesy of BBOXX Ltd.).

In terms of the effectiveness of off-grid solar-based electrification at the household level, a total of 124 million people have benefited from using off-grid solar between 2010 and 2016 — 100 million people have used pico-solar products like solar lanterns (< 11 Wp), and 24 million have used SHS [25].

## 1.2. LIMITATIONS OF SHS

Despite being the natural technology choice to tackle electrification woes, there are multiple reasons why SHS have not been able to achieve scale or fully eradicate energy poverty. This section details the inherent problems endemic to state-of-the-art SHS.

### 1.2.1. Cost

Even though the sun's energy is freely available, the system for converting the free resource into useful electricity — SHS — incurs significant costs. Especially given the target segment for electrification, cost remains a stumbling block for SHS. As of 2016, while the PV module costs for SHS reached \$1–2/Wp, the total initial system costs were significantly higher, ranging from around \$4–15/Wp for different systems across Africa [26]. These cost figures vary greatly over time and across regions. However, in general, the initial costs of SHS are typically more than 75% of the total lifetime costs, and these upfront costs can be equivalent to a low-income rural household's earnings over a year [27].

While a direct impact on technology costs depends largely on the technology learning curves, there are still other avenues where technical and technological interventions in the context of SHS can yield direct dividends while alleviating cost-related woes. These other 'avenues' are also problems translatable to present-day SHS technical design, as explained in Section 1.2.2 to Section 1.2.6.

### 1.2.2. Battery in an SHS

The battery is a vital component of the SHS, enabling energy storage of the PV output (output power generated by the PV modules), which can be utilized in the absence of sunlight. However, the sizable proportion of upfront battery costs in total system costs makes the battery the most expensive SHS component. This fact, coupled with the low battery lifetimes (sometimes even as low as 3 years [28]), makes battery-costs the most relevant in SHS design. Battery-costs recur not just in terms of the upfront costs, but also in terms of the replacements during SHS lifetime, thereby making battery lifetime a critical parameter in SHS applications [29]. Additionally, accurate sizing of the battery can impact battery lifetime [30], underlining the importance of battery lifetime as a design parameter to be taken into account while dimensioning an SHS, which also has implications on the total system costs. Therefore, the battery lifetime needs to be estimated based on the anticipated application in the context of SHS at the SHS design stage.

### 1.2.3. Optimal system sizing

SHS dimensioning or sizing comprises the PV sizing (the rated output in Wp), battery sizing (the rated energy capacity), and the sizing of the power converters (rated power). PV sizing mainly depends on the total energy needed from the PV generator [3], which in turn depends on the load profile. A lower than adequate PV size results in system failure or a high number of loss of load events, i.e., loss of load probability (LLP). On the other hand, a larger than adequate PV size results in wastage of energy along with higher system costs.

The battery is the most expensive SHS component while suffering from low lifetimes as compared to other SHS components. Additionally, a smaller than adequate battery size will result in failure to meet the load requirements, while an oversized battery will drastically increase the upfront costs of the system. Moreover, battery replacements are often an additional hassle in the context of remote rural areas.

---

[3]The PV module is also be called as the PV generator, as in the context of SHS, the PV module is the only source of power generation.

For a given electricity demand, the optimal system size will reduce the wastage of energy in the form of excess power generation, increase the power supply availability, and increase the estimated battery lifetime while keeping the upfront costs as low as possible. Therefore, the optimal sizing of SHS is a critical task for designing the SHS to cater to off-grid electricity needs.

### 1.2.4. LOAD DEMAND IN OFF-GRID SYSTEMS

Load demand of a household can be quantified in the form of an electrical load profile. A load profile can be defined as the power demand of an energy system mapped over time. A load profile not only captures the electricity demand of the user but also serves as a vital input to the electrical system design. Especially in the case of off-grid power systems like the SHS, reliable apriori knowledge of the load profile is extremely helpful in the electrical sizing the system (i.e., deciding the PV rating and the battery capacity).

In fact, load profile, even if coarsely estimated, is almost always the starting point in an off-grid, standalone PV system design [31]. Load profiles can have a profound impact on the performance as well as design decisions in off-grid systems [32]. A better knowledge of load profile makes for a more optimal off-grid electrical system design. Conversely, the lack of an appropriate load profile leads to either oversizing or undersizing the system, thereby causing an unhealthy trade-off between system costs and power availability [33].

Moreover, there is a lack of load profile data for off-grid users, especially when considering electricity needs above basic lighting and mobile phone charging. Additionally, it is challenging to design an energy system for a user without an electricity footprint in the past. Furthermore, even if the basic electricity demands are met, the electricity needs of a user in the off-grid context keep increasing with time [33, 34]. Lastly, the off-grid sector has seen the growth of the so-called super-efficient DC appliances in the last few years [35]. Therefore, in order to design and dimension off-grid SHS, load profiles are needed that not only capture different levels of electricity usage, but also take into account the load consumption in line with the currently available super-efficient DC appliances. Hence, constructing load profiles for various levels of electrification would be one of the first problems to be tackled in this dissertation.

### 1.2.5. POWER AVAILABILITY

Power availability is another limitation of SHS when compared to conventional grid extension. While state-of-the-art SHS are extremely useful for powering a few DC appliances and LED lights, they still face a power ceiling that prevents the users from using high power appliances like pumps, washing machines, etc. The limited nature of the PV power production, coupled with a limited capacity of the PV module and battery storage, means that the households in question are often restricted not just to the appliance choice but also the duration of appliance usage. Again, this translates back to the challenge of optimal sizing, while also being able to accommodate a growing load profile.

### 1.2.6. CLIMBING UP THE ELECTRIFICATION LADDER

As mentioned in Section 1.2.4, the electricity needs of a household keep increasing with time. This phenomenon can be visualized in the form of the so-called energy ladder, as referred to in literature before [36]. Specifically in the context of electrification, it is also

referred to as the electrification ladder [37, 33]. Figure 1.8 illustrates the concept of the electrification ladder. At the lowest rung is an unelectrified household with no access to electricity, represented by a fossil-based fuel source (e.g., kerosene lamp). Higher rungs of the ladder represent the increase in the number of appliances and therefore, the overall electricity demand.
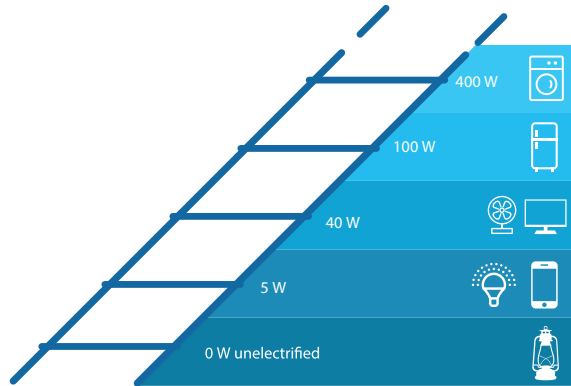


Figure 1.8: Concept illustration of the electrification ladder. As a household scales up the ladder, the electricity demand increases through the addition of higher power (or greater number of) appliances relative to the preceding rungs of the ladder. The power levels of the appliances are indicative only.

In their current form, present-day SHS are only able to fulfill the electricity needs in the lower rungs of the electrification ladder. Simplistic oversizing or over-stacking of PV and battery in an incumbent SHS to reach highest levels of electrification might be economically unviable. This is where the role of rural microgrids could be explored to achieve higher levels of electrification, especially as a solution that goes further than standalone SHS yet without incurring the usual problems associated with conventional grid extension. This also opens up multiple avenues of exploration. For instance, the specific benefits for going from standalone SHS to rural microgrids, and the optimal microgrid topology with decentralized power generation and storage while taking into account the spatial spread of the households, are topics that can be suitably addressed through scientific investigation. This will be one of the topics to be explored in this dissertation, as explained in Section 1.5. A comparison between SHS and microgrids as potential electrification pathways is discussed in detail in Chapter 2.

**Multi-tier framework for measuring household electricity access**    The different rungs of the conceptual electrification ladder can be alternatively viewed through the multi-tier framework (MTF) for measuring household electricity access [38], which describes 5 distinct tiers of household electricity access. This is discussed in detail in Chapter 2. While the electrification ladder is a useful concept to visualize the increasing electricity needs of a household, the MTF gives a quantified categorization of the energy demand per tier of electricity access, as discussed later in Section 2.1.1. In this dissertation, the MTF will be used for the quantified distinction of different levels of electricity demand to be satisfied through off-grid solar-based electrification.

## 1.3. Scope, Objective and Research questions

### 1.3.1. Scope of this dissertation

As discussed in Section 1.2, the state-of-the-art SHS is limited by several problems that are largely inter-related. The greater issue of attaining SDG 7 and eradicating energy poverty warrants a multi-disciplinary approach spanning technology, policy, business, finance, user-centered design, amongst others. However, owing to the technical nature of this dissertation, the scope of the work discussed in this dissertation is limited to the extent where technology can address the problems described in Section 1.2. Therefore, special focus is laid on the problems described in Section 1.2.2 to Section 1.2.6, without directly looking at cost itself as a problem to be specifically solved. Keeping this in mind, the objective and research questions for the work conducted in this dissertation are described below.

### 1.3.2. Main objective

The main objective of this dissertation is stated as follows.

"*To analyze the technological limits of Solar Home Systems (SHS) in terms of power level, availability and energy storage for achieving universal electrification.*"

### 1.3.3. Research Questions

The main objective can be broken down into the following research questions.

RQ₁ What are the main (technical) limitations of the present electrification pathways in achieving universal electrification? *Ch2*

RQ₂ How to construct load profiles for the various levels of off-grid electrification that enable the design of off-grid solar-based solutions? *Ch3*

RQ₃ How to estimate battery lifetime for a given SHS application at the SHS design stage? *Ch4*

RQ₄ How to optimize the SHS size to satisfy the energy needs for various levels of electrification, while also ensuring maximum levels of power availability, minimizing excess energy generation, and maximizing battery lifetime? *Ch5*

RQ₅ What are the quantitative benefits on the battery storage sizing and power availability when going from standalone SHS to SHS-based microgrids that enable power sharing? *Ch6*

RQ₆ How to find the optimal microgrid topology for interconnection of SHS in remote off-grid regions, taking into account the spatial spread of the households? *Ch7*

## 1.4. Research publications

The research publications relevant to this dissertation are listed below along with the corresponding chapters that are based on them.

**1**

### Journal publications

J$_1$ **N. Narayan**, Z. Qin, J. Popovic-Gerber, J. C. Diehl, P. Bauer, M. Zeman. Stochastic load profile construction for the multi-tier framework for household electricity access using off-grid DC appliances, *Energy Efficiency*, In Topical Collection of Journal Energy Efficiency on Off-grid Appliances and Smart Controls for Energy Access, Springer 2018. **(Ch 3)**

J$_2$ **N. Narayan**, T. Papakosta, V. Vega-Garita, Z. Qin, J. Popovic-Gerber, P. Bauer, M. Zeman. Estimating battery lifetimes in Solar Home System design using a practical modelling methodology, *Applied Energy*, Volume 228, 2018, Pages 1629-1639, ISSN 0306-2619. **(Ch 4)**

J$_3$ **N. Narayan**, A. Chamseddine, V. Vega-Garita, Z. Qin, J. Popovic-Gerber, P. Bauer, M. Zeman. Exploring the boundaries of Solar Home Systems (SHS) for off-grid electrification: Optimal SHS sizing for the multi-tier framework for household electricity access. *Applied Energy*, 240, 2019, Pages 907-917. **(Ch 5)**

J$_4$ **N. Narayan**, A. Chamseddine, V. Vega-Garita, Z. Qin, J. Popovic-Gerber, P. Bauer, M. Zeman. Quantifying the Benefits of a Solar Home System-Based DC Microgrid for Rural Electrification. Energies, 2019, 12(5), 938. **(Ch 6)**

J$_5$ **N. Narayan**, M. Tagliapietra, Z. Qin, J. Popovic-Gerber, P. Bauer, and M. Zeman. Optimal microgrid layout using Geographic Information System and graph theory concepts, submitted. **(Ch 7)**

J$_6$ **N. Narayan**, V. Vega-Garita, Z. Qin, J. Popovic-Gerber, P. Bauer, and M. Zeman. The long road to universal electrification: A critical look at present pathways and challenges, submitted. **(Ch 2)**

J$_7$ Y. Yu, **N. Narayan**, V. Vega-Garita, J. Popovic-Gerber, Z. Qin, M. Wagemaker, P. Bauer, M. Zeman. Constructing Accurate Equivalent Electrical Circuit Models of Lithium Iron Phosphate and Lead–Acid Battery Cells for Solar Home System Applications in *Energies*, 2018 (special issue on Battery Storage Technology for a Sustainable Future), doi: https://doi.org/10.3390/en11092305. **(Appendix A)**

### Conference publications

C$_1$ **N. Narayan**, T. Papakosta, V. Vega-Garita, J. Popovic-Gerber, P. Bauer and M. Zeman, "*A simple methodology for estimating battery lifetimes in Solar Home System design*," 2017 IEEE AFRICON, Cape Town, 2017, pp. 1195-1201. doi: 10.1109/AFRICON.2017.8095652. **(Ch 4)**

C$_2$ T. den Heeten, **N. Narayan**, J. C. Diehl, J. Verschelling, S. Silvester, J. Popovic-Gerber, P. Bauer and M. Zeman, "Understanding the present and the future electricity needs: Consequences for design of future Solar Home Systems for off-grid rural electrification," *2017 International Conference on the Domestic Use of Energy (DUE)*, Cape Town, 2017, pp. 8-15. doi: 10.23919/DUE.2017.7931816. **(Partly Ch 2)**

C₃  **N. Narayan**, V. Vega-Garita, Z. Qin, J. Popovic-Gerber, P. Bauer and M. Zeman, "A modeling methodology to evaluate the impact of temperature on Solar Home Systems for rural electrification," 2018 IEEE International Energy Conference (ENERGYCON), Limassol, Cyprus, 2018, pp. 1-6. doi: 10.1109/ENERGYCON.2018.8398756 **(Appendix B)**

C₄  **N. Narayan**, B. O-Malik, L. Mackay, Z. Qin, J. Popovic-Gerber, P. Bauer and M. Zeman, "*Decentralized Control-Scheme for DC-Interconnected Solar Home Systems for Rural Electrification*," 2019 IEEE International Conference on DC Microgrids (ICDCM), Matsue, Japan, 2019, pp. 1-6. **(Appendix C)**

## 1.5. DISSERTATION LAYOUT

Figure 1.9 illustrates the interdependency between the various chapters in the dissertation. Additional thematic separations have been identified, along with the research questions that will be answered and the research publications that the chapters are based on, as seen in Figure 1.9.

### CHAPTER 1. INTRODUCTION

This chapter introduces the background, motivation, scope, objective, research questions, and layout of the dissertation.

### CHAPTER 2. UNIVERSAL ELECTRIFICATION: A CRITICAL LOOK AT PRESENT PATHWAYS AND CHALLENGES

This chapter discusses the 3 main electrification pathways, viz., grid extension, centralized microgrids, and standalone solar-based solutions like pico-solar and SHS while understanding their relative merits and demerits. Additionally, the main bottlenecks with SHS for large scale electrification and moving up the electrification ladder are discussed. This chapter sets the general directions for the technological explorations presented in the rest of the dissertation.

### CHAPTER 3. LOAD PROFILE CONSTRUCTION

This chapter presents the methodology followed to quantify the electricity demand of the households for various tiers of electricity access in terms of load profiles. In the context of electrification, reliable data for load profiles is often non-existent or limited to the lowest tiers of electricity access. Additionally, the off-grid appliances are rapidly evolving, with the advent of the so-called super-efficient off-grid dc appliances, like TV, fan, etc. This chapter details the construction of a stochastic load profile construction tool, resulting in representative load profiles for various tiers of electricity consumption while considering the super-efficient off-grid dc appliances.

### CHAPTER 4. ESTIMATING BATTERY LIFETIME IN SOLAR HOME SYSTEMS

Estimating battery lifetime is a critical task for SHS design. However, it is also a complex task due to the reliance on experimental data or modelling cell level electrochemical phenomena for specific battery technologies and application use-case. This chapter presents a practical, non-empirical battery lifetime estimation methodology specific
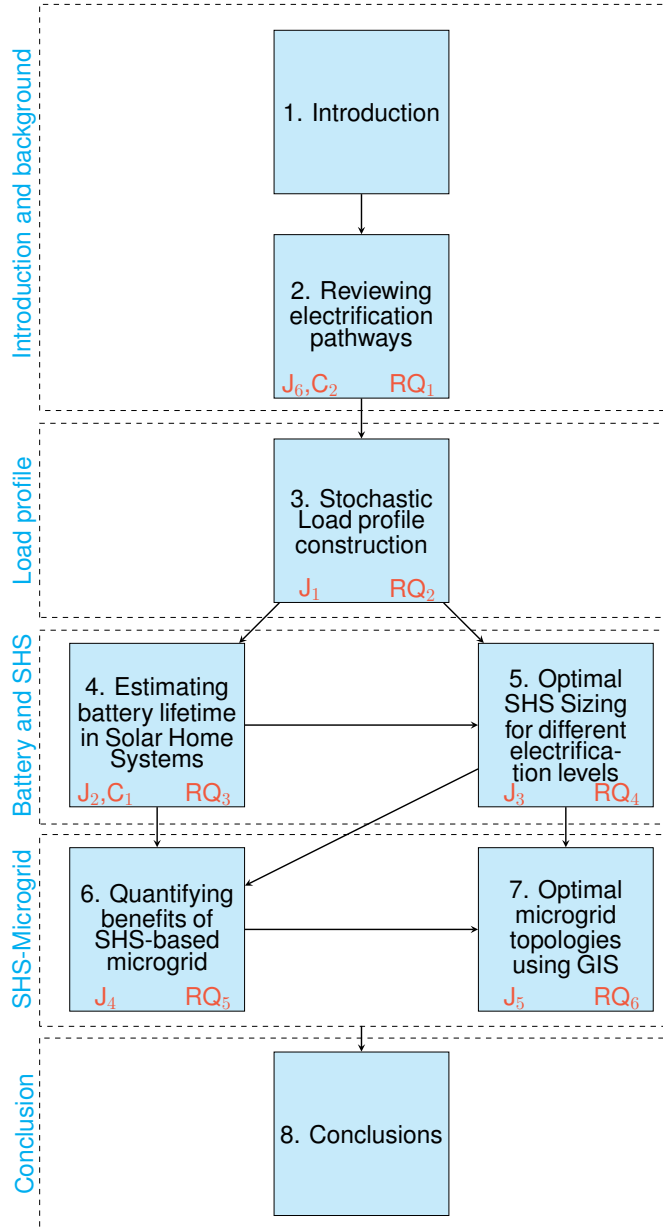
Figure 1.9: Dissertation layout showing the interdependencies between chapters and corresponding research questions.

to the application and the available candidate battery choices. An application-specific SHS simulation is carried out, and the battery activity is analyzed. A practical dynamic

battery lifetime estimation method is introduced, which captures the fading capacity of the battery dynamically through every micro-cycle.

### CHAPTER 5. OPTIMAL SYSTEM SIZING FOR SHS

This chapter explores the possibilities of using SHS for climbing up the energy ladder. An optimal standalone system size is calculated for each tier of energy consumption, taking into account the battery lifetime, temperature impact on SHS performance, power supply availability in terms of LLP, and excess PV energy. The optimal system sizing methodology relies on a multi-objective optimization using a genetic algorithm.

### CHAPTER 6. QUANTIFYING BENEFITS OF INTERCONNECTED SHS-BASED DC MICROGRID

As standalone SHS are inadequate in meeting the electricity needs of higher tiers of electrification, an alternate solution is explored in this chapter with SHS having relatively lower battery sizes while sharing energy. A modular and scalable architecture for such a bottom-up, interconnected SHS-based architecture is introduced, and the benefits of the microgrid over standalone SHS are quantified in terms of lower battery sizes and the defined system metrics like LLP.

### CHAPTER 7. OPTIMAL MICROGRID TOPOLOGIES USING GEO-INFORMATION SYSTEM (GIS) FOR MICROGRID PLANNING THROUGH SHS INTERCONNECTION

Optimal microgrid topologies are usually based on merely a comparison between a standard set of topologies, like ring, bus, spider, and radial topology. This chapter presents a GIS-based methodology that looks at the geo-spatial spreads of households in remote off-grid settlements. The GIS-based household points obtained are then transformed in a planar coordinate system so that graph theory-based concepts like Minimum Spanning Tree can be applied. Thus, various topologies are considered apart from those existing in microgrid literature. The graph theory-based approach yields an interesting trade-off between total installed microgrid cabling needed to establish the interconnectivity and the potential operational parameters like line losses and line congestion.

### CHAPTER 8. CONCLUSIONS

This chapter contains the key conclusions and point-by-point answers to the research questions. Additionally, it explains the scientific implications of the research findings and its broader significance for the society. Finally, future work and recommendations are discussed.

### APPENDICES

Three appendices are presented in this dissertation.

- **Appendix A** Equivalent electrical circuit models of lithium iron phosphate and lead-acid battery cells for solar home system applications are presented in this appendix chapter. This work is based on experiments performed at the cell level for the two battery technologies.

- **Appendix B** A modeling methodology to evaluate the temperature impact on SHS (in terms of PV yield and battery lifetime) is discussed in this appendix chapter.

**1**

- **Appendix C** A decentralized control scheme for interconnected solar home systems for dc microgrids is presented in this appendix chapter. Simulation results are also discussed for a case study with 5 households exchanging power.

## REFERENCES

[1] IEA, *Energy Access Outlook 2017 - From Poverty to Prosperity*. Organization for Economic Cooperation and Development, International Energy Agency, 1 ed., 2017.

[2] International Energy Agency, *Energy Access Outlook 2017 - from poverty to prosperity*. IEA, 2017.

[3] United Nations, "Sustainable development goals." `https://www.un.org/sustainabledevelopment/sustainable-development-goals/`. Accessed: 2017-05-19.

[4] R. Spalding-Fecher, "Health benefits of electrification in developing countries: a quantitative assessment in south africa," *Energy for Sustainable Development*, vol. 9, no. 1, pp. 53–62, 2005.

[5] S. Ray, B. Ghosh, S. Bardhan, and B. Bhattacharyya, "Studies on the impact of energy quality on human development index," *Renewable energy*, vol. 92, pp. 117–126, 2016.

[6] B. Pillot, M. Muselli, P. Poggi, and J. B. Dias, "Historical trends in global energy policy and renewable power system issues in sub-saharan africa: The case of solar pv," *Energy policy*, vol. 127, pp. 113–124, 2019.

[7] J. Sušnik and P. van der Zaag, "Correlation and causation between the un human development index and national and personal wealth and resource exploitation," *Economic Research-Ekonomska Istraživanja*, vol. 30, no. 1, pp. 1705–1723, 2017.

[8] E.-j. Quak, "Lighting and electricity services for off-grid populations in sub-sahara africa," *Knowledge, evidence and learning for development, Tech. Rep.*, 2018.

[9] Global LEAP, "The State of the Off-Grid Appliance Market," tech. rep., Global LEAP Lighting and Energy Access Partnership, 2016.

[10] S. Buluswar, Z. Friedman, P. Mehta, S. Mitra, and R. Sathre, *50 Breakthroughs - Critical scientific and technological advances needed for sustainable global development*. LIGTT, Institute for Globally Transformative Technologies, Lawrence Berkeley National Lab, 2014.

[11] ESMAP, "State of Electricity Access Report 2017," tech. rep., World Bank Group, ESMAP and SE4ALL, 2017.

[12] D. F. Barnes and H. Samad, *Measuring the Benefits of Energy Access: A Handbook for Development Practitioners*. Inter-American Development Bank, 2018.

[13] Lighting Global, Bloomberg New Energy Finance and GOGLA, "Off-grid solar market trends report 2016," *Bloomberg New Energy Finance and Lighting Global in cooperation with the Global Off-Grid Lighting Association (GOGLA)*, 2016.

[14] E. F. Merchant, "Irena: Global renewable energy prices will be competitive with fossil fuels by 2020." `https://www.greentechmedia.com/articles/read/irena-renewable-energy-competitive-fossil-fuels-2020#gs.3y8akc`. Accessed: 2019-02-30.

[15] IRENA, "Renewable Power Generation Costs in 2017," *International Renewable Energy Agency, Tech. Rep.*, 2018.

[16] I. I. U. World Bank, and World Health Organization, "Tracking SDG7: The energy progress report 2018," tech. rep., International Energy Agency, International Renewable Energy Agency, United Nations Statistics Division, World Bank, and World Health Organization, 2018.

[17] D. Palit and K. R. Bandyopadhyay, "Rural electricity access in south asia: Is grid extension the remedy? a critical review," *Renewable and Sustainable Energy Reviews*, vol. 60, pp. 1505–1515, 2016.

[18] T. Urmee, D. Harries, and A. Schlapfer, "Issues related to rural electrification using renewable energy in developing countries of asia and pacific," *Renewable Energy*, vol. 34, no. 2, pp. 354–357, 2009.

[19] N. Narayan, J. Popovic, J. C. Diehl, S. Silvester, P. Bauer, and M. Zeman, "Developing for developing nations: Exploring an affordable solar home system design," in *2016 IEEE Global Humanitarian Technology Conference (GHTC)*, pp. 474–480, Oct 2016.

[20] N. Otuki, "Half of kenya power clients use sh10 daily." `https://www.businessdailyafrica.com/economy/Half-of-Kenya-Power-clients-use-Sh10-daily/3946234-4643380-tmq6js/index.html`. Accessed: 2019-01-28.

[21] Gabriel Davies, Matt Tilleard and Lucy Shaw, "Private mini-grid firms deserve a chance to compete against slow utilities in africa." `https://www.greentechmedia.com/articles/read/a-faster-path-to-rural-electrification#gs.4p99x3`. Accessed: 2017-05-19.

[22] IEA, *World Energy Outlook 2016*. Organization for Economic Cooperation and Development, International Energy Agency, 1 ed., 2016.

[23] Global Off-Grid Lighting Association, "Global off-grid solar market report - semi-annual sales and impact data," tech. rep., GOGLA, Lighting Global and Berenschot, 2018.

[24] Lighting Global, "Solar home system kit quality standards version 2.5," *Lighting Global, Tech. Rep.*, December 2018.

[25] IRENA, "Off-grid renewable energy solutions to expand electricity access: An opportunity not to be missed," *International Renewable Energy Agency, Tech. Rep.*, 2019.

**1**

[26] IRENA, "Solar PV in Africa: Costs and Markets," *International Renewable Energy Agency, Tech. Rep.*, 2016.

[27] T. Urmee, D. Harries, and H.-G. Holtorf, *Overview of Financing Mechanisms for Solar Home Systems in Developing Countries*, pp. 49–77. Cham: Springer International Publishing, 2016.

[28] Good Solar Initiative, *Quality Charter: Technical and Service Quality Standards for Accredited Solar Suppliers.* SNV Netherlands Development Organisation, 2016.

[29] N. Narayan, T. Papakosta, V. Vega-Garita, J. Popovic-Gerber, P. Bauer, and M. Zeman, "A simple methodology for estimating battery lifetimes in solar home system design," in *2017 IEEE AFRICON*, pp. 1195–1201, Sept 2017.

[30] N. Narayan, T. Papakosta, V. Vega-Garita, Z. Qin, J. Popovic-Gerber, P. Bauer, and M. Zeman, "Estimating battery lifetimes in solar home system design using a practical modelling methodology," *Applied Energy*, vol. 228, pp. 1629 – 1639, 2018.

[31] A. H. Smets, K. Jäger, O. Isabella, R. Van Swaaij, and M. Zeman, *Solar Energy, the Physics and Engineering of Photovoltaic Conversion Technologies and Systems.* UIT Cambridge, 2016.

[32] S. Treado, "The effect of electric load profiles on the performance of off-grid residential hybrid renewable energy systems," *Energies*, vol. 8, no. 10, pp. 11120–11138, 2015.

[33] T. D. Heeten, N. Narayan, J. C. Diehl, J. Verschelling, S. Silvester, J. Popovic-Gerber, P. Bauer, and M. Zeman, "Understanding the present and the future electricity needs: Consequences for design of future solar home systems for off-grid rural electrification," in *2017 International Conference on the Domestic Use of Energy (DUE)*, pp. 8–15, April 2017.

[34] M. Gustavsson, "With time comes increased loads: An analysis of solar home system use in lundazi, zambia," *Renewable Energy*, vol. 32, no. 5, pp. 796–813, 2007.

[35] N. Narayan, Z. Qin, J. Popovic-Gerber, J.-C. Diehl, P. Bauer, and M. Zeman, "Stochastic load profile construction for the multi-tier framework for household electricity access using off-grid dc appliances," *Energy Efficiency*, Nov 2018.

[36] I. Bisaga and P. Parikh, "To climb or not to climb? investigating energy use behaviour among solar home system adopters through energy ladder and social practice lens," *Energy research & social science*, vol. 44, pp. 293–303, 2018.

[37] B. Tenenbaum, C. Greacen, T. Siyambalapitiya, and J. Knuckles, *From the bottom up: how small power producers and mini-grids can deliver electrification and renewable energy in Africa.* World Bank Publications, 2014.

[38] M. Bhatia and N. Angelou, *Beyond Connection, Energy Access Redefined.* The World Bank, 2015.

# 2

# THE LONG ROAD TO UNIVERSAL ELECTRIFICATION: A CRITICAL LOOK AT PRESENT PATHWAYS AND CHALLENGES

*We will make electricity so cheap that only the rich will burn candles*

Thomas A. Edison

## ABSTRACT

In this chapter, the three different electrification pathways — grid extension, centralized microgrids, and standalone solar-based solutions like pico-solar and SHS — are critically examined while understanding their relative merits and demerits. Grid extension can provide broad-scale access at low LCOE values but requires a certain electricity demand threshold and population density to justify investments. To a lesser extent, centralized (off-grid) microgrids also require a minimum demand threshold and knowledge of the electricity demand. Solar-based solutions are the main focus in terms of off-grid electrification in this chapter, in line with the scope of this dissertation, as mentioned in

Chapter 1. In recent times, decentralized solar-based off-grid solutions like pico-solar and SHS have shown the highest adoption rates and promising impetus with respect to basic lighting and electricity for powering small appliances. However, the burning question is — *from lighting a million to empowering a billion – can solar home systems get us there?* The two main roadblocks for SHS are discussed, and the requirements from the ideal electrification pathway are introduced. A bottom-up, interconnected SHS-based electrification pathway is proposed that can form the missing link among the present electrification pathways.

## OUTLINE

This chapter contains 7 sections. Section 2.1 introduces the problem of universal electrification with the 3 electrification pathways presently in use. Sections 2.2–2.4 discuss each of the electrification pathways in detail. Section 2.5 presents the significant challenges hindering the state-of-the-art SHS from becoming the electrification pathway of choice in the long run. Section 2.6 describes the requirements from an ideal pathway that can overcome the current challenges and discusses the comparative qualities of each electrification pathway. Section 2.7 the challenges with the SHS-based vision towards universal electrification. Finally, Section 2.8 concludes the chapter with closing thoughts on universal electrification.

## 2.1. INTRODUCTION

Universal electrification is a monumental challenge facing humankind today. Just under a billion people globally lacked access to any form of electricity at the end of 2017 [1], an (inadequate) improvement since 2000, when there were 1.7 billion people without electricity [2]. Three main solutions have been tried, with varying degrees of success, in the last decade to increase the umbrella of electrification. These are:

1. Grid extension

2. Off-grid micro (or mini-) grids

3. Standalone household level solutions like pico-solar and solar home systems (SHS)

While solar-based standalone solutions have gained prominence in the last few years, the overall electrification efforts have not been rapid enough. The UN also took note of the progress on SDG 7, saying it "remains too slow to be on track to meet the global energy targets for 2030" [3].

### 2.1.1. MULTI-TIER FRAMEWORK FOR MEASURING ELECTRICITY ACCESS

Before proceeding to understand the electrification pathways, it is first essential to understand the concept and significance of the multi-tier framework for measuring household electricity access.

In the past, governments have often defined electricity access as a connection to an electrical grid, whether or not that connection is reliable. Additionally, large sections of the people (e.g., a whole village) have also been called electrified if a small percentage of the households is electrified [4]. Until the previous decade, electricity access was

Table 2.1: Multi-tier matrix for measuring access to household electricity supply. Sourced from [5].

| | Tier 1 | Tier 2 | Tier 3 | Tier 4 | Tier 5 |
|---|---|---|---|---|---|
| **Energy and peak power rating** | > 12 Wh & > 3 W | > 200 Wh & > 50 W | > 1 kWh & > 200 W | > 3.4 kWh & > 800 W | > 8.2 kWh & > 2 kW |
| **Availability (hrs/day)** | > 4 | > 4 | > 8 | > 16 | > 23 |
| **Availability (hrs/evening)** | > 1 | > 2 | > 3 | > 4 | > 4 |
| **Reliability** | — | — | — | < 14 disruptions per week | < 3 disruptions per week |
| **Quality** | — | — | — | Voltage problems do not affect the use of desired appliances | |
| **Affordability** | — | — | — | Cost of 365 kWh/year < 5% of household income | |
| **Legality** | — | — | — | Bill is paid to the utility or authorized representative | |
| **Health & Safety** | — | — | — | Absence of past accidents and high risk perception in the future | |

largely looked at as a have or have-not condition. However, such oversimplification is a dangerously narrow view of understanding and acting towards the electricity access problem. Such binary metrics were therefore considered insufficient, and a multi-tier framework (MTF) was proposed in [5], which captures the multi-dimensional nature of electricity access. Table 2.1 presents the MTF as described in [5].

In terms of the electrification ladder mentioned previously in Chapter 1 in Figure 1.8, the climb up the ladder can now be alternatively seen as the movement across the tiers of the MTF.

**SCOPE OF THIS CHAPTER**

In this chapter, the three main electrification pathways currently in use are analyzed while discussing the relative merits and demerits for each pathway. Special attention is paid to the solar-based off-grid electrification. This is because off-grid renewable energy-based electrification has emerged in the last decade as a mainstream, cost-competitive alternative to grid-based electricity. For instance, between 2011 and 2016 alone, more than 133 million people benefited from off-grid renewables [6]. We critically look at some of the most pressing problems that off-grid solar-based electrification is/will be facing in achieving scale en route to universal electrification.

Furthermore, it must be noted that technology is only one part of the larger puzzle of electrification. Business and policy aspects also need significant attention, but the scope of this chapter is largely limited to the technical and technological considerations of electrification.

## 2.2. PATHWAY 1: GRID EXTENSION

Grid-based electricity refers to a household having its electricity derived from a local network that is connected to the larger transmission network, where the grid is typically powered by large centralized power plants. Grid extension refers to the act of expanding the national grid's network to provide electricity access. Grid extension includes installing medium voltage distribution lines as well as adding new connections to the households needing electricity access [7].

Grid extension has historically been the most common way to provide electricity access to un(der-)electrified regions and communities. Apart from being a common

**2**

approach, it can also be the most cost-effective way to provide electricity access at very high levels of electricity demand, e.g., for tier 4 and tier 5 electricity access.

However, grid extension is cost-effective only if the target region has a certain population density and energy demand. Otherwise, the extension efforts are almost certain to incur losses. For example, 55% of all customers serviced by Kenya Power and Lighting Corporation (KLPC) spend less than $3 a month on electricity, pushing the payback period of a typical KLPC grid connection to 44 years, even for higher levels of consumption [8]. The high investment costs for grid extension have been estimated in the order of €22750/km for transmission line and €12000/km for distribution line in most African countries; in comparison, the grid-based retail electricity tariffs in these countries could range from €0.04/kWh (subsidized) to over €0.23/kWh (non-subsidized) [9]. Inadequate revenues also result in progressive deterioration of the reliability of the transmission and distribution network. Unsurprisingly, the compounding effects of these inadequate revenues led to 81% of sub-Saharan African utilities reporting net financial losses in 2013 [10]. Unfortunately, the present reality is that conventional African utilities tend to run a loss every time they connect to a rural customer [8].

While the lack of affordability by the consumers can hamper the viability of the national grid as an electrification option, there are also examples where the infrastructure lags the people's ability to pay. There are several countries where people above the poverty line, who could potentially afford to pay for electricity but still do not have access due to infrastructural issues. For example, it was estimated that in sub-Saharan Africa, 120 million people were living above the poverty line without access to electricity [2]. Other factors like topographical issues, regulatory hurdles, and sparse populations can also make the investment and maintenance of grid extension less favourable compared to off-grid solutions [2].



Figure 2.1: So close, yet so far: A rural household in Aligarh, Uttar Pradesh (India) with installed SHS. Grid lines have passed close to the house for years, yet the household was without any grid-based electricity until 2017. Photo credit: Gaurav Manchanda.

Fieldwork carried out in 2017 related to this PhD project also highlighted the complex

issues at the grass-roots level related to the limitations of national grid outreach [11]. Figure 2.1 depicts a "powerful" image; it captures the harsh reality of electricity access for a rural household in a state in Northern India. A single solar panel can be seen on the rooftop that also has cow dung cakes drying in the sun, which will be used as cooking fuel once dried. Making up the powerful irony in the picture are the grid lines passing tantalizingly close to the house, which had no grid-based electricity access until 2017 despite the presence of the grid in the region for several years.

### CHICKEN AND EGG PROBLEM?

Grid-based electrification in low-income countries is often seen as a chicken and egg problem. Having multiple areas for development to be pursued with inadequate budgets, low-income countries often do not have the means to invest in large-scale grid electrification. On the other hand, lack of electrification, as discussed before in Section 1.1.1, keeps the progress towards development stymied.

### 2.2.1. COMPETITION WITH OFF-GRID RENEWABLES

A significant factor that has led to grid expansion losing out on the cost-effectiveness front for rapid electrification is the rise of the off-grid solutions. In particular, solar-based off-grid solutions like pico-solar SHS have enjoyed tremendous success in recent years as the electrification solution of choice. This has mainly been due to the massive drop in prices of most pico-solar and SHS components. For example, PV price has fallen by more than 80% from 2009 to 2017; LED lights and Li-ion batteries have dropped by 80% and 73% respectively between 2010 and 2016 [6]. Moreover, national grids often heavily depend on fossil fuels for power generation and are therefore counterproductive to progress on other SDGs like SDG 13 (climate action) and SDG 11 (sustainable cities and communities).

However, it is usually a complex task to declare grid extension better or worse than an off-grid alternative. Investigating the viability of grid extension for a particular target location must take into account not just its distance from the existing grid, but also the expected energy consumption and relative off-grid standalone system costs. Figure 2.2 simplistically illustrates the conceptual cost curve as a function of distance assuming a certain energy demand and fixed off-grid system cost. The point where the grid extension costs and off-grid costs meet forms the breakeven distance for that particular case. To the left of that distance, the grid-extension option is more economically favourable, while an off-grid solution is favourable to the right of that breakeven distance.

Figure 2.3 depicts a conceptual comparison of breakeven annual electricity consumption as a function of upfront SHS system costs for a given target region. It is assumed that different target regions would have different mean distances from the grid leading to different curves. The annual electricity consumption as outlined by the MTF is also marked for the various tiers on this conceptual graph. Grid extension will be a cheaper option if the annual consumption of a household in the target region is more than the breakeven electricity level given by the curve. Although a conceptual illustration, it can be seen that the capital SHS costs need to be much lower to be able to justify a standalone system for higher tiers of consumption.

Therefore, it can be said that the precise determination of the viability of grid extension for the electrification of a particular target location depends on multiple factors as seen in
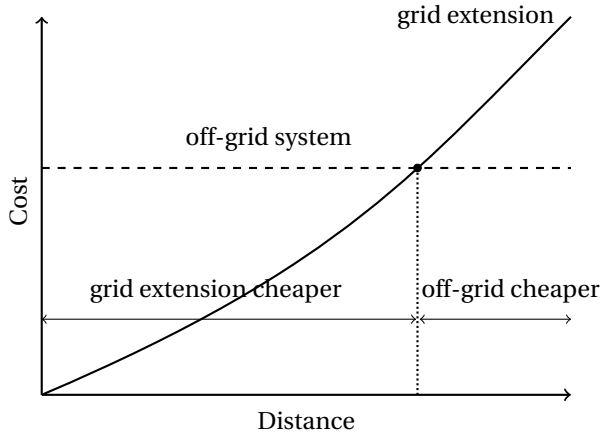
Figure 2.2: Conceptual comparison of off-grid system and grid-extension cost-curves as a function of distance from the existing grid (adapted from [7]). Off-grid system costs are independent of distance.

Figure 2.2 and Figure 2.3. Furthermore, other non-technical factors like policy, regulations, and topography could pose additional challenges for grid extension.
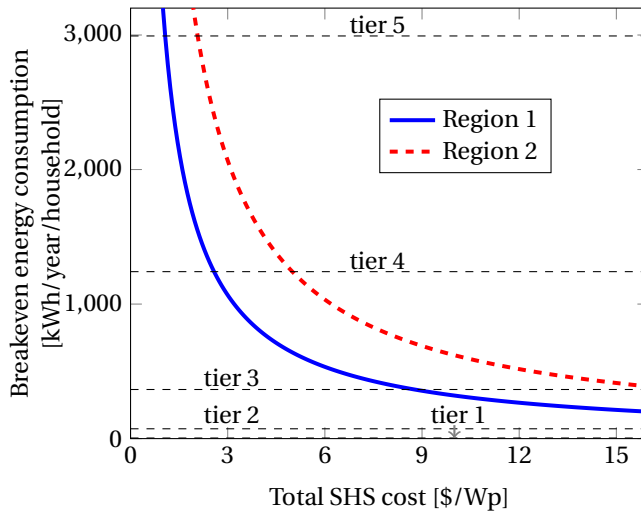


Figure 2.3: Illustrative breakeven annual consumption as a function of SHS upfront costs for two different regions (adapted from [12]). The different tier consumptions of the MTF are also marked for reference. Tier 1 is not clearly visible given the y-axis scale, as the annual energy consumption for tier 1 level is merely 4.38 kWh.

## 2.3. Pathway 2: (Off-grid) centralized microgrids and mini-grids

### 2.3.1. Clarification in terminology

When it comes to off-grid electrification, there are no universally accepted definitions for, or distinctions between, mini-grids and microgrids. Several different definitions exist. For example, the IEA has defined mini-grids as "small grid systems linking a number of households and other consumers" [13]. Although not specified in the context of off-grid electrification, the National Renewable Energy Laboratory (NREL) defined microgrids as "a group of interconnected loads and distributed energy resources that acts as a single controllable entity with respect to the grid" [14]. Mini-grids have also been defined as small-scale distribution networks producing electricity from small generators, typically operating below 11 kV, and providing power to one or more local communities [4]. In the context of electrification, generally, mini-grids and microgrids operate isolated from the grid. Hence, this electrification pathway is referred to as "off-grid".

Some definitions also take into account power levels, although these limits may also vary from one definition to another. For example, the Alliance for Rural Electrification (ARE) defines mini-grids as having capacities ranging from 10 kW to 10 MW, and micro-grids as being similar to mini-grids with generation capacities of 1–10 kW. In general, mini-grids and microgrids are standalone electrical power systems that serve multiple consumers through wired connections, powered by PV modules, diesel gensets, or/and wind turbines [7]. A microgrid has a connotation of being smaller in power capacity, as also seen in some of the power capacity-based definitions above.

**Note:**    For the remainder of this dissertation, the term "microgrids" will be consistently used in the context of off-grid electrification. However, many of the arguments and ideas discussed could also be interchangeably applied also to mini-grids, especially when centralized power generation is considered.

### 2.3.2. Centralized microgrids

Microgrids for off-grid electrification can further be classified based on the power generation technology used. For example, solar PV, biomass, micro-hydro, wind, diesel, etc. Hybrid microgrids are also possible, which use two or more power generation technologies. Energy storage technologies like batteries are frequently used in microgrid projects to improve the availability of power supply. The most common storage technologies are lead-acid and lithium-ion batteries. Sometimes, diesel is also used to replace the battery in a hybrid microgrid, although this option incurs running fuel costs. Usually, the power generation is centralized, i.e., the power generation occurs centrally, and there is a distribution network responsible for supplying power to the consumers. In this dissertation, the main focus is on solar PV as the power generation technology of choice, owing to its historically low prices, modular nature, and ease of installation.

An example of a centralized microgrid architecture is shown in Figure 2.4. The term centralized refers to the central power generation and storage, which is shown in Figure 2.4 in the form of solar PV and battery storage. Additionally, given the recent proliferation of the so-called super-efficient DC appliances (as discussed later in Chapter 3), the microgrid

depicted in Figure 2.4 assumes a DC architecture.
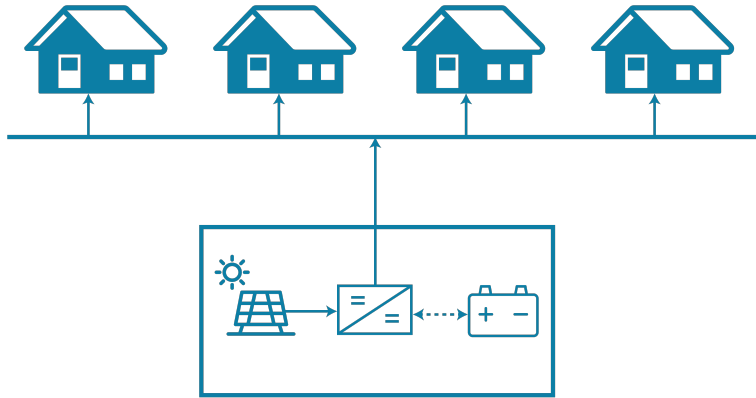


Figure 2.4: An illustration of a centralized (DC) microgrid architecture. The term centralized refers to the central power generation (solar PV) and storage (battery). Each house is assumed to have a set of (DC) loads.

### CENTRALIZED VS. DECENTRALIZED

Microgrids-based off-grid electrification is often referred to as being decentralized. It must be cautiously noted that the classification of these systems being decentralized stems from collectively viewing the myriads of such microgrids juxtaposed with the central national grid. In that specific context, these microgrid systems can be together viewed as autonomous, and hence a decentralized way of delivering electricity. However, in terms of architecture, rural microgrids are usually centralized with central power generation and storage. Therefore, these off-grid microgrids have been classified as centralized microgrids in this dissertation.

### 2.3.3. MICROGRIDS VS. GRID EXTENSION

Where national electricity grids fail to reach, microgrids can step in with several benefits. Microgrids score over grid extension over several categories, as described below.

1. **Transmission and connection costs.** One of the biggest gains for microgrids in comparison to grid extension comes in the form of minimizing transmission costs, which can be up to 40% of the total grid-based electricity costs [15]. On the other hand, as the microgrids usually serve areas within 5 km of the installation, they incur minimal transmission losses compared to the grid. Typical mini-grid retail tariffs in Africa have seen to range from €0.1/kWh to €1.2/kWh, depending on local conditions and operators [9]. Average per connection capital cost of starting a microgrid has been estimated to start from as low as $50, as compared to the average per connection costs of grid extension, which have been estimated at $500 [15].

2. **Empowering local population.** Furthermore, traditional national grids are largely a vertically integrated and regulated monopoly. On the other hand, rural microgrids

can be highly empowering to the local consumer population, not just in terms of the benefits of electricity itself, but in terms of local entrepreneurship opportunities. These microgrids also have the potential to improve gender equality through greater involvement of women in the value chain [16].

3. **Reliability of power supply.** In terms of reliability, microgrids can often perform better than ailing grids in urban and peri-urban areas of low- and middle-income countries. For example, private sector microgrids have reportedly observed 98% up-time in Tanzania as compared to the national grid's reported usable voltage range availability of 47% in Dar es Salaam [8].

4. **Integrating renewables.** In terms of generating power technology, microgrids are perfectly poised to utilize renewables, as opposed to grids. Since most of the microgrids are to be installed from scratch, opting for renewable sources of energy like solar PV is much more economical in both capital costs as well as fuel costs. This way, the route to achieving SDG 7 can be without adversely affecting the overall climate targets and hampering the progress towards other SDGs.

   Furthermore, while there are many renewable energy technologies available, solar PV is the most viable and widely suited, as there is abundant sunshine in the electricity-starved regions most of Asia and Africa, except for a few locations due to excessive rains. In comparison, other renewable energy sources like (micro-)hydroelectric power have to depend on site-specific resources like a perennial stream.

The efficacy of (rural) microgrids in electrification has been established beyond doubt. The undeniable potential, as well as the necessity of rural microgrids, has been mentioned in several studies on future scenarios. In one of its scenarios, the IEA estimates 140 million people in Africa to receive electricity access through mini-grids by 2040, necessitating the development of between 100,000 to 200,000 mini-grids [13].

### 2.3.4. Microgrids vs. standalone SHS

Figure 2.5 shows a comparative plot of the total installed capacity of off-grid solar energy sources for the years 2010 and 2016. A phenomenal growth in capacity can be seen for off-grid solar, underlining a positive trend and a momentum that is poised to continue. Figure 2.6 shows a similar statistic for the number of people gaining access to electricity through off-grid solar between 2010 and 2016. The remarkable fact is that despite a much smaller number proportion of people affected by the microgrids (nearly 124 million through standalone PV as compared to 2.2 million tier 1 and 2 level PV microgrid and 9 million including hybrid microgrids in 2016 [17]), the total installed capacity of PV microgrids is much more sizable at around 296 MW than SHS at around 215 MW and pico-solar at 58 MW, as seen in Figure 2.5. This can is attributed to the fact that the installed capacity of the microgrids, which are usually at a community scale, can be much higher than SHS and pico-solar, which are limited to the household level.

Compared to standalone systems like SHS, microgrids offer multiple advantages, as discussed below.

**2**
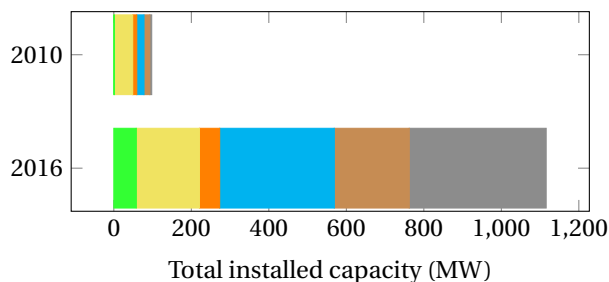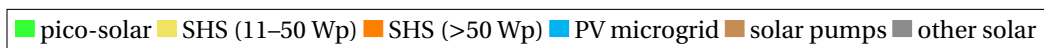


Figure 2.5: Capacity of different installed off-grid solar energy sources including SHS, pico-solar, solar PV minigrids, solar pumps, and other uncategorized off-grid solar PV applications (data from [17]).
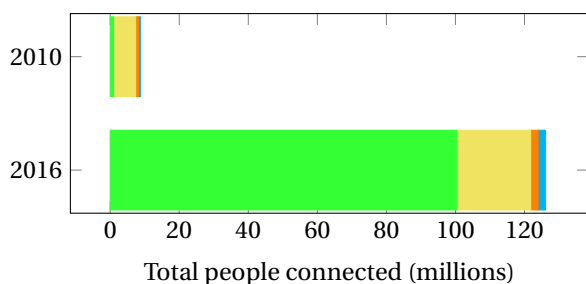


Figure 2.6: Number of people with improved electricity access to off-grid solar energy sources including SHS, pico-solar and solar PV minigrids (data from [17]).

1. **High power loads.** Higher installed power capacity of the microgrids by definition allows for higher power loads. Thus, people can potentially enjoy higher tiers of electricity access, as opposed to smaller standalone systems like SHS or pico-solar products, which often tend to keep the consumers locked in with respect to the choice of appliances.

2. **Load variance.** Higher load variance can be achieved through microgrids as multiple households are connected [18]. This leads to the added benefit of better utilization of the installed resources like PV and battery, provided the given levels of load consumption are commensurate with the installed power capacity.

3. **Productive use of energy (PUE).** Productive use of energy implies the use of energy for supplementing income generating activities [19]. Usually, PUE appliances like power tools, pumps, etc. are of higher power rating than basic consumptive household appliances like fans, TV, and a small fridge [20]. These are better supported by

microgrids than SHS. More on PUE is discussed in Section 3.1.2.

4. **Community buildings and loads.** Microgrids are also suited for community buildings like schools and hospitals, where a single SHS will not suffice. Additionally, community level loads can be met by microgrids more easily than SHS.

5. **Cheaper unit system costs.** Compared to SHS, microgrids can fundamentally attain cheaper unit system costs due to economies of scale. However, the overall system cost can pose a significant challenge in the beginning.

### 2.3.5. Disadvantages of centralized microgrids

Microgrids also come with a distinct set of disadvantages that are holding back this electrification pathway from achieving its full potential. These demerits are described below.

1. **High capital expenditures(CAPEX).** High CAPEX costs are a major barrier leading to slow uptake of microgrids for electrification. Unlike biomass plants, which have low CAPEX and high operational expenditures (OPEX), PV microgrids have high CAPEX and low OPEX. High CAPEX can be an impediment, especially if the microgrid is operating on a private or community-owned model, as opposed to a utility-owned model.

2. **Arrival of the national grid.** The arrival of the national grid has complicated consequences. On the one hand, the advent of the grid could be a perfect ending to a microgrid story as the microgrid could (potentially) seamlessly integrate with the grid. On the other hand, it could also bring about technical as well as financial consequences. As a thumb rule, grid tariffs are usually lower than microgrid tariffs due to cross-subsidization as well as economies of scale [9]. Additionally, certain technical standards need to be met before a microgrid could connect with the main grid, e.g., voltage and frequency regulation, and islanding capabilities. Microgrids can turn into stranded assets if the arrival of the grid is not planned for. Regulatory frameworks need to exist from the start if the integration of microgrids with the national grid is desired.

3. **Need for demand threshold.** Similar to national grids, albeit, at a lower level, microgrids need a certain demand threshold to justify their initial investment.

4. **Operational involvement with consumers.** Although the OPEX costs are relatively low in PV microgrids, high operational involvement is needed from the microgrid operators in terms of interaction with hundreds or thousands of households for revenue collection. This part is unique to rural microgrids, as opposed to large solar farms where the plant developers have minimal operational involvement. The participation of well-established players has therefore been negligible in terms of rural microgrids as opposed to smaller private entities.

5. **Overall demand estimation.** The peak power rating for the central installation is hinged on the demand estimation of (usually) hitherto un(der-)electrified community. In some cases, the installation might even be oversized to account for the

**2**

future demand of the microgrid. Lower than expected consumption patterns could lead to a risk of inadequate revenues, while higher than expected consumption could lead to potential blackouts.

## 2.4. Pathway 3: Solar-based standalone systems

This electrification pathway includes solar-based standalone systems like pico-solar (solar lanterns) and SHS. As discussed in Chapter 1, SHS are standalone PV systems rated 11 Wp and above, usually not more than 350 Wp and mostly less than 100 Wp. Solar lanterns or pico-solar products are defined to have rated PV power of less than 11 Wp [21]. Sometimes, further categorization of SHS and pico-solar exists, based on either wattage (for SHS), like 11–21 Wp, 21–50 Wp, 50–100 Wp, and > 100 Wp, or based on services provided (for pico-solar), like single light, single light + mobile charging, multiple lights + mobile charging [22]. In any case, it is expected that pico-solar products can enable tier 1 access, while SHS can enable at least tier 2 access.



(a) A solar LED lantern (d.light S30) with 0.3 Wp solar module and integrated 60 lm LED [23]

(b) A solar home system (d.light X850) with a 40 Wp panel and DC appliances [24]

Figure 2.7: Examples of a pico-solar product (solar lantern) and an SHS from the company d.light. Images obtained from [21].

Figure 2.7 shows examples of pico-solar and SHS products currently being used in the off-grid market, helping to accelerate (decentralized) electrification. Figure 2.8 shows a symbolic representation of SHS in a household along with a schematic block diagram representation. The SHS consists of a PV module, a suitably sized battery, power electronics for power conversion, and a set of DC loads.

Since pico-solar is limited to tier 1 access only, SHS is a more viable alternative for decentralized electrification, and therefore, discussed in greater detail in the following sections. Installation of SHS has improved the lives of off-grid consumers in multiple ways, e.g., creating job opportunities, enhancing business revenue, unlocking additional work hours, and increasing monthly income, among others [25].

### 2.4.1. SHS vs. grid and microgrids

Present day SHS enjoys several advantages as the pathway of choice in accelerating towards last-mile electrification targets. Some of these advantages are discussed below.

(a) SHS symbol

(b) Block diagram of an SHS
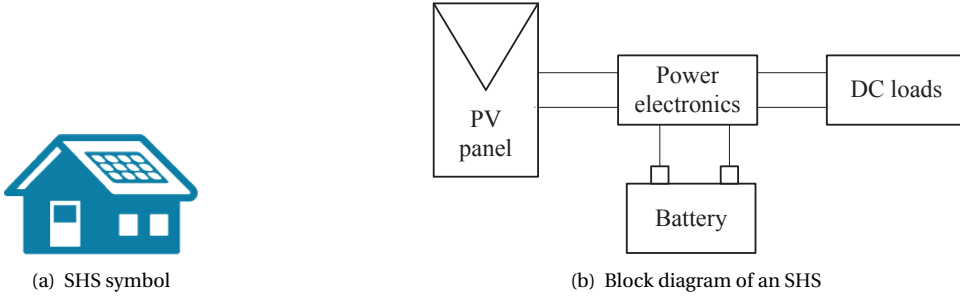
Figure 2.8: Symbolic and block diagram representations of an SHS.

1. **Least cost option.** Even though SHS score poorly in terms of LCOE ($/kWh) or unit system costs ($/Wp), they are by definition able to offer least total system costs by catering to a single household, as opposed to centralized microgrids and grids, which need to attain a certain scale of consumers to justify lower costs. SHS are an economically more appealing choice when facing conditions like long distances from the grid, low density of population, and low electricity demands. Of course, the affordability of the user depends largely on the target regions and specific financing mechanisms available, which is a different topic altogether, and not within the purview of this dissertation.

2. **Last mile connectivity.** Historically, grid-based electricity has taken the longest to reach the remotest corners of a country. In terms of last mile connectivity, while rural microgrids perform better than national grids, SHS perform even better than microgrids as the electricity demand threshold is the lowest for SHS. Often, governments themselves subsidize the uptake of SHS to augment the national electrification efforts.

3. **Use of DC appliances.** Many SHS providers are opting for a full DC system to save on conversion losses. BBOXX, a company active in East Africa, supplies its SHS consumers with its in-house portfolio of DC appliances. In Cambodia, the use of AC appliances and inverters is discouraged, and end users are also advised to use efficient DC appliances with their SHS [26]. These so-called super-efficient DC appliances can significantly reduce the strain on SHS size for delivering the same amount of electricity, thereby shifting the total cost distribution of an SHS along with resulting in cost savings [27, 2]. Additionally, the extent of the increasingly efficient DC options available in the market today, as catalogued extensively in [28, 19], proves further the impetus that DC-based SHS enjoy going forward. More on these efficient appliances can be found in Chapter 3.

4. **Better service through technology.** The use of technology like data acquisition and remote monitoring can significantly impact consumer satisfaction and uptake, which is otherwise a usual pain-point for SHS. Internet of things (IoT) is increasingly being used for implementing smart SHS to facilitate easy data acquisition and

analysis. For example, BBOXX, an SHS company operational in Rwanda, utilized its SMART Solar platform in nearly 20000 SHS to better understand the user needs, enabling them to create scalable business models for energy access [29]. This leads to not just better user insights but also faster service and higher SHS user satisfaction.

5. **Rapid growth and adoption.** Scaling up is often easier for SHS as opposed to microgrids, because microgrids are often a customized solution from one installation to another. On the other hand, an SHS (from the same manufacturer) for a given size can be produced over and over given the product demand. This has enabled rapid growth and adoption of SHS. As seen in Figure 2.6, between 2010 and 2016, the number of people gaining electricity access through SHS went from 7.2 to 23.5 million people [17]. As of 2017, off-grid solar solutions have provided improved energy access to 73 million households [21].

## 2.5. Present issues with SHS-based electrification

The most directly significant barrier that prevents widespread adoption of SHS is the unit system cost. Technologically, this can be most directly addressed only in the form of declining component costs. From a business point of view, it comes down to innovative business models tailored to suit the target region and community. From a policy point of view, subsidies could also play a role. These considerations are outside the scope of the work discussed in this dissertation. However, even if the adoption of present SHS were to scale to a billion units radically, there are still two major drawbacks that will hold back existing SHS from being the perfect pathway towards universal electrification. These issues are discussed in this section.

### 2.5.1. Climbing the electrification ladder

Owing to its standalone nature, SHS is dimensioned to cater to a particular level of load demand. Dimensioning or sizing is often a critical exercise; an oversized SHS leads to an expensive system leading to wastage of energy and unaffordability to a considerable portion of the target population, while an undersized SHS leads to insufficient power availability that may cause user dissatisfaction and lower technology adoption rates. Therefore, SHS need to be optimally sized for a given load demand [30]. However, as is clearly evidenced in literature and observed in the field, one of the consequences of providing access to electricity is the increase in electricity demand itself. That is, the demand for electricity often increases with time [31, 32, 27]. Therefore, in time (sometimes, in less than a year), the perfectly dimensioned SHS becomes obsolete and untenable to cater to the growing demands of the user. In other words, a particular SHS size is insufficient to enable the climb up the electrification ladder.

Figure 1.8 illustrated the concept of the electrification ladder. As a person or household moves up the electricity ladder, the quality and quantity of electricity demand increases, which can also be viewed as movement across the tiers in the context of the MTF. State-of-the-art SHS typically supply up to tier 2 level of electricity, and sometimes to tier 3. Even though a dedicated SHS for tier 3, 4 or 5 could be custom made, often it is not the best solution because: (i) it would be at the cost of discarding the previously perfectly

dimensioned lower tier SHS, as households seldom demand a direct tier 4 or 5 level access and usually climb up the electrification ladder (ii) at higher levels of electricity demand, the storage costs would significantly drive up the total system costs [30, 33].

In general, the level of electrification is often a dynamic requirement as the electricity needs increase with time. The current SHS-based electrification is largely inflexible to this requirement. Appliances for productive use of energy and communal loads, which are also usually commensurate with tiers 4 and 5 of electricity access, can also not be powered with typical state-of-the-art SHS power levels.

### 2.5.2. THE PARADOX OF SHS-BASED ELECTRIFICATION - WATT'S THE MATTER!

State-of-the-art SHS are usually limited to 100 Wp. This leads to a paradoxical predicament as shown in the conceptual illustration in Figure 2.9, which maps the appliance costs versus power rating space. The highlighted region represents the range of the typical SHS in terms of power delivery and the usual DC appliances used in such an SHS. These appliances are the so-called super-efficient DC appliances.
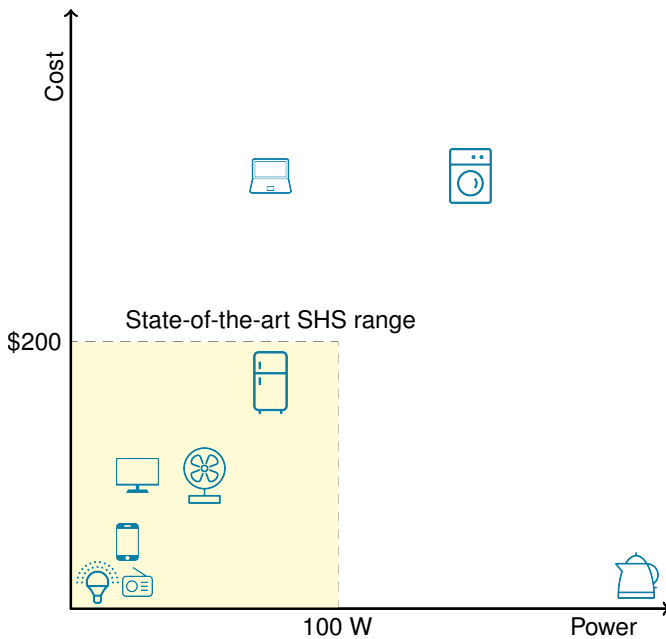


Figure 2.9: A concept graph illustrating the mapping between power rating of the various home appliances and their costs. Note: the price level is just an indicative number, as the prices differ greatly across vendors and geographies.

Horizon appliances like washing machines are definitely outside the scope of the present day SHS, both in terms of power and in terms of price, as denoted by the icon in the upper right corner in the graph. However, a 70 W laptop charger can be easily powered by a 100 Wp SHS, while the appliance (laptop) itself might be well outside the

range of typical appliances afforded by an SHS consumer. Ironically, some appliances like water kettles and rice cookers are already cheap enough (sub $5–10) for low-income communities to buy, but cannot be powered by the SHS due to the high-power rating of the appliances (e.g., a kW or more for the water kettle). In a Cambodian field study carried out as part of this PhD project in 2016, inadequate power level has already been noted as a shortcoming of the present SHS. The local users expressed interest in powering water kettles and rice cookers with their SHS. The field study was conducted to mainly find out the future needs of SHS users in rural Cambodia. Figure 2.10 shows photos from the fieldwork [27].



(a) Simulation game to engage the SHS users on their future electricity needs and appliance wishlist

(b) Visual representation to understand the expected times of the future appliance usage
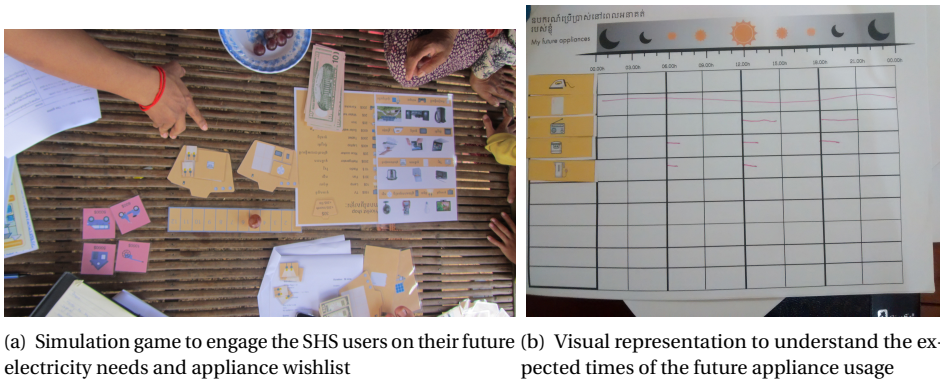
Figure 2.10: Photos from the fieldwork carried out in Cambodia as part of this PhD project [27]. Photo credit: Thomas den Heeten.

### SILVER LINING OR RISK OF STAGNANCY?

Considering the above two issues, therefore, the biggest criticism for SHS comes in the form of its impermanence as an electrification pathway. It has been often regarded as merely a short-term solution [34]. Despite the undeniable momentum in accelerating up to tier 2 level electricity access, SHS has been largely seen as a stopgap solution to provide lighting and some basic appliances until the advent of the national grid.

The deployment of SHS leads to the unlocking of the latent electricity demand of the consumers, thereby paving the way for the need for higher power solutions like microgrids and grid extension. On the one hand, the silver lining is that an increased demand might justify the installation of higher power systems like centralized microgrids and grid extension. On the other hand, the delays and other roadblocks associated with grid extension and microgrid installation might keep the consumers locked in at a certain tier of electricity access.

In general, from lighting a million to empowering a billion, solar home systems in their present form can only take us part of the way.

## **2.6.** **THE HOLY GRAIL OF UNIVERSAL ELECTRIFICATION**

Now that the three electrification pathways have been discussed in detail along with the challenges and opportunities they face, we can think of the ideal pathway for achieving universal electrification. In line with the scope of this dissertation, the focus is on off-grid solar-based electrification in this discussion.

Figure 2.11 shows the different electrification pathways mapped onto a plot of ease of electrification versus power level. Decentralized solutions like pico-solar and SHS perform much better on the ease of electrification, while the grid performs far better on the power levels. In other words, current electrification pathways present an inherent trade-off between the on-demand electrification versus on-demand power consumption. Centralized microgrids perform somewhat in the middle on both counts.
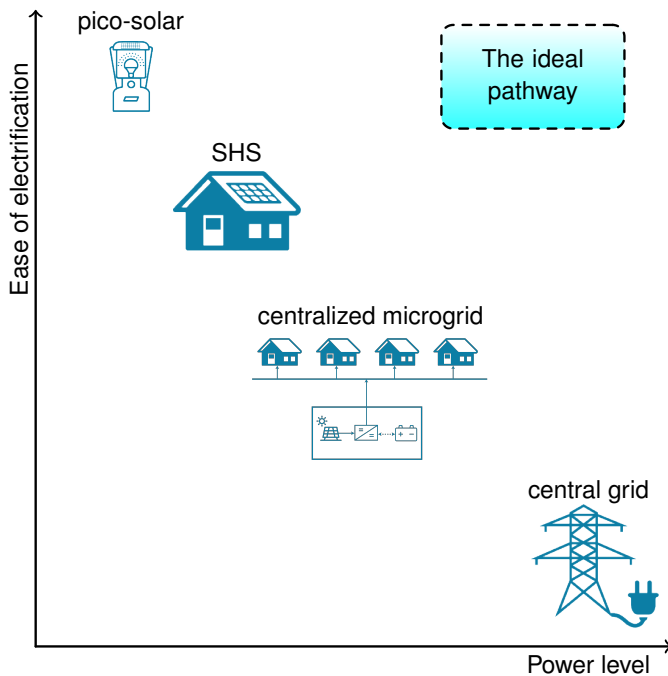


Figure 2.11: A concept graph illustrating the comparison between the different electrification pathways on a plot of the ease of electrification versus power demand.

The holy grail of universal electrification is represented in Figure 2.11 in the top right corner as the ideal electrification pathway that can provide rapid electrification while catering to on demand power consumption commensurate with higher tiers of electricity consumption. This solution has to be as easy for rapid adoption as SHS while addressing the current shortcomings plaguing SHS from becoming a truly sustainable electrification solution. The requirements from such an ideal off-grid solar solution that can overcome the issues mentioned in Section 2.5 can be listed as follows.

1. **Climbing up the electrification ladder.** The solution should be expandable to

cater to growing household needs as well as scalable to accommodate increasing numbers of the systems in the off-grid communities.

2. **High power appliances**. The solution should enable the use of high-power appliances.

3. **Retrofitting.** The solution should be able to work with other existing SHS.

4. **Future-ready.** The advent of the electricity grid in the future should preferably not render the present solution completely obsolete.

## 2.6.1. SHS-BASED MICROGRID: A MEANS TO GET THERE?

In the absence of fundamental technological breakthroughs that can radically affect component costs or choice of energy technology, an SHS-based microgrid can be a means to at least approach the ideal pathway. Figure 2.12 shows this concept, where a meshed DC grid can be created through the interconnection of existing SHS already operating on DC. Such a microgrid can grow in time, as opposed to a centralized microgrid that is relatively rigid with respect to initial system sizes.
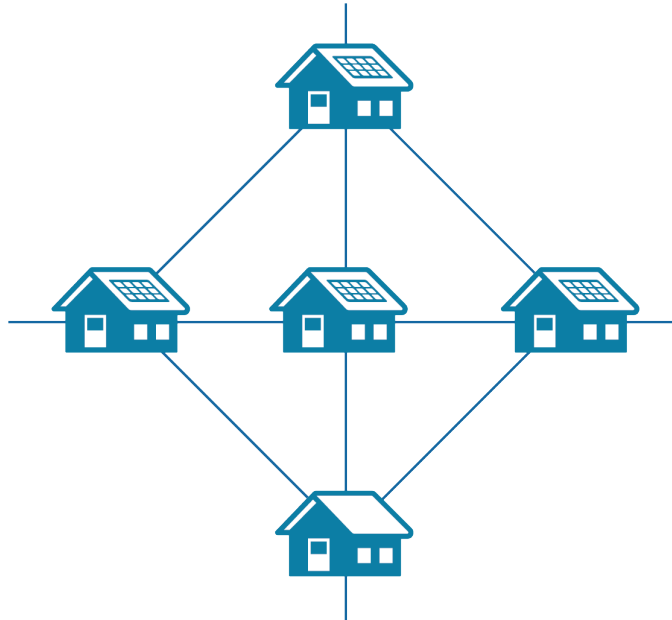


Figure 2.12: Concept illustration of a bottom-up, scalable, interconnected SHS-based meshed DC microgrid [18]. The bottom house is shown without any SHS, indicating the possibility of purely consumptive houses joining such a microgrid.

This concept has seen multiple proponents in recent literature [35, 36]. However, the existing projects in practice are mostly limited to tiers 1 to 2 with 12 V battery and 12 V distribution. In order to enable higher tiers of consumption, such microgrids need to make use of higher voltage distribution as it minimizes distribution losses [37]. The

quantification of benefits from these microgrids has been covered in Chapter 6 and in a recent publication [18].

Such bottom-up, organically growing microgrids that are born out of the interconnection of existing SHS can enable energy sharing. Additional advantages of such microgrids would include reduced system sizes as compared to standalone SHS and the capability to power appliances meant for productive use of energy. Furthermore, if and when the national grid does arrive, this microgrid can already serve as a ready distribution grid (otherwise, grid extensions are merely reduced to providing electricity to just the peripheries of villages, or the microgrids are left as stranded assets). Such bottom-up microgrids need to be an essential piece of the electrification puzzle, which not only complement other electrification technologies and efforts but also become a logical transition step from standalone systems like SHS. In this way, it also helps in preserving the sanctity of the SHS electrification pathway, which is already underway with remarkable momentum.

### ADVANTAGES OF AN SHS-BASED, DECENTRALIZED, BOTTOM-UP MICROGRID

Compared to standalone electrification, following can be summarized as the main advantages of an interconnected SHS-based microgrid [18].

1. **DC architecture.** Exploiting the DC nature of its interconnected building blocks (DC), this can grow as a meshed DC microgrid.

2. **Excess energy sharing.** Interconnecting SHS enables excess energy sharing between the households.

3. **Reduced system size.** A direct consequence of 2 is that the system sizes can be lower than the standalone case for meeting the same power availability requirement.

4. **Productive use of energy.** High power appliances enabling PUE can be easily supported in an interconnected SHS microgrid. Productive use of energy can supplement income-generating activities and therefore lead to a higher degree of ownership in the microgrid for the users.

5. **Climbing up the electrification ladder.** Climbing up the tiers of MTF will require much lower increments in energy storage per household as opposed to a standalone SHS climb up the tiers.

6. **Retrofitting and 'future-fitting'.** Interconnected SHS-based microgrid not only helps in reusing the existing SHS but also ensures that a DC distribution grid exists for the national grid expansion if and when it reaches the target region.

**Note:** This is only one possible solution and by no means the silver bullet for attaining universal electrification. Nonetheless, given the current state of off-grid electrification, the massive investments in the off-grid sector and the inevitable climb up the electrification ladder, this seems to be the most promising route to scale electrification.

## 2.6.2. Comparison of the various electrification pathways

Table 2.2 presents a qualitative comparison of the electrification pathways presented in
this chapter. The different aspects considered are in the context of universal electrification
only. As discussed before and seen in Table 2.2, each of the three present-day electrification pathways have relative merits and demerits, while the decentralized SHS-based
microgrids generally perform well across the different aspects of comparison. The scalability and adoption aspect deserves a special mention, as that is a particular pain-point
in addressing the urgency of accelerated electrification. SHS can potentially continue
with their current momentum in adoption, but the level of electricity access will still be
limited, as discussed in Section 2.5. Interconnected SHS-based microgrids, on the other
hand, can scale just as wide as SHS, but also grow in size due to interconnectivity.

Table 2.2: A qualitative comparison of the different electrification pathways on various aspects.

| Aspect | SHS | Centralized microgrids | Central grid | Decentralized SHS-based DC microgrids |
|---|---|---|---|---|
| MTF tiers | Tier 2–3 | Tiers 1–5 (fixed) | Tiers 1–5 | Tiers 1–5, flexible |
| Implementation ease | Very high | Medium | Low | High |
| Scaling the electrification ladder | Very low | Low | High | High |
| AC/DC | DC | AC, DC, hybrid | AC | DC |
| Community loads/PUE | No | Yes if planned | Yes | Yes, depends on the microgrid size |
| Scalability & adoption | Very high | Limited | Limited | High |

### Decentralized paradigm: History repeats, but time to leapfrog into the future

The dawn of the electrical era, in fact, saw decentralized generation plants, together with
batteries supplying electricity via DC grids to nearby areas [38]. Then came along the AC
generation and distribution system, with its technological advances at the time, and the
centralized electrification paradigm, which is still a mainstay of the electricity networks
around the world. However, when it comes to the 21st-century goals of electrification with
its contemporary opportunities and unique challenges, we have distinct technological
advantages with decentralized DC electrification.

From power electronics to decentralized solar PV generation and battery storage to
super-efficient DC appliances, the advances in technology can allow us to leapfrog towards a cleaner, sustainable electricity network based on DC when considering the daunting task of universal electrification. Additionally, accelerating towards off-electrification
allows to leapfrog towards a bottom-up and decentralized electricity network paradigm.
The time is opportune to make significant strides in electrification targets and 'power'
through towards SDG 7. Therefore, bottom-up, decentralized DC microgrid based on
interconnected SHS is not just an alternative to consider but also a logical choice.

## 2.7. CHALLENGES FOR THE SHS-BASED ELECTRIFICATION VISION

The vision of SHS-based electrification described in Section 2.6.1 requires a few technical challenges to be solved first for SHS design at the lower tiers of electrification before thinking of the integration of SHS into a microgrid network for higher tiers of electrification. This necessitates following challenges to be tackled, as also described in Section 1.2.

**Knowledge of the load profiles** Load profile is the basic first step needed when thinking of optimally designing an off-grid system while reducing costs and maximizing power availability. Therefore, for an off-grid system like SHS, a better knowledge of the expected load profiles can lead to better system design. Conversely, a poor knowledge of the expected load profile can lead to oversizing of the system, leading to increased system costs, or undersizing of the system, leading to unacceptable power availability. However, load profiles are a scarce commodity for system designers in the context of electrification, especially when dealing with hitherto un(der-)electrified target regions.

**Battery lifetime estimation** Battery is a vital system component in an SHS owing to its relatively low lifetime with high costs amongst all SHS components. Along with intial investment or upfront costs, battery costs recur in the form of replacements during the SHS lifetime. As battery lifetime also depends on battery size, a reasonable estimate of battery lifetime at the SHS design stage can equip the system designer to balance the upfront and replacement costs based on the specific project application. However, battery lifetime needs to be estimated at the SHS design stage taking into account the expected battery cycling for a given level of electricity demand.

**Optimal system sizing** Given a particular load profile or electricity demand, an optimal system size will maximize the power supply availability, maximize the battery lifetime, while minimizing the total system upfront costs and excess power production. This turns into a multi-objective optimization problem. Therefore, the challenges related to knowledge of load profiles, battery lifetime estimation at the SHS design stage, and optimal SHS sizing would be tackled first in Chapters 3, 4, and 5, respectively. Consequently, the benefits for going towards a decentralized DC microgrid based on SHS interconnection are explored in Chapter 6. Optimal microgrid topologies are investigated in Chapter 7 using a geographic information system (GIS)-based approach.

## 2.8. CONCLUSION

The 3 different pathways for electrification, viz., grid extension, centralized microgrids, and standalone solar-based solutions like SHS, each come with their own set of limitations. SHS have been a promising solution so far in achieving up to tier 2 level electrification. However, in its current state, SHS can only light the way but is far from being the electrifying solution to achieve universal electrification. While decentralized solutions like pico-solar and SHS can provide on-demand electrification, the central grid can provide higher levels of power commensurate with tier 4 and tier 5. For climbing up the electrifica-

tion ladder and enabling the use of high power appliances, an interconnected SHS-based DC microgrid can overcome many of the limitations of SHS as well as centralized micro-grids. Such a bottom-up microgrid could well be the missing link between the present electrification pathways, forming an integral part of the universal electrification jigsaw.

**2**

## REFERENCES

[1] International Energy Agency, *World Energy Outlook 2018.* IEA, 2018.

[2] International Energy Agency, *Energy Access Outlook 2017 - from poverty to prosperity.* IEA, 2017.

[3] UN, "The Sustainable Development Goals Report," tech. rep., United Nations, 2018.

[4] B. Tenenbaum, C. Greacen, T. Siyambalapitiya, and J. Knuckles, *From the bottom up: how small power producers and mini-grids can deliver electrification and renewable energy in Africa.* World Bank Publications, 2014.

[5] M. Bhatia and N. Angelou, *Beyond Connection, Energy Access Redefined.* The World Bank, 2015.

[6] IRENA, "Off-grid renewable energy solutions to expand electricity access: An opportunity not to be missed," *International Renewable Energy Agency, Tech. Rep.*, 2019.

[7] H. Louie, *Off-grid electrical systems in developing countries.* Springer, 2018.

[8] Gabriel Davies, Matt Tilleard and Lucy Shaw, "Private mini-grid firms deserve a chance to compete against slow utilities in africa." `https://www.greentechmedia.com/articles/read/a-faster-path-to-rural-electrification#gs.4p99x3`. Accessed: 2017-05-19.

[9] M. Franz, N. Peterschmidt, M. Rohrer, and B. Kondev, "Mini-grid policy toolkit," *EUEI-PDF, ARE and REN21, Tech. Rep.*, 2014.

[10] IEG, *World Bank Group Support to Electricity Access, FY2000–FY2014.* World Bank Group, 2014.

[11] G. Manchanda, "Augmenting the diffusion of solar home systems for rural electrification — An Indian perspective," Master's thesis, Delft University of Technology, the Netherlands, 2017.

[12] T. Levin and V. M. Thomas, "Can developing countries leapfrog the centralized electrification paradigm?," *Energy for Sustainable Development*, vol. 31, pp. 97–107, 2016.

[13] IEA, *Africa Energy Outlook - A focus on energy prospects in sub-Saharan Africa.* Organization for Economic Cooperation and Development, International Energy Agency, 2014.

[14] NREL, "Microgrids." `https://www.nrel.gov/grid/microgrids.html`. Accessed: 2018-10-13.

[15] S. Buluswar, Z. Friedman, P. Mehta, S. Mitra, and R. Sathre, *50 Breakthroughs - Critical scientific and technological advances needed for sustainable global development.* LIGTT, Institute for Globally Transformative Technologies, Lawrence Berkeley National Lab, 2014.

[16] IBRD | The World Bank Group, *Mini-Grids and Gender Equality : Inclusive Design, Better Development Outcomes.* World Bank Group, ESMAP and Climate Investment Funds, 2017.

[17] IRENA, "Measurement and estimation of off-grid solar, hydro and biogas energy," *International Renewable Energy Agency, Tech. Rep.*, 2018.

[18] N. Narayan, A. Chamseddine, V. Vega-Garita, Z. Qin, J. Popovic-Gerber, P. Bauer, and M. Zeman, "Quantifying the benefits of a solar home system-based dc microgrid for rural electrification," *Energies*, vol. 12, no. 5, 2019.

[19] H. Olk and J. Mundt, "Photovoltaics for Productive Use Applications. A catalogue of DC-Appliances," *Deutsche Gesellschaft für Internationale Zusammenarbeit (GIZ) GmbH*, 2016.

[20] N. Narayan, Z. Qin, J. Popovic-Gerber, J.-C. Diehl, P. Bauer, and M. Zeman, "Stochastic load profile construction for the multi-tier framework for household electricity access using off-grid dc appliances," *Energy Efficiency*, Nov 2018.

[21] Lighting Global and Dalberg Advisors, "Off-grid solar market trends report," tech. rep., Lighting Global, Dalberg Advisors, GOGLA, ESMAP, 2018.

[22] Global Off-Grid Lighting Association, "Global off-grid solar market report - semi-annual sales and impact data," tech. rep., GOGLA, Lighting Global and Berenschot, 2018.

[23] d.light, "S30 Solar LED Lantern." `https://www.dlight.com/product/s30/`. Accessed: 2017-08-12.

[24] d.light, "X850 Solar Home System." `https://www.dlight.com/product/x850/`. Accessed: 2017-08-12.

[25] GOGLA, "Powering Opportunity — The Economic Impact of Off-Grid Solar," *Global Off-Grid Lighting Association (GOGLA) and Altai Consulting*, 2018.

[26] Good Solar Initiative, *Quality Charter: Technical and Service Quality Standards for Accredited Solar Suppliers.* SNV Netherlands Development Organisation, 2016.

[27] T. D. Heeten, N. Narayan, J. C. Diehl, J. Verschelling, S. Silvester, J. Popovic-Gerber, P. Bauer, and M. Zeman, "Understanding the present and the future electricity needs: Consequences for design of future solar home systems for off-grid rural electrification," in *2017 International Conference on the Domestic Use of Energy (DUE)*, pp. 8–15, April 2017.

**2**

[28] Lighting Global, Bloomberg New Energy Finance and GOGLA, "Off-grid solar market trends report 2016," *Bloomberg New Energy Finance and Lighting Global in cooperation with the Global Off-Grid Lighting Association (GOGLA)*, 2016.

[29] I. Bisaga, N. Puźniak-Holford, A. Grealish, C. Baker-Brian, and P. Parikh, "Scalable off-grid energy services enabled by iot: A case study of bboxx smart solar," *Energy Policy*, vol. 109, pp. 199–207, 2017.

[30] N. Narayan, T. Papakosta, V. Vega-Garita, Z. Qin, J. Popovic-Gerber, P. Bauer, and M. Zeman, "Estimating battery lifetimes in solar home system design using a practical modelling methodology," *Applied Energy*, vol. 228, pp. 1629 – 1639, 2018.

[31] M. Gustavsson, "With time comes increased loads: An analysis of solar home system use in lundazi, zambia," *Renewable Energy*, vol. 32, no. 5, pp. 796–813, 2007.

[32] F. Benavente, A. Lundblad, P. E. Campana, Y. Zhang, S. Cabrera, and G. Lindbergh, "Photovoltaic/battery system sizing for rural electrification in bolivia: Considering the suppressed demand effect," *Applied energy*, vol. 235, pp. 519–528, 2019.

[33] N. Narayan, A. Chamseddine, V. Vega-Garita, Z. Qin, J. Popovic-Gerber, P. Bauer, and M. Zeman, "Exploring the boundaries of solar home systems (shs) for off-grid electrification: Optimal shs sizing for the multi-tier framework for household electricity access," *Applied Energy*, vol. 240, pp. 907 – 917, 2019.

[34] D. Chattopadhyay, M. Bazilian, and P. Lilienthal, "More power, less cost: transitioning up the solar energy ladder from home systems to mini-grids," *The Electricity Journal*, vol. 28, no. 3, pp. 41–50, 2015.

[35] B. Soltowski, S. Strachan, O. Anaya-Lara, D. Frame, and M. Dolan, "Using smart power management control to maximize energy utilization and reliability within a microgrid of interconnected solar home systems," in *7th Annual IEEE Global Humanitarian Technologies Conference, GHTC 2017*, pp. 1–7, 2017.

[36] S. Groh, D. Philipp, B. E. Lasch, and H. Kirchhoff, "Swarm electrification: Investigating a paradigm shift through the building of microgrids bottom-up," in *Decentralized Solutions for Developing Economies*, pp. 3–22, Springer, 2015.

[37] M. Nasir, H. A. Khan, N. A. Zaffar, J. C. Vasquez, and J. M. Guerrero, "Scalable solar dc micrigrids: On the path to revolutionizing the electrification architecture of developing communities," *IEEE Electrification Magazine*, vol. 6, no. 4, pp. 63–72, 2018.

[38] S. Mandelli, J. Barbieri, R. Mereu, and E. Colombo, "Off-grid systems for rural electrification in developing countries: Definitions, classification and a comprehensive literature review," *Renewable and Sustainable Energy Reviews*, vol. 58, pp. 1621–1646, 2016.

# 3

# LOAD PROFILE CONSTRUCTION

*If knowledge can create problems, it is not through ignorance that we can solve them*

Isaac Asimov

## ABSTRACT

To improve access to electricity, decentralized, solar-based off-grid solutions like Solar Home Systems (SHS) and rural microgrids have recently seen a prolific growth, as discussed in Chapter 2. However, electrical load profiles for these systems, usually the first step in determining the electrical sizing of off-grid energy systems, are often non-existent or unreliable, especially when looking at the hitherto un(der)-electrified communities. This chapter aims to construct load profiles at the household level for each tier of electricity access as set forth by the Multi-tier Framework (MTF) for measuring household electricity access. The loads comprise dedicated off-grid appliances, including the so-called super-efficient ones that are increasingly being used by SHS, reflecting the off-grid appliance market's remarkable evolution in terms of efficiency and price. This study culminated in devising a stochastic, bottom-up load profile construction methodology with sample load profiles constructed for each tier of the MTF. The methodology exhibits several advantages like scalability and adaptability for specific regions and communities based on community-specific measured or desired electricity usage data. The resulting load profiles for different tiers shed significant light on the technical design directions that current and future off-grid systems must take to satisfy the growing energy demands of the un(der)-electrified regions. Finally, a constructed load profile was also compared with a measured load profile from an SHS active in the field in Rwanda, demonstrating the usability of the methodology.

**OUTLINE**

This chapter contains 5 sections. Section 3.1 introduces the requirement of load profiles within off-grid systems and the development in super-efficient DC appliances for off-grid electrification. Sections 3.2 discusses the literature review and the relevant load profile parameters. Section 3.3 describes the methodology used to construct the load profiles. Section 3.4 discusses the results and also presents a comparison of the constructed tier 1 load profile with SHS load data obtained from the field in Rwanda. Finally, Section 3.5 concludes the chapter with additional recommendations related to load profile construction.

## 3.1. INTRODUCTION

### 3.1.1. MULTI-TIER FRAMEWORK FOR HOUSEHOLD ELECTRICITY ACCESS

Section 2.1.1 already introduced the concept of the MTF. The central idea behind the MTF is to view electrification in terms of the quality and quantity of the energy services supplied to the user. The underlying premise is that different energy service attributes, as listed in Table 2.1, define the electricity usage that satisfies the various human needs. Human needs broadly encompass the following categories: (a) lighting, (b) entertainment and communication, (c) food preservation, (d) mechanical loads and labor-saving, (e) cooking and water heating, (f) space cooling and heating [1]. The household level energy use is bound to be increasing with time as more households rise out of (energy) poverty [2]. Moving up the tiers makes more and better quality energy services available that could satisfy more of these human needs. The notion of this tier-based framework is independent of the type of technology that enables the electrification. However, as discussed in Chapters 1 and 2, the focus of the energy technology is confined to SHS in this dissertation.

### 3.1.2. OFF-GRID APPLIANCES

Since the dawn of electricity, the electricity appliance market has always been under a constant state of evolution. However, until recently, most major advents of electrical appliances and devices in the developing world have largely been on the heels of their success in the developed world. Examples include mobile phones and LED lights. This trend has now been broken, and a number of dedicated, so-called super-efficient off-grid appliances are being designed specifically for the off-grid markets [4, 5]. Examples include electric fans, TVs [6], and refrigerators, all of which can work easily with off-grid PV on DC as well as consume just a fraction of the energy costs of the traditional, mainstream counterparts. Moreover, high quality off-grid products tailor-made for the low-income markets combined with innovative business models and falling component costs have enabled the rapid market growth.

Envisioning universal electricity access by 2030 would require the support of off-grid, standalone systems as well. The use of super-efficient appliances will greatly help in this regard, as seen in Figure 3.1. The higher cost of bundling super-efficient appliances is more than compensated by the lower cost of the PV and battery due to reduced system size needed to deliver the same energy services. In this particular example, an average annual cost reduction of 32% can be achieved [3]. In general, coupling super-efficient
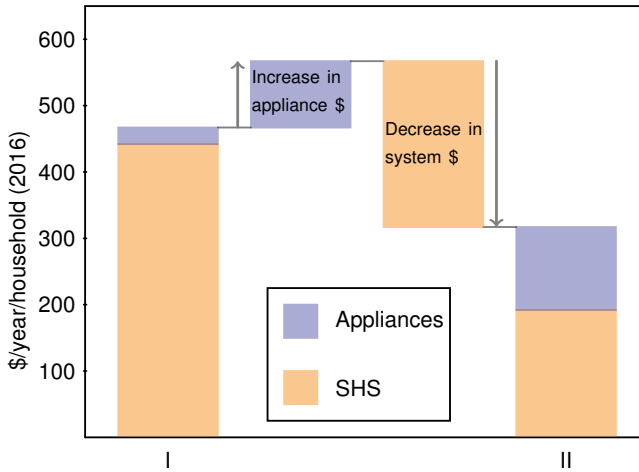
Figure 3.1: Impact of using super-efficient appliances in overall system costs. Assuming universal electricity access by 2030, annual average cost per household powered by SHS and using four light bulbs, a television, a fan, a mobile phone charger and a refrigerator. I: SHS with standard appliances; II: SHS with super-efficient appliances. Use of super-efficient appliances leads to an overall decrease in total costs. Adapted from [3].

devices has been seen as a means to delivering the same, if not better energy services at lower costs, while also increasing the momentum of the energy access efforts [7].

Moreover, many of these appliances can be used for their productive use of energy, i.e., using the appliances for improving the productivity and supplementing income [8]. Productive use of energy (PUE) is different from the usual, consumptive use of energy, in that the productive use is labor-saving and supplements the income generation capabilities of the user. Some examples are in small enterprises (sewing machines, power drills) and farming (solar pumps). The biggest advantage of PUE comes in the form of benefits towards both poverty reduction as well as stability and viability of energy supply, due to increased ability to pay for the energy services, and less reliance on subsidies [9]. However, not all dedicated off-grid appliances available today can be classified in the super-efficient category. For instance, washing machines and air coolers still have a long way to go in terms of efficiency improvements.

It is interesting to note that super-efficient appliances are also being promoted from the policy side by governments, and are not necessarily limited to the off-grid sector. For example, by providing production subsidies to appliance manufacturers, the Super Efficient Equipment Program (SEEP) aims at reducing energy consumption in Indian households [10]. International collaborative programs like CLASP are also working towards improving energy efficient appliances.

### 3.1.3. IMPORTANCE OF LOAD PROFILES

A load profile can be defined as the power demand of an energy system mapped over time. A load profile not only captures the energy demand of the user but also serves as a vital input to the electrical system design. Especially in the case of off-grid power systems like

the SHS, reliable apriori knowledge of the load profile is extremely helpful in the electrical sizing the system (i.e., deciding the PV rating and the battery capacity).

In fact, load profile, even if coarsely estimated, is almost always the starting point in an off-grid, standalone PV system design [11]. Load profiles can have a profound impact on the performance as well as design decisions in off-grid systems [12]. A better knowledge of load profile makes for a more optimal off-grid electrical system design. Conversely, the lack of an appropriate load profile leads to either oversizing or undersizing the system, thereby causing an unhealthy trade-off between system costs and power availability [13].

An over-utilization will result in frequently empty batteries and loss-of-load events. Particularly in the context of first-time SHS users, this may result in loss of faith and trust in solar-based electrification, as was experienced during the fieldwork done in rural Cambodia related to the work reported in [13]. On the other hand, under-utilization would have a detrimental financial impact. This is because the user would pay more for effectively utilizing only a fraction of the power generation potential of the system. In terms of the levelized cost of electricity (LCOE), a grossly underutilized system would result in a high LCOE. In a market segment where purchase power, cost price, and profit margins are sensitive parameters, a high LCOE is definitely unattractive, whether or not there are subsidies in play.

### 3.1.4. NEED FOR LOAD PROFILE CONSTRUCTION
The following points necessitate the requirement for load profile construction.

- **Difficult to estimate** It is tough to estimate the energy consumption behaviour in off-grid communities if the electricity access has hitherto been limited.

- **Starting point** The load profile is the starting point in off-grid system design. In the absence of existing load profiles, as is the case with most off-grid locations, reliable load profile construction is crucial.

- **Growth enabling** Load profile construction for not just the present but an estimated future usage would benefit the off-grid system designers to enable the growth of the energy consumption in their off-grid systems.

### 3.1.5. HIGHLIGHTS
For the goal of achieving an optimal SHS design, the work described in this chapter endeavours to construct load profiles by mapping the energy usage for various tiers of electricity access. While multiple studies in the past have discussed load profile construction (as discussed in Section 3.2.1), this chapter focuses specifically on stochastic load profile construction for the various tiers of the MTF for electricity access. Following are the main highlights of this chapter.

1. A fully adaptable, scalable, and bottom-up load profile construction methodology is presented, which can be customized for different regions and user groups.

2. The constructed load profiles include the latest trends in dedicated off-grid appliances for each tier of the MTF for household electricity access.

3. Off-grid appliances for productive use of energy are included while constructing the load profiles.

4. The stochastic load profile construction model is validated through a comparison with a measured one from an active SHS in the field.

5. The impact of load profiles on off-grid system design is discussed.

## 3.2. BACKGROUND

This section discusses a brief literature review on the existing load profile construction methodologies, and details the load profile parameters and the types of off-grid electrical appliances considered in this study.

### 3.2.1. LITERATURE REVIEW

Load profile construction can be a complex task for the rural off-grid scenario. The electrical consumption of the target users is often increasing with time, as the process of electrification itself contributes to greater energy needs because of improvement in living standards [14]. It is therefore important for rural off-grid initiatives to enable communities to move beyond basic lighting and phone charging [15].

However, the complex causality of electricity access with socio-economic development significantly impacts energy modelling approaches, while most electrification impact assessments estimate a linear growth in electricity demand [16]. Limited knowledge of electricity demand can negatively impact off-grid system dimensioning. Similarly, it has been noted that most studies do not assume a dynamic demand over the years, and do not consider the evolution of the future load demand, which severely undermines long-term planning [17]. As seen in [17], 74.4% of energy demand forecasting approaches adopted in the reported case studies consider no evolution in the energy demand.

Fortunately, thanks to its multi-layered approach, the MTF for household electricity access can be instrumental in overcoming some of these problems. The tier-based electrification makes it easier to categorically cater to different tiers of energy usages. Additionally, while the jump from, say, tier 1 to tier 2 might happen quickly for certain households, it would still take much longer to reach tier 4 or 5. Using MTF as a categorical sieve for modelling energy demand and consequently designing electrical systems still makes a better case for the future than assuming a fixed demand. Moreover, use of interviews and surveys can be used additionally to complement and calibrate the load profiles based on the MTF, thereby making them more robust as well as customized to local contexts.

In the case of rural (off-grid) electrification projects, use of only interviews to model the energy demand may not be the best way forward. Currently, energy demand estimation is often carried out solely through interviews and surveys due to lack of historical data. However, research-surveys for predicting electricity consumptions can be error-prone. As high as 426 Wh/day per consumer of mean absolute error has been observed over a study of eight rural mini-grids in Kenya [18]. In [19], the load profiles are compared in a minigrid from interviews as well as measured data, concluding that purely interview-based data falls short in accurately estimating energy needs. Therefore, interviews, when used

as the only tool, need not be the best indicators of actual load consumption, especially if delicate system design and sizing is going to be based on the load profiles constructed from interview data. However, a stochastic load profile construction approach can gain greatly from interview data in terms of calibration and limits.

Existing energy modelling methods have in general been investigated by [20] in the context of developing economies. Econometric (macro-scale) and end-use are the two most common approaches being used, with the latter able to produce more realistic projections. Given the task of estimating household energy demand and constructing load profiles for the same, modelling end-use consumption is more suited. In [21], two main approaches in modelling user data and generating load profiles are identified, viz., top-down and bottom-up approaches.

Top-down approaches work on aggregate data, which does not distinguish energy consumption due to individual users. Pattern recognition and clustering methods to generate load profiles as well as for short/mid-term load forecasting are used in [22]. However, this is oblivious to appliance level data. Similarly, clustering-based methodologies are used to peruse large datasets and construct 'new' load profiles based on the existing data in [23] and [24]. Load aggregation and sampling times of measured data to determine optimal sampling times and aggregation levels are discussed in [25].

Based on the top-down approach, these models lack appliance level data and are not specifically suitable for off-grid applications. Reliance on historical aggregate data is a drawback of these models, as they are intrinsically incapable of modelling technological advances that are discontinuous in nature [21]. Therefore, top-down approach is deemed inadequate to be used for modelling the energy consumption in the form of load profiles for the purpose of electrification of remote, off-grid households that are hitherto un(der)-electrified, while also taking into account the latest developments in dedicated off-grid appliances.

On the other hand, bottom-up approaches work with individual users, and often even with appliance level data. Bottom-up approaches can be classified as Statistical Methods (SMs) or Engineering Methods (EMs). While SMs use regression analysis or artificial neural networks to estimate end-user energy consumptions, and use historical data, EMs account for energy consumption at individual user levels on the basis of power ratings and use of equipment [21]. These do not necessarily rely on historical or measured data, but measured data can be used for calibration. To construct load profiles while incorporating the off-grid appliances, only the EM methods can be used. Moreover, as one goes to a smaller scale, like a household level, load profiles need to be more appliance oriented than what the top-down approaches can offer. This is because demand and supply needs to be optimally matched in planning and operation. The maximum demand and variability decreases with increasing number of appliances and users [26]. Therefore, for smaller mini-grids and SHS, the peaks are even more disruptive and the demand and supply matching even more difficult. Consequently, a good peek into the load consumption profile at the design stage is crucial. Therefore, a bottom-up approach is chosen for stochastic load profile construction in this study.

Bottom-up approach is used in [27], which uses datasets for hundreds of Finnish urban households to construct load profile from each load behaviour. Underlying loads and appliances were obtained from other studies at the time (2006). Probability factors

were taken from public reports and other available data. However, this study was primarily in the urban scenario, with contemporary loads, and considering hourly mean power levels.

In [28], a bottom-up approach to construct load profiles specifically for off-grid areas is discussed. While [28] comes closest to this study for creating a bottom-up methodology for constructing load profiles for rural off-grid systems, there are additional aspects that are considered in the study described in this chapter, which will be incorporated in the methodology described in Section 3.3. These are described below.

(a) Special focus on dedicated, super-efficient, off-grid (DC) appliances and related trends.

(b) Formulating an analytical approach to include the coincidence factor as a design parameter for stochastic load profile construction.

(c) Each load per tier constrained by a maximum usage per day.

(d) Use of a measured load profile from an SHS in Rwanda to compare and validate the constructed load profile.

(e) Constructing daily load profiles for an entire year so as to also account for inter-day variations. The methodology could be further complemented with interviews and data monitoring for seasonal recalibration if necessary.

### 3.2.2. LOAD PROFILE PARAMETERS

The important load profile parameters that referred in this work are discussed in this section. Additionally, implications of the load parameters on the off-grid energy system are also discussed.

#### PEAK AND AVERAGE LOADS

Peak load is the maximum power value the load profile takes over the period of consideration, while the average load is the mean load power. The electrical dimensioning of the energy system must be able to support the peak load power. In SHS, this is usually done with adequately rated power electronic converters. Information on average loads is in itself insufficient to appropriately size the systems and often error-prone [29].

#### ENERGY DEMAND

The energy demand is the integral of instantaneous power demand, i.e., the summation of all load consumption events during the period of consideration. This has implications on the amount of electrical energy the generator like PV module has to produce in the system.

$$E = \int_0^T P_L(t)\,dt \tag{3.1}$$

Where $E$ is the total energy demand, $P_L(t)$ is the instantaneous load power, and $T$ is the time interval under consideration. Consequently, the mean daily energy, which is defined as the average daily energy consumption over the given year, can be obtained as follows.

$$\overline{E_{\text{daily}}} = \frac{\sum_{i=1}^{365} \int_{0}^{24h} P_{L_i}(t)\,dt}{365} \tag{3.2}$$

Where $\overline{E_{\text{daily}}}$ is the mean daily energy, $P_{L_i}(t)$ is the instantaneous load power on day $i$.

#### LOAD FACTOR
Load factor is defined as the ratio of the average load power to the peak load power as shown in Equation 3.3. Higher the load factor, flatter the load profile, indicative of a load demand with fewer variations. On the other hand, a low load factor is indicative of high variability in the load profile.

$$\text{Load Factor} = \frac{P_{L,\text{Avg}}}{P_{L,\text{Peak}}} \tag{3.3}$$

Where $P_{L,\text{Avg}}$ and $P_{L,\text{Peak}}$ are the average and the peak power values of the load profile over a particular day.

#### COINCIDENCE FACTOR
Coincidence factor (CF) is defined as the ratio of the peak load power in the load profile to the total rated power of all the installed appliances in the energy system, as shown in Equation 3.4 [19]. It is a measure of the likelihood of all the loads constituting the load profile functioning simultaneously. This can hugely impact the electrical dimensioning of the system.

$$\text{CF} = \frac{P_{L,\text{Peak}}}{P_{L,\text{Tot}}} \tag{3.4}$$

Where $P_{L,\text{Tot}}$ is the total installed load.

### 3.2.3. TYPES OF APPLIANCES
Section 3.1.2 has already introduced the so-called super-efficient appliances increasingly being produced and used in the rural, off-grid regions. [30] reports a dedicated survey on off-grid appliances to investigate the appliance-products reflecting the greatest off-grid consumer demand, as well as driving the greatest electricity access. This survey, carried out in Africa, Latin America, and South Asia, considered a total of 19 appliances for off-grid household usage. The appliances considered in the survey have been listed in Table 3.1.

The table also mentions the typical power ratings and the needs that these appliances can fulfill. This survey and its results reported in [30] have been taken as the base for the selection of the loads that can meet the energy needs and can help in the construction of the load profiles. These loads can now be used in constructing the load profiles for the various tiers of electricity access as outlined by the MTF.

## 3.3. METHODOLOGY
This section details the overall methodology used for the stochastic construction of the load profiles, along with the mathematical model that forms the core of the methodology.

Table 3.1: List of off-grid appliances as ranked in [30]. The 'Needs' column refers to the same human needs a to f as mentioned in Section 3.1.1.

| S. No. | Appliance | Needs | Typical Rating [W] |
|---|---|---|---|
| 1 | LED Lighting | a | 1 - 5 |
| 2 | Mobile charging/ banks | b | 3 - 20 |
| 3 | Television | b | 10 - 50 |
| 4 | Radio | b | 2 - 5 |
| 5 | Fridges | c | 40 - 400 |
| 6 | Fan | f | 15 - 100 |
| 7 | Laptop | b | 30 - 100 |
| 8 | Solar water pumps | d | 40 - 800 |
| 9 | Tablets | b | 12 - 50 |
| 10 | Rice cooker | e | 200 - 250 |
| 11 | Clothes iron | d | 150 - 2000 |
| 12 | Grinders | d | 750 - 1000 |
| 13 | Hand power tools | d | 100 - 1000 |
| 14 | Hair clippers | d | 15 - 50 |
| 15 | Small speaker systems | b | 5 - 10 |
| 16 | Rice mills | d | 200 - 500 |
| 17 | Sewing machines | d | 40 - 100 |
| 18 | Soldering iron | d | 20 - 60 |
| 19 | Tea kettles | e | 100 - 800 |

### 3.3.1. LOAD CLASSIFICATION

Out of the 19 listed off-grid appliances listed in Table 3.1, a total of 16 appliances were considered in this study, with an air cooler as an additional appliance. These loads are then classified into the 5 tiers (T-1 to T-5) of household electricity access as outlined by the MTF (Table 2.1). Every tier is a superset of the preceding tier with more appliances.

This classification is captured in Table 3.2, where the considered load appliances are listed along with their power rating, quantity, and other operating constraints that are used as inputs to the mathematical model, as described in Section 3.3.2. Table 3.2 assumes typical values of operational constraints to demonstrate the applicability of the described methodology. These values are expected to be customized per target region or community.

Additionally, four dedicated appliances that contribute to productive use of energy (PUE) are considered as well in tier 5, viz., hand power tools, water pump, grinder/miller, and sewing machine. Note that the so-called super-efficient off-grid appliances are considered wherever applicable. However, some high power appliances, although DC and off-grid, are still in the process of undergoing advancements in the off-grid market, and therefore need not necessarily be 'super-efficient' like the LEDs and TV. For example, washing machine and air coolers. The appliances, and their specific datasheets, wherever applicable, are mentioned in the Appendix at the end of this chapter.

Table 3.2: Various operational constraints and inputs to the load profile construction methodology. T-1:T-5 = Tier 1:Tier 5.

| Load $j$ | Rating $P$ [W] | | | | | $T_{\min}$ [min] | $T_{\max}$ [min] | $T_{\mathrm{m}}$ [h] | | | | | $n_{\min}$ [-] | $n_{\max}$ [-] | W1 start time | W1 length [h] | W2 start time | W2 length [h] | Quantity $q$ [-] | | | | |
|---|---|---|---|---|---|---|---|---|---|---|---|---|---|---|---|---|---|---|---|---|---|---|---|
| | T-1 | T-2 | T-3 | T-4 | T-5 | | | T-1 | T-2 | T-3 | T-4 | T-5 | | | | | | | T-1 | T-2 | T-3 | T-4 | T-5 |
| LED Lighting | 2 | 2 | 2 | 2 | 2 | 30 | 240 | 6 | 8 | 8 | 12 | 12 | 1 | 12 | 4 | 2 | 18 | 6 | 3 | 5 | 5 | 8 | 12 |
| Mobile Phone Charging | 3 | 3 | 3 | 3 | 3 | 5 | 120 | 6 | 8 | 8 | 8 | 8 | 1 | 12 | 0 | 1 | 6 | 18 | 2 | 3 | 3 | 5 | 5 |
| Radio | 0 | 3 | 3 | 3 | 3 | 5 | 240 | 0 | 8 | 8 | 12 | 12 | 1 | 10 | 7 | 13 | 0 | 0 | 0 | 2 | 2 | 2 | 2 |
| Fan | 0 | 15 | 20 | 35 | 35 | 5 | 600 | 0 | 8 | 8 | 12 | 16 | 1 | 10 | 7 | 12 | 0 | 0 | 0 | 1 | 2 | 4 | 4 |
| TV | 0 | 12 | 18 | 29 | 29 | 5 | 240 | 0 | 8 | 8 | 12 | 12 | 1 | 10 | 7 | 7 | 17 | 6 | 0 | 1 | 1 | 2 | 2 |
| Fridge | 0 | 0 | 54 | 54 | 54 | 5 | 30 | 0 | 0 | 3 | 8 | 24 | 5 | 15 | 5 | 19 | 0 | 0 | 0 | 0 | 1 | 1 | 1 |
| Tablet | 0 | 0 | 18 | 18 | 18 | 5 | 120 | 0 | 0 | 6 | 12 | 12 | 1 | 10 | 0 | 1 | 6 | 18 | 0 | 0 | 1 | 1 | 1 |
| Kettle | 0 | 0 | 0 | 400 | 400 | 5 | 15 | 0 | 0 | 0 | 1 | 1 | 1 | 8 | 7 | 14 | 0 | 0 | 0 | 0 | 0 | 1 | 1 |
| Laptop | 0 | 0 | 0 | 60 | 60 | 5 | 240 | 0 | 0 | 0 | 6 | 6 | 1 | 10 | 0 | 1 | 6 | 18 | 0 | 0 | 0 | 1 | 1 |
| Rice Cooker | 0 | 0 | 0 | 200 | 200 | 30 | 30 | 0 | 0 | 0 | 1.5 | 1.5 | 1 | 3 | 10 | 2 | 17 | 3 | 0 | 0 | 0 | 1 | 1 |
| Clothes Iron | 0 | 0 | 0 | 150 | 150 | 5 | 20 | 0 | 0 | 0 | 2 | 2 | 1 | 2 | 6 | 16 | 0 | 0 | 0 | 0 | 0 | 1 | 1 |
| Washing machine | 0 | 0 | 0 | 70 | 70 | 15 | 120 | 0 | 0 | 0 | 2 | 2 | 0 | 1 | 6 | 14 | 0 | 0 | 0 | 0 | 0 | 1 | 1 |
| Air cooler | 0 | 0 | 0 | 500 | 500 | 30 | 120 | 0 | 0 | 0 | 4 | 12 | 0 | 8 | 9 | 9 | 0 | 0 | 0 | 0 | 0 | 1 | 1 |
| Power tools | 0 | 0 | 0 | 0 | 100 | 5 | 60 | 0 | 0 | 0 | 0 | 10 | 2 | 10 | 6 | 14 | 0 | 0 | 0 | 0 | 0 | 0 | 1 |
| Grinders/Millers | 0 | 0 | 0 | 0 | 750 | 10 | 120 | 0 | 0 | 0 | 0 | 10 | 2 | 10 | 6 | 14 | 0 | 0 | 0 | 0 | 0 | 0 | 1 |
| Sewing Machine | 0 | 0 | 0 | 0 | 40 | 5 | 120 | 0 | 0 | 0 | 0 | 10 | 3 | 20 | 6 | 14 | 0 | 0 | 0 | 0 | 0 | 0 | 1 |
| Water Pump | 0 | 0 | 0 | 0 | 750 | 5 | 30 | 0 | 0 | 0 | 0 | 4 | 0 | 2 | 5 | 12 | 0 | 0 | 0 | 0 | 0 | 0 | 1 |

### 3.3.2. MODEL PARAMETERS

The parameters of the mathematical model used in the methodology are defined in Table 3.3. The model assumes that a load can be operated in an allowed usage window multiple times for finite durations, as defined by the parameters and their constraints. The values for these parameters (including boundary values where applicable) along with details of the load appliance used for constructing the load profile can be seen in Table 3.2. It must be noted that these input values have a bearing on the model output, and can be tailored by the system designer using the described methodology for the specific user group being catered to.

As the data resolution in this study is 1 minute, functioning time $f$ (Table 3.3) is a 1440 (1 day long) length vector in MATLAB having ones and zeroes (1s and 0s) to indicate activity or inactivity of any load.

#### USAGE WINDOW

The idea of the usage window is illustrated in Figure 3.2. The concept illustration shows a usage window ($W$) spanning 9 hours from 09.00 to 18.00. Two occurrences of variable duration of a load rated 150 W can be seen, from 11.00 to 12.00 and 15.00 to 18.00. Additionally, the cycle times ($T_i$), number of instances ($n$), starting times ($t_i$) and power

Table 3.3: Parameters used for the stochastic load profile construction.

| Parameter | Definition | Notation | Type |
|---|---|---|---|
| Load type | Type of load in use. For example, TV, LED lights, etc, chosen from the LCM | $j$ | Input |
| Total load type | Total load types per category | $N$ | Input |
| Rated power | Rated power per load | $P$ | |
| Cycle time | Duration for which a load is operational | $T$ | Generated |
| Maximum Usage | Maximum number of hours a load is allowed to operate during the day | $T_m$ | Input |
| Instances | Number of times a load is operated in the allowed usage window | $n$ | Generated |
| Usage window | The allowed time window within which the loads are expected to be used | $W$ | Input |
| Quantity of loads | The number of loads of each type | $q$ | Input |
| Start time | Start time of a load instance within the usage window | $t$ | Generated |
| Load occurrence | The $i^{th}$ occurrence of a load cycle | $i$ | Generated |
| Dynamic Window | Dynamic window calculated as more load occurrences reduce the usage window | $W_{dyn}$ | Generated |
| Functioning time | Day long time interval showing the precise time stamps when the load is active or inactive | $f$ | Output |
| Peak window | The usage window where multiple appliances can potentially function simultaneously | $W_{peak}$ | Generated |
| Coincidence Factor | a design input between 0.2 and 1 that denotes the likelihood of appliances functioning simultaneously | $CF$ | Input |

rating ($P$) have been marked.

### PEAK WINDOW AND COINCIDENCE FACTOR

Peak window is that subset of the total allowed usage window that intersects with the usage window of other loads. This is an important input parameter for the model, as depending on the coincidence factor, multiple loads will operate in the peak window at the same time or around each other.

Figure 3.3 illustrates the concept of the peak window. The load usage window $W_j$ is shown for 3 different appliances $W_1$ to $W_3$, and the intersecting time duration $W_{peak}$ is shown. For tiers 4 and 5, lower powered applications like LED lighting, mobile phone charging, and radio are not considered for determining the peak window.

**Using coincidence factor**   The concept of coincidence factor (CF) described in Section 3.2.2 is an important load profile parameter, which can have implications on the

**3**
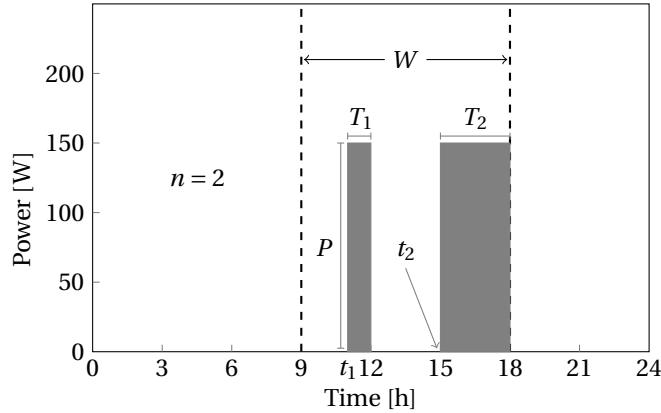


Figure 3.2: Concept illustration of load usage window ($W$) and load occurrence during the day.
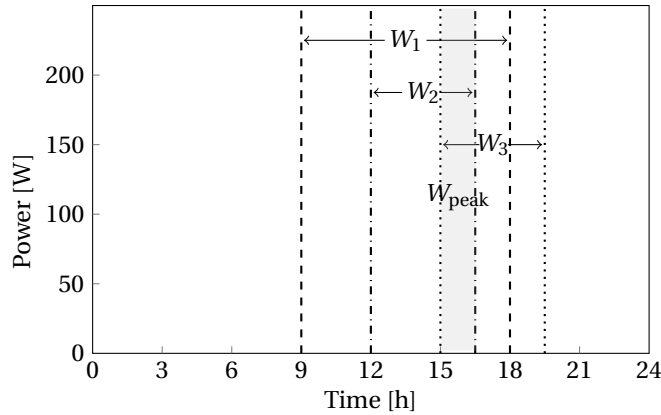


Figure 3.3: Concept illustration of peak window (shaded region) as an intersection of 3 different load usage windows.

off-grid system design to cater to the load profile. The coincidence factor measure is used as an attribute that impacts the probability of a load occurrence in the peak window. The probability of load occurrence times $t_{ij}$ within the peak window is considered to follow a normal distribution with the mean centered around the middle of the peak window. Equation 3.5 describes the normal probability density function with a mean $\mu$ and standard deviation $\sigma$. It is known that 99.7% of the values drawn from the normal distribution are within $3\sigma$ distance from the mean.

$$P(x) = \frac{1}{\sigma\sqrt{2\pi}} e^{-(x-\mu)^2 / 2\sigma^2} \tag{3.5}$$

Figure 3.4 illustrates the normal probability distribution of load occurrence being superimposed on the peak window. A high coincidence factor would imply a much narrower distribution compared to a lower coincidence factor. Minimum coincidence factor
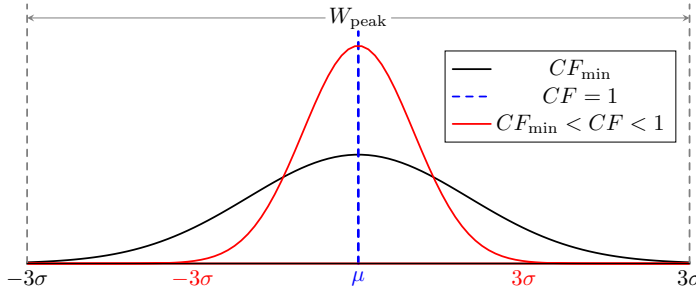
Figure 3.4: Normal probability distribution of load occurrence in the peak window.

gives rise to a normal distribution that just fits within the window, with the peak window boundary marking the $3\sigma$ limits for the normal distribution. Maximum coincidence factor of 1 would imply a distribution with $\sigma = 0$ and therefore the occurrence guaranteed at the center of the peak window.

Additionally, this is used to derive a relationship between CF and sigma as shown in Equation 3.6. $CF_{\text{min}}$ is fixed at 0.2 in this study.

$$\sigma = \frac{1 - CF}{1 - CF_{\text{min}}} \times \frac{W_{\text{peak}}}{6} \tag{3.6}$$

### RANDOMNESS AND CONSTRAINTS

As the model stochastically builds a load profile in a bottom-up manner by constructing load usages during the day, randomness was incorporated in the model. There are 3 main parameters that are quantified randomly withing the usage windows. These are: cycle times, starting times within the usage window(s), and the number of instances of load occurrence.

Moreover, the starting time for the specific occurrence in the peak window is handled using a normal distribution and the coincidence factor as explained in Section 3.3.2. The load profile construction efforts described in this chapter have been executed in MATLAB, and the randomness has been achieved with the help of the internal random number generator of MATLAB.

Additionally, there are several constraints that the various parameters are bound by. These are listed as follows.

1. $i \in [1, n_j]$

2. $j \in [1, N]$

3. $n_j \in [n_{j_{\text{min}}}, n_{j_{\text{max}}}]$, where $n_{j_{\text{min}}}$ and $n_{j_{\text{max}}}$ are the lower and upper bounds of the number of instances of load occurrence for load $j$ in a window respectively.

4. $T_{ij} \in [T_{j_{\text{min}}}, T_{j_{\text{max}}}]$ where $T_{j_{\text{min}}}$ and $T_{j_{\text{max}}}$ are the lower and upper bounds of the cycle times respectively.

5. $\sum_{i=1}^{n_j} T_{ij} \leq T_{\text{m},j}$

6. $t_{ij} \in W_j \; \forall \; ij$. Additionally, $t_{ij} + T_{ij} \in W_j$

These constraints change across the different load categories. The values of each of these constraints for the various loads and different tiers have been captured in Table 3.2.
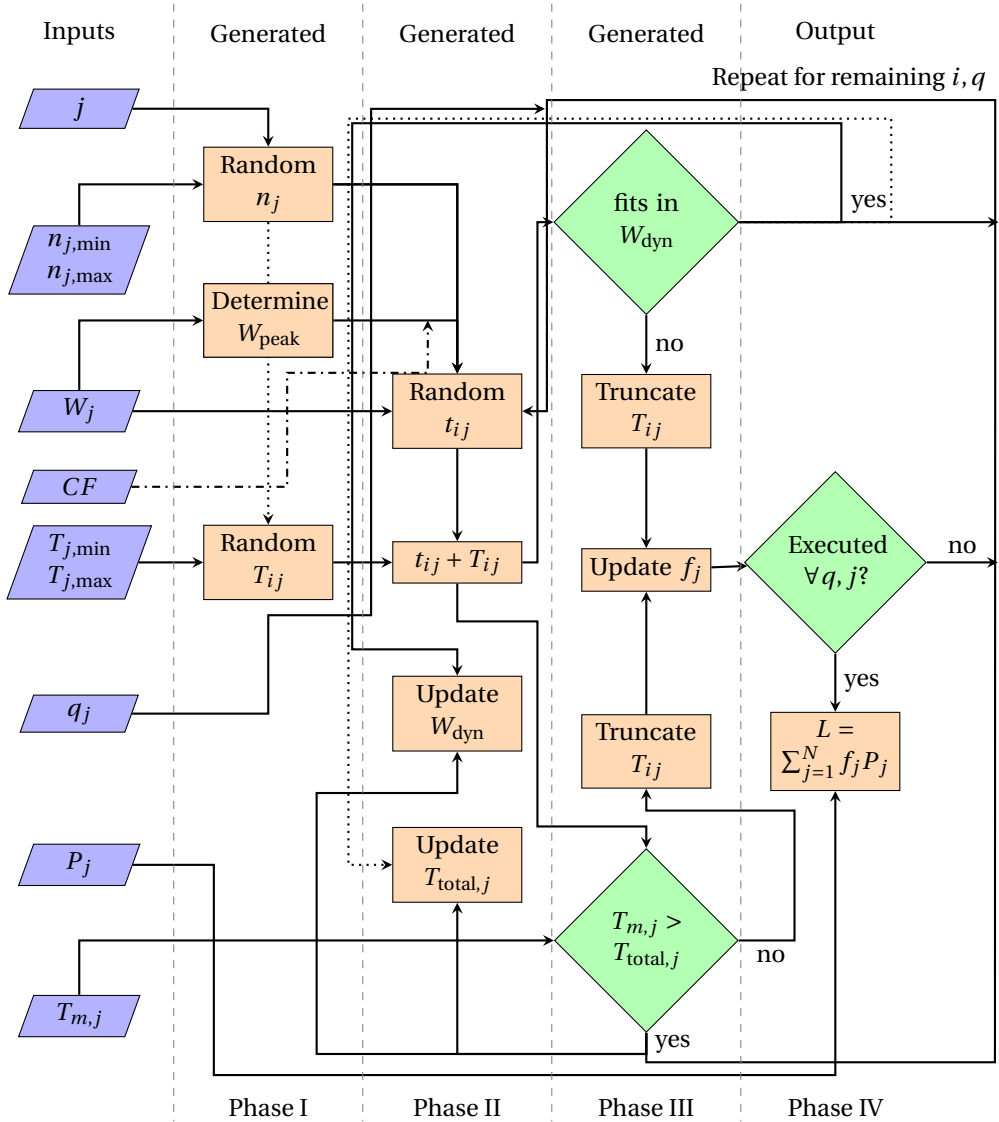


Figure 3.5: Flowchart illustrating the stochastic load profile estimation for one day. The process is repeated for the whole year across every tier.

### 3.3.3. STOCHASTIC LOAD PROFILE MODEL

The stochastic load profile construction methodology is illustrated through the flowchart presented in Figure 3.5. The methodology is executed in MATLAB in four distinct phases. They are as described below.

1. Phase I: **Stochastic generation** In this phase, for every load $j$, the number of instances $n_j$ of load occurrence during the day is randomly generated using the random number generator in MATLAB. Then, for each load instance occurrence $i$, a cycle time $T_{ij}$ is randomly generated. The peak window $W_{\text{peak}}$ is also determined in this phase. The various constraints, quantity of loads, rated power, and coincidence factor ($CF$) are also taken as inputs in this phase.

2. Phase II: **Occurrence Distribution** The occurrence time instance $t$ of every load instance $i$ is determined randomly in this step. Note that one occurrence is deliberately considered inside the peak window, using normal probability distribution with parameters derived from the coincidence factor, as explained in Equation 3.4 in Section 3.3.2. The occurrence $t_i$ occurs inside the allowed window(s) $W$, so that in general $t_{ij} \in W_j$. The cycle time $T_i$ is added to $t_i$. At this time, Phase III is executed to validate the cycle time of the load. If valid, then Phase II is executed again for the next load instance $i$. If invalid, then the cycle time is constrained according to either of 2 criteria as mentioned in Phase III, and then Phase II is executed for the next load instance $i$. If $i$ was already the same as $n$, then Phase II is implemented for the next load of the same type if the quantity $q > 1$. If the functioning window $f$ has been generated for all $q$ then the execution proceeds to the next load $j$. For every execution of Phase II, the allowed window is shrunk based on the cycle time occurrence of the executed load instance. Therefore an updated, shrunken, dynamic window $W_{\text{dyn}}$ is available for the next load occurrence. The total usage hours of any load is also kept track of in this phase.

3. Phase III: **Validation and Correction** Phase III concerns with validation based on 2 criteria, viz., $\sum_{i=1}^{n_j} T_{ij} \leq T_{m,j}$ and $t_{ij} + T_{ij} \in W_j$. That is, the cycle time is truncated if it spills out of the dynamic window. Alternately, it is truncated if the sum total of all load occurrences is greater than the allowed usage hours, a constraint coming from the MTF. After every execution of Phase II, Phase III validates the result, and Phase II is executed again accordingly. The methodology thus operates between Phase II and Phase III until the functioning time $f_j$ is populated for each $q$ of all $j$.

4. Phase IV: **Aggregation** At this point, the functioning windows $f_j$ have been stochastically generated for all the loads. Finally, the load profile is aggregated taking the quantity $q$ of the loads and the power rating $P$ into account as shown in Equation 3.7.

$$L = \sum_{j=1}^{N} f_j P_j \tag{3.7}$$

Where L is the final load profile vector of length 1440, owing to the 1-minute resolution of $f$. The load profile generation is repeated 365 times for a yearly load profile.

**3**

The procedure described is valid for the generation of the load profile for N loads within the user group. The same procedure can be followed with different inputs and constraints to obtain the load profiles from various tiers. The reader is referred to Table 3.2 to peruse the entire list of inputs and constraints as used in this study.

**ASSUMPTIONS IN THE METHODOLOGY**

There are a few careful assumptions in the presented methodology. These are:

1. No occurrence of the load takes place outside the usage window. Therefore, the choice of usage window largely dictates the particular load's contribution in the overall load profile. The usage windows shown in Table 3.2 have been considered as the typically expected values, which could be made more precise as usage preference data is available from the field.

2. For some of the loads, like laptop, tablet, and mobile phone charging, the loads in these cases specifically denote just the charging of the devices' battery and not the usage of the loads itself.

3. The load power is constant throughout its occurrence and is equal to the rated power. The only exception to this is the refrigerator, as explained below.

It must also be noted that the methodology presented here is strictly for load profile construction, and not for load forecasting.

**THE CASE OF THE REFRIGERATOR**

Unlike the rest of the loads, the fridge's energy consumption is rated differently and therefore deserves special treatment. The power consumption behaviour of the fridge is not taken to be at rated power at all times. This is because manufacturers often specify two parameters, the rated power and the daily energy consumption under testing conditions.

For example, an off-grid DC-powered fridge is rated at 40 W with a daily energy consumption of 114 Wh at 32.2°C ambient temperature [31]. The daily energy mentioned translates to a steady consumption of 4.75 W, much lower than the rated power of 40 W. This is because the daily energy only denotes the consumption when the fridge is largely in standby, and otherwise switches on due to self-checks. This neglects the switching on of the fridge due to external events like the door opening and new food addition, etc.

The methodology described in this study assumes the rated standby and self-check consumption without external events. Additionally, the load instances $i$ occurring through the day are considered to be the external events causing the fridge to switch on and consume 40 W for the cycle times $T_i$. Just as the other loads, the number of event instances will be constrained as $i \in [1, n]$ and $n \in [n_{\min}, n_{\max}]$.

**3.3.4. ADVANTAGES OF THE METHODOLOGY**

The load profile construction methodology developed in this study has several advantages, as listed below.

1. **Scalability** The load profiles constructed in this study were at a household level, given the background of electricity access and the MTF. However, as the methodology is bottom-up, the same method can be used to scale up the scope from

household to neighbourhood or even village level. The coincidence factor will need to be appropriately changed.

2. **Randomness** The stochastic nature of the load profiles embodies uncertainty, reflecting human behaviour. For example, there is consistency with the usage windows for each load. However, the number of times of load usage and the cycle times are still inconsistent within constraints. This allows for multiple load profile generations within the same set of given input data constraints.

3. **Yearly load profile** The yearly load profile contains unique daily load profiles. For instance, the load profile constructed for day 1 can be quite different from that of, say, day 200 in a given year. This is a welcome change from the yearly load profiles that are simply the same daily load repeated 365 times. This is helpful in sizing an off-grid system and understanding the system's battery behaviour over a larger span of time.

4. **Adaptability** The procedure described is flexible enough to incorporate more or different appliances in the future or even change the specifications of any load that makes up the load profile. The load profiles can be further customized based on precise demographic inputs and requirements from a specific community through fieldwork, for instance.

5. **Ease of system design** Due to increasing needs of the off-grid population, SHS designers often need to oversize their systems to enable future growth of consumption. This could be planned better with the methodology which helps quantify the energy consumption in the form of load profiles.

## 3.4. Results and Discussions

Based on the inputs described in Table 3.2 to the methodology described in Figure 3.5, different load profiles are obtained for the various tiers of the MTF. For ease of discussion, only the daily load profiles are shown here and discussed.

All the data from the generated load profiles have been made freely accessible at *DOI: 10.4121/uuid:c8efa325-87fe-4125-961e-9f2684cd2086.*

### 3.4.1. Stochastic load profiles for MTF

Figure 3.6 shows a tier 1 load profile for a representative day from the year-long load profile. As only a handful of loads operate in this case, both the peak power and the energy consumption is the lowest compared to the rest of tiers.

Figure 3.7 shows a daily tier 2 load profile for a representative day. Similar to tier 1 load profile, the characteristic peak occurs in the evening with moderate consumption during the day.

Figure 3.8 shows a daily tier 3 load profile for a representative day. An additional base load can be seen in this case due to the fridge. As described earlier, the consumption of the fridge is not modelled based on the duty cycle. Instead, a base average consumption is assumed from the manufacturer's data, and the external usage events are modelled.
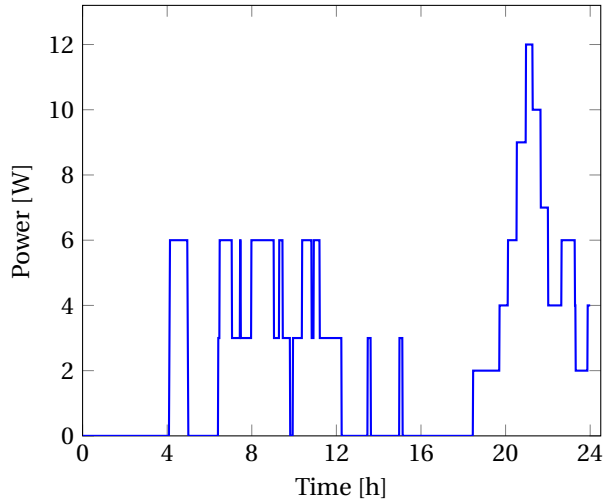
Figure 3.6: Load profile of an off-grid household with tier 1 electricity access for a representative day. Total energy consumption for this day is 60 Wh with a peak of 12 W.
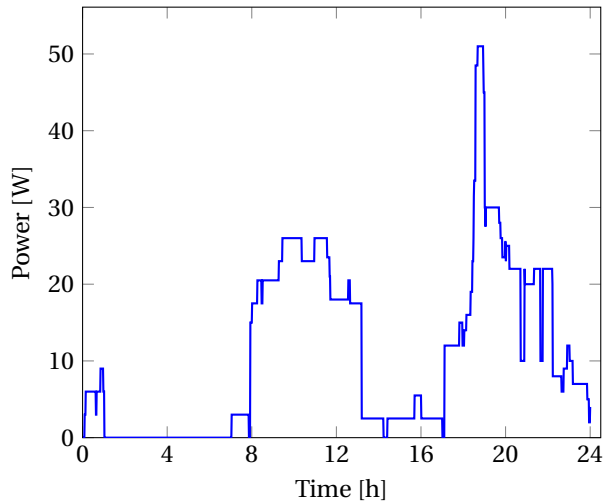


Figure 3.7: Load profile of an off-grid household with tier 2 electricity access for a representative day. Total energy consumption for this day is 262 Wh with a peak of around 51 W.

Figure 3.9 shows a daily tier 4 load profile for a representative day. Due to the high power appliances used in this category, the peak power (around 1 kW) is much more pronounced.

Figure 3.10 shows a daily tier 5 load profile for a representative day. As this tier is assumed to contain appliances that support PUE as well, a very high peak of 2.5 kW can be seen. Moreover, the peaks of all the load profiles lie in the peak window based on the
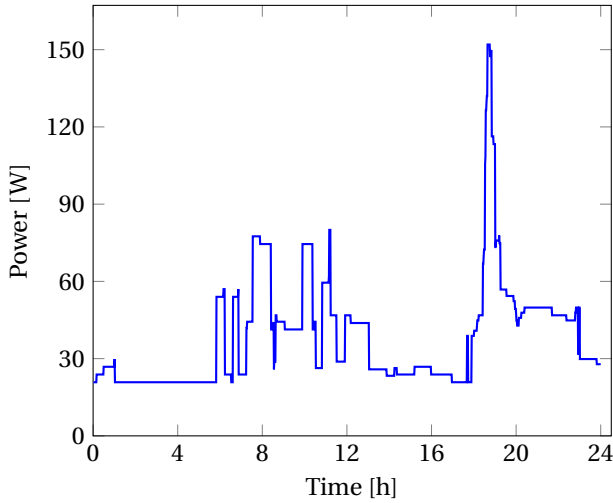
Figure 3.8: Load profile of an off-grid household with tier 3 electricity access for a representative day. Total energy consumption for this day is 914 Wh with a peak of around 150 W.
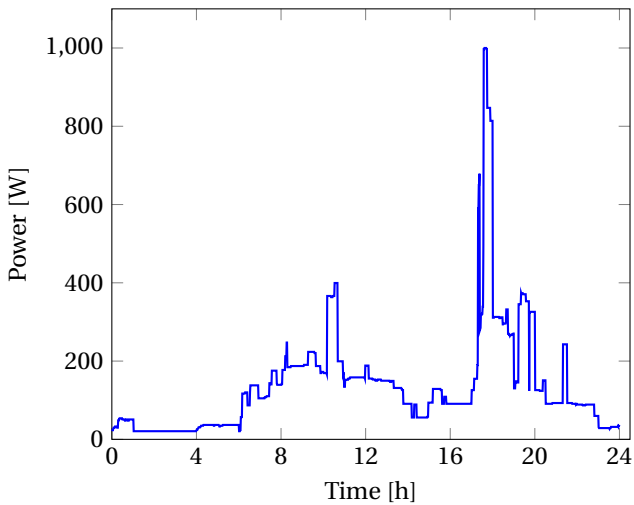


Figure 3.9: Load profile of an off-grid household with tier 4 electricity access for a representative day. Total energy consumption for this day is 3.29 kWh with a peak of around 1 kW.

coincidence factor as explained in Section 3.3.2.

### 3.4.2. LOAD PROFILES: MAIN PARAMETERS

The main parameters of the load profiles discussed in Section 3.2.2 have been captured in Table 3.4.

Here, $P_{\max}$ is the maximum value attained by $P_{L,\text{Peak}}$ throughout the year, while $P_{\min}$
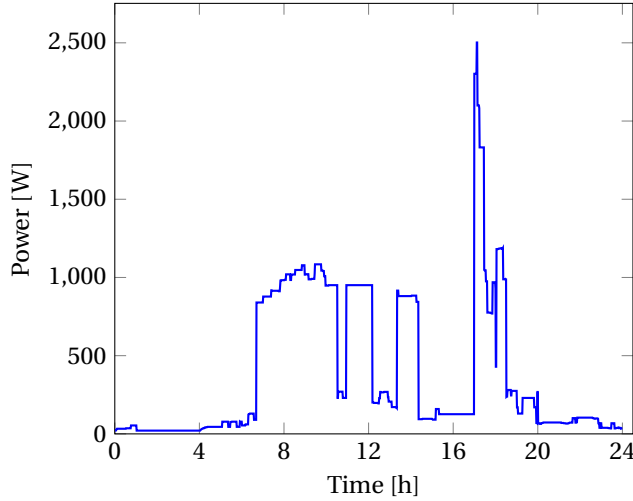
Figure 3.10: Load profile of an off-grid household with tier 5 electricity access supporting PUE loads for a representative day. Total energy consumption for this day is 9.34 kWh.

Table 3.4: Maximum peak power $P_{max}$, minimum peak power $P_{min}$, average daily energy $\overline{E_{daily}}$ and load factor for the load profiles for each tier based on the 1-year generated load profile.

|  | Tier 1 | Tier 2 | Tier 3 | Tier 4 | Tier 5 |
|---|---|---|---|---|---|
| $P_{max}$ (W) | 12 | 51 | 154 | 1670 | 3081 |
| $P_{min}$ (W) | 6 | 35 | 113 | 583 | 1732 |
| $\overline{E_{daily}}$ (Wh) | 50 | 218 | 981 | 3952 | 9531 |
| Load factor (-) | 0.17 | 0.18 | 0.26 | 0.10 | 0.13 |

is the minimum value. When compared with the energy and power limits mentioned by the MTF (Table 2.1), it can be seen that the constructed load profiles (in terms of $\overline{E_{daily}}$ and $P_{max}$) conform to these limits. The only exception is tier 3, where the $P_{max}$ is lower than the minimum limit as mentioned in the MTF. This is because of the super-efficient appliances already available and in use, which impact the overall power consumption. The impact of the efficiency of these appliances is more apparent in tier 3 than the lower tiers. The higher tiers 4 and 5 are still seeing advances being made in terms of dedicated, high power, efficient, off-grid appliances.

It must be noted that the existing solar lanterns, SHS or mini-grid solutions only span tiers 1 to 3 in terms of off-grid electrification. There is still a long way to go before most current off-grid communities can reach tier 4 and 5 consumptions. Nonetheless, climbing up the rural electrification ladder is inevitable, and when the expected tier 4 and 5 consumptions are reached, viable energy solutions need to be in place.

The higher tier load profiles can be seen to have lower load factors due to the tall peaks of the high power appliances. This would have severe implications on the battery size and the battery lifetime of standalone systems like SHS if that were to solely satisfy

these load profiles.

The values obtained in Table 3.4 can be tailored based on the kind of loads being used and the corresponding usage restrictions that are captured in Table 3.2, which is the expected use of this methodology.

### 3.4.3. Implications on system design

This section outlines the implications of the tier-based load profiles on the system design for the tiers. A standalone solar PV and battery-based (off-grid) energy system is considered in a location with around 4.5 equivalent sun hours (ESH), which is usual for most tropical and equatorial regions.

Tier 1 load profile shown in Figure 3.6 could be typically satisfied with a 15 to 20 Wp PV module and corresponding battery storage. This is already being done in the field by pico-solar products or smaller SHS designs. The tier 2 load demand shown in Figure 3.7 could be typically satisfied with around 50 Wp PV module and corresponding battery size for a location in the tropical belt, which is what a present-day small SHS can provide. Finding the optimal battery size requirement would need a more detailed analysis based on the year-long load profile and the specific meteorological data.

Tier 3 load profile would need around 250 Wp of PV, which is about the typical size of a contemporary residential solar panel used in the developed world. Only a handful SHS providers currently operate with such PV dimensions when catering to household level, standalone, off-grid SHS. Tier 4 load profile would need almost 1 kWp of PV module. A load peak of around 1 kW (Figure 3.9) and overall peak of 1.67 kW (Table 3.4 would have implications on the optimal dimensioning of the battery and the power electronics of the system, which needs a dedicated analysis.

Tier 5 load profile shows a load peak of around 2.5 kW (Figure 3.10) and an overall peak of around 3 kW due to the high power appliances that enable PUE. A standalone system would demand a PV of around 2.5 kWp and corresponding battery and power electronics to match. This shows that supporting the high power, dedicated, PUE-enabling appliances is going to be an exacting challenge on the size of a standalone system like SHS. Guaranteeing zero loss-of-load events would call for a highly oversized standalone system. A microgrid with distributed generation might be a more suited option [1].

### 3.4.4. Comparison with field data

At the time of conducting the work described in this chapter, most prevalent SHS and other off-grid systems deployed at household level were only catering up to tier 2, or in some cases, tier 3 level electricity access. BBOXX, an SHS provider in Rwanda, East Africa offers a portfolio of efficient DC appliances along with the SHS. Figure 3.11 shows a single day load profile of an off-grid SHS from BBOXX capable of powering 3 LED lights (1.2 W nominal consumption) and a USB port for charging a mobile phone and a portable radio. The consumption limits would deem this to be a tier 1 load profile. Also shown is a stochastically generated load profile, with different inputs matching those corresponding to the appliances of the SHS in the field. The generated profile seems to match the measured one closely, especially with respect to the peak load in the peak window in

---

[1]Note that these system sizes are back-of-the-envelope approximations, and a thorough analysis is needed to comment on the system sizes that satisfy particular system metrics, which is exclusively dealt with in Chapter 5
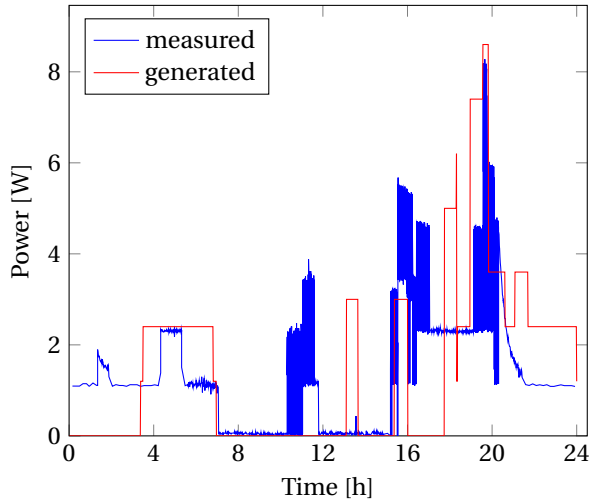
Figure 3.11: Comparison of a generated stochastic load profile with the measured load consumption over a single day of a household in Rwanda powered by an SHS from BBOXX.

the evening. The total daily energy of the measured load profile is 35.7 Wh, while that of the generated one is 34.7 Wh, representing a 2.9% error. Furthermore, the load factor of the measured load profile is 0.18 while that of the generated load profile is 0.17. A much greater match can naturally be achieved if needed by adjusting the operational constraints. However, the comparison here is to merely exemplify the usefulness of the described methodology.

## 3.5. CONCLUSIONS

This chapter described a bottom-up, stochastic load profile construction methodology to quantify the energy needs for the various tiers of the MTF. The loads were entirely composed of dedicated, off-grid, and in some cases the so-called super-efficient, appliances. Advantages like scalability, adaptability, and randomness of the proposed methodology were identified. A method for incorporating coincidence factor as a design input for the methodology was also introduced. Several stochastic load profiles were created using the described methodology, and their impact on standalone system design for the different load profiles has been underlined. The impact of appliances enabling productive use of energy was also investigated through a tier 5 load profile construction. The utility of this methodology can be greatly augmented with the availability of local data and complemented with targeted surveys per target community/region.

The load profile construction methodology described in this chapter is expected to greatly help various off-grid electrical system designers in constructing load profiles and customizing energy solutions to cater to the growing energy needs of the un(der)-electrified population.

In the next chapter, estimating battery lifetime is discussed for SHS-specific applications utilizing the load profiles constructed through the methodology described in this

chapter.

## RECOMMENDATIONS AND FUTURE WORK

The methodology described assumes rated power consumption of these DC appliances throughout the usage of the appliance. In reality, some appliances may consume differently based on their usage. For now, only the fridge has been treated as a special case. Other examples could include the starting power consumption of an appliance, or the varying power consumption of an LCD TV depending on the screen illumination, which can be quite different from the rated power. In the absence of actual power consumption profiles of these up-and-coming DC appliances, the current load profile construction methodology is considered to be sufficient. More light will be hopefully shed in the future by the real-time data gathered from SHS in the field. Seasonal implications on the load vary for different locations, and were not considered in this study. However, these can also be added as an additional parameter based on location specific information; the input table (Table 3.2) can be updated based on context specific knowledge, potentially complemented by field studies.

**3**

## ACKNOWLEDGEMENT

## REFERENCES

[1] B. Tenenbaum, C. Greacen, T. Siyambalapitiya, and J. Knuckles, *From the bottom up: how small power producers and mini-grids can deliver electrification and renewable energy in Africa*. World Bank Publications, 2014.

[2] C. Wolfram, O. Shelef, and P. Gertler, "How Will Energy Demand Develop in the Developing World?," *Journal of Economic Perspectives*, vol. 26, no. 1, pp. 119–138, 2012.

[3] IEA, *Energy Access Outlook 2017 - From Poverty to Prosperity*. Organization for Economic Cooperation and Development, International Energy Agency, 1 ed., 2017.

[4] A. A. Phadke, A. Jacobson, W. Y. Park, G. R. Lee, P. Alstone, and A. Khare, "Powering a home with just 25 watts of solar pv. super-efficient appliances can enable expanded off-grid energy service using small solar power systems," tech. rep., Lawrence Berkeley National Laboratory (LBNL), Berkeley, CA (United States), 2015.

[5] Global LEAP, "The State of the Off-Grid Appliance Market," tech. rep., Tech. rep. Washington, DC: Global LEAP Lighting and Energy Access Partnership, 2016.

[6] W. Y. Park and A. A. Phadke, "Adoption of energy-efficient televisions for expanded off-grid electricity service," *Development Engineering*, vol. 2, pp. 107 – 113, 2017.

[7] REN21, *Renewables 2017 Global Status Report*. Paris, REN21 Secretariat, 2017.

[8] GIZ, *Photovoltaics for Productive Use Applications - A Catalogue of DC-Appliances.* Deutsche Gesellschaft für Internationale Zusammenarbeit (GIZ) GmbH, 2016.

[9] A. L. Kooijman-van Dijk, *The Power to Produce: The role of energy in poverty reduction through small scale Enterprises in the Indian Himalayas.* University of Twente, 2008.

[10] B. Troja, "A quantitative and qualitative analysis of the super-efficient equipment program subsidy in India," *Energy Efficiency*, vol. 9, no. 6, pp. 1385–1404, 2016.

[11] A. H. Smets, K. Jäger, O. Isabella, R. Van Swaaij, and M. Zeman, *Solar Energy, the Physics and Engineering of Photovoltaic Conversion Technologies and Systems.* UIT Cambridge, 2016.

[12] S. Treado, "The effect of electric load profiles on the performance of off-grid residential hybrid renewable energy systems," *Energies*, vol. 8, no. 10, pp. 11120–11138, 2015.

[13] T. D. Heeten, N. Narayan, J. C. Diehl, J. Verschelling, S. Silvester, J. Popovic-Gerber, P. Bauer, and M. Zeman, "Understanding the present and the future electricity needs: Consequences for design of future solar home systems for off-grid rural electrification," in *2017 International Conference on the Domestic Use of Energy (DUE)*, pp. 8–15, April 2017.

[14] M. Gustavsson, "With time comes increased loads: An analysis of solar home system use in lundazi, zambia," *Renewable Energy*, vol. 32, no. 5, pp. 796–813, 2007.

[15] S. Hirmer and P. Guthrie, "The benefits of energy appliances in the off-grid energy sector based on seven o ff -grid initiatives in rural Uganda," *Renewable and Sustainable Energy Reviews*, vol. 79, no. May, pp. 924–934, 2017.

[16] F. Riva, H. Ahlborg, E. Hartvigsson, S. Pachauri, and E. Colombo, "Electricity access and rural development: Review of complex socio-economic dynamics and casual diagrams for more appropriate energy modelling," *Energy for Sustainable Development*, vol. 43, pp. 203–223, 2018.

[17] F. Riva, A. Tognollo, F. Gardumi, and E. Colombo, "Long-term energy planning and demand forecast in rural areas of developing countries: classification of case studies and insights for a modelling perspective," *Energy Strategy Reviews*, vol. 20, pp. 71–89, 2017.

[18] C. Blodgett, P. Dauenhauer, H. Louie, and L. Kickham, "Accuracy of energy-use surveys in predicting rural mini-grid user consumption," *Energy for Sustainable Development*, vol. 41, pp. 88–105, 2017.

[19] E. Hartvigsson and E. O. Ahlgren, "Comparison of load profiles in a mini-grid: Assessment of performance metrics using measured and interview-based data," *Energy for Sustainable Development*, vol. 43, pp. 186–195, 2018.

[20] S. C. Bhattacharyya and G. R. Timilsina, "Modelling energy demand of developing countries: Are the specific features adequately captured?," *Energy Policy*, vol. 38, no. 4, pp. 1979–1990, 2010.

[21] L. G. Swan and V. I. Ugursal, "Modeling of end-use energy consumption in the residential sector: A review of modeling techniques," *Renewable and Sustainable Energy Reviews*, vol. 13, no. 8, pp. 1819–1835, 2009.

[22] G. Tsekouras, P. Kotoulas, C. Tsirekis, E. Dialynas, and N. Hatziargyriou, "A pattern recognition methodology for evaluation of load profiles and typical days of large electricity customers," *Electric Power Systems Research*, vol. 78, no. 9, pp. 1494 – 1510, 2008.

[23] T. Räsänen, D. Voukantsis, H. Niska, K. Karatzas, and M. Kolehmainen, "Data-based method for creating electricity use load profiles using large amount of customer-specific hourly measured electricity use data," *Applied Energy*, vol. 87, pp. 3538–3545, 2010.

[24] J. Nuno, M. António, and L. Ribeiro, "A new clustering algorithm for load profiling based on billing data," *Electric Power Systems Research*, vol. 82, no. 1, pp. 27 – 33, 2012.

[25] I. A. Sajjad, G. Chicco, and R. Napoli, "A probabilistic approach to study the load variations in aggregated residential load patterns," in *2014 Power Systems Computation Conference*, pp. 1–7, Aug 2014.

[26] P. Boait, V. Advani, and R. Gammon, "Estimation of demand diversity and daily demand profile for off-grid electrification in developing countries," *Energy for Sustainable Development*, vol. 29, pp. 135–141, 2015.

[27] J. V. Paatero and P. D. Lund, "A model for generating household electricity load profiles," *International Journal of Energy Research*, vol. 30, no. 5, pp. 273–290, 2006.

[28] S. Mandelli, M. Merlo, and E. Colombo, "Novel procedure to formulate load profiles for off-grid rural areas," *Energy for Sustainable Development*, vol. 31, pp. 130–142, 2016.

[29] H. Louie and P. Dauenhauer, "Effects of load estimation error on small-scale off-grid photovoltaic system design , cost and reliability," *Energy for Sustainable Development*, vol. 34, pp. 30–43, 2016.

[30] Global LEAP, "Off-grid appliance market survey," tech. rep., Tech. rep. Washington, DC: Global LEAP Lighting and Energy Access Partnership, 2015.

[31] SunDanzer, "DCR50 DC powered refrigerator," *Datasheet*, 2016.

[32] Phocos, "Led Light SL 1220CF120," *Datasheet*, 2016.

[33] Samsung, "Mobile phone Guru Plus," *Datasheet*, 2016.

**3**

[34] Global LEAP, "Global leap awards - 2016 buyer's guide for outstanding off-grid fans and televisions," tech. rep., Tech. rep. Washington, DC: Global LEAP Lighting and Energy Access Partnership, 2016.

[35] HP, "HP Pro Tablet EE G1," *Datasheet*, 2016.

[36] Panasonic, "Automatic Rice Cooker SR-3NA-5," *Datasheet*, 2016.

[37] Hotspot Energy, "Solar/DC Air Conditioner DC4812VRF," *Datasheet*, 2016.

**3**

## APPENDIX

Table 3.5 lists down the loads used in the study. The model number and basic specifications of the loads are mentioned, along with the corresponding source wherever applicable.

Table 3.5: List of appliances used for constructing the load profile.

| Loads | Sample model number | Source |
|---|---|---|
| LED Lighting | SL 1220CF120 | [32] |
| Mobile Phone | Samsung Guru Plus | [33] |
| Radio | Fosera, FS106 | [8] |
| Fan | ONergy 10" BOX FAN, FS91, ONergy 16" PEDESTAL FAN, FS92, Ceiling Fan ME-103-DC | [8], [34] |
| TV | Fosera DC TV 15.6" 12 V, D.light design 18.5" LE185N91C,Mobisol 24" MSDV2310MY-308C1 | [34] |
| Fridge | Solar Chill, FS52 , Sundanzer DCR 50, DCR 165 | [31],[8] |
| Tablet | HP Pro Tablet 10 EE G1 | [35] |
| Kettle | Solar DC Kettle SE520, FS65 | [8] |
| Laptop | Generic Laptop | - |
| Rice Cooker | SR-3NA-S | [36] |
| Clothes Iron | Solar DC Power Iron Dry/ Spray style-12V SL100S, FS192 | [8] |
| Washing Machine | Washing Machine CERAD, FS127 | [8] |
| Air cooler | DC Solar Air Conditioner, DC4812VRF | [37] |
| Power tools | Bosch 18V Lithium Ion 4-Tool Combo Kit (CLPK414-181), FS84 | [8] |
| Grinders/Millers | Grain Mill Solar Milling, FS32 | [8] |
| Sewing Machine | Sewing Machine CERAD, FS73 | [8] |
| Water Pump | Solar Surface Slow Pump Dankoff, FS10 | [8] |

# 4

# ESTIMATING BATTERY LIFETIME IN SOLAR HOME SYSTEMS

*It has become appallingly obvious that our technology has exceeded our humanity*

Albert Einstein

## ABSTRACT

The battery is a vital but usually the most expensive part of an SHS. As the battery has the least lifetime among other SHS components, it is also the first to fail. Estimating battery lifetime is a critical task for SHS design. However, it is also a complex task due to the reliance on experimental data or modelling cell level electrochemical phenomena for specific battery technologies and application use-case. This chapter presents a practical, non-empirical battery lifetime estimation methodology specific to the application and the available candidate battery choices. An application-specific SHS simulation is carried out, and the battery activity is analyzed. A practical dynamic battery lifetime estimation method is introduced, which captures the fading capacity of the battery dynamically through every micro-cycle. This method is compared with an overall non-empirical battery lifetime estimation method, and the dynamic lifetime estimation method is found to be more conservative but practical. Cyclic ageing of the battery is thus quantified and the relative lifetimes of 4 battery technologies are compared, viz. Lead-acid gel, Flooded

This chapter is based on the following publications:

1. N. Narayan, T. Papakosta, V. Vega-Garita, Z. Qin, J. Popovic-Gerber, P. Bauer, & M. Zeman. (2018). Estimating battery lifetimes in Solar Home System design using a practical modelling methodology. *Applied Energy*, 228, 1629-1639.

2. N. Narayan, T. Papakosta, V. Vega-Garita, J. Popovic-Gerber, P. Bauer and M. Zeman, "A simple methodology for estimating battery lifetimes in Solar Home System design," *2017 IEEE AFRICON*, Cape Town, 2017, pp. 1195-1201. doi: 10.1109/AFRCON.2017.8095652.

lead-acid, Nickel-Cadmium (NiCd), and Lithium Iron Phosphate (LiFePO$_4$) battery. For the same SHS use-case, State-of-Health (SOH) estimations from an empirical model for LiFePO$_4$ is compared with those obtained from the described methodology, and the results are found to be within 2.8%. Based on the intended application and battery manufacturer's data, the practical methodology described in this chapter can potentially help SHS designers in estimating battery lifetimes and therefore making optimal SHS design choices.

### OUTLINE

This chapter is divided into five sections. Section 4.1 introduces the work described in the chapter, while Section 4.2 outlines the necessary technical background and the focus of this study. Section 4.3 discusses the specific application use-case and describes the methodology used. Section 4.4 discusses the results and compares the estimated battery lifetime from the proposed methodology with an experimentally obtained model for LiFePO$_4$ battery. Finally, Section 4.5 concludes the discussion on the battery lifetime estimation methodology.

## 4.1. INTRODUCTION

The battery is a vital component of the SHS, enabling energy storage of the PV output. However, the sizable proportion of upfront battery costs makes the battery the most expensive SHS component, as seen in Figure 4.1. This fact, coupled with the low battery lifetimes (sometimes as low as 3 years [1]), makes battery-costs the most relevant in SHS design. Battery-costs recur not just in terms of the upfront costs, but also in terms of the replacements during SHS lifetime, thereby making battery lifetime a critical parameter in SHS applications.
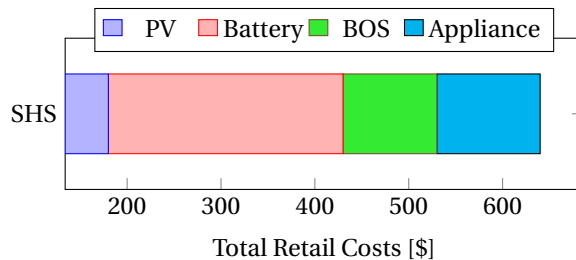


Figure 4.1: Split-up of upfront costs of SHS components for powering a 19" TV, radio, lights and a mobile phone charger in 2014 (data from [2]).

Additionally, the accurate sizing of the battery can impact the battery lifetime [3]. This is because an increase in battery size for the same application reduces the average Depth of Discharge (DOD) for the battery [4], as seen below in Section 4.3. Therefore, the sizing of the battery in an SHS presents itself as an interesting balance between upfront costs (size) and lifetime [5].

Battery lifetime is thus seen as a vital parameter to be considered in SHS design, especially in the cost-sensitive context of electrification.

### 4.1.1. LITERATURE STUDY

Battery lifetime estimation models can be broadly classified under two categories, viz. performance-based models and cycle counting models.

In performance-based models, the performance values of the battery are simulated based on certain performance parameters. When the particular parameter drops below a pre-determined value, the end of life (EOL) is reached for the battery. These can be classified into 4 different categories.

(i) **Electrochemical Models** that need extensive information on the chemical and physical interactions occurring within the battery in order to accurately model the battery. Despite the efforts to simplify these models while effectively estimating the dynamically changing states (SOC and SOH) [6], the lack of detailed information such as Li-ion concentration, diffusion coefficients, reaction rates, ionic conductivity, reduce the applicability of these models specially when different battery technologies are to be compared.

(ii) **Equivalent Electrical Circuit Models** that represent the battery as an equivalent electrical circuit comprising electrical elements like resistors, capacitors, voltage, and current sources. These kind of models can also include the thermal stresses related to fast charging to develop optimal charging profiles [7]. A combined electrochemical-thermal model has also helped in recent studies to develop health-aware strategies for fast charging of Li-ion battery, underlining the importance of being able to model SOH in battery applications [8].

(iii) **Analytical Models** with empirical data fitting are constructed by interpolating and fitting empirical data obtained through experiments.

(iv) **Artificial neural networks (ANN)** can establish a relationship between the system outputs and input operating conditions, given a large enough dataset [9].

Performance-based models can rely on experimental methods that observe and measure the battery degradation through time, or on semi-empirical approaches that represent the fade mechanisms using equations that fit a particular type of cell. These models can also be constructed by including the physiochemical effects behind the side reactions of a particular set of chemical compounds endemic to particular cell chemistries. Therefore, the main limitation of all of the underlying approaches for performance-based models is that they are constructed for specific cells, under certain environment conditions, and tested through a limited amount of time [10]. Additionally, some semi-empirical approaches do not consider the effect of parameters like DOD [11]. For models relying on ANN, a vast amount of data is first needed for the neural network to be trained reliably. In general, it can be said that to construct reliable performance-based models, it not only costs time per specific intended application and use-case needed but also raises concerns on the accuracy of these approaches if they were to be used under a different set of conditions wherein the same battery technology undergoes a different stress pattern🦇.

---

🦇In this PhD project, it was also endeavoured to create dynamic performance models of lead-acid gel and LiFePO$_4$ battery types for SHS applications. To this end, cell level experiments were conducted to construct equivalent electrical circuit models. This is described in Appendix 8.4.3.

Unlike performance-based models, cycle counting or **weighted Ah-throughput** (charge processed by the battery) models are able to determine parameters which can be linked to their EOL, for instance, Ah-throughput (the amount of energy processed by the battery), cycles, or time since manufacturing [9]. A comparison study in the past has shown accurate results for lifetime prediction with weighted Ah-throughput model [12]. These models are mainly based on the data provided by the manufacturers, assuming that the battery is able to achieve an overall Ah-throughput throughout its life under certain specific stress factors like DOD and temperature. Palmgren-Miner (PM) rule is one of the most common examples that fit in the category of cycle counting models. The different lifetime estimation models are compared in Table 4.1.

Table 4.1: Comparison of the performance-based and cycle-counting models in the context of battery life estimation. Adapted from [9].

| Model type | Model example | Merits | Demerits |
|---|---|---|---|
| Performance-based | Electro-chemical | Very high accuracy | Complex |
| | | | Low-speed |
| | Equivalent Electrical Circuit Model | Good prediction of dynamic behaviour | Depends on experimental data for accuracy |
| | | | Not suitable for lifetime prediction as is |
| | Analytical model with empirical data fitting | Ease of simulation using the model due to the analytical functions | Effects of various stress factors need to be combined from the experimental data |
| | | Good accuracy | Large amount of data needed |
| | Artificial Neural Networks (ANN) | Reasonable accuracy with high speed | Adequate training of ANN requires a large dataset |
| | | Knowledge of battery mechanisms not needed | |
| Cycle-counting | Palmgren-Miner (PM) rule | Deviations from standard operating conditions captured well | Although non-empirical in itself, relies on empirical data from the manufacturer |
| | | Simple implementation | |

There have been a few cycle-counting-based lifetime estimation models discussed in the past in [13, 14, 15], and most notably in [5], where the authors discuss a simple

methodology for non-empirical battery lifetime estimation. However, while [13] assumes an arbitrary duration of a cycling event 6400 seconds long, [14] uses only temperature as a stress factor but not for battery storage specifically, [15] employs off-line cycle-counting through rainflow counting algorithm but using DOD as the only stress factor for battery degradation, and [5] does not take into account dynamic capacity fading and temperature as an additional stress factor. The work described in [16] presents a lifetime estimation of lead-acid battery, but also does not consider dynamic capacity fading, and the capacity loss is only estimated after one entire year of simulation using rainflow counting algorithm.

This chapter focuses on a non-empirical, cycle-counting approach for the estimation of the battery lifetime while also taking into account important battery stress factors like DOD and temperature. Given the off-grid SHS application, where the typical battery C-rates are C/20 to C/10 [17, 18], the C-rates are considered to be low enough to not be included as a critical stress factor. The dynamic capacity fading model proposed here is capable of estimating the State of Health (SOH) after every micro-cycle-based degradation while the battery is under operation. Additionally, multiple technologies are used in this study, demonstrating the usefulness of the proposed methodology across multiple battery technologies without having to model the electrochemical processes at the cell level for the different technologies.

### 4.1.2. CONTRIBUTIONS OF THIS CHAPTER
Following are the main contributions of this chapter.

- A methodology to estimate the battery lifetime in a practical way using the application-based, expected battery usage and the battery data provided by the manufacturer. The methodology is applicable across battery technologies.

- Insight into performance of 4 different battery technologies for the SHS application.

- A dynamic capacity fading model that quantifies the fractional degradation caused by the micro-cycles of battery activity.

## 4.2. BATTERY LIFETIME
### 4.2.1. BATTERY PARAMETERS
Some of the important battery parameters that this work refers to are discussed in this section.

**State of Charge and Depth of Discharge**    The state of charge (SOC) indicates battery charge as a fraction of the initial capacity, while the depth of discharge (DOD) refers to the capacity discharged as a fraction of the initial capacity. They are treated as a complement of each other.

The DOD can be calculated from the battery discharge current over a discharging interval as shown in Equation 4.1.

$$DOD = \frac{\int_{t_i}^{t_f} I_{\text{discharge}}.dt}{C_i} \tag{4.1}$$

where $t_f$ is the time at the end of the discharge interval process, $t_i$ is the initial time, $I_{discharge}$ is the current, and $C_i$ the initial battery capacity.

**Cycle-life**    Cycle-life is defined as the number of charge/discharge cycles that a battery can undergo maintaining a specified percentage of its initial capacity, after which batteries reach the end of life (EOL). The EOL is usually defined as 80% of the initial rated battery capacity [19].

**State of Health (SOH)**    State of Health refers to the fraction of the rated battery capacity actually available for cycling. As the battery ages, the SOH reduces, and 80% SOH is often defined as the EOL for a battery. The battery ageing can be classified into two categories, viz., cyclic ageing and calendar ageing.

**Cyclic ageing**    Cyclic ageing is related to the decrease in battery capacity while the battery is undergoing cycling. Cyclic ageing plays a larger role in cases where operation times are relatively longer than idle periods, like in off-grid SHS.

**Calendar ageing**    Calendar ageing is related to the decrease in battery capacity while the battery is under storage and not in use, and therefore, independent of charge/discharge cycles. Calendar ageing plays a predominant role in cases where operation times are shorter than idle periods [20]. This work takes into account only the cyclic ageing process. In other words, this work models the application-specific, battery induced capacity fading and the resulting battery lifetime.

**Active SOC/DOD**    Active SOC/DOD refers to the State-of-Charge or Depth-of-Discharge of the battery while the battery is in operation [5]. The concept of active SOC/DOD helps in looking at only those SOC/DOD points that actively contribute towards cyclic ageing of a battery, which is the focus of this work.

### 4.2.2. CAUSES OF BATTERY DEGRADATION

The loss of active lithium, principally at the anode, is the main reason for lithium-ion cell degradation. The mechanical stresses induced by cycling and temperature gradients lead to contraction and expansion, eventually increasing the cell impedance and reducing the cell capacity [20]. Electrode pore clogging, passive layer growth, and lithium metal plating are consequences of the undesired side reaction that takes place inside the Lithium-ion cells [21]. In the case of lead-acid batteries, the major degradation processes that decrease performance and provoke end of service life are anodic corrosion, active mass degradation, and loss of adherence to the grid plate [22]. Furthermore, the continuous loss of water in vented cells and the production of lead sulphate (in the electrodes) out of the active materials of the cell facilitates the ageing process [23]. NiCd cells suffer from hydrogen production when overcharged and when exposed to a temperature higher than nominal temperature; therefore, the accurate detection of the end-of-charge process is fundamental to avoid battery damage [24]. In NiCd cells, Cd crystallization happens

under particular cycling and storage conditions, causing a reduction of active material while reducing the active surface dedicated to the electrochemical reaction [19].

Battery lifetime is directly related to battery usage, and therefore the way in which the battery cycling occurs and the environmental conditions affect the natural ageing of batteries. One of the principal factors to take into account is the DOD range of operation, which defines the usable capacity of the battery, and therefore, the battery range of operation. Another parameter that profoundly impacts battery ageing is cell temperature, where an increase in temperature translates into a higher electrochemical activity that instantaneously improves cell performance but in the long term fosters side reactions that consume the active materials, thereby diminishing battery capacity [25]. The kinetics of the electrochemical reaction also relates to the charge and discharge rates imposed by the applications. Therefore, the methodology introduced in the next section takes into account the influence of temperature and cycling to quantify their impact on lifetime.

## 4.3. METHODOLOGY

The methodology followed in this study is composed of multiple steps. Section 4.3.1 describes the extraction of lifetime data from the battery datasheet as a function of temperature and DOD. Section 4.3.2 details the SHS-based inputs used in the methodology. Sections 4.3.3 and 4.3.4 discuss the two models that are proposed and used in this study, viz. the overall battery usage model and the dynamic capacity fading model.

### 4.3.1. BATTERY DATA FROM THE MANUFACTURER

Battery manufacturers usually provide the battery cycle-life characteristics as a function of DOD and temperature, for example, in [26]. The data from these curves are extracted, and lookup-functions are created.

**Battery technology**  Four different battery technologies are chosen for this study, viz., sealed Lead-Acid or Lead-Acid gel (LA-gel), Lithium-Iron Phosphate (LiFePO$_4$), flooded Lead-Acid (LA), and Nickel-Cadmium (NiCd) battery. The corresponding datasheets used are [26, 27, 28, 29] respectively. While the merits and demerits of using one battery technology over the other for SHS application is a different subject of discussion altogether, the reason for including these different technologies in this study is to illustrate the usefulness of the described methodology to estimate the battery lifetime irrespective of the underlying battery chemistry.

**Temperature linearity**  For cycling at a given DOD level, it is observed that the cycle life shows a linear temperature dependency, at least in the range of 20 to 45 °C, a temperature range typically mentioned in the datasheets. This behaviour is illustrated in Figure 4.2 for the flooded lead-acid battery.

**Polynomial approximations**  The linearity on temperature dependency is exploited to create polynomial approximation functions. A 4$^{th}$ order polynomial approximation for the battery lifetime curves for the above-mentioned technologies is given by the following set of Equations.
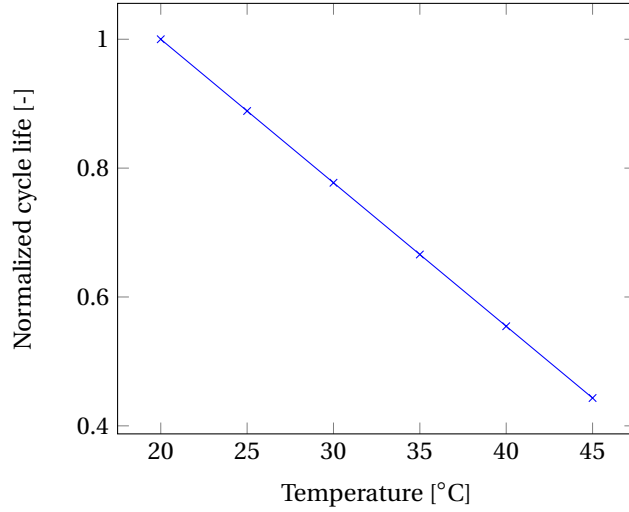
Figure 4.2: Normalized cycle life with temperature for a flooded lead-acid battery at 30% DOD with a reference temperature of 20°C. Data sourced from [28]).

$$n(T, DOD) = n(T_{\text{ref}}, DOD) - f(T_{\text{avg}})D_n(DOD) \tag{4.2}$$

$$n(T_{\text{ref}}) = p_4 d^4 + p_3 d^3 + p_2 d^2 + p_1 d + p_0 \tag{4.3}$$

$$f = p_{l_1} T_{\text{avg}} + p_{l_0} \tag{4.4}$$

$$D_n = p_{d_4} d^4 + p_{d_3} d^3 + p_{d_2} d^2 + p_{d_1} d + p_{d_0} \tag{4.5}$$

Where

$$n(T, DOD) = \text{Cycle life for a given temperature and DOD}$$
$$f = \text{A linear factor}$$
$$D_n = \text{Difference of } n \text{ between two temperatures}$$
$$p_0 \text{ to } p_4 = \text{Polynomial fitting coefficients at } T_{ref}$$
$$p_{l_1}, p_{l_0} = \text{Fitting coefficients for determining}$$
$$\text{the linear factor}$$
$$p_{d_0} \text{ to } p_{d_4} = \text{Fitting coefficients for difference}$$
$$\text{between two temperature curves}$$
$$T_{\text{avg}} = \text{Average operating temperature}$$
$$T_{\text{ref}} = \text{Reference operating temperature}$$
$$d = \text{Battery DOD}$$

A reconstruction of the battery lifetime curves depending on temperature and DOD from the battery datasheet is shown in Figure 4.3 for a flooded lead-acid battery. These

curves are then approximated as polynomial 'lookup' functions that can be used in battery lifetime estimation based on the application-specific battery usage.
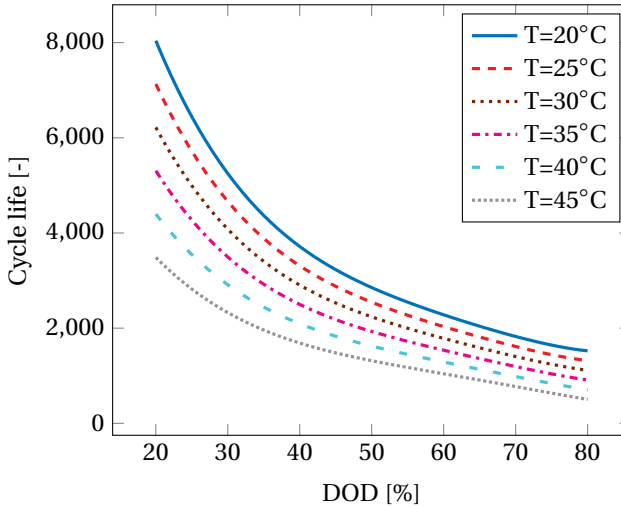


Figure 4.3: Reconstruction of battery cycle-life curves based on DOD for flooded lead-acid battery(data sourced from [28]).

It must be noted that many manufacturers do not explicitly distinguish between the ambient temperature and the actual battery operating temperature, and some even mention the battery cycle-life curves at ambient temperature [28, 26]. It is difficult to accurately determine the battery temperature, as it depends on several local operating conditions outside the electrical functioning of the system. In this study, the battery operating temperatures are taken to be at ambient levels, especially given the slow C-rates for the SHS batteries.

### 4.3.2. SHS APPLICATION AND LOAD PROFILE
An SHS application was considered as the use-case for investigating the battery usage and estimating the battery lifetime. The various inputs used for the SHS use-case for are described below.

#### LOAD PROFILE
As discussed before in Chapter 3, load profiles were constructed for the various tiers of the multi-tier framework based on the stochastic load profile construction methodology. For the SHS use-case described in this chapter, a tier 3 load profile was used, in line with the consumption limits outlined by the MTF [30]. This was done taking into account the efficient DC appliances that are on the rise in the off-grid market. Several works in the recent past have indicated a sharp rise in the availability as well as popularity of the so-called super-efficient DC appliances [2, 31, 32]. The operational (DC) loads that make up the load profile are LED lights, mobile phone charging, radio, TV, fridge, and a tablet, as described in Chapter 3.

**METEOROLOGICAL INPUTS**

The meteorological inputs to the model were obtained from the tool Meteonorm [33], which includes irradiance, wind speed and temperature. A sample geographical location experiencing an average of 5.5 equivalent sun hours per day was considered. The data resolution of the inputs to the model was 1-minute. Although far from instantaneous, it is assumed that a one-minute data resolution provides reasonable accuracy to incorporate the intermittency of the PV generation and the load profile.

**SHS PV SIZE**

The selected PV module is Jinko Solar JKM265P rated 265 Wp. One PV module is enough to cover the average daily energy needs for the given load profile. Additionally, the extra DC yield helps to compensate for the system inefficiencies. The PV output is modelled and corrected for thermal losses. As it is not the primary focus of this chapter, the detailed PV model is described in Appendix B.

**SHS BATTERY SIZE**

Loss of Load probability (LLP) was chosen as the optimizing parameter for finding the desired battery size. LLP is a metric defined as the ratio of the expected amount of downtime (system failure) of the system while delivering the demanded power, to the total amount of time the system was designed to deliver power for. The concept of LLP has been explained in a previous work in [4], and is explored in detail in Chapter 5, containing detailed SHS-level modeling and simulation. A battery size of 1440 Wh was considered for the given load profile and the chosen solar panel. This PV-battery combination guaranteed an LLP of 1.8% for the given load profile, i.e., this was the minimum storage size with the required PV size that could guarantee a total loss of load of 1.8% throughout the 1 year of simulation. The LLP optimization approach for the given load profile can be seen in Figure 4.4, where the chosen battery size and the corresponding LLP are marked on the graph.

**SHS SIMULATION**

An SHS model was constructed in MATLAB to simulate the functioning of the SHS for a year. Based on the load profile and the modelled PV output, the simulation was run over an arbitrary calendar year to obtain the battery usage pattern. It should be noted that the battery was limited to a maximum DOD limit of 80% in the simulation. The battery efficiency was assumed to be constant throughout the simulation, and certain constant efficiencies were assumed after a comparative study based on literature [34, 35, 36, 37, 38]. The efficiencies assumed are 85%, 90%, 78%, 93%, for flooded LA, LA-gel, NiCd, and LiFePO$_4$ respectively. Additionally, a constant electronic power conversion efficiency of 95% was assumed for the SHS. These efficiency numbers can also be specifically changed depending on the data from the manufacturer or the choice of a particular battery for the application without impacting the efficacy of the described methodology.

### 4.3.3. OVERALL BATTERY USAGE MODEL

In the overall battery usage method, the lifetime is estimated based on the overall battery usage that is extracted from the 1-year SHS simulation. The main parameters for
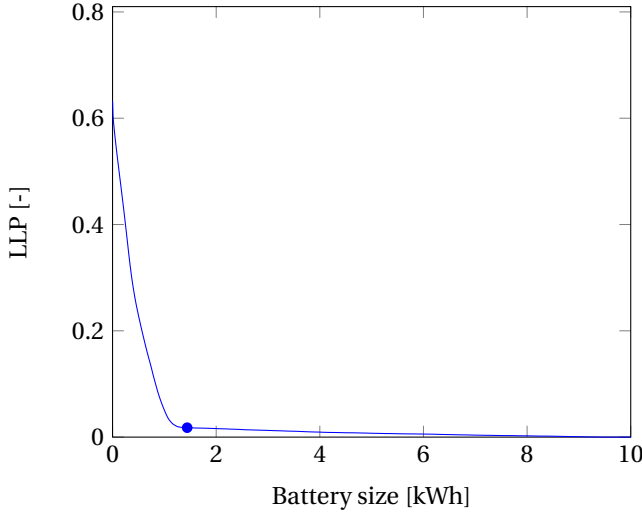
Figure 4.4: Loss of load probability (LLP) curve for the given load profile with varying storage sizes. A battery size of 1440 Wh (marked on the graph) is deemed sufficient through this analysis, resulting in an LLP of 1.8%.

estimating the battery lifetime are the average DOD and average temperature in battery operation. These were derived from the battery usage in two different ways, viz. the coarse average DOD and the micro-cycle zero-crossings-based approach.

#### Coarse average approach

This is the less computationally demanding approach of the two, where the required average DOD and temperature values are simply taken as the average of all the data points throughout the simulation, as shown in Equation 4.6.

$$\overline{DOD} = \frac{\sum_{i=1}^{N} DOD_i}{N}$$
$$\overline{T} = \frac{\sum_{i=1}^{N} T_i}{N} \tag{4.6}$$

Where $\overline{DOD}$ and $\overline{T}$ are the average DOD and temperature, $N$ is the total number of data points in the simulation.

While computationally less intensive, a simple average does not capture the battery usage well. This is because not only does this method include the extraneous, inactive battery periods, but also the battery processes different amounts of energy throughput under different DODs. Therefore, a more weighted approach needs to be used for taking this into account.

#### Zero-crossing (ZC) approach

In the micro-cycle zero-crossing (ZC) approach, micro-cycles of battery activity are defined based on the zero-crossings of the battery current. Therefore, only the active battery

cycling periods are considered. This concept was introduced in a recent publication from the authors [5].

A micro-cycle in this context is defined as a small cycle of variable duration that exists between two consecutive current zero crossings; this is typically much shorter than a full charge-discharge cycle. This method involves taking into account all the zero current transitions given the 1 minute data resolution.

Figure 4.5 illustrates this concept. In this case, the active DOD should only be considered for the durations that the battery is cycling. Therefore, the states with battery current $I_{battery} = 0$ are ignored. Note that the concept can be equivalently explained if the battery power $P_{battery}$ is considered instead of $I_{battery}$. In that case, the area of each micro-cycle would give the energy that the battery cycles in that interval.
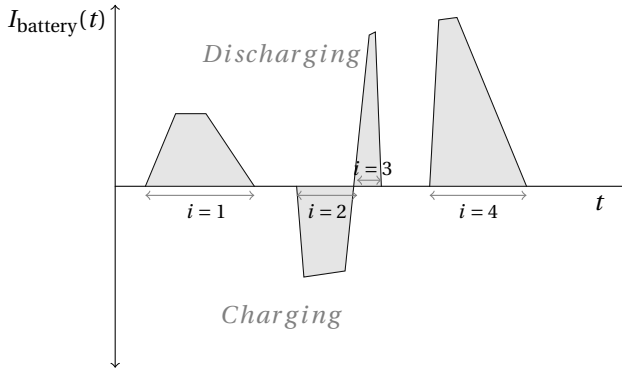


Figure 4.5: An illustrative battery current waveform showing arbitrary micro-cycle intervals, where $i$ is the micro-cycle number.

Finally, with the micro-cycle zero-crossing data extracted from the battery simulation, the average active DOD can be calculated as shown in Equation 4.7.

$$\overline{DOD} = \frac{\sum\limits_{i=1}^{N} \overline{DOD_i}.E_{thr_i}}{\sum\limits_{i=1}^{N} E_{thr_i}} \tag{4.7}$$

Where $\overline{DOD}$ : Combined average active DOD due to all the micro-cycles, $\overline{DOD_i}$ : Average active DOD in the $i^{th}$ micro-cycle, $E_{thr_i}$ : Total energy throughput in the $i^{th}$ micro-cycle, $N$ : total number of ZC-based micro-cycles.

The average temperature is calculated based on the duration of the ZCs as follows.

$$\overline{T} = \frac{\sum\limits_{i=1}^{N} \overline{T_i}.T_{ZC_i}}{\sum\limits_{i=1}^{N} T_{ZC_i}} \tag{4.8}$$

Where $\overline{T}$ : Combined average temperature due to all the micro-cycles, $\overline{T_i}$ : Average temperature in the $i^{th}$ micro-cycle, $T_{ZC_i}$ : Total duration of the $i^{th}$ micro-cycle.

### LIFETIME ESTIMATION BASED ON OVERALL BATTERY USAGE

Once the $\overline{DOD}$ is known, the cycle-life number $n$ is then obtained from the look-up functions described in Section 4.3.1. The battery lifetime is then estimated as shown in Equation 4.9 below [5].

$$L = n \times \overline{DOD} \times \frac{2 \times E_{\text{nom}}}{\sum\limits_{i=1}^{N} E_{\text{thr}_i}} \tag{4.9}$$

Where ($L$) is the battery lifetime in years, and $E_{\text{nom}}$ is the nominal battery energy capacity in Wh.

**Assumptions under overall battery usage methodology**    In the overall battery usage methodology, there are a few crucial assumptions that serve the balance between the complexity of implementation and accuracy. These are as follows.

1. The battery performs throughout the 1-year simulation without any loss in capacity.

2. The battery performance in terms of the dynamic SOC is irrespective of its SOH. That is, the SOC of the battery is not corrected for its faded capacity during the simulation.

3. Only one year of intended battery usage is enough to be able to linearly extrapolate the battery usage and hence the cycle life.

The major drawback of this method is that there is no loss in capacity of the battery during the simulation. Instead, the battery lifetime is estimated based on the overall battery usage for one year. It would be more accurate to estimate the battery lifetime while taking the capacity fading into account dynamically in the battery performance, as discussed in the next section.

### 4.3.4. DYNAMIC CAPACITY FADING MODEL

The dynamic capacity model fundamentally differs from the overall battery usage method for battery lifetime estimation, in that this model dynamically assesses the damage caused due to the stress factors after every ZC micro-cycle. This model is implemented through a process explained in the flowchart illustrated in Figure 4.6.

The SHS simulation starts as in the overall battery usage method, with SOH = 100%. The simulation is executed in 3 stages using the model. In Stage A, the battery activity is probed within the SHS simulation. Zero-crossings (ZCs) are recorded, and the capacity damage computations within this model start when the battery activity data is extracted for a ZC-based micro-cycle. This includes evaluating the average battery DOD ($\overline{DOD_i}$), the energy throughput ($E_{\text{thr}_i}$) and the average temperature ($\overline{T_i}$) for the $i^{\text{th}}$ ZCs micro-cycle as shown in Equations 4.7 and 4.8.

In Stage B, the total number of cycles $n(\overline{T_i}, \overline{DOD_i})$ possible at the DOD and temperature levels is calculated using the polynomial lookup functions described in Section 4.3.1. Additionally, the proportional number of cycles ($\alpha_i(E_{\text{thr}_i}, E_{\text{nom}}), \overline{DOD_i}$) spent under the same DOD and temperature levels for the $i$th ZCs micro-cycle is calculated as a function
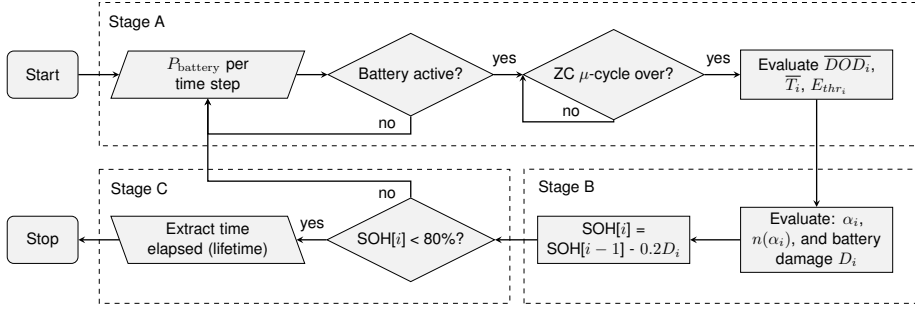
Figure 4.6: Flowchart explaining the dynamic capacity fading model for lifetime estimation.

of the energy throughput ($E_{\text{thr}_i}$) and the nominal battery capacity ($E_{\text{nom}}$), as shown in Equation 4.10.

$$\alpha_i = \frac{E_{\text{thr}_i}}{2 \times E_{\text{nom}} \times \overline{DOD_i}} \tag{4.10}$$

The damage ($D_i$) incurred to the battery life is then calculated using the Palmgren-Miner rule. This rule states that the lifetime of a component after undergoing a series of load events is reduced by a finite fraction corresponding to each of the load events. This fraction is the ratio between the number of cycles the element has undergone under a particular stress factor (or load event) to the total expected number of expected cycles until EOL under that stress factor [9, 13]. Equation 4.11 represents the Miner's rule.

$$D = \sum_{i=1}^{E} D_i = \sum_{i=1}^{E} \frac{\alpha_i}{n(\alpha_i)} \tag{4.11}$$

Where $\alpha_i$: number of cycles spent under a stress factor $\sigma_i$ (DOD and temperature), $n(\alpha_i)$: total number of cycles for the EOL to be reached, $E$: number of events taken place until the EOL condition is reached, $D$: total damage accumulated, and $D_i$: damage at the battery for each one of these events. This damage is then scaled and subtracted from the current SOH. The damage scaling is done to ensure that when the total damage $D = 1$, the SOH is 80%.

Stage C involves checking for the EOL of the battery after every ZC micro-cycle of activity. If the SOH has reached 80% or below (or, in other words, if the damage $D$ equals a value of 1.), the simulation ends, and the SOH data is extracted as a function of time. If SOH is > 80%, the simulation continues in Stage A with the updated SOH. The stages repeat until the battery accumulates enough damage to reach its EOL. Note that the DOD values are all dynamic, i.e., the DOD values are computed based on the updated battery capacity after every micro-cycle.

### SALIENT FEATURES OF THE DYNAMIC CAPACITY FADING MODEL
The dynamic capacity fading model is a significant upgrade over the overall battery usage model both in complexity and accuracy with which the micro-degradation per ZC micro-cycle is assessed. It has the following salient features.

1. **High resolution** Given that the model captures the micro-cycle degradation, the dynamic capacity fading model serves with a high degree of resolution of the battery degradation. Thus, the model can potentially capture the micro-degradation in a time-step as small as the time resolution of the input data used for the application.

2. **Dynamic battery parameters** Battery parameters like DOD and SOC are updated after every ZC micro-cycle based on the degraded battery capacity. Therefore, the battery performance is not independent of the capacity fading.

3. **SOH estimation** The model allows for SOH to be estimated after every micro-cycle, which is not possible with the overall battery usage model.

4. **Technology independent** Given that the model is independent of electrochemical processes for its implementation, it can be used for any battery technology. In this study it is used to estimate the battery lifetime for 4 battery technologies.

5. **Application independent** Without any loss of generality, this model can be used to estimate the battery lifetimes for other applications too, especially those applications where the battery cycling undergoes cycling at similar C-rates as those of SHS.

6. **Usefulness at battery level** Most performance-based experimentally constructed models are based on cell-level experiments, and the same battery technology might exhibit different characteristics at the battery level. With the proposed model, one can pick a candidate battery product and proceed to estimate the battery lifetime at the system design stage.

## 4.4. Results and discussions

### 4.4.1. Battery Usage

The battery experiences a wide range of DOD levels due to the intermittent nature of the incident solar irradiance on the SHS and the varying load profile. This can be seen from Figure 4.7 that shows the normalized frequency of the different DOD levels throughout the year for the lead-acid gel battery under 2 cases, viz. considering the overall battery DOD data and only the active battery DOD data.

The active battery data points were considered based on the zero-crossings, as described in Section 4.3.3. As seen in Figure 4.7, the two different cases differ in their DOD levels. Between 10% to 70% DOD the active DOD occur relatively more frequently. However, in the very shallow (0–10%), and very deep DOD levels (70–80%), the trend is reversed, showing a lesser occurrence of active DODs, underlining the periods of inactivity of the battery. This corresponds to when the battery was either full (not needed to power the load) or empty (could not power the load). Moreover, the maximum limit of the DOD shown in the histogram is 80%, owing to the lower limit of the battery SOC fixed at 20% in the simulation.

Additionally, the battery cycling related data is extracted using both the coarse average and the ZCs approach. The results are shown in Table 4.2.
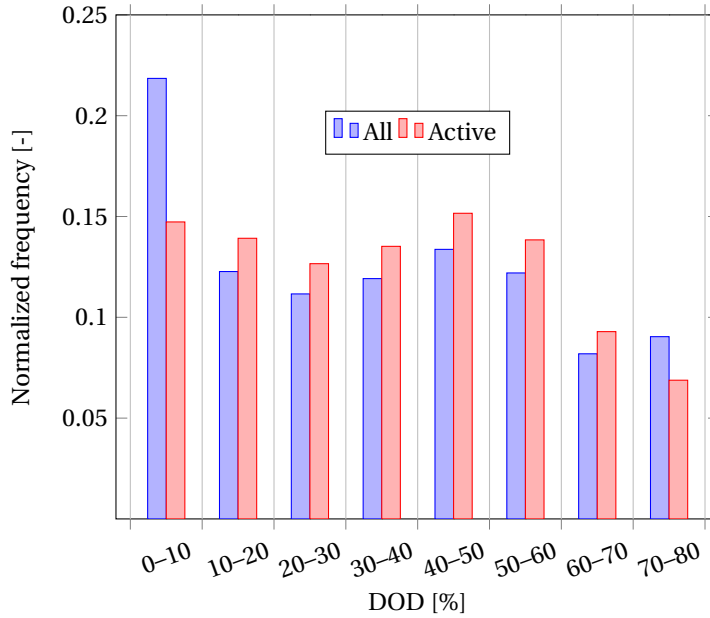
Figure 4.7: Normalized frequency of the DODs experienced by the lead-acid gel battery for both the overall battery DOD data and only the active battery DOD data.

A difference can be seen across the 4 battery technologies for the various battery parameters. In general, the coarse average-based DOD is more optimistic than the ZCs-based DOD for all the technologies. The difference in the DOD using the same method for different batteries comes from the fact that the different batteries have different operating efficiency, and therefore need to cycle differently in order to meet the storage demand of the given SHS application. Similarly, the energy throughputs of the different battery technologies are also different. The coarse-average temperature is the same for every battery technology based on the meteorological data, while the ZCs-based temperature is slightly different, depending on the duration of the ZC-cycles (Equation 4.8), which differ across technologies.

LiFePO$_4$ fares the best across the different battery statistics, while the NiCd battery fares the worst. Lead-acid gel battery performs slightly better than its flooded counterpart. In general, the more efficient the battery, the lower the DOD as well as temperature and energy throughput for the exact same application. Consequently, the cycle life will also be higher than that of a battery with lower efficiency, as seen in Section 4.4.2 below.

Even though the average DOD values between the two methods differ only by about 1–1.5%, this difference can be significantly amplified based on the battery size chosen and the SHS load requirements. For example, oversizing the battery (lower LLP) would have resulted in a larger difference between the coarse average and the ZCs-based active DOD calculations. Going forward, the more conservative ZCs-based battery lifetime results are discussed, as using a coarse average-based estimation can yield to an optimistic prediction of battery lifetime.

Table 4.2: Usage statistics for the 4 battery technologies over 1 year of SHS simulation. LA: lead-acid, CA: Coarse average-based, ZC: Zero crossings-based.

| Battery | $\overline{DOD}$ (%) | | $\overline{T}$ (°C) | | $E_{thr}$ (kWh/ year) |
|---|---|---|---|---|---|
| | CA | ZC | CA | ZC | |
| Flooded LA | 37.81 | 38.21 | 27.16 | 26.94 | 613.9 |
| LA gel | 36.23 | 36.73 | 27.16 | 26.78 | 589.7 |
| NiCd | 39.77 | 40.04 | 27.16 | 27.2 | 647.7 |
| LiFePO$_4$ | 35.11 | 35.66 | 27.16 | 26.7 | 575.7 |

### 4.4.2. LIFETIME ESTIMATION
Based on the battery usage discussed in Section 4.4.1, the battery lifetime is estimated based on the methodologies described in Section 4.3.

#### OVERALL BATTERY USAGE-BASED LIFETIME ESTIMATION
The results for the overall battery usage-based estimated lifetimes are shown in Table 4.3.

Table 4.3: Cycle life and battery lifetime in years, based on the overall battery usage-based lifetime estimation. LA: Lead-acid.

| Technology | Cycle life (-) | Lifetime (years) |
|---|---|---|
| Flooded LA | 3329 | 6 |
| LA gel | 3796 | 6.8 |
| NiCd | 1662 | 3 |
| LiFePO$_4$ | 16450 | 29.4 |

Following the battery usage statistics discussed in Section 4.4.1, the battery lifetime follows a similar relative trend. LiFePO$_4$ comprehensively outperforms the other battery technologies, having an estimated battery lifetime of nearly 5 times the lead-acid batteries and almost 10 times the NiCd battery.

#### DYNAMIC LIFETIME ESTIMATION
Based on the dynamic lifetime estimation method described in Section 4.3.4, the battery lifetimes for the SHS use-case were estimated for the 4 battery technologies. The results for the dynamic capacity fading-based lifetime estimation are shown in Figure 4.8. For comparison, the results from the overall battery usage-based estimation method are also plotted.

As seen in Figure 4.8, the dynamic lifetime estimation is found to be much more conservative, with lifetimes for LA-gel, LA-flooded, NiCd, LiFePO$_4$ batteries as 5.6, 5.1, 2.86, and 16.7 years, which are 18%, 14%, 3%, and 43% less than the corresponding overall usage-based lifetime estimates, respectively. This is attributed to the fact that dynamic lifetime degradation captures the micro-degradation of the battery capacity for every micro-cycle. Consequently, the battery is progressively degraded as it enters the next
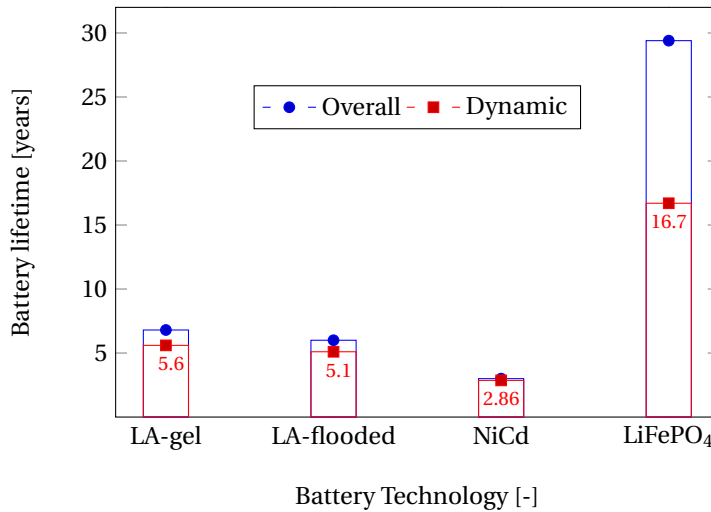
Figure 4.8: Dynamic battery lifetime estimation results for the 4 battery technologies in comparison with the results using the overall battery usage method.

micro-cycle with a faded capacity, instead of calculating the lifetime based on overall usage of one year where the battery performs identically without any degradation. Therefore, the dynamic capacity fading model-based lifetime estimation is considered more practical and realistic. Additionally, the longer the battery lasts, the more pronounced effect of dynamic capacity fading. Therefore, from NiCd to LiFePO$_4$ the deviation from the overall battery lifetime estimation method is increasing.

Of course, it must be noted that the methodology described here relies on the manufacturer's datasheet, and therefore the relative lifetime estimation for this particular SHS application need not be extendable to all battery products from the same technology. This is because different battery products from the same technology often display varying cycle lives depending on the construction geometry, propriety manufacturing processes, amongst others.

A comparison of this model is also made with an experimentally obtained empirical model for capacity fading of LiFePO$_4$, as explained in Section 4.4.3.

### 4.4.3. COMPARISON WITH AN EMPIRICAL BATTERY LIFETIME ESTIMATION MODEL

As an experimental validation of the dynamic lifetime estimation model at the battery pack level can take an impractically long time, the accuracy of the model was compared to the results obtained from another experimentally created, empirical-based lifetime estimation model based on LiFePO$_4$ battery technology as described in [39]. The empirical model can been described by the Equations 4.12 and 4.13 [39].

$$cf = \sum_{i}^{E} \Big( (k_{s1}SOC_{dev,i}.e^{k_{s2}.SOC_{avg,i}} + k_{s3}.e^{k_{s4}.SOC_{dev,i}})$$
$$.e^{\left(-\frac{Eg}{R}\left(\frac{1}{T_i} - \frac{1}{T_{ref}}\right)\right)} \Big) Ah_i \qquad (4.12)$$

Where $cf$ is the capacity fading experienced by the battery due to all the cycling events E, $i$ is an event for an arbitrary length of time, $Ah_i$ is the total charge processed during event $i$, $E$ is the total number of events.

The temperature dependence term comes from the Arrhenius equation, where $k_{s1}$ to $k_{s4}$ are constants determined experimentally and reported in [39], $SOC_{dev,i}$ is the normalized standard deviation from $SOC_{avg}$ in event $i$. This value is derived from Equation 4.13 [5].

$$SOC_{dev} = \sqrt{\frac{3}{\Delta Ah_m} \int_{Ah_{m-1}}^{Ah_m} (SOC(Ah) - SOC_{avg})^2 . dAh} \qquad (4.13)$$

To be applied in the SHS application discussed in this study, Equation 4.12 was adapted to the battery usage obtained in the SHS use-case. Similar to the approach discussed in Section 4.3.4, the capacity fading was calculated per cycling event (ZC micro-cycle) with the help of Equations 4.12 and 4.13. Consequently, the battery lifetime was found to be 14.3 years, about 14.2% deviation from the dynamic battery lifetime estimation method.

The State of Health (SOH) is also calculated based on the empirical method, which is discussed along with the other SOH results in Section 4.4.3 below.

### STATE OF HEALTH (SOH)

While the lifetime results mentioned above give a measure of the overall battery life for the given application, the SOH results over time give a measure of the rate of the capacity fading for different battery technologies. For the given battery lifetime estimation modelled in this study, the State of Health (SOH) was computed for the different batteries under operating conditions, i.e., taking only cyclic ageing into account.

The results are plotted in Figure 4.9. For the same starting battery capacity, the slowest fading rate is seen to be experienced by the LiFePO$_4$ battery, while the fastest rate (steepest slope) is experienced by the considered NiCd battery. The SOH results seem to show a near-linear trend over time.

Additionally, the SOH is plotted for the empirical lifetime estimation model for the same SHS use-case considered, as shown in Figure 4.9. The SOH from the empirical model follows the dynamic lifetime estimation method-based SOH (both for LiFePO$_4$) closely, especially up to 89% SOH. After year 10, the SOH estimates start to deviate. The SOH deviations at the various year-marks differ by a maximum of 2.8%. However, it must be noted that the comparison with empirical model is only valid for the LiFePO$_4$ battery technology and as such the degree of accuracy shown by this comparison cannot be extended to other technologies solely on this basis. No empirical models were found for the other technologies at the time of writing this chapter, which could enable a similar
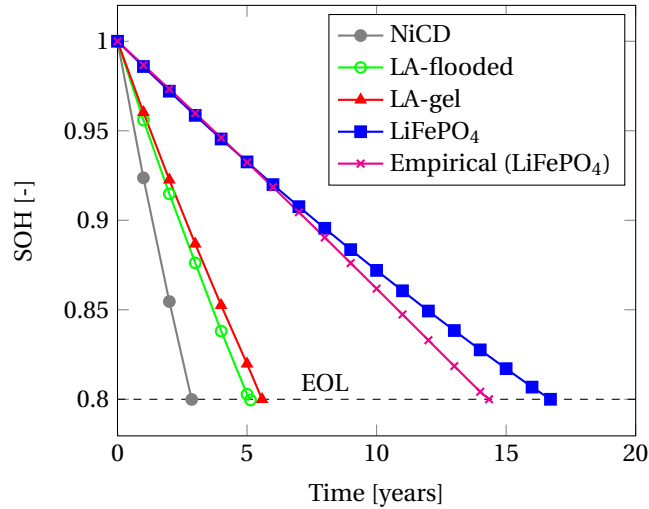
Figure 4.9: SOH for the different battery technologies as estimated by the dynamic lifetime method. The black dashed line denotes the end of life.

comparison for the SHS use-case for the exact same stress factors as considered in the proposed methodology.

In summary, the main difference between the 2 proposed models, viz. the overall usage model, and the dynamic capacity fading model, is the increased complexity and accuracy of the dynamic capacity fading model. Within the overall battery usage model, the coarse average approach is rather crude but quick, while the ZC micro-cycle-based approach is more computationally demanding. However, the overall battery usage model is not without its assumptions, as discussed in Section 4.3.3. The dynamic capacity fading model is the most complex but remarkably matches the experimentally derived empirical model until about 89% SOH.

### 4.4.4. RELEVANCE FOR SHS DESIGN

In the context of SHS application, the battery lifetime estimation exercise is quite relevant, as mentioned previously in Section 4.1. This is even more relevant in the off-grid electrification segment, where system reliability plays a critical role in technology adoption.

Compared to a typical PV module that lasts 25 years, an SHS battery usually lasts much less. Therefore, the battery will need to be replaced in the SHS lifetime. Having a larger battery size leads to lower levels of average DOD while cycling. Thus, a larger battery size not only increases the lifetime but also consequently reduces the number of battery replacements needed in the SHS lifetime. This presents an interesting trade-off between the upfront costs and battery replacement costs; the cost of having an increased lifetime (and therefore increased battery size) for the same application is the increased upfront costs that come along with a larger battery size. Therefore, estimating the battery lifetime at the SHS design stage can help optimize this delicate trade-off between upfront costs and battery replacement costs. The methodology described in this chapter was

used to investigate the impact of SHS battery sizing on battery lifetime to underline the importance of estimating battery lifetime at the SHS design stage. This can be found in Chapter 5, where SHS is optimally sized while taking battery lifetime into account.

## 4.5. CONCLUSION

This chapter described a practical methodology for estimating the battery lifetime without needing to model the electrochemical processes within the battery or needing dedicated experiments. Moreover, this methodology uses available battery data from the manufacturer for candidate battery technologies at hand. The methodology is applicable irrespective of the battery technology, as it is independent of the technology-specific electro-chemical processes. The methodology can also be extended to other applications experiencing similar battery C-rates without loss of generality. The described methodology is expected to help SHS designers make informed decisions with respect to the battery storage at the system sizing stage.

Dynamic capacity fading model introduced in this chapter was deemed more practical than the overall battery usage model. For a given load profile and specific SHS system size, the estimated lifetimes for LA-gel, LA-flooded, NiCd, LiFePO$_4$ batteries were 5.6, 5.1, 2.86, and 16.7 years, respectively using the dynamic capacity fading model. Comparison of this proposed dynamic model with an experimentally derived empirical model of LiFePO$_4$ battery yielded very close results, with the SOH values over time being within 2.8% of each other.

The battery lifetime estimation methodology described in this chapter is also used in Chapter 5 to perform a multi-objective optimization for determining optimal system sizes for SHS.

## REFERENCES

[1] Good Solar Initiative, *Quality Charter: Quality Standards for Accredited Solar Suppliers.* Good Solar Initiative, 2016.

[2] A. A. Phadke, A. Jacobson, W. Y. Park, G. R. Lee, P. Alstone, and A. Khare, "Powering a home with just 25 watts of solar pv. super-efficient appliances can enable expanded off-grid energy service using small solar power systems," tech. rep., Lawrence Berkeley National Laboratory (LBNL), Berkeley, CA (United States), 2015.

[3] N. Narayan, J. Popovic, J. C. Diehl, S. Silvester, P. Bauer, and M. Zeman, "Developing for developing nations: Exploring an affordable solar home system design," in *2016 IEEE Global Humanitarian Technology Conference (GHTC)*, pp. 474–480, Oct 2016.

[4] T. D. Heeten, N. Narayan, J. C. Diehl, J. Verschelling, S. Silvester, J. Popovic-Gerber, P. Bauer, and M. Zeman, "Understanding the present and the future electricity needs: Consequences for design of future solar home systems for off-grid rural electrification," in *2017 International Conference on the Domestic Use of Energy (DUE)*, pp. 8–15, April 2017.

[5] N. Narayan, T. Papakosta, V. Vega-Garita, J. Popovic-Gerber, P. Bauer, and M. Zeman, "A simple methodology for estimating battery lifetimes in solar home system design," in *2017 IEEE AFRICON*, pp. 1195–1201, Sept 2017.

[6] C. Zou, C. Manzie, D. Nešić, and A. G. Kallapur, "Multi-time-scale observer design for state-of-charge and state-of-health of a lithium-ion battery," *Journal of Power Sources*, vol. 335, pp. 121–130, 2016.

[7] C. Zou, X. Hu, Z. Wei, and X. Tang, "Electrothermal dynamics-conscious lithium-ion battery cell-level charging management via state-monitored predictive control," *Energy*, vol. 141, pp. 250 – 259, 2017.

[8] C. Zou, X. Hu, Z. Wei, T. Wik, and B. Egardt, "Electrochemical estimation and control for lithium-ion battery health-aware fast charging," *IEEE Transactions on Industrial Electronics*, vol. 65, pp. 6635–6645, Aug 2018.

[9] V. Marano, S. Onori, Y. Guezennec, G. Rizzoni, and N. Madella, "Lithium-ion batteries life estimation for plug-in hybrid electric vehicles," in *2009 IEEE Vehicle Power and Propulsion Conference*, pp. 536–543, Sept 2009.

[10] M. Dubarry, B. Y. Liaw, M.-S. Chen, S.-S. Chyan, K.-C. Han, W.-T. Sie, and S.-H. Wu, "Identifying battery aging mechanisms in large format li ion cells," *Journal of Power Sources*, vol. 196, no. 7, pp. 3420 – 3425, 2011.

[11] V. Agarwal, K. Uthaichana, R. A. DeCarlo, and L. H. Tsoukalas, "Development and validation of a battery model useful for discharging and charging power control and lifetime estimation," *IEEE Transactions on Energy Conversion*, vol. 25, pp. 821–835, Sept 2010.

[12] R. Dufo-López, J. M. Lujano-Rojas, and J. L. Bernal-Agustín, "Comparison of different lead-acid battery lifetime prediction models for use in simulation of stand-alone photovoltaic systems," *Applied Energy*, vol. 115, pp. 242 – 253, 2014.

[13] M. A. Tankari, M. B. Camara, B. Dakyo, and G. Lefebvre, "Use of ultracapacitors and batteries for efficient energy management in wind -diesel hybrid system," *IEEE Transactions on Sustainable Energy*, vol. 4, pp. 414–424, April 2013.

[14] M. Musallam and C. M. Johnson, "An efficient implementation of the rainflow counting algorithm for life consumption estimation," *IEEE Transactions on Reliability*, vol. 61, pp. 978–986, Dec 2012.

[15] T. Dragičević, H. Pandžić, D. Skrlec, I. Kuzle, J. M. Guerrero, and D. S. Kirschen, "Capacity optimization of renewable energy sources and battery storage in an autonomous telecommunication facility," *IEEE Transactions on Sustainable Energy*, vol. 5, pp. 1367–1378, Oct 2014.

[16] T. M. Layadi, G. Champenois, M. Mostefai, and D. Abbes, "Lifetime estimation tool of lead-acid batteries for hybrid power sources design," *Simulation Modelling Practice and Theory*, vol. 54, pp. 36 – 48, 2015.

[17]  D. G. für Sonnenenergie, *Planning and Installing Photovoltaic Systems: A Guide for Installers, Architects and Engineers*. Planning and Installing, Taylor & Francis, 2008.

[18]  P. Mohanty, T. Muneer, and K. Mohan, *Solar Photovoltaic System Applications*. Springer, 2016.

[19]  M. R. Palacin and A. de Guibert, "Why do batteries fail?," *Science*, vol. 351, no. 6273, pp. 1253292–1253292, 2016.

[20]  P. Keil, S. F. Schuster, J. Wilhelm, J. Travi, A. Hauser, R. C. Karl, and A. Jossen, "Calendar Aging of Lithium-Ion Batteries," *Journal of The Electrochemical Society*, vol. 163, no. 9, pp. A1872–A1880, 2016.

[21]  M. T. Lawder, P. W. C. Northrop, and V. R. Subramanian, "Model-Based SEI Layer Growth and Capacity Fade Analysis for EV and PHEV Batteries and Drive Cycles," *Journal of The Electrochemical Society*, vol. 161, no. 14, pp. A2099–A2108, 2014.

[22]  P. Ruetschi, "Aging mechanisms and service life of lead-acid batteries," *Journal of Power Sources*, vol. 127, no. 1-2, pp. 33–44, 2004.

[23]  K. Brik and F. Ben Ammar, "Causal tree analysis of depth degradation of the lead acid battery," *Journal of Power Sources*, vol. 228, pp. 39–46, 2013.

[24]  J. C. Viera, M. González, J. C. Anton, J. C. Campo, F. J. Ferrero, and M. Valledor, "NiMH vs NiCd batteries under high charging rates," *INTELEC, International Telecommunications Energy Conference (Proceedings)*, 2006.

[25]  J. Wang, P. Liu, J. Hicks-Garner, E. Sherman, S. Soukiazian, M. Verbrugge, H. Tataria, J. Musser, and P. Finamore, "Cycle-life model for graphite-LiFePO4 cells," *Journal of Power Sources*, vol. 196, no. 8, pp. 3942–3948, 2011.

[26]  Hoppecke, Germany, *Installation , commissioning and operating instructions for valve-regulated stationary lead-acid batteries - Solar Battery Data Sheet*, 2013.

[27]  Valence | Lithium Ion Phosphate Battery Manufacturer, "Valance battery cyclelife curves." url=https://www.valence.com/why-valence/long-lifecycle/, 2017. Date last accessed: 2017-05-03.

[28]  Hoppecke, Germany, *Installation , commissioning and operating instructions for vented stationary lead-acid batteries - Solar Battery Data Sheet*, 2013.

[29]  Alpha Technologies, Inc., United States, *Alpha Power - Industrial Ni-Cd Batteries Standard Range Technical Manual*, 2009.

[30]  M. Bhatia and A. Nicolina, *Capturing the Multi-Dimensionality of Energy Access*. Live Wire, 2014/16. World Bank, Washington, DC. ©World Bank, 2014.

[31]  Global LEAP, "The State of the Off-Grid Appliance Market," *Tech. Rep.*, 2016.

**4**

[32] H. Olk and J. Mundt, "Photovoltaics for productive use applications. a catalogue of dc-appliances," *Deutsche Gesellschaft für Internationale Zusammenarbeit (GIZ) GmbH*, 2016.

[33] Meteotest, "(software) meteonorm ver 7.1," 2014.

[34] B. Dunn, H. Kamath, and J.-m. Tarascon, "Electrical energy storage for the Grid : A Battery of choices," *Science Magazine*, vol. 334, no. 6058, pp. 928–936, 2011.

[35] P. Van den Bossche, F. Vergels, J. Van Mierlo, J. Matheys, and W. Van Autenboer, "SUBAT: An assessment of sustainable battery technology," *Journal of Power Sources*, vol. 162, no. 2 SPEC. ISS., pp. 913–919, 2006.

[36] K. Hojckova, J. Jelinek, M. Schneider, N. Spittler, and I. Varju, "Evaluation of battery storage technologies for sustainable and rural electrification in sub-saharan africa," *Regional Academy on the United Nations*, 2014.

[37] X. Luo, J. Wang, M. Dooner, and J. Clarke, "Overview of current development in electrical energy storage technologies and the application potential in power system operation," *Applied Energy*, vol. 137, pp. 511–536, 2015.

[38] R. M. Herritty and J. Midolo, "Nickel cadmium batteries for photovoltaic applications," in *Thirteenth Annual Battery Conference on Applications and Advances. Proceedings of the Conference*, pp. 255–257, Jan 1998.

[39] L. Lam, "A practical circuitbased model for state of health estimation of liion battery cells in electric vehicles," Master's thesis, Delft University of Technology, August 2011.

**4**

# 5

# EXPLORING SHS BOUNDARIES FOR ELECTRIFICATION: OPTIMAL SHS SIZING

*As long as poverty, injustice and gross inequality persist in our world, none of us can truly rest*

Nelson Mandela

## ABSTRACT

Optimal system sizing for SHS is a vital task as both oversizing and undersizing a system can be detrimental to system cost and power availability, respectively. This chapter presents an optimal SHS sizing methodology that minimizes the loss of load probability (LLP), excess energy dump, and battery size while maximizing the battery lifetime. A genetic algorithm-based multi-objective optimization approach is utilized to determine the optimal SHS sizes. The potential for SHS to cater to every tier of the Multi-tier framework (MTF) for measuring household electricity access is examined. The optimal system sizes for standalone SHS are found for different LLP thresholds. Results show that beyond tier 2, the present day SHS sizing needs to be expanded significantly to meet the load demand. Additionally, it is deemed untenable to meet the electricity needs of the higher tiers of MTF purely through standalone SHS without compromising one or more of the system metrics. A way forward is proposed to take the SHS concept all the way up the energy ladder such that load demand can also be satisfied at tier 4 and 5 levels.

**OUTLINE**

This chapter is divided into five sections. Section 5.1 introduces the chapter, underlining the motivation for optimal system sizing and presenting a literature review. Section 5.2 describes the various parameters and metrics used in the study. Section 5.3 details all the steps considered in the methodology, while Section 5.4 discusses the results and their implication on the utility of SHS as a solution for electrifying higher tiers of the MTF. Finally, Section 5.5 concludes the chapter with the closing thoughts.

## 5.1. INTRODUCTION

In this chapter, an optimal sizing methodology is introduced to optimally size SHS for every tier of the MTF, which gives insights on the level of PV and battery storage needed to enable electrification across the various tiers.

### 5.1.1. IMPORTANCE OF OPTIMAL SHS SIZING

SHS sizing comprises the PV sizing, battery sizing, and the sizing of the power converters. PV sizing mainly depends on the total energy needed from the PV generator, which in turn depends on the load profile. A lower than adequate PV size results in system failure or a high number of loss of load events, i.e., high loss of load probability (LLP). LLP is a system metric that quantifies the system's reliability in meeting the load demand, as explained in detail in Section 5.2.1. A higher than adequate PV size, however, increases the amount of energy dumped — or the non-utilization of solar energy — when the load is satisfied and the battery is full.

Power converter sizing mainly depends on the peak power of the PV and the load. Some degree of dimensioning flexibility can be achieved depending on the undersizing of the converter. A lower than peak power of the converter may not be suited for peak power operation but can perform more efficiently at most of the other operating points. This depends mainly on the frequency of occurrence of the different power levels expected throughout the operation of the converter. Thus, a suitably lower than peak sized converter can lead to cost savings. Compared to PV and power converter, however, battery sizing is far more involved.

The battery is a vital component of the SHS that not only enables energy storage of the PV output but also caters to the load when there is no solar generation. However, the battery is the most expensive SHS component while suffering from low lifetimes as compared to other SHS components. Additionally, a smaller than adequate battery size will result in failure to meet the load requirements (high LLP), while an oversized battery will drastically increase the upfront costs of the system. Also, a larger battery size can lead to lower depth of discharge (DOD) levels, and therefore higher lifetime, whereas a smaller battery size can lead to lower lifetimes due to the deep DOD levels [1, 2]. Usual battery lifetimes are much lower than typical PV module lifetime of 25 years. Therefore, a higher battery lifetime is advantageous as it means fewer replacements during the SHS lifetime. Battery costs and lifetime thus have an intricate relationship, making battery sizing extremely relevant albeit challenging in SHS design. Battery sizing and lifetime can, therefore, be considered as critical parameters when dimensioning an SHS.

An optimal SHS size can thus be considered as one that results from an SHS dimen-

sioning exercise that minimizes the LLP, excess energy, and battery size while maximizing the battery lifetime.

### 5.1.2. LITERATURE STUDY

In general terms, most sizing-based studies utilize sizing criteria that result in a good trade-off between the system reliability (or power availability) and system investment cost. Previous studies have dealt with the sizing problem by only looking at one or two metrics, including LLP [3, 4], system cost, and battery lifetime [5]. LLP has been considered as an objective in [6] as well as a constraint. In [7], the main objective function was to minimize the total SHS investment cost, while keeping LLP ≤ 2%. LLP was also used as the primary sizing criterion for an off-grid PV-battery system in Bolivia [8], where the system size was determined for three different case studies: a household, school, and health center.

Additionally, battery lifetime has been included as a key parameter in a single weighted objective optimization for a PV array, diesel generator and battery system to minimize battery degradation and fuel consumption [9]. Similarly, the optimal sizing of a PV-battery-diesel generator hybrid system has been investigated [10], paying special attention to system cost and environmental impact of the off-grid system. In this case, the levelized cost of electricity and the carbon footprint of energy are defined as the main metrics that must be minimized.

Other sizing methods are based on intuitive "rules of thumb". The concept of days of autonomy (DOA) for battery sizing, which consists of finding the storage size that can fulfill the load for a predefined amount of days in the absence of solar generation is an example [11]. Another example is the concept of nights of autonomy (NOA). Both the DOA and NOA concepts are discussed in Section 5.2.2. More complex optimization methods have been introduced over the past years, especially iterative optimization approaches where the system performance for the objective is iteratively evaluated across the decision variable space [12, 13]. For instance, a standalone PV-battery system has been dimensioned based on loss of power probability and life cycle cost using an iterative procedure in [14].

However, the main drawback of these techniques is that the system is only optimized based on one objective function. Therefore, a system with multiple trade-offs, or objective functions, has not been completely tackled, especially for the application of solar home systems. In comparison, multi-objective optimization (MOO) techniques offer better applicability. Nowadays, MOO techniques based on artificial intelligence are widely used, which are generally more robust, and are better equipped to deal with multi-objective optimization problems [15]. Among them, Genetic Algorithms (GA) are powerful meta-heuristic techniques that are capable of reaching global optima with high accuracy and appropriate computational speed [16]. Former studies using MOO techniques in PV systems show different focus areas compared to our study. In [17], authors quantify the trade-offs between economic and environmental performances of rural solar PV projects. Authors in [18] use a sizing algorithm based on Particle Swarm Optimization (PSO) for a PV-battery-hydrogen fuel cell-based hybrid system. There is a clear research gap in literature with respect to studies focusing on optimal sizing of present-day SHS, especially taking into account battery lifetime as one of the objectives.

In this study, the different SHS parameters need to be optimized simultaneously,

making the MOO a necessity. Consequently, in this study, we use a GA algorithm for the task of optimal sizing of an SHS for different electrification levels defined by the MTF. In this optimization, the PV rating, battery capacity, and converter sizes are obtained taking into account the most optimum combination of LLP, excess energy, battery size, and battery lifetime.

### 5.1.3. CONTRIBUTIONS OF THIS CHAPTER

Following are the main contributions of this chapter.

1. An optimal sizing methodology for SHS is presented that minimizes the LLP, excess energy, and battery size while maximizing the battery lifetime specific to SHS applications.

2. For the first time, optimal SHS sizing is investigated for the various tiers of MTF for household electricity access.

3. Inadequacies of standalone SHS are highlighted for higher tiers of electrification and a possible alternative is proposed for climbing the so-called electrification ladder.

## 5.2. SYSTEM METRICS AND PARAMETERS

### 5.2.1. SYSTEM METRICS

The system metrics used in this work are discussed below.

#### LOSS OF LOAD PROBABILITY

The Loss of Load probability is a measure of the system downtime. It is defined as the ratio of the amount of time the system fails to deliver the demanded power to the total amount of operation time the system was designed to deliver power for [4]. For modelling and simulating off-grid systems, this is an application specific or a user-defined constraint. For example, in [4], the LLP over a year was constrained to 1.8%, and in [19], a similar metric had a minimum limit of 2%.

$$LLP = \frac{\sum_{i=1}^{N} t_{\text{downtime},i}}{N} \tag{5.1}$$

where $t_{\text{downtime},i}$ takes a value of 1 if the system fails to deliver the expected load demand in the $i$th time interval, and 0 if the system fully meets the load requirement; $N$ is the time period of interest. Since the system is modelled with a 1-min data resolution, $t_{\text{downtime},i}$ is updated every minute, while a 1-year long period of interest yields an N value of 525600.

The choice of LLP can also be dependent on the application. For instance, [11] states that the recommended LLP values for domestic illumination, appliances, and telecommunications applications are 0.01, 0.1, and 0.0001 respectively.

**UNSATISFIED LOAD ENERGY ($E_{\text{fail}}$)**

$E_{\text{fail}}$ quantifies the unmet energy demand in kWh over a given period of time. In this study, it is mathematically defined as the summation of the unsatisfied energy over a year for each time interval $i$, as shown in Equation 5.2.

$$E_{\text{fail}} = \sum_{i=1}^{N} E_{\text{unsatisfied},i} \tag{5.2}$$

**ENERGY DUMP ($E_{\text{dump}}$) AND DUMP RATIO ($R_{\text{dump}}$)**

This is the total amount of energy that is unused when the local battery is full and the load demand is met while the PV can still generate more power. In this study, this value is considered over a period of 1 year for the system. In order to make relative comparisons easier, a term dump ratio is introduced, which is the ratio between the total energy dump of the system in a year divided by the annual load energy need, as seen in Equation 5.3.

$$R_{\text{dump}} = \frac{E_{\text{dump}}}{E_{\text{load,year}}} \tag{5.3}$$

**SHS SIZE**

SHS size corresponds to the electrical dimensions of PV, battery and the power converters. Typically, this is specific to the rated power of the PV in Wp, total battery capacity in Wh, and peak power rating in W of the converter.

**BATTERY LIFETIME**

This is the lifetime in years of operation after which the battery capacity reduces to below 80% of its nominal rated capacity. At the end of this period, the battery is said to have reached its end of life (EOL).

### 5.2.2. SYSTEM PARAMETERS

The following are the other important system parameters that are referred to in this chapter.

**STATE OF CHARGE AND DEPTH OF DISCHARGE**

This has already been described in Chapter 4 in Section 4.2.1.

**STATE OF HEALTH**

State of Health (SOH) is indicative of the fraction of the nominal rated battery capacity actually available for cycling.

**DAYS OF AUTONOMY (DOA)**

Days of autonomy refers to the number of days a particular battery size is capable of powering the full load demand assuming there is no PV generation. This is often used in approximate battery sizing. For example, a battery size in Wh can potentially be written as shown in Equation 5.4.

$$E_{\text{batt}} = \frac{E_{\text{load}} \cdot n_{\text{DOA}}}{DOD \cdot \eta_{\text{batt}}} \tag{5.4}$$

where $E_{load}$ is the load energy requirement over a day, $n_{DOA}$ is the number of days of autonomy, $\eta_{batt}$ is the average battery efficiency, and $\overline{DOD}$ is the average DOD of the intended battery cycling. Practitioners often use DOA or NOA to size the battery as a "rule of thumb". However, this can lead to inaccurate and suboptimal system sizing, as shown later in Section 5.4.1.

### NIGHTS OF AUTONOMY (NOA)

Nights of autonomy refers to the number of nights (night = non-sunlight hours of the day) where a battery can completely power the load demand assuming no PV generation to recharge the battery. This is also used in approximate battery sizing. For example, a battery size in Wh can potentially be written as shown in Equation 5.5.

$$E_{batt} = \frac{E_{nightload} \cdot n_{NOA}}{\overline{DOD} \cdot \eta_{batt}} \tag{5.5}$$

where $E_{nightload}$ is the load energy requirement in the non-sunlight hours in a day, and $n_{NOA}$ is the number of nights of autonomy.

## 5.3. METHODOLOGY

The various steps employed in the methodology of this study are described in this section. Section 5.3.1 presents the inputs to the SHS model, Section 5.3.2 presents the architecture of the system, Section 5.3.3 describes a dynamic PV output modeling method, Section 5.3.4 describes the steps involved in battery lifetime modelling, Section 5.3.5 discusses the power management scheme used in the standalone SHS, Section 5.3.6 describes the steps used to evaluate the converter rating, and Section 5.3.7 details a genetic algorithm (GA)-based multi-objective optimization (MOO) approach for SHS sizing.

### 5.3.1. INPUTS TO THE SHS MODEL

#### LOCATION AND METEOROLOGICAL INPUTS TO THE SHS MODEL

Since the ground level meteorological data was not readily available for the remote rural areas, the data for an Indian city (with 5 Equivalent sun hours of irradiance per day) was taken from the Meteonorm software database [20]. The meteorological data is assumed to be representative of other remote areas in similar latitudes in the tropical regions. The data used in this study has a resolution of 1 minute.

The main meteorological inputs used in the SHS model are: (a) Ambient temperature ($T_{amb}$), (b) Direct Normal Irradiance ($G_{DNI}$), (c) Diffused Horizontal Irradiance ($G_{DHI}$), (d) Global Horizontal Irradiance ($G_{GHI}$), and (e) Wind speed ($v_w$).

#### LOAD PROFILES FOR THE MTF

Stochastic load profiles constructed for the various tiers of the MTF in Chapter 3 were used as inputs in this study. Figure 5.1 shows a sample load profile for a representative day from the constructed 1-year load profile for a tier 2 household. The household-level load datasets for all the tiers have been obtained from [21]. Table 3.4 summarizes the important load profile characteristics for each tier of the MTF.
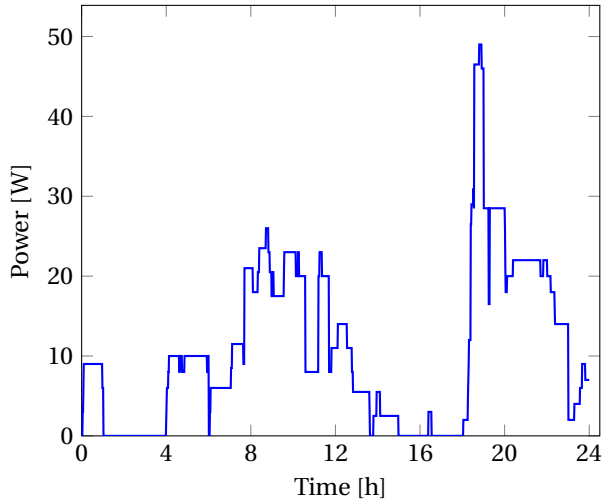
Figure 5.1: 1-day load profile of an off-grid household with tier 2 electricity access. The total energy consumption for this day is 257 Wh with a peak of around 49 W. Data sourced from [21].

### 5.3.2. MODULAR SHS ARCHITECTURE

Climbing up the so-called rural electrification ladder requires expansion of the off-grid system to cater to increased load demand. A modular architecture for SHS is therefore proposed that could potentially allow for expansion of the system at the household level. Figure 5.2 shows the modular architecture.
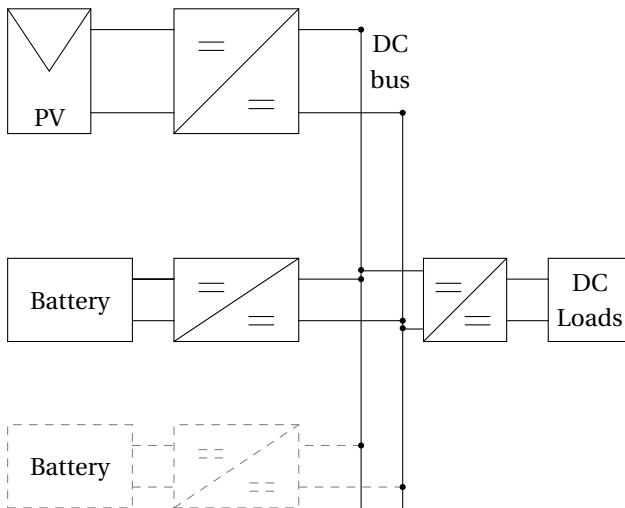


Figure 5.2: Modular DC architecture for an SHS that enables intra-household growth option. Dashed battery with converter illustrates the modular capability.

All the SHS components, viz., PV, battery, and DC loads, are connected to the central

DC bus via converters. Expansion of the system can be achieved by adding more of the SHS components to the DC bus via a converter, as shown in Figure 5.2 with the dashed battery at the bottom. The DC bus can be operated at 12 V, 24 V or 48 V. As more high power loads are connected, a higher bus voltage is recommended to keep the current and therefore cable losses low.

### 5.3.3. Dynamic PV output

The dynamic PV output for each minute is calculated based on an elaborate PV model as illustrated in Figure 5.3.
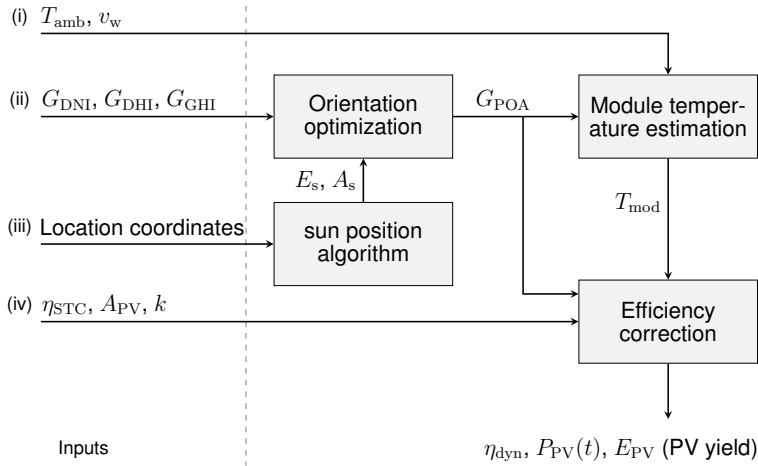


Figure 5.3: Flowchart explaining the steps involved in calculating the dynamic PV output.

There are 4 different kinds of inputs used. Firstly, the location coordinates in terms of latitude and longitude are used to determine the sun position throughout the year. The two main parameters that quantify the sun position are the sun azimuth ($E_s$) and the sun altitude ($A_s$).

Secondly, the ground level irradiance data for the location is used, as mentioned in Section 5.3.1. Along with $E_s$ and $A_s$, the PV module orientation optimization model uses $G_{DNI}$, $G_{DHI}$, and $G_{GHI}$ to evaluate the module azimuth and tilt that maximizes the plane of array irradiance ($G_{POA}$). Additionally, the $G_{POA}$ is computed for the optimal azimuth and tilt.

The dynamic efficiency ($\eta_{dyn}$) of the PV module can be quite different than its rated efficiency ($\eta_{STC}$). As $\eta_{dyn}$ depends on both the module temperature ($T_{mod}$) and $G_{POA}$, the module temperature needs to be estimated. The fluid dynamic model is used to estimate $T_{mod}$ by using $T_{amb}$, wind speed ($v_w$), and the calculated $G_{POA}$ as inputs [11]🦇.

Finally, the PV efficiency is corrected and the dynamic efficiency $\eta_{dyn}$ is calculated using the module area ($A_{PV}$), the temperature coefficient of power for the PV module ($k$), and $\eta_{STC}$. The selected PV module is Jinko Solar JKM265P. Although the rated power is 265

---

🦇More details can be found in Appendix B
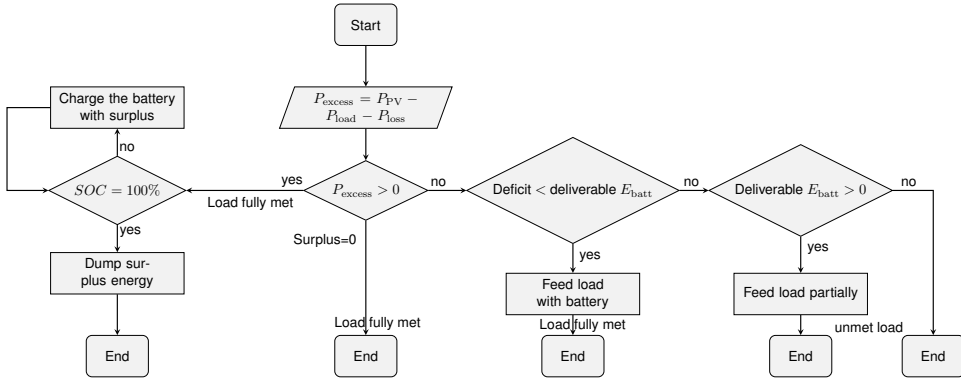
Figure 5.4: Flow chart explaining the power management scheme used in the standalone SHS model; it represents the algorithm followed in every time step. Note that dumped energy could be viewed as PV power production curtailment in practice, leading to potential under-utilization of solar energy.

Wp, a normalized dynamic PV output scaled down to 10 Wp is considered for the optimal sizing methodology. The detailed methodology for modelling the dynamic PV output has been described in a previous work done by the authors in [4].

### 5.3.4. Estimating battery lifetime

In this study, a valve regulated lead acid (VRLA) battery is considered as the energy storage device. The practical battery lifetime estimation method presented in Chapter 4 is used in this study. As explained in Chapter 4, the model uses battery manufacturers' datasheets to refer to the cycle life curves at different temperatures [22]. A constant round-trip efficiency of 90% is considered for the VRLA battery [1].

For each micro-cycle of battery activity determined by a current zero-crossing, the proportional number of cycles spent under the DOD and temperature levels, is then evaluated, as shown in Equation 4.10. The partial damage incurred by the battery in each micro-cycle is calculated as shown in Equation 4.11. This damage is then scaled and subtracted from the present SOH, so that when the cumulative damage becomes 1, the SOH reaches 80%. When the SOH falls below 80%, the simulation ends, and this time at which the simulation ends is the battery lifetime ($L$) in years.

It should be noted that as the cycle-life curves are taken from the manufacturer's datasheets, choice of a different battery product or type will impact the lifetime calculations.

### 5.3.5. Power management scheme for standalone SHS

The algorithm used for power management in every time step (1 minute) is shown in Figure 5.4. $E_{\text{batt}}$ refers to the battery capacity in Wh in any time step.

As shown in the flowchart, at the start of every time step $t$, the excess power or the

load deficit is computed as shown in Equation 5.6.

$$P_{\text{excess}} = P_{\text{PV}} - P_{\text{load}} - P_{\text{loss}} \tag{5.6}$$
$$P_{\text{deficit}} = P_{\text{load}} - (P_{\text{PV}} - P_{\text{loss}})$$

Where $P_{\text{loss}}$ is the combined power lost in the PV and load converters. If $P_{\text{excess}} > 0$, then the load is fully met, and the excess energy either goes to charge to the battery, or dumped if the battery is full.

The case where $P_{\text{excess}} < 0$ means that there is an energy deficit and has to be fed from the battery. If $E_{\text{batt}} - E_{\text{batt,min}} \geq$ the energy deficit for the time step, then the load is fully met. In the case where the battery cannot feed the load fully or at all, then the unmet load results in $E_{\text{fail}}$. At the instant where $E_{\text{fail}} > 0$, LLP = 1 for the given time step. It must be noted that a C-rate limit of 5C was imposed on the battery operation. This process repeats for every time step until the one year simulation is over, corresponding to 1 year of the load data and meteorological data.

### 5.3.6. Converter rating
The power converters shown in Figure 5.2 need to be appropriately rated. Power rating of each converter is chosen depending on its intended application as seen below.

#### PV converter sizing
The PV converter optimal size was selected based on the sizing ratio $R_S$ defined in Equation 5.7.

$$R_S = \frac{P_{\text{PV,Peak}}}{P_{\text{Nom,conv}}} \tag{5.7}$$

Where $P_{\text{PV,Peak}}$ is the peak PV power and $P_{\text{Nom}}$ is the rated converter power. Therefore, a sizing ratio $R_S < 1$ implies oversizing of the converter.

In the studies conducted in [23, 24], the effect of varying $R_S$ on the total yearly energy output from the PV converter was analyzed. The PV array output depends on the geographical location, and rarely has an output that is equal to or larger than its rated peak power. Hence, having $R_S = 1$ or lower for a relatively small time during the year is unnecessary. In this study, the same approach for finding the optimal $R_S$ was performed. The yearly energy yield from the PV module was obtained for values of $0.5 \leq R_S \leq 1.5$ as shown in Figure 5.5.

The figure shows that for $R_S = 0.9$, the maximum energy yield is obtained. However, for $R_S = 1.27$, 96% of the maximum yield is obtained. Hence, for an around 41% reduction in the sizing ratio (from 0.9 to 1.27), only 4% of the energy yield is lost. Therefore, an $R_S$ of 1.27 was selected as the optimal sizing ratio to obtain the PV converter rating $P_{\text{Nom,conv}}$, as it is the highest sizing ratio (and therefore most sizing gains) that guarantees more than 95% of maximum achievable yield. Moreover, past studies on solar converter sizing have concluded that a converter could be undersized by up to 30% of the PV array Wp rating, as undersizing causes an insignificant reduction ($\leq 5\%$) in the total yearly energy yield compared to the reduction in its cost [23, 24].

#### Load converter sizing
The load converter was sized according to the peak load for each tier. Hence, for the load converter, $P_{\text{Nom}} = P_{\text{max}}$, which are the values found in Table 3.4.
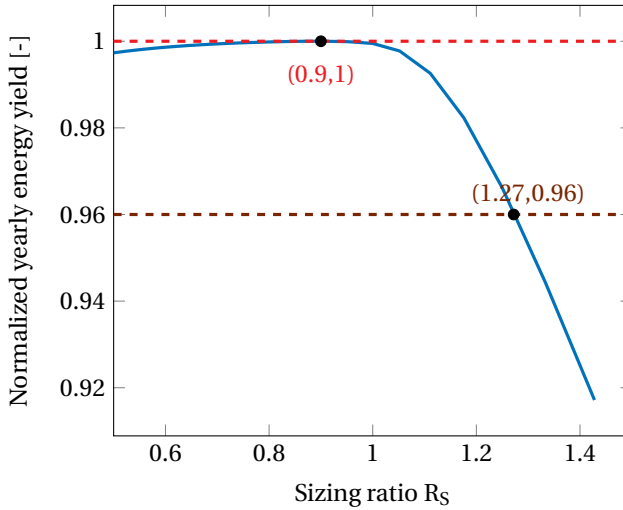
Figure 5.5: Normalized energy yield VS $R_S$

**BATTERY CONVERTER SIZING**

The battery converter is a bidirectional converter that processes power by charging or discharging the battery based on the excess PV generation or greater load demand respectively. Hence, it should be sized appropriately to allow the maximum net charge or discharge power to go in/out of the battery. The $P_{\text{Nom}}$ for the battery converter is then taken as the maximum between the $P_{\text{deficit}}$ and $P_{\text{excess}}$ values.

### 5.3.7. MULTI-OBJECTIVE OPTIMIZATION FOR STANDALONE SHS SIZING

Optimal SHS sizing is a complex task that brings to the fore the intricate interplay between the different SHS component sizes and the various system metrics described in Section 5.2.1. For example, a larger battery size can lead in general to longer battery lifetimes (at the cost of increased initial investments), while a smaller battery size will result in loss of load events (high LLP) as there won't be enough stored energy to power the load in the non-sunlight hours. Similarly, a lower than adequate PV size will result in high LLP. However, an indiscriminate increase in PV size will result in high $E_{\text{dump}}$ values, which is a waste of energy and should be avoided as much as possible. While an increase in PV or battery size increases the initial system costs, a high $E_{\text{dump}}$ value increases the levelized cost of kWh of the system.

**DECISION VARIABLES**

For the optimal SHS sizing, 3 variables determine the performance of the system based on the various metrics. These are: PV size (Wp), battery size (Wh), and converter ratings (W). However, as seen in Section 5.3.6, the converter rating is dependent on the PV size and the load. The load profile is a given for the specific SHS application (MTF tier-based usage). Therefore, the primary independent decision variables used in this study are:

(1) the PV size (Wp) and

(2) the battery size (Wh).

## OBJECTIVES

The main objectives can be written as (a) to minimize total cost (b) to minimize LLP and (c) to minimize $E_{\text{dump}}$ (or $R_{\text{dump}}$). However, the total system cost can be considered as a sum total of PV cost, battery cost, and the converter cost. Each of these costs are directly proportional to the rating of the SHS components. Additionally, the battery costs consist of both the initial costs and the replacement costs, owing to the lowest lifetime amongst the other SHS components. As the replacement costs go down with increasing battery lifetime, minimizing the total battery costs is the same as minimizing the battery size while maximizing the battery lifetime (although battery size and lifetime are not mutually independent variables).

The converter sizes are again dependent on the PV and load and therefore cannot be independently minimized to lower the costs. PV size is in a way already reflected in minimizing the dumped energy ($E_{\text{dump}}$). Therefore, the objective of minimizing total SHS costs can be crystallized down to the objectives of minimizing battery size, maximizing battery lifetime while minimizing $E_{\text{dump}}$ and $LLP$. This adaptation of the cost objective into battery size and lifetime helps in avoiding the actual costs in \$ or €, for example, and maintains the generality of the methodology and the results.

Consequently, the following objectives are used for multi-objective optimization in this study.

(1) to minimize the battery size

(2) to maximize the battery lifetime

(3) to minimize the $LLP$ and

(4) to minimize the $R_{\text{dump}}$.

## CONSTRAINTS

Constraints are necessary in the MOO process to curtail optimization run times and eliminating unwanted navigation of the algorithm employed within the search space. In this study, constraints were placed on the $LLP$ and the $E_{\text{dump}}$. Although $LLP$ and $E_{\text{dump}}$ form part of the objective set, the additional constraints augment the efficiency of the optimization computation. The constraints used in the MOO can be stated as:

(1) $LLP \leq 10\%$

(2) $E_{\text{dump}} \leq$ yearly load or $R_{\text{dump}} \leq 1$.

## GENETIC ALGORITHM-BASED MOO

For performing a multi-objective optimization (MOO), the genetic algorithm toolbox of MATLAB was utilized. The *gamultiobj* function within the GA toolbox of MATLAB is based on a Non-dominated Sorting GA (NSGA)-II variant [25]. Figure 5.6 outlines the steps contained in the GA-based MOO used in this study. The functioning of the genetic algorithm can be explained as follows.
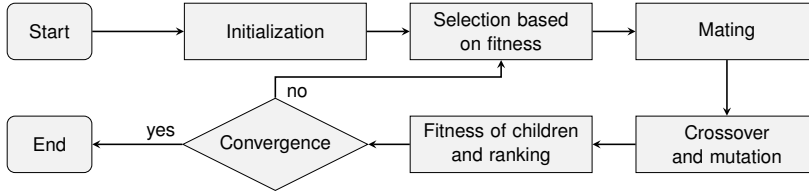
Figure 5.6: Flow chart showing the steps followed in the GA-based MOO.

1. **Initialization**. The initialization step involves generating a random population of 'N' individuals which represent the first generation. Each individual has a set of characteristics, which are the PV and battery capacity in Wp and Wh, respectively. For example, for an individual X:

$$X = [PV_X, Batt_X] \tag{5.8}$$

   The final step of initialization also includes evaluating the fitness.

2. **Fitness-based selection**. In this step, the fitness of each individual is assessed according to the objective functions:

$$\text{Obj.functions} = \begin{cases} \text{Min} : LLP \\ \text{Max} : L \\ \text{Min} : E_{\text{dump}} \\ \text{Min} : E_{\text{batt}} \end{cases}$$

   and the fittest individuals are selected for the mating, while the rest are disregarded.

3. **Mating**. A pair from the pool of fittest individuals is selected, producing two offspring individuals that share characteristics from each of the parents. The process is repeated until a new population of 'N' individuals is obtained.

4. **Crossover and mutation**. These two stochastic operators serve to randomly alter the characteristics of some of the "child" population to maintain some variability in the algorithm.

5. **Fitness of children**. The same fitness assessment and selection takes place for the children individuals, which represent the new generation.

6. **Checking convergence criteria** The convergence criteria used are:

   (a) $G_i = G_{\text{max}}$, where $G_i$ is the $i$th generation

   (b) $\Delta_{S_i} \leq \Delta_{S,\text{max}}$ for each objective, where $\Delta_{S_i}$ is the spread between the objectives for $G_i$ and $G_{i+1}$.

If the convergence criteria are met, the optimization process stops. Otherwise, the optimization process repeats from Step 2 until convergence is reached. In Table 5.1, the parameters and convergence criteria used in this study are shown.

Table 5.1: GA parameters and stopping conditions used in this study.

| Parameter | Symbol | Value |
|---|---|---|
| Population size | $N_{\text{max}}$ | 25 |
| Generation limit | $G_{\text{max}}$ | 500 |
| Spread tolerance | $\Delta_{S,\text{max}}$ | $10^{-4}$ |

It must be noted that the a multi-objective optimization need not lead to unique optimization solutions. Instead, a Pareto set of solutions is usually obtained, which (in terms of GA) are the individuals with fitness functions that are non-dominated by any other individual in the search space. Here, dominance refers to the attribute of an individual to score lower (better) than all other individuals for that particular fitness function. For example, an individual $x$ dominates $y$ in the population when [26]:

$$f_i(x) \leq f_i(y) \quad \forall\, i \quad \text{and} \tag{5.9}$$
$$f_i(x) < f_i(y) \quad \text{for at least 1 } i$$

## 5.4. Results and discussions

### 5.4.1. Dependence of SHS parameters on size

As described in Section 5.3.7, there is a complex interplay of the various SHS parameters with respect to the SHS size. In this section, the impact of sizing on each of the system metrics ($LLP$, $R_{\text{dump}}$, and lifetime) is presented.

#### LLP

Figure 5.7 presents a contour plot depicting the variations in $LLP$ depending on the PV and battery size for a tier 3 load profile with VRLA battery. It can be seen that the same $LLP$ can be achieved by either increasing the battery size or the PV size. Moreover, minimal sizing can be achieved if the knee point of the curve is chosen for a given $LLP$. However, the knee point, or the least distance of the curve from the origin, is a least-cost operating point only if the PV and battery are equally cheap or expensive.

In other words, for the same technology costs ($/Wp and $/Wh), the least-cost operating point is the knee point. Deviations from the knee point to achieve least-cost sizing is possible if the ratio between the technology costs is precisely known. Additionally, also shown in Figure 5.7 are the battery sizes based on the days of autonomy and nights of autonomy, represented as vertical lines. It can be seen how a "rule of thumb" of 2 DOA using a "back of the envelope" method to arrive at battery size (Equation 5.4) can result in oversizing of the battery, as even for 1 DOA, Equation 5.4 yields a battery size of 1363 Wh for a VRLA battery assuming an 80% DOD. Using NOA method need not be very precise either, and also depends largely on the proportion of the load profile that falls in the non-sunlight hours. The exact $LLP$ achieved using such methods will also depend on the operational PV module size. In general, these "rule of thumb"-based approaches can lead to inaccurate battery sizing leading to either an expensive or an inadequately reliable system.
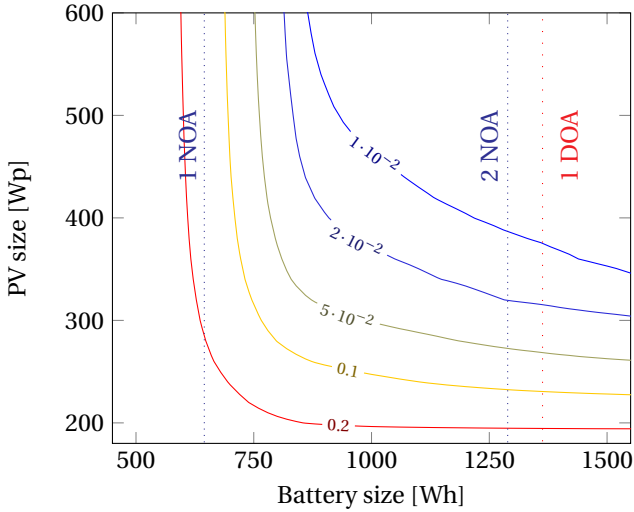
Figure 5.7: *LLP* contours based on PV and (VRLA) battery sizes for a tier 3 load profile.
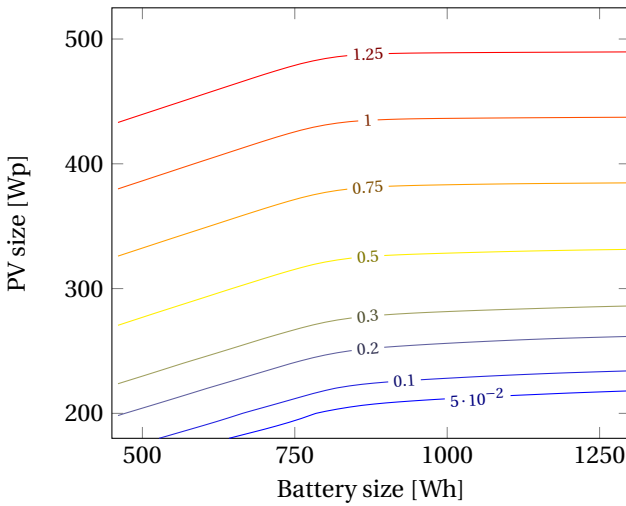


Figure 5.8: $R_{\text{dump}}$ contours based on PV and (VRLA) battery sizes for a tier 3 load profile.

#### DUMP RATIO

Figure 5.8 presents a contour plot depicting the variations in $R_{\text{dump}}$ depending on the PV and battery size for a tier 3 load profile with VRLA battery. As seen in the figure, the $R_{\text{dump}}$ increases with increasing PV size. To an extent the increase in battery size helps in reducing the dump ratio. However, after around 900 Wh, the increase in battery is almost irrelevant for the considered PV and battery size range. It can already be seen that an interesting trade-off emerges between *LLP* and $R_{\text{dump}}$. For example, to maintain an

*LLP* of 0.05 and below (Figure 5.7), almost 300 Wp of PV module is necessary. On the other hand, a 300 Wp of PV module size will guarantee an $R_{\text{dump}}$ of at least 0.3 as seen in Figure 5.8.

**Battery lifetime**

The trade-off between *LLP* and $R_{\text{dump}}$ becomes more intricate when the battery lifetime is considered into the mix. Figure 5.9 presents a contour plot depicting the variations in battery lifetime (*L*) in years depending on the PV and battery size for a tier 3 load profile with VRLA battery.
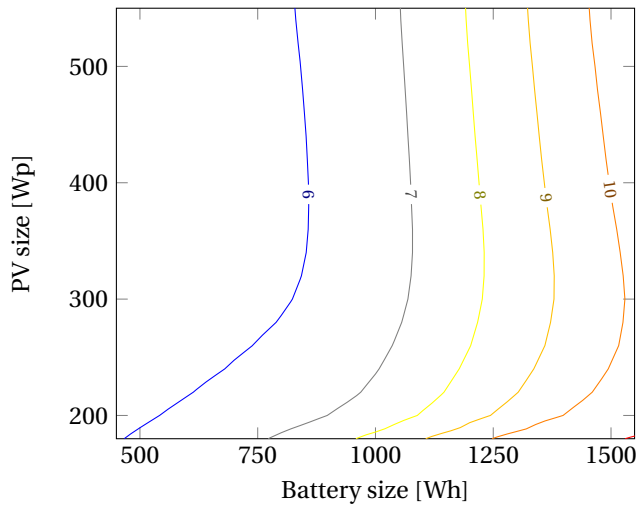


Figure 5.9: Lifetime contours in years based on PV and (VRLA) battery sizes for a tier 3 load profile.

For the same PV size, the battery lifetime increases with increasing battery size. For the same battery size, the lowest PV size leads to relatively lowest battery activity and therefore highest lifetime. As the PV size increases for the same battery size, the battery lifetime initially decreases due to increasing battery activity contributing to higher cyclic ageing. However, at the higher end of the PV sizing range, the battery is being operated largely at relatively lower DOD levels, leading to relatively higher lifetimes than the medium PV range.

### 5.4.2. Multi-objective optimization for SHS sizing

Based on the methodology described in Section 5.3.7, a multi-objective optimization was performed for the various objectives. Consequently, different Pareto fronts are obtained that give the optimal PV and battery sizes that dominate at least one objective function without being worse off in the other objectives, as shown in Equation 5.9. Figure 5.10 shows for the tier 3 case the Pareto set of points for *LLP*, $R_{\text{dump}}$, which also perform optimally with respect to the other objectives of lifetime and battery size. As expected, the solution space is bounded by the constraints specified in Section 5.3.7.
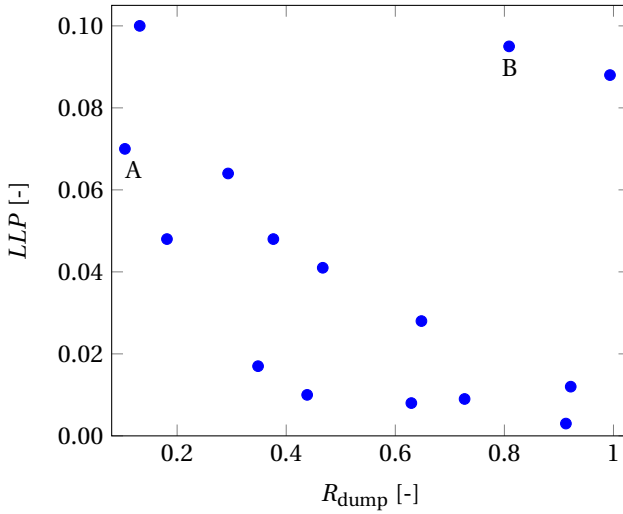
Figure 5.10: *LLP* VS $R_{dump}$ for a Pareto set of points for the tier 3 case. Points A and B perform differently on the 4 objectives, but still form a part of the Pareto set of system solutions.

**5**
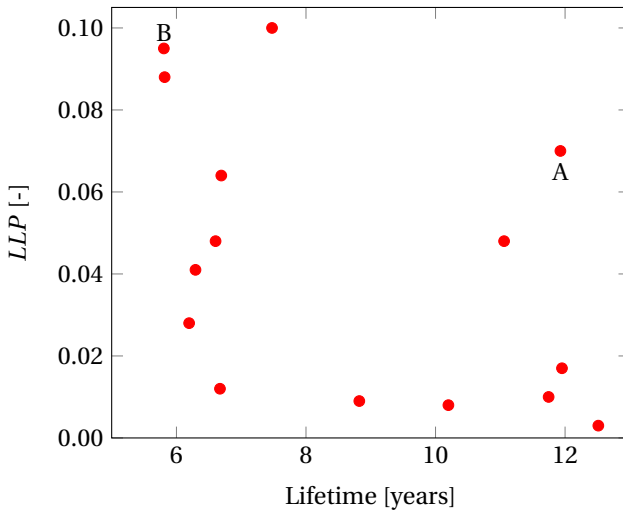


Figure 5.11: *LLP* VS lifetime for a Pareto set of points for the tier 3 case. Points A and B perform differently on the 4 objectives, but still form a part of the Pareto set of system solutions.

Figure 5.11 and Figure 5.12 depict the same Pareto set of points for the system metrics of *LLP* and lifetime, and lifetime and $R_{dump}$, respectively. Some of the points that were too close to each other have been removed for clarity. It can be seen that the various system sizes represented by the points in the Pareto set perform differently across the various system metrics. As long as the different objectives are not weighted, the applied methodology does not favour a particular system size over another. Therefore, the task of
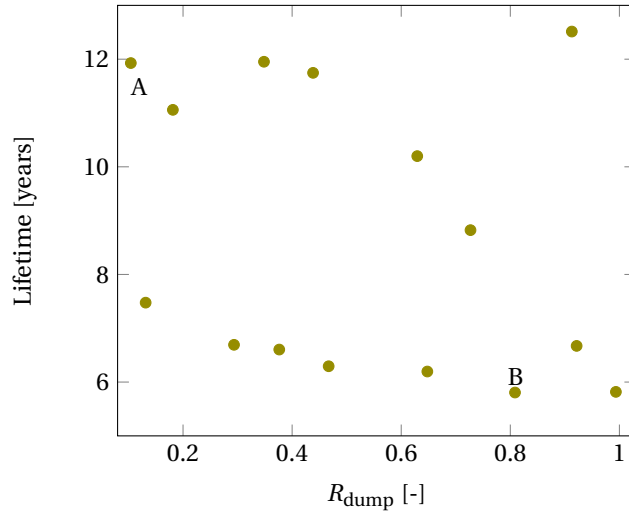
Figure 5.12: Lifetime VS $R_{\text{dump}}$ for a Pareto set of points for the tier 3 case. Points A and B perform differently on the 4 objectives, but still form a part of the Pareto set of system solutions.

optimal SHS sizing for a particular tier will depend on selecting an optimal size based on additional filters and categorization, as described below in Section 5.4.2.

It should be noted that the GA-based MOO chooses the Pareto front based on the performance across all 4 objective functions and not just the 2 functions described in these figures. Therefore, each figure shows the Pareto points that satisfy not only the two objective functions represented on the x and y-axes, but all four objective functions stated in Section 5.3.7. This is illustrated with the help of 2 labeled Pareto points A and B in Figures 5.10 to 5.12. Point A satisfies a very high battery lifetime as well as a low $R_{\text{dump}}$ (11.93 years and 0.1 respectively), but shows a relatively high $LLP$ (0.07). Furthermore, the battery size, which is also an objective to be minimized in the optimization, is not explicitly represented in the Pareto fronts in Figures 5.10 to 5.12, but is playing an equally important role in the selection of optimal Pareto points. For example, point A leads to a storage size of 1800 Wh for tier 3 SHS. On the other hand, point B, which seems to be specifically non-dominant for the $LLP$, Lifetime and $R_{\text{dump}}$ simultaneously (0.095, 5.81, and 0.81 respectively), actually has the lowest battery size (720 Wh), and is therefore part of the Pareto front.

#### OPTIMAL SHS SIZES FOR TIERS OF THE MTF

Similar to the results shown in Figure 5.10 to Figure 5.12, the MOO was performed for all the tiers of the MTF. To determine the optimal system sizes per tier, a selection has to be made from the Pareto set of points allowing relative trade-offs. Firstly, three different categories of $LLP$ are defined, viz., (a) $LLP \leq 0.1$, (b) $LLP \leq 0.05$, and (c) $LLP \leq 0.02$. Secondly, the smallest battery size that satisfies the above LLP criteria in each category are chosen. This gives rise to unique PV-battery size combinations per tier. Accordingly, the final optimal SHS sizes for every tier of the MTF is shown in Table 5.2. The table also

Table 5.2: Optimal SHS sizes that satisfy the different LLP criteria, along with the required converter sizes and the performance of these system sizes on the system metrics.

| $LLP$ [-] | Tier | PV (Wp) | Battery [Wh] | Converter [W] | | | Lifetime [Years] | $R_{dump}$ [-] | $LLP$ [-] |
|---|---|---|---|---|---|---|---|---|---|
| | | | | PV | Load | Battery | | | |
| $\leq 0.1$ | 1 | 20 | 60 | 15 | 12 | 15 | 6.2 | 0.82 | 0.047 |
| | 2 | 70 | 210 | 53 | 51 | 52 | 5.9 | 0.48 | 0.1 |
| | 3 | 380 | 720 | 285 | 154 | 259 | 5.8 | 0.81 | 0.1 |
| | 4 | 1620 | 2520 | 1215 | 1670 | 1660 | 5.4 | 0.89 | 0.099 |
| | 5 | 4050 | 5300 | 3038 | 3081 | 2961 | 5.7 | 0.99 | 0.089 |
| $\leq 0.05$ | 1 | 20 | 60 | 15 | 12 | 15 | 6.2 | 0.82 | 0.047 |
| | 2 | 80 | 240 | 60 | 51 | 59 | 6.3 | 0.65 | 0.039 |
| | 3 | 340 | 860 | 255 | 154 | 229 | 6.0 | 0.56 | 0.042 |
| | 4 | 1500 | 2880 | 1125 | 1670 | 1661 | 5.7 | 0.73 | 0.046 |
| | 5 | 3800 | 6150 | 2850 | 3081 | 2777 | 6.1 | 0.84 | 0.0431 |
| $\leq 0.02$ | 1 | 20 | 70 | 15 | 12 | 15 | 6.8 | 0.80 | 0.019 |
| | 2 | 90 | 290 | 68 | 51 | 67 | 7.5 | 0.85 | 0.019 |
| | 3 | 420 | 1020 | 315 | 154 | 288 | 6.7 | 0.92 | 0.012 |
| | 4 | 1740 | 3560 | 1305 | 1670 | 1660 | 7 | 1.0 | 0.017 |
| | 5 | 4000 | 6600 | 3000 | 3081 | 2924 | 6.45 | 0.93 | 0.029 |

shows the system metrics for the particular PV and battery size along with the converter sizes.

Based on the methodology followed in Section 5.3.6, the converter sizes follow the PV rating and load profile. The PV and battery sizes, however, are a direct result of selection of a particular PV-battery combination from the Pareto set. Based on the LLP threshold, the selection of the lowest battery size to meet the LLP criteria gives an interesting mix of system sizes. For instance, as seen in Table 5.2, the $LLP \leq 5\%$ criterion sees lower PV and higher battery sizes as compared to $LLP \leq 10\%$ for tiers 3 to 5. This leads to relatively lower $R_{dump}$ values.

### THE LIMITS OF STANDALONE SHS

As seen in Table 5.2, the PV and battery sizes increase drastically between the tiers, especially when going towards tiers 4 and 5. Additionally, it can be seen that no optimal solutions exist with the given constraints for tier 5 for $LLP \leq 2\%$. This is because larger-sized SHS that could potentially satisfy the LLP criterion would still end up compromising the dump criterion while also leading to extremely high battery sizes. This clearly shows that there is a limit to the level of electricity access a standalone SHS can provide.

For tiers 1 to 3, a small increment in system size (due to climbing up the tiers for instance) can be easily achieved, especially in a way such that low $LLP$ values are guaranteed. However, tiers 4 and 5 require significant increase in system sizing, and without the kind of reliability (low LLP) achievable at the lower tiers. Additionally, the presence of high power loads also increases the required converter ratings in tiers 4 and 5. If the

LLP threshold is further lowered to ≤ 1%, even tier 4 has no optimal solution based on the Pareto points. The lowest achievable *LLP* for tier 4 within the given constraints is 1.5%.

**State-of-the-art SHS**

It should be noted that the concept of LLP as a vital parameter in system sizing is usually not followed in state-of-the-art SHS. For example, present-day SHS capable of powering up to tier 2 level loads, are sized from 50 Wp, 300 Wh (for an SHS operational in East Africa) to 100 Wp, 1 kWh (for an SHS operational in Cambodia). While this may lead to suboptimal use of the SHS components of PV and battery, having a sizing approach without a reasonable approximation of LLP targets for standalone SHS catering to higher tiers could amplify the suboptimal usage.

Additionally, as most deployed state-of-the-art SHS are rated less than 200 Wp, there is a long way to go if SHS are to enable higher tiers of electrification as ubiquitously as they have been effective with tiers 1 (as pico-solar products) and 2. While tier 3 level electrification still seems to be within reach of state-of-the-art SHS, tier 4 and tier 5 level electrification demand a much bigger expansion from the standalone SHS, which may not be practical to implement when additional aspects like financial viability are considered in off-grid contexts.

**Another approach to climbing up the electrification ladder**

In the absence of a central grid connection in many of these off-grid regions where SHS are currently deployed, the best way to achieve tier 4 or tier 5 level of electricity access is via a microgrid. However, a centralized islanded microgrid with central PV and storage requires high CAPEX investments, which is also why standalone SHS have seen far greater proliferation than centralized rural microgrids. Moreover, the level of electrification is often a dynamic requirement, as the electricity needs keep increasing with time [27, 28]. In such a case, it is more practical to envisage a bottom-up SHS-based microgrid borne out of the interconnection of standalone SHS, as discussed earlier in Chapter 2. This would enable the sharing of excess energy between the households while improving the overall system metrics and potentially reducing the battery storage size.

## 5.5. Conclusion

This study detailed an extensive methodology for the optimal sizing of SHS for every tier of the multi-tier framework for household electricity access. The genetic algorithm-based multi-objective optimization performed gave insights on the delicate interdependencies of the various system metrics on the SHS sizing. Moreover, meeting the energy demand of higher tiers, especially tier 5 is shown to be untenable with purely standalone SHS. Optimal system sizes for each tier of the MTF are presented, and the implications of these system sizes are discussed from the perspective of state-of-the-art SHS. Finally, an SHS interconnection-based microgrid is proposed as a potential means to climb up the so-called electrification ladder, especially to easily enable tier 4 and tier 5 levels of electricity access. The work presented in this chapter is expected to shed light on the complex, multi-dimensional issue of electrification from the point of view of technical system design while exploring the intricate interdependencies of SHS parameters.

The optimal SHS sizes obtained for the various LLP thresholds serve as a reference for quantifying the benefits of a decentralized, interconnected SHS-based microgrid on the system metrics in Chapter 6.

## REFERENCES

[1] N. Narayan, T. Papakosta, V. Vega-Garita, Z. Qin, J. Popovic-Gerber, P. Bauer, and M. Zeman, "Estimating battery lifetimes in solar home system design using a practical modelling methodology," *Applied Energy*, vol. 228, pp. 1629 – 1639, 2018.

[2] N. Narayan, T. Papakosta, V. Vega-Garita, J. Popovic-Gerber, P. Bauer, and M. Zeman, "A simple methodology for estimating battery lifetimes in solar home system design," in *2017 IEEE AFRICON*, pp. 1195–1201, Sept 2017.

[3] V. Vega-Garita, D. D. Lucia, N. Narayan, L. Ramirez-Elizondo, and P. Bauer, "Pv-battery integrated module as a solution for off-grid applications in the developing world," in *2018 IEEE International Energy Conference (ENERGYCON)*, pp. 1–6, June 2018.

[4] N. Narayan, V. Vega-Garita, Z. Qin, J. Popovic-Gerber, P. Bauer, and M. Zeman, "A modeling methodology to evaluate the impact of temperature on solar home systems for rural electrification," in *2018 IEEE International Energy Conference (ENERGYCON)*, pp. 1–6, June 2018.

[5] N. Narayan, Z. Qin, J. Popovic, P. Bauer, and M. Zeman, "Evaluating the techno-economic feasibility of battery technologies in the context of solar home systems," in *2018 20th European Conference on Power Electronics and Applications (EPE'18 ECCE Europe)*, pp. P.1–P.10, Sept 2018.

[6] O. Ekren and B. Y. Ekren, "Size optimization of a pv/wind hybrid energy conversion system with battery storage using response surface methodology," *Applied Energy*, vol. 85, no. 11, pp. 1086 – 1101, 2008.

[7] R. Hosseinalizadeh, H. S. G, M. S. Amalnick, and P. Taghipour, "Economic sizing of a hybrid (pv–wt–fc) renewable energy system (hres) for stand-alone usages by an optimization-simulation model: Case study of iran," *Renewable and Sustainable Energy Reviews*, vol. 54, pp. 139 – 150, 2016.

[8] F. Benavente-Araoz, A. Lundblad, P. E. Campana, Y. Zhang, S. Cabrera, and G. Lindbergh, "Loss-of-load probability analysis for optimization of small off-grid pv-battery systems in bolivia," *Energy Procedia*, vol. 142, pp. 3715 – 3720, 2017. Proceedings of the 9th International Conference on Applied Energy.

[9] S. Chalise, J. Sternhagen, T. M. Hansen, and R. Tonkoski, "Energy management of remote microgrids considering battery lifetime," *The Electricity Journal*, vol. 29, no. 6, pp. 1 – 10, 2016.

[10] M. Bortolini, M. Gamberi, A. Graziani, and F. Pilati, "Economic and environmental bi-objective design of an off-grid photovoltaic–battery–diesel generator hybrid energy system," *Energy Conversion and Management*, vol. 106, pp. 1024 – 1038, 2015.

**5**

[11] K. Jäger, O. Isabella, A. H. Smets, R. Van Swaaij, and M. Zeman, *Solar Energy: The physics and engineering of photovoltaic conversion, technologies and systems*. UIT Cambridge, 2016.

[12] I. Kougias, S. Szabó, F. Monforti-Ferrario, T. Huld, and K. Bódis, "A methodology for optimization of the complementarity between small-hydropower plants and solar pv systems," *Renewable Energy*, vol. 87, pp. 1023 – 1030, 2016. Optimization Methods in Renewable Energy Systems Design.

[13] W. D. Kellogg, M. H. Nehrir, G. Venkataramanan, and V. Gerez, "Generation unit sizing and cost analysis for stand-alone wind, photovoltaic, and hybrid wind/pv systems," *IEEE Transactions on Energy Conversion*, vol. 13, pp. 70–75, March 1998.

[14] R. Ayop, N. M. Isa, and C. W. Tan, "Components sizing of photovoltaic stand-alone system based on loss of power supply probability," *Renewable and Sustainable Energy Reviews*, vol. 81, pp. 2731 – 2743, 2018.

[15] T. Khatib, A. Mohamed, and K. Sopian, "A review of photovoltaic systems size optimization techniques," *Renewable and Sustainable Energy Reviews*, vol. 22, pp. 454 – 465, 2013.

[16] M. D. Al-Falahi, S. Jayasinghe, and H. Enshaei, "A review on recent size optimization methodologies for standalone solar and wind hybrid renewable energy system," *Energy Conversion and Management*, vol. 143, pp. 252–274, 2017.

[17] E. De Schepper, S. Lizin, B. Durlinger, H. Azadi, and S. Van Passel, "Economic and environmental performances of small-scale rural pv solar projects under the clean development mechanism: the case of cambodia," *Energies*, vol. 8, no. 9, pp. 9892–9914, 2015.

[18] M. Paulitschke, T. Bocklisch, and M. Böttiger, "Sizing algorithm for a pv-battery-h2-hybrid system employing particle swarm optimization," *Energy Procedia*, vol. 73, pp. 154–162, 2015.

[19] F. A. Bhuiyan, A. Yazdani, and S. L. Primak, "Optimal sizing approach for islanded microgrids," *IET Renewable Power Generation*, vol. 9, no. 2, pp. 166–175, 2015.

[20] Meteotest, "(software) meteonorm ver 7.1," 2014.

[21] N. Narayan, "Electrical power consumption load profiles for households with dc appliances related to multi-tier framework of household electricity access." `https://doi.org/10.4121/uuid:c8efa325-87fe-4125-961e-9f2684cd2086`, 2018.

[22] "Installation , commissioning and operating instructions for valve-regulated stationary lead-acid batteries - solar battery data sheet," 2015.

[23] X. Camps, G. Velasco, J. de la Hoz, and H. Martín, "Contribution to the pv-to-inverter sizing ratio determination using a custom flexible experimental setup," *Applied Energy*, vol. 149, pp. 35 – 45, 2015.

**5**

[24] S. Islam, A. Woyte, R. Belmans, and J. Nijs, "Undersizing inverters for grid connection-what is the optimum?," *Proceedings of PV in Europe*, pp. 780–783, 2002.

[25] MATLAB, *gamultiobj Algorithm.* Natick, Massachusetts: The MathWorks Inc., 2018.

[26] D. Kalyanmoy, *Multi objective optimization using evolutionary algorithms.* John Wiley and Sons, 2001.

[27] T. D. Heeten, N. Narayan, J. C. Diehl, J. Verschelling, S. Silvester, J. Popovic-Gerber, P. Bauer, and M. Zeman, "Understanding the present and the future electricity needs: Consequences for design of future solar home systems for off-grid rural electrification," in *2017 International Conference on the Domestic Use of Energy (DUE)*, pp. 8–15, April 2017.

[28] N. Narayan, Z. Qin, J. Popovic-Gerber, J.-C. Diehl, P. Bauer, and M. Zeman, "Stochastic load profile construction for the multi-tier framework for household electricity access using off-grid dc appliances," *Energy Efficiency*, Nov 2018.

**5**

# 6

# QUANTIFYING THE BENEFITS OF SHS-BASED DC MICROGRIDS

*There is hopeful symbolism in the fact that flags do not wave in a vacuum*

Arthur C. Clarke

## ABSTRACT

As seen in Chapter 5, state-of-the-art SHS can only provide electricity access with adequate power supply availability up to tier 2, and to some extent, tier 3 levels of the Multi-tier Framework (MTF) for measuring household electricity access. When considering system metrics of loss of load probability (LLP) and battery size, meeting the electricity needs of tiers 4 and 5 is untenable through SHS alone. Alternatively, a bottom-up microgrid composed of interconnected SHS is proposed in this chapter. Such an approach can enable the so-called climb up the rural electrification ladder. The impact of the microgrid size on the system metrics like LLP and energy deficit is evaluated. Finally, it is found that the interconnected SHS-based microgrid can provide more than 40% and 30% gains in battery sizing for the same LLP level as compared to the standalone SHS sizes for tiers 5 and 4 of the MTF, respectively, thus quantifying the definite gains of an SHS-based microgrid over standalone SHS. This study paves the way for visualizing SHS-based rural DC microgrids that can not only enable electricity access to the higher tiers of the MTF with lower battery storage needs but also make use of existing SHS infrastructure, thus enabling a technologically easy climb up the rural electrification ladder.

## OUTLINE

This chapter is divided into five sections. Section 6.1 introduces the chapter and presents a literature review. Section 6.2 describes in detail the methodology used in the study.

Section 6.3 discusses the results and their implication while quantifying the benefits on the various system metrics of going from standalone SHS to an SHS-interconnected microgrid. Finally, Section 6.4 concludes the chapter with the closing thoughts on the interconnection benefits and recommendations for future work.

## 6.1. INTRODUCTION

In this chapter, an alternative, bottom-up, SHS-based microgrid is proposed as a solution to achieve higher tiers of electrification, and the benefits of such an interconnected SHS-based microgrid are quantified over standalone SHS.

### 6.1.1. LITERATURE STUDY

#### INADEQUACY OF CONTEMPORARY SHS

Most plug-and-play SHS for households currently being offered in the off-grid market segment belong to the 11 Wp to 100 Wp category [1, 2]. For locations with 4 or more equivalent sun hours per day of solar insolation (a common attribute for locations in the equatorial and tropical areas), such a PV rating can easily satisfy the electricity needs up to tier 2 (Table 2.1), provided adequate battery storage is present in the system. However, there is a scarcity of SHS-based solutions that cater to higher tiers of the MTF. For instance, tier 4 requirements are stated to be more than 3.4 kWh per day, which requires more than 800 Wp of rated PV in the SHS, which is a far cry from contemporary SHS ratings available in the field (typically around 100 Wp or less)[1, 3]. The study presented in Chapter 5 on optimal sizing of SHS while increasing the battery lifetime, decreasing the excess unused energy, and reducing the LLP concluded that standalone SHS are not tenable to be used for tier 4 and tier 5 level electrification. In fact, the lowest LLP attainable by an optimally sized SHS catering to tier 5 electricity demand was seen to be 0.029 [3], while several off-grid projects keep 0.02 as a lower limit of the LLP [4, 5]. For off-grid systems, typical LLP values based on the specific application can be 0.01 and 0.0001 for domestic illumination and telecommunications respectively [6]. Moreover, due to the mismatch between the electricity demand and production, which is to some extent abated with the help of battery storage, there is usually some amount of energy that is wasted, leading to underutilization of the PV-generated energy. This utilized energy in standalone SHS in literature has been seen to be as much as 31%, for simulated SHS installed in Bangladesh [7]. For SHS installed in Rwanda, around 65% of the generated energy remains unutilized [8]. The SHS considered in these studies are currently catering to tier 1 and tier 2 users only. For higher tier usage, the scaling up of PV and battery size needed to meet the energy demand would mean that the unutilized component of generated energy also scales up in magnitude, thus leading to more "wasted energy". Even though contemporary SHS mostly cater to tier 1 and tier 2 usage, the climb up the electrification ladder is inevitable. Hence, there is a need to also focus on the larger goal of being able to satisfy the higher tier energy demands. As contemporary standalone SHS suffer from the aforementioned drawbacks, a microgrid-based electrification needs to be explored, especially for meeting the electricity demands of the higher tiers. This is because microgrids can potentially cater to much higher power needs as opposed to single SHS with only one PV panel at the household level. Furthermore, grid-extension, which is the third option apart from

standalone systems and microgrids, has not been considered in this chapter as for the majority of the unelectrified population it is not a cost-effective solution, as also discussed in Chapter 2.

### RURAL MICROGRIDS

In the absence of a central grid connection in many of the un(der)-electrified off-grid regions where SHS are currently deployed, the best way to achieve tier 4 or tier 5 level of electricity access is via a microgrid. In the past, rural microgrids in literature have encompassed different categorizations: centralized [9] and decentralized microgrids [10]; grid-connected [11] and islanded (or off-grid) [12]; AC [13], DC [14] and hybrid [15]; Renewable energy-based [16] and hybrid energy-based (with diesel) [17]. However, given the falling PV prices, solar-based solutions like pico-solar products and SHS have already seen a very high rate of proliferation and acceptance. Additionally, the SHS available in the field are mostly DC-based, i.e. without AC components. Therefore, the focus of this study is mainly on islanded solar-based rural DC microgrids. Such a microgrid can be implemented in three ways, viz.,

1. **a centralized microgrid**, with central PV generation and centralized storage;

2. **a semi-decentralized microgrid**, with central PV generation and decentralized storage, or vice-versa;

3. **a fully decentralized microgrid**, with decentralized PV generation, decentralized storage, and DC distribution.

Compared to standalone SHS at the household level, a centralized islanded microgrid with central PV and storage requires high CAPEX investments, and few private players want to set up such a centralized endeavour with the high risks currently associated with such an investment. Semi-decentralized microgrids are also being explored, with a central village solar kiosk, with individual households having some loads and a basic energy storage unit like battery. This can sometimes also be implemented in the form of a single entrepreneur operating the kiosk and leasing out batteries that are charged from the centralized PV [18]. This does not strictly qualify as a microgrid, as there is no distribution grid present. Additionally, semi-decentralized solutions have also been limited by the extent of the electricity they are able to provide.

### BOTTOM-UP, DECENTRALIZED INTERCONNECTED SHS-BASED RURAL MICROGRIDS

In general, the level of electrification is often a dynamic requirement, as the electricity needs keep increasing with time [19, 20]. For example, households might not need a direct tier 4 or tier 5 connection but might move from tier 3 to tier 4 over a span of time. This would mean that the planned microgrid has to expand and scale up with the increase in the energy demand. In such a case, it is more practical to envisage a bottom-up SHS-based microgrid born out of the interconnection of standalone SHS. This would lead to a reduced storage requirement as the households will be able to depend on the excess generation of other households in the microgrid network. Moreover, since the lower tier electrification is already underway through SHS in large parts of the world, an interconnected SHS-based decentralized rural DC microgrid is an option that

is easier to retrofit when visualizing future rural microgrids. The advantages of such an interconnected SHS-based microgrid has already been discussed in Section 2.6.1.

The idea of bottom-up, decentralized rural DC microgrids that can grow organically with time has seen more proponents in literature [21, 22]. However, existing studies like [23, 22] mainly identify the financial benefits of interconnecting SHS. The advantage of demand diversity, that is the load profile peaks of different households occurring at different points in time, due to SHS interconnection, is captured in [8]. Moreover, these studies, based on existing SHS, are limited to tiers 1 to 2 with 12 V battery and distribution. Scaling up the energy ladder would demand high power loads, and therefore a much higher voltage for DC distribution. Additionally, higher power loads that enable productive use of energy are not considered in these studies. Moreover, there is insufficient information in literature on the quantified benefits of microgrid over SHS in terms of system sizing and other system metrics like power supply availability and excess energy.

Therefore, this chapter focuses on the concept of bottom-up SHS-based microgrids that can grow organically based on the electricity demand and the affordability of the households in a given location. Furthermore, this chapter endeavours to quantify the benefits of such an interconnected SHS-based microgrid over standalone SHS.

### 6.1.2. Contributions of this chapter

Following are the main contributions of this chapter.

- A bottom-up, organically growing microgrid is modeled that enables climbing up the rural electrification ladder through energy sharing.

- The benefits of SHS interconnectivity over standalone SHS for enabling higher tiers of electricity access are quantified in the form of system metrics of storage size, loss of load probability and excess energy.

- A modular SHS-based architecture is proposed that can not only enable modular intra-household expansion of the SHS but also allow for inter-household scalability of a meshed DC microgrid.

## 6.2. Methodology

### 6.2.1. Location and meteorological inputs

Meteonorm software database was used to obtain the meteorological data of a city in India (that enjoys 5 equivalent sun hours of irradiance per day) as the ground level meteorological data was not readily available for the remote rural areas [24]. This data can be assumed to be representative of other areas in similar latitudes, as most of the un(der)-electrified areas lie in the tropical latitudes enjoying comparable equivalent sun hours. The meteorological data is composed of ambient temperature, wind speed, and ground level irradiance, which are all required for modelling the dynamic PV output for SHS. This has been extensively discussed in Chapter 5. The data used in this study also has a resolution of 1 minute.

### 6.2.2. Stochastic load profiles

Similar to Chapter 5, stochastic load profiles were used as inputs in this study for the various levels of MTF. The construction of these household level load profiles has been detailed in Chapter 3 and published in [20]. Figure 6.1 shows sample load profiles from a representative day for tier 4 and tier 5 level electrified households. The household-level load profiles for all the tiers differ on a day-to-day basis; the datasets have been obtained from [25].
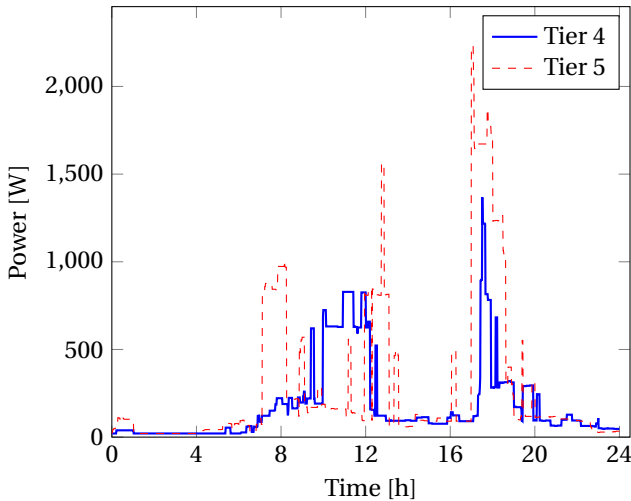


Figure 6.1: 1-day load profiles for tier 4 and tier 5 levels of electricity consumption. Data sourced from [25].

As the focus of the work is to determine the adequacy, and quantify the benefits of, an SHS-based microgrid for higher tiers of electrification as compared to standalone SHS, only tiers 4 and 5 have been considered in this study while modelling the energy exchange between the SHS in the microgrid.

### 6.2.3. System metrics and parameters

The system metrics used in this work are discussed below.

#### Loss of Load Probability (LLP)

This has been already discussed in Section 5.2.1. In Chapter 5, different LLP thresholds were investigated for SHS applications.

#### Unsatisfied load energy ($E_{\text{fail}}$)

This has also been already discussed in Section 5.2.1.

#### Energy Dump ($E_{\text{dump}}$)

This has also been already discussed in Section 5.2.1.

**Per household metrics**

To translate the SHS level metrics to the microgrid level, certain per household metrics are defined as the average metric per household in the microgrid. Specifically, these are:

- Average *LLP* per household:

$$\overline{LLP} = \frac{\sum_i^H LLP}{H} \tag{6.1}$$

   where H is the total number of households in the microgrid.

- Average $R_{\text{dump}}$ per household:

$$\overline{E_{\text{dump}}} = \frac{\sum_i^H E_{\text{dump}}}{H} \tag{6.2}$$

- Average $E_{\text{fail}}$ per household:

$$\overline{E_{\text{fail}}} = \frac{\sum_i^H E_{\text{fail}}}{H} \tag{6.3}$$

### 6.2.4. Optimal standalone SHS sizes for the MTF

Based on the multi-objective optimization for SHS sizing described in Chapter 5, optimal SHS sizes were identified as described in Section 5.4.2. Table 5.2 captures these optimal SHS sizes, which will serve as the reference for comparing the performance of the interconnected SHS-based microgrid across the same system metrics on a per household basis.

As seen in Table 5.2, tiers 4 and 5 required very high sizes of standalone SHS battery sizes. No standalone SHS size could satisfy the *LLP* threshold of ≤ 2% for tier 5 within the given constraints of the study [3].

### 6.2.5. SHS interconnection-based DC microgrid

An interconnected SHS-based DC microgrid is expected to enable the excess energy sharing between the households while improving the overall system metrics of *LLP* and $E_{\text{dump}}$. This section details the steps involved in modeling the energy exchange between different SHS in such a microgrid. A concept illustration of such an interconnected SHS-based microgrid was shown in Figure 2.12. One of the houses in the figure is shown without an installed SHS (illustrated as a non-PV rooftop on the bottommost house), indicating that "load only" consumptive households can also be potentially part of such a microgrid to leverage the excess energy being produced from the PV of other SHS in the microgrid.

**Modular SHS-based microgrid architecture**

Climbing up the so-called rural electrification ladder requires the architecture to support the expansion of the off-grid system to cater to increased load demand. On the other hand, the architecture should also allow for easy interconnectivity with other SHS to form a meshed DC microgrid. Therefore, a modular architecture for SHS is proposed that could potentially allow for expansion of the system at the household level, while also enabling scaling up of the microgrid size. Figure 6.2 shows the modular architecture.
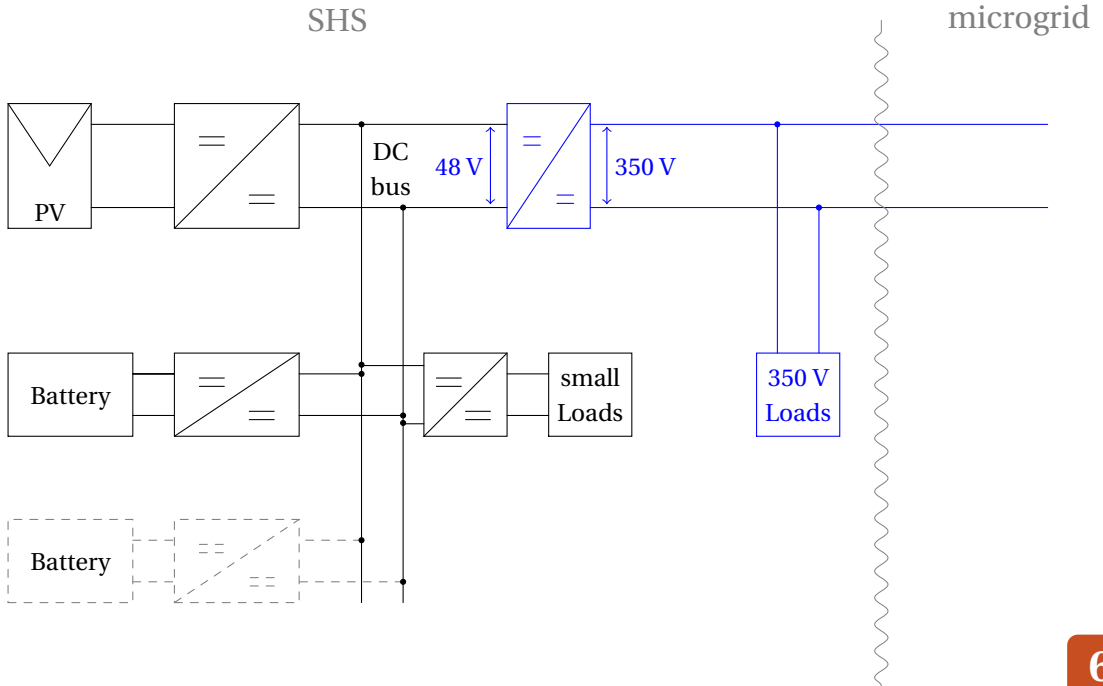
Figure 6.2: Modular DC architecture for an SHS-based DC microgrid that enables intra-household growth option as well as scalability in the form of a meshed DC microgrid. Dashed battery with converter illustrates the modular capability. Similar modular expandability can be considered for loads and PV too. The additional hardware needed to go from standalone SHS to microgrid, along with the high power loads at 380V that the microgrid can support, are denoted in blue colour.

All the SHS components and DC loads are connected to the central DC bus via converters. The SHS can be modularly expanded as shown in Figure 6.2 with the dashed battery at the bottom. The DC bus is assumed to be operated at a reference of 48 V, which has been tested in rural DC microgrid pilot in the past [27]. For the higher power loads, whether within a household (for tier 4/tier 5) or more communal loads like solar pumps, the higher voltage line is available that is operated at a reference of 350 V. This helps to keep the current and therefore cable losses low. Additionally, such an architecture also helps in scaling up this meshed DC microgrid, where more of such SHS of different sizes could be interconnected. It is assumed that the power exchange capacity of such an architecture is only limited by the power demand of the high power loads on the 350 V bus.

**POWER MANAGEMENT SCHEME FOR INTERCONNECTED SHS-BASED MICROGRID ARCHITECTURE**
The detailed PV and storage modeling at every SHS level has been covered extensively in previous works by the authors in [28, 3, 26]. The power management scheme implemented at the SHS level was shown in the flowchart in Figure 5.4.

Note that a fully decentralized microgrid architecture will also benefit from a decentralized control scheme at the SHS level🦇. While going from SHS level to the interconnected SHS microgrid, additional information needs to be considered in every time step. Figure 6.3 shows the algorithm for the interconnected power management scheme. The same algorithm that occurs at every time step $t$ in Figure 5.4 takes place in this scenario, and is repeated for each of the total number of households 'H'. In this step, the $LLP$, $E_{dump}$, $E_{fail}$ and $E_{batt}$ for each household are calculated.
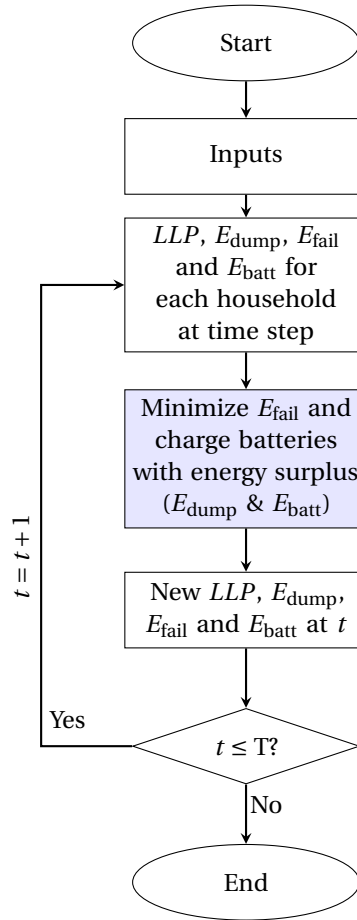


Figure 6.3: Steps involved in the modeling of energy sharing between the SHS for a given number of households. $T$ denotes the total time period of simulation. Apart from minimizing $E_{fail}$, the shaded block involves sharing energy surplus, as detailed in Figure 6.4.

The most important step in this algorithm is the energy sharing process that occurs towards the end of the time step, as indicated by the shaded process block in the flowchart

---

🦇While this is not the focus of this chapter, a decentralized control scheme for DC-interconnected SHS has been discussed in Appendix C
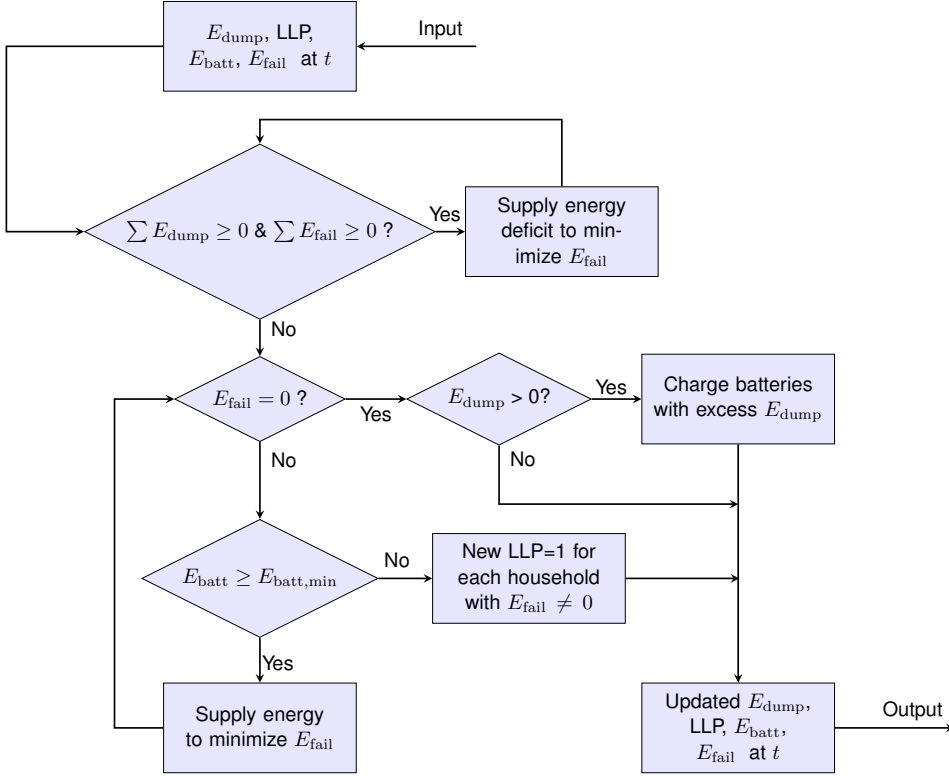
Figure 6.4: Algorithm for sharing the excess energy based on the ranking of load deficit (in terms of $E_{\text{fail}}$ and battery depth of discharge (DOD)).

in Figure 6.3. During this step, the energy sharing between the households takes place to balance the overall energy surplus and deficit in the microgrid. The entire process is detailed in Figure 6.4.

First, the $LLP$, $E_{\text{fail}}$ and $E_{\text{dump}}$ for each household are taken as inputs. The total dump obtained is used as the first measure to eliminate the energy deficit of the households in an ascending order as shown in Equation 6.4.

$$E_{\text{fail},t} = [E_{\text{fail},1,t}, E_{\text{fail},2,t}, ....E_{\text{fail},H,t}] \tag{6.4}$$

where $E_{\text{fail},t}$ is the ordered array containing the energy deficit per household for time step $t$, $E_{\text{fail},i,t}$ is the energy deficit in time step $t$ for the $i^{th}$ household, and $E_{\text{fail},i} \leq E_{\text{fail},i+1}$. Hence, the household with the lowest energy deficit is the first to be supplied from the energy dump, and so on for the remaining households. Prioritizing the households with a low $E_{\text{fail}}$ minimizes the number of households with an $E_{\text{fail}} > 0$ for time step $t$. This results in reducing the average $LLP$ for the SHS community in the microgrid.

If there are still more households left with energy deficit, then the SHS batteries of the rest of the microgrid come into play. This happens when $E_{\text{dump},t} = 0$ & $\sum_{i=1}^{H} E_{\text{fail},i,t} > 0$.

The available battery storage is then sorted in a descending order, where the SHS with the highest available battery energy is the first to supply energy to minimize the deficit.

$$E_{\text{batt},t} = [E_{\text{batt},1,t}, E_{\text{batt},2,t}, ... E_{\text{batt},H,t}] \qquad (6.5)$$

where $E_{\text{batt},t}$ is the matrix containing the battery per household for time step $t$, $E_{\text{batt},i,t}$ is the battery energy in time step $t$ for the $i^{th}$ household, and $E_{\text{batt},i,t} \geq E_{\text{batt},i+1,t}$. The energy deficit minimization process ends when

1. $\sum_{i=1}^{H} E_{\text{fail},i,t} = 0$ or

2. $E_{\text{batt},i} = E_{\text{batt,min},i} \quad \forall \quad E_{\text{batt},i}$

After this process, any household that still has an energy deficit has an $LLP = 1$ for that time step. In the case where all the energy deficit is satisfied but some excess energy still remains from $E_{\text{dump}}$, the batteries in the microgrid are recharged. This can be done in multiple ways. In this study, 3 different excess energy sharing mechanisms are explored for charging the batteries with excess energy.

### A DOD-BASED PROPORTIONAL EXCESS ENERGY SHARING

$$E_{\text{charge},i,t} = x_{i,t} \cdot \sum_{i=1}^{H} E_{\text{dump},i,t} \qquad (6.6)$$

$$\text{Where } x_{i,t} = \frac{DOD_{i,t}}{\sum_{i=1}^{H} DOD_{i,t}} \qquad (6.7)$$

Where $x_{i,t}$ is the share of $i^{th}$ household out of the remaining surplus energy, $E_{\text{dump},i,t}$ is the excess energy available from the $i^{th}$ household at time step $t$, and $E_{\text{charge},i,t}$ is the energy allocated for sharing the battery of the $i^{th}$ household at time step $t$. Hence, the household with the highest DOD obtains the highest share from the available combined excess energy.

The concept of depth of discharge (DOD)-based proportional excess energy sharing can be best illustrated in the following example. Suppose there are 4 SHS (SHS1, SHS2, SHS3, and SHS4) with respective battery DOD levels of 10%, 20%, 30%, and 40% at time $t$ wherein the individual load deficits have already been already taken care of. Suppose there is still a total excess $E_{\text{dump}}$ of 1 kWh available, while each battery has a rated capacity of 2 kWh. Consequently, through the DOD-based, proportional excess energy sharing method described in Equations 6.6 and 6.7, the 4 batteries will be recharged. Figure 6.5 shows the battery energy before and after the total excess energy is distributed. The recharged energy for each battery will also be in the proportion of 1:2:3:4 (as the DOD), and therefore each battery receives 100 Wh, 200 Wh, 300 Wh, and 400 Wh, respectively.

### PRIORITY EXCESS ENERGY SHARING

In this method, the excess energy is shared amongst the batteries in a ranked manner. The batteries are prioritized based on the DOD. Therefore, the highest DOD battery first receives the excess energy until it is full, then the next highest DOD-level battery gets the
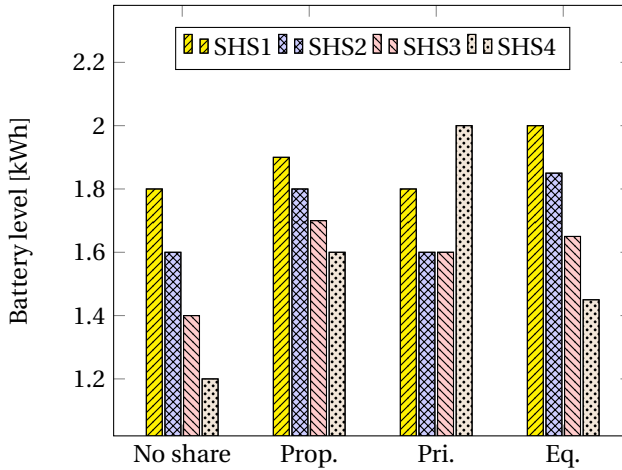
Figure 6.5: Battery energy levels for the 4 SHS batteries without sharing and after the combined excess energy distribution based on proportional (Prop.) energy sharing, priority (Pri.) energy sharing, and equal (Eq.) energy sharing. The rated battery capacity is also shown as the dashed line in the plot.

energy, if any, until it is full, and so on. In the context of the above example in Figure 6.5, the priority sharing would ensure that battery 4, owing to its highest DOD gets fully charged to 2 kWh. The remaining 200 Wh goes to battery 3, which charges up to 1.6 kWh, same as battery 2 at the end of the time step.

#### EQUAL EXCESS ENERGY SHARING
In this method, the excess energy is shared equally amongst the batteries irrespective of their DOD. Therefore, in the context of the example shown in Figure 6.5, the equal sharing would result in each battery getting 250 Wh of energy. It can be seen that battery 1 does not charge beyond 2 kWh, its maximum capacity, leading to a waste of 50 Wh. The equal sharing method can, therefore, be suboptimal in excess energy sharing.

It is interesting to note that these methods for sharing of the excess energy do not necessarily create a uniform SOC across the microgrid. That is, SOC balancing of SHS batteries in the microgrid is not the aim of these excess energy sharing methods.

#### CASE STUDY: HOMOGENEOUS MICROGRIDS
Two different case studies have been considered, viz., a homogeneous microgrid of tier 4 SHS and a homogeneous microgrid of tier 5 SHS. Having a homogeneous microgrid makes for easier comparison in terms of the system metric gains per household. However, the study can also be extended to heterogeneous microgrids consisting of SHS belonging to different tiers and sizes.

**Tier 4 microgrid**    Based on the optimal SHS sizes mentioned in Table 5.2, each SHS was modelled with a PV size of 1740 Wp and battery size of 3560 Wh. Additionally, the microgrid size was varied between 2 to 50 households. The averaged load profile per household for the homogeneous tier 4 microgrid of 50 households is shown in Figure 6.6

along with the load profile for a single household for a representative day in the one-year long simulation.



Figure 6.6: Comparison of 1-day load profile for a tier 4 standalone SHS and an averaged load profile per household for the SHS-based microgrid with 50 households for the same day. The demand diversity can be seen to significantly reduce the peak average load.

**Tier 5 microgrid**    Similar to the tier 4 case, each SHS was modelled based on the optimal SHS sizes (mentioned in Table 5.2), viz., a PV size of 4000 Wp and battery size of 6600 Wh. Additionally, the microgrid size was varied between 2 to 50 households. The averaged load profile per household for the tier 5 microgrid for 50 households is shown along with the load profile for a standalone SHS for tier 5 in Figure 6.7.

### SCOPE OF THE SHS-BASED MICROGRID STUDY
It should be noted that the concept of the interconnected SHS-based microgrid is explored from the point-of-view of the overall benefits of energy sharing between SHS and the maximum potential consequent improvement in the system metrics for the microgrid as a whole. Accordingly, the study described in this chapter assumes perfect knowledge of the battery states of every SHS for sharing energy.

## 6.3. RESULTS AND DISCUSSION
Based on the modeling methodology described in Section 6.2.5, two SHS-based homogeneous microgrids were modeled comprising tier 4 and tier 5 households respectively. Firstly, the concept of energy sharing in the microgrid as explained in Section 6.2.5 is demonstrated in a scaled down case of 2 SHS. Secondly, using the optimal SHS sizes of PV and battery for tier 4 and 5 as shown in Table 5.2, the microgrid was simulated for an increasing number of households. The performance of the overall system in terms of $LLP$ and $E_{\text{fail}}$ per household for increasing mcirogrid sizes is analyzed in Section 6.3.3. Finally,
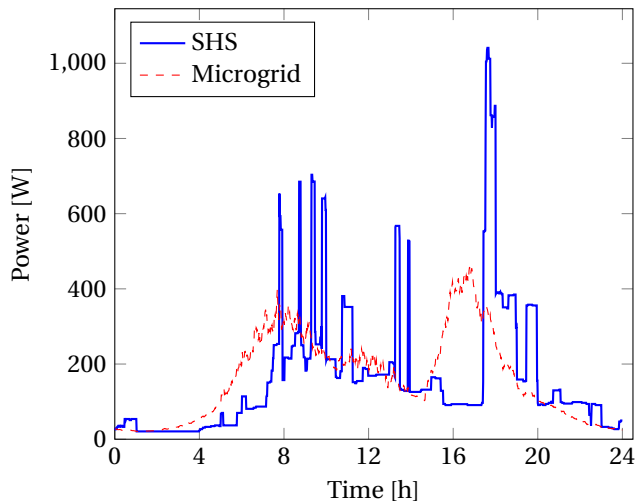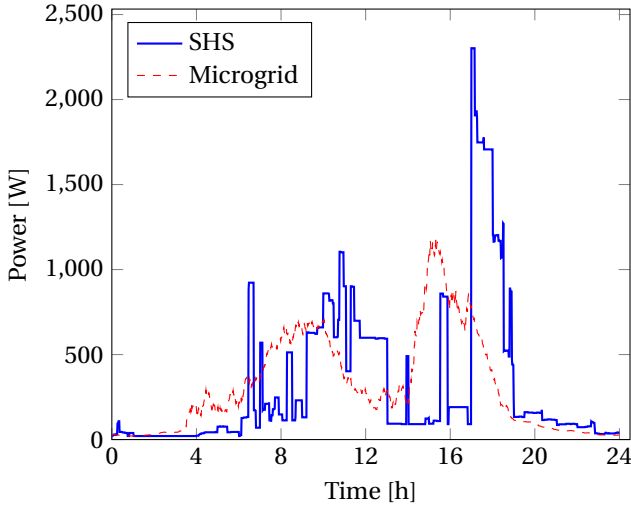
Figure 6.7: Comparison of 1-day load profile for a tier 5 standalone SHS and an averaged load profile per household for the SHS-based microgrid with 50 households for the same day. The demand diversity can be seen to significantly reduce the peak average load.

the benefits in the system sizing for the individual SHS participating in the microgrid case is also shown in Section 6.3.4.

### 6.3.1. ENERGY EXCHANGE IN THE SHS-BASED MICROGRID

To study the energy exchange behaviour, a reduced size of 2 SHS is initially considered in the microgrid. Figures 6.8–6.10 depict the various parameters of the two SHS participating in the microgrid over a period of 32 hours during the 1 year of simulation. It can be seen in Figure 6.8 that there is a relatively low PV production in the region around 6 hours, and higher PV production in the regions around 10-14 hours, and again around 30 hours. Consequently, as seen in Figure 6.9, both the SHS batteries are fully depleted at hour 6. Conversely, both the batteries are fully charged after the excess PV production around hour 30. After the initial high PV production around hour 12, however, only Battery 1 is fully charged.

The most remarkable feature of the energy sharing can be seen (in Figure 6.10) from the fact that neither SHS shows a positive $E_{fail}$ while there is even 1 non-empty battery. Additionally, until both the batteries are fully charged, the total $E_{dump}$ value in the interconnected system is 0. A proportional excess energy sharing scheme was considered to charge the battery with excess energy in this case.

### 6.3.2. COMPARISON OF BATTERY CHARGING USING EXCESS ENERGY

Figure 6.11 shows the comparison between the 3 modes of excess energy-based battery charging (described in Section 6.2.5) in tier 5 homogeneous microgrid in terms of average *LLP* per household. The performance is measured over an increasing microgrid size up to 10 households. As seen in the figure, the priority excess sharing method yields the
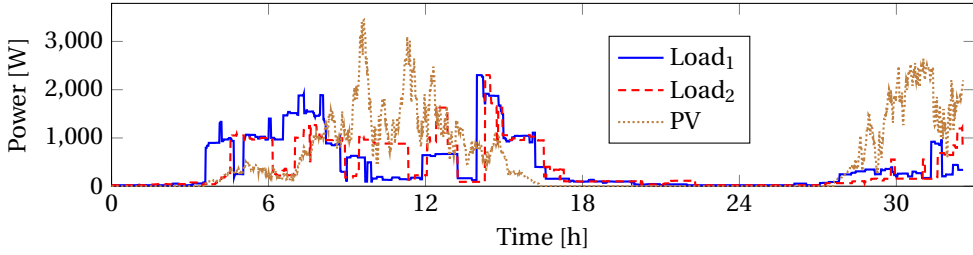
Figure 6.8: Load demand for each SHS and the PV generation per SHS at every time step.
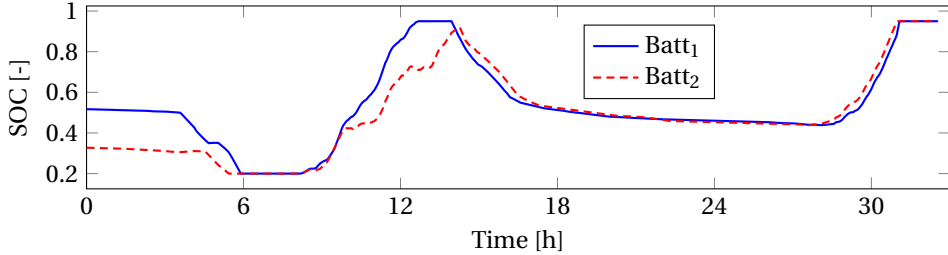


Figure 6.9: Battery SOC for each SHS at every time step.
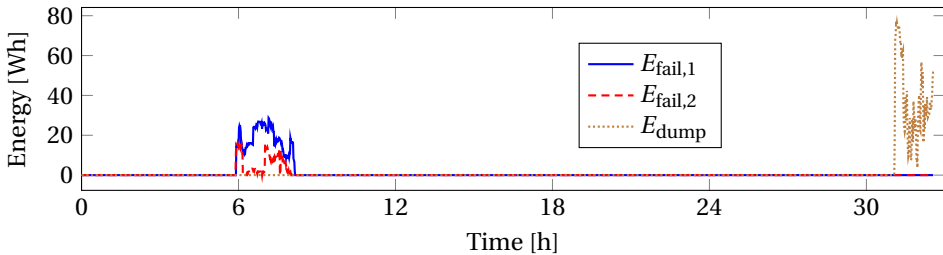


Figure 6.10: $E_{fail}$ for the 2 SHS and total $E_{dump}$ at every time step.

worst performing results. Proportional excess sharing method and equal sharing method perform almost similarly for most microgrid sizes. Given the relative performance, for the rest of the results, only the proportional sharing method for sharing excess energy is considered for the rest of the analysis while modeling the energy exchange in the microgrid.

### 6.3.3. IMPACT OF MICROGRID SIZE
Figure 6.12 shows the LLP per household for tier 4 and tier 5 homogeneous microgrids for different microgrid sizes, up to a maximum of 50 houses. Each SHS in tier 4 has a PV and battery size of 1740 Wp and 3560 Wh respectively, while each tier 5 SHS has a PV and battery size of 4 kWp and 6600 Wh respectively.

It can be seen that the gains in the average *LLP* per household due to the microgrid largely "saturate" after around 15 households for tier 4, and around 20 households for
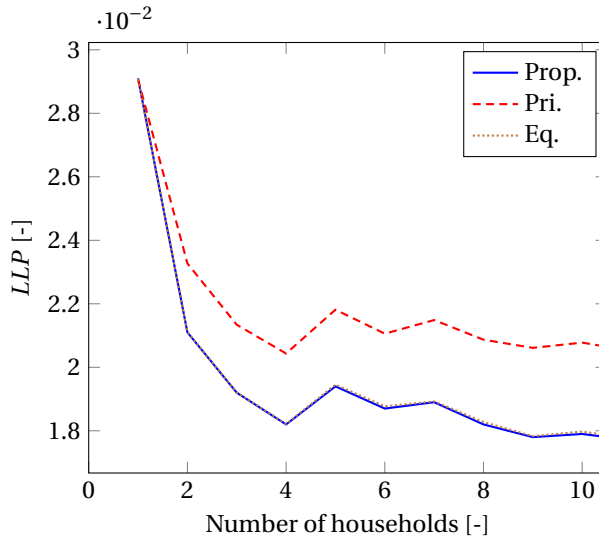
Figure 6.11: Performance comparison of the 3 excess energy-based battery charging methods in terms of LLP for varying homogeneous (tier 5) microgrid sizes. The 3 methods are proportional (Prop.), priority (Pri.), and equal (Eq.) energy sharing
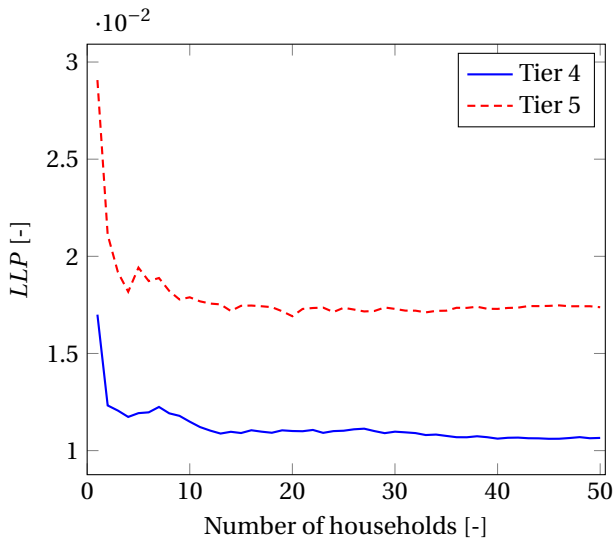


Figure 6.12: Impact of increasing microgrid size on LLP per household for homogeneous microgrids of tiers 4 and 5.

tier 5, respectively. This is because the load profiles per household for a given tier are quite similar, with the load profile peaks still reasonably close to each other. Therefore, the gains in these system metrics will significantly increase if there is a larger intra-day

variability between the load profiles for the various households. Additionally, it can be seen that the average *LLP* for tier 5 falls below 2%, which was not possible with purely standalone SHS, wherein the minimum achievable *LLP* was 2.9% (Table 5.2).
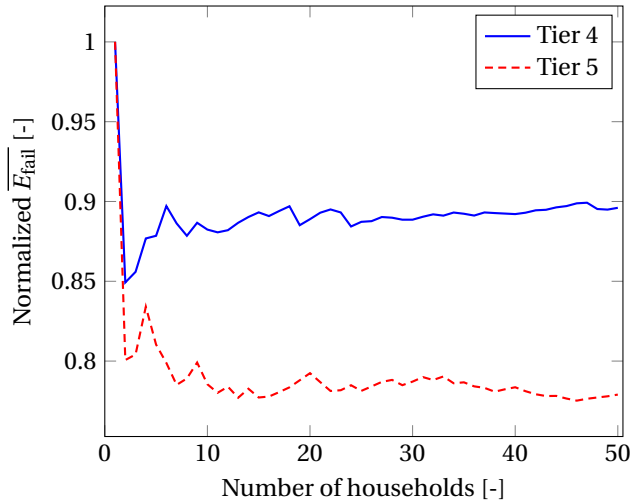


Figure 6.13: Variations in normalized average $E_{\text{fail}}$ per household for homogeneous microgrids composed of tiers 4 and 5.

The average $E_{\text{fail}}$ per household also experiences a considerable decline with increasing size of the microgrid, as shown in Figure 6.13, where the normalized average $E_{\text{fail}}$ is represented for easy comparison between the tier 4 and tier 5 microgrids. The case with a single household is treated as the base value for normalization. The gains in average $E_{\text{fail}}$ per household in the microgrid seems to largely stagnate after around 10 households for both tier 4 and tier 5. While the tier 5 microgrid is able to achieve a reduction of 20% in the normalized average $E_{\text{fail}}$ per household, the tier 4 microgrid is able to achieve a reduction of 10%.

It should be noted that this does *not* mean that the microgrid size should not grow to more than 10 households. The fluctuations in these system metrics with every increasing microgrid size is attributed to the individual variability that an additional household's load profile brings to the overall microgrid load profile. Figure 6.14 shows the impact of increasing microgrid size on the peak average load profile for the set of tier 5 load profiles considered in this study.

The peak average load largely decreases with increasing microgrid size, up to around 10 households, beyond which there is much less reduction. Moreover, each additional load profile brings about a tiny fluctuation in the peak average load, depending upon how coinciding the individual load profile peak is with that of the overall microgrid. Consequently, greater variability in the load demand across the SHS will lead to greater energy exchange and therefore better performance in terms of the system metrics. Naturally, the use of any demand-side management technique resulting in a higher load profile variability would result in more significant gains in each of the system metrics.
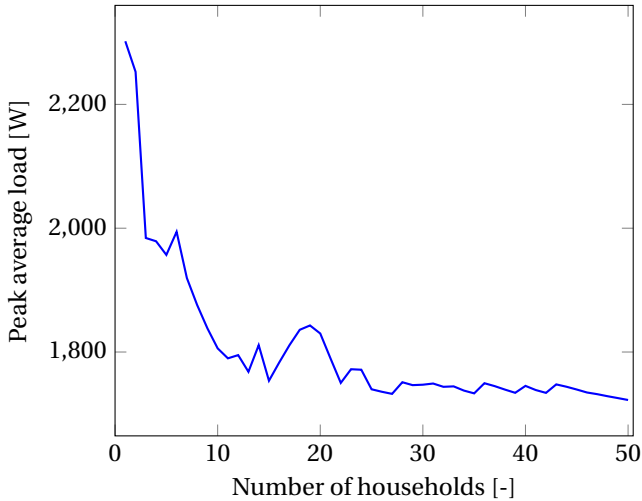
Figure 6.14: Change in peak average load with increasing microgrid size for tier 5.

In general, it can be said that an increase in microgrid size will improve the system metrics until a certain size, beyond which the gains in these metrics will largely stagnate. This directly follows from the fact that the variations in the total load profile for any cluster increase with cluster size until a certain point, beyond which the incremental variations in the cluster load profile are minimal. As the performance gains in the system metrics are limited by the load profile variability, these gains are expected to improve when considering heterogeneous microgrids, i.e., microgrids comprising households belonging to mixed tiers of the MTF.

### 6.3.4. BENEFITS OF MICROGRID ON SHS SIZING

For the same level of performance on system metrics like LLP, an SHS-based microgrid can offer a significant advantage in the individual SHS sizing compared to a standalone SHS. This is evident from Figure 6.15 as shown below, where for a particular microgrid size (number of households), the average *LLP* of the microgrid is evaluated across different SHS battery sizes.

A microgrid size of 20 households has been considered in Figure 6.16 as that size was seen to be enough (Figure 6.12) for average *LLP* of both tiers 4 and 5 to stabilize. The x and y-axes refer to the battery sizes and average *LLP* values respectively in the homogeneous tier 5 microgrid. Three different PV sizes are used corresponding to the optimal PV sizes obtained in Table 5.2 for each of the LLP thresholds.

It can be seen that the general nature of the LLP curve depending on the battery size remains the same as that of an individual standalone SHS as seen in other studies [3]. The main difference is that with the energy sharing capability in the microgrid, the same system sizing would enable better performance. This can be seen while comparing the 3 circular brown marks corresponding to the standalone system sizes from Table 5.2, with the 3 rectangular green marks corresponding to the same LLP threshold and PV size

Figure 6.15: Variations in average *LLP* per household over battery size for a homogeneous tier 5 microgrid with 20 households. The points marked correspond to the different battery sizes for the standalone (circular dots) and microgrid case (green rectangles), respectively.

but lower battery sizes for the tier 5 microgrid case. More than 2 kWh of battery size can be saved to meet the same LLP threshold. In other words, battery sizing gains of 41% (i.e., a 41% lower battery size) can be achieved for tier 5 SHS by energy sharing with the microgrid as opposed to a standalone operation to meet *LLP* = 0.1. The gains are lower but still significant at 19.7% to meet *LLP* of 0.029, which was the minimum LLP achievable by an optimally sized tier 5 standalone SHS (Table 5.2).

A similar analysis is performed on a homogeneous tier 4 microgrid with 20 households to quantify the benefits achieved in terms of SHS battery sizes. This is shown in Figure 6.16. Similar to the tier 5 case, for all the 3 LLP thresholds shown in Table 5.2, significant battery sizing gains can be achieved through the microgrid when compared to standalone SHS to meet the same LLP requirements. At 1740 Wh (blue rectangular mark in Figure 6.16), a 31% lower sized battery is needed to meet an LLP threshold of 0.1 for a tier 4 microgrid, as opposed to a standalone SHS with a battery size of 2520 Wh (Table 5.2). Thus, the benefits of energy sharing in an SHS-based microgrid have been quantified in this study.

Most importantly, as the microgrid proposed in this study is SHS-based, the main problems of centralized PV battery installations with substantial component costs can be avoided. Additionally, each SHS belongs to a different household participating in the microgrid, as opposed to centralized microgrids with lack of clear ownership.

## 6.4. CONCLUSIONS

This study presented a detailed methodology for modelling an interconnected SHS-based microgrid. A modularly expandable and scalable microgrid architecture is proposed. Moreover, meeting the energy demand of higher tiers like tier 4 and tier 5 is shown to be possible with this approach of bottom-up, interconnected SHS-based microgrid as
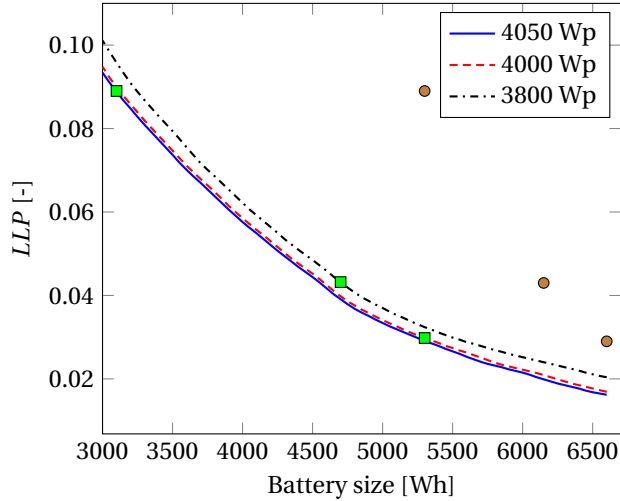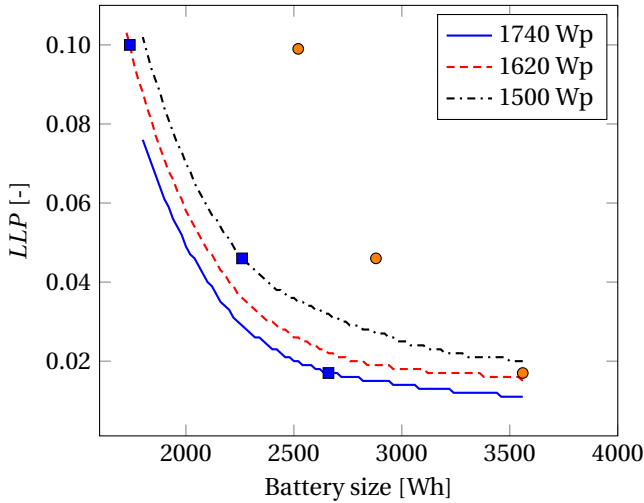
Figure 6.16: Variations in average *LLP* per household over battery size for a homogeneous tier 4 microgrid with 20 households. The points marked correspond to the different battery sizes for the standalone (circular orange dots) and microgrid case (blue rectangles), respectively.

**6**

opposed to standalone SHS. The energy sharing between the different SHS is modeled and its positive impact on the system metrics quantified. It is shown that battery sizing gains of more than 40% can be achieved at the tier 5 level with interconnectivity as compared to standalone SHS to meet the same loss of load probability threshold. It should be noted that the sizing gains and better performance with respect to the system metrics can increase even further depending on the demand diversity in the load profiles. Furthermore, such a bottom-up microgrid can also help in utilizing high power appliances, especially the ones that cater to productive use of energy.

### RECOMMENDATIONS AND FUTURE WORK
The interconnected SHS-based microgrid described in this chapter assumes perfect knowledge of the dynamic behaviour of every SHS. For a truly decentralized bottom-up expansion of such an envisioned microgrid, decentralized power management should be considered. Additionally, optimal microgrid topologies should be studied for such a decentralized microgrid. Moreover, the effects of load profile variations within the microgrid along with load and PV generation uncertainty can also be examined.

### REFERENCES

[1] Lighting Global and Dalberg Advisors, "Off-grid solar market trends report," tech. rep., Lighting Global, Dalberg Advisors, GOGLA, ESMAP, 2018.

[2] N. Narayan, J. Popovic, J. C. Diehl, S. Silvester, P. Bauer, and M. Zeman, "Developing for developing nations: Exploring an affordable solar home system design," in *2016 IEEE Global Humanitarian Technology Conference (GHTC)*, pp. 474–480, Oct 2016.

[3]  N. Narayan, A. Chamseddine, V. Vega-Garita, Z. Qin, J. Popovic-Gerber, P. Bauer, and M. Zeman, "Exploring the boundaries of solar home systems (shs) for off-grid electrification: Optimal shs sizing for the multi-tier framework for household electricity access," *Applied Energy*, vol. 240, pp. 907 – 917, 2019.

[4]  F. A. Bhuiyan, A. Yazdani, and S. L. Primak, "Optimal sizing approach for islanded microgrids," *IET Renewable Power Generation*, vol. 9, no. 2, pp. 166–175, 2015.

[5]  F. Benavente-Araoz, A. Lundblad, P. E. Campana, Y. Zhang, S. Cabrera, and G. Lindbergh, "Loss-of-load probability analysis for optimization of small off-grid pv-battery systems in bolivia," *Energy Procedia*, vol. 142, pp. 3715 – 3720, 2017. Proceedings of the 9th International Conference on Applied Energy.

[6]  A. Smets, K. Jäger, O. Isabella, R. Van Swaaij, and M. Zeman, *Solar Energy - The physics and engineering of photovoltaic conversion, technologies and systems.* 02 2016.

[7]  H. Kirchhoff, "Identifying hidden resources in solar home systems as the basis for bottom-up grids," in *Decentralized Solutions for Developing Economies*, pp. 23–32, Springer, 2015.

[8]  B. Soltowski, J. Bowes, S. Strachan, and O. limpo Anaya-Lara, "A simulation-based evaluation of the benefits and barriers to interconnected solar home systems in east africa," in *2018 IEEE PES/IAS PowerAfrica*, pp. 491–496, IEEE, 2018.

[9]  A. Chaurey and T. Kandpal, "A techno-economic comparison of rural electrification based on solar home systems and pv microgrids," *Energy Policy*, vol. 38, no. 6, pp. 3118 – 3129, 2010. The Role of Trust in Managing Uncertainties in the Transition to a Sustainable Energy Economy, Special Section with Regular Papers.

[10]  A. Bani-Ahmed, M. Rashidi, and A. Nasiri, "Coordinated failure response and recovery in a decentralized microgrid architecture," in *2017 IEEE Energy Conversion Congress and Exposition (ECCE)*, pp. 4821–4825, Oct 2017.

[11]  Y. Xia, W. Wei, Y. Peng, P. Yang, and M. Yu, "Decentralized coordination control for parallel bidirectional power converters in a grid-connected dc microgrid," *IEEE Transactions on Smart Grid*, vol. 9, pp. 6850–6861, Nov 2018.

[12]  Z. Wang, F. Liu, Y. Chen, S. H. Low, and S. Mei, "Unified distributed control of standalone dc microgrids," *IEEE Transactions on Smart Grid*, vol. 10, pp. 1013–1024, Jan 2019.

[13]  Z. Liu, M. Su, Y. Sun, L. Li, H. Han, X. Zhang, and M. Zheng, "Optimal criterion and global/sub-optimal control schemes of decentralized economical dispatch for ac microgrid," *International Journal of Electrical Power and Energy Systems*, vol. 104, pp. 38 – 42, 2019.

[14]  M. Baranwal, A. Askarian, S. Salapaka, and M. Salapaka, "A distributed architecture for robust and optimal control of dc microgrids," *IEEE Transactions on Industrial Electronics*, vol. 66, pp. 3082–3092, April 2019.

**6**

[15] M. S. Rahman, M. J. Hossain, J. Lu, and H. R. Pota, "A need-based distributed co-ordination strategy for ev storages in a commercial hybrid ac/dc microgrid with an improved interlinking converter control topology," *IEEE Transactions on Energy Conversion*, vol. 33, pp. 1372–1383, Sep. 2018.

[16] H. R. Baghaee, M. Mirsalim, G. B. Gharehpetian, and H. A. Talebi, "Decentralized sliding mode control of wg/pv/fc microgrids under unbalanced and nonlinear load conditions for on- and off-grid modes," *IEEE Systems Journal*, vol. 12, pp. 3108–3119, Dec 2018.

[17] K. Gong, E. Lenz, and U. Konigorski, "Decentralized frequency control of a ddg-pv microgrid in islanded mode," in *2015 23rd Mediterranean Conference on Control and Automation (MED)*, pp. 292–297, June 2015.

[18] "Rural Spark - Energy Kit." `http://www.ruralspark.com/products/energy-kit/`. (Date last accessed 2015-10-12).

[19] T. D. Heeten, N. Narayan, J. C. Diehl, J. Verschelling, S. Silvester, J. Popovic-Gerber, P. Bauer, and M. Zeman, "Understanding the present and the future electricity needs: Consequences for design of future solar home systems for off-grid rural electrification," in *2017 International Conference on the Domestic Use of Energy (DUE)*, pp. 8–15, April 2017.

[20] N. Narayan, Z. Qin, J. Popovic-Gerber, J.-C. Diehl, P. Bauer, and M. Zeman, "Stochastic load profile construction for the multi-tier framework for household electricity access using off-grid dc appliances," *Energy Efficiency*, Nov 2018.

[21] B. Soltowski, S. Strachan, O. Anaya-Lara, D. Frame, and M. Dolan, "Using smart power management control to maximize energy utilization and reliability within a microgrid of interconnected solar home systems," in *7th Annual IEEE Global Humanitarian Technologies Conference, GHTC 2017*, pp. 1–7, 2017.

[22] S. Groh, D. Philipp, B. E. Lasch, and H. Kirchhoff, "Swarm electrification: Investigating a paradigm shift through the building of microgrids bottom-up," in *Decentralized Solutions for Developing Economies*, pp. 3–22, Springer, 2015.

[23] S. Groh, D. Philipp, B. E. Lasch, and H. Kirchhoff, "Swarm electrification-suggesting a paradigm change through building microgrids bottom-up," in *Developments in Renewable Energy Technology (ICDRET), 2014 3rd International Conference on the*, pp. 1–2, IEEE, 2014.

[24] Meteotest, "(software) meteonorm ver 7.1," 2014.

[25] N. Narayan, "Electrical power consumption load profiles for households with dc appliances related to multi-tier framework of household electricity access." `https://doi.org/10.4121/uuid:c8efa325-87fe-4125-961e-9f2684cd2086`, 2018.

[26] N. Narayan, V. Vega-Garita, Z. Qin, J. Popovic-Gerber, P. Bauer, and M. Zeman, "A modeling methodology to evaluate the impact of temperature on solar home systems

**6**

for rural electrification," in *2018 IEEE International Energy Conference (ENERGY-CON)*, pp. 1–6, June 2018.

[27] A. Jhunjhunwala, A. Lolla, and P. Kaur, "Solar-dc microgrid for indian homes: A transforming power scenario," *IEEE Electrification Magazine*, vol. 4, no. 2, pp. 10–19, 2016.

[28] N. Narayan, T. Papakosta, V. Vega-Garita, Z. Qin, J. Popovic-Gerber, P. Bauer, and M. Zeman, "Estimating battery lifetimes in solar home system design using a practical modelling methodology," *Applied Energy*, vol. 228, pp. 1629 – 1639, 2018.

**6**

# 7

# OPTIMAL MICROGRID LAYOUT USING GEOGRAPHIC INFORMATION SYSTEM (GIS)

*The saddest aspect of life right now is that science gathers knowledge faster than society gathers wisdom*

Isaac Asimov

## ABSTRACT

As discussed in Chapter 6, bottom-up meshed DC microgrids born out of the interconnection of SHS are instrumental to achieving higher tiers of electrification while maintaining scalability. However, there is limited knowledge when considering the possible layouts for such microgrids, as conventional microgrid topology (layout) studies are limited to certain standard layouts, like spider, ring, bus, and radial layouts. The optimal microgrid layouts in the context of (remote) rural electrification can be quite different from the conventional layouts, because of various reasons like geographical spread, lack of structured housing layouts, etc., thereby necessitating a different methodology altogether when thinking of microgrid planning for rural electrification. In this chapter, a geographic information system (GIS)-based methodology is introduced, which takes into account the actual geographic spread of households in remote areas. After GIS-based data processing, graph theory concepts are used to minimize the layout costs. A total of 42 different remote sites around the world are considered in the study. The proposed integrated methodology is explained in this chapter with an example of its application to a sample of the remote areas from the 42 different sites. The results of the layout comparisons show how the conventional microgrid layouts can be easily outperformed in terms of network length

by the microgrid layouts arrived at through the integrated approach proposed in the methodology, highlighting the usefulness of the approach.

## OUTLINE

This chapter is divided into five sections. Section 7.1 introduces the work described in the chapter with a literature review on the other studies that have used geographic information systems (GIS) for planning electricity networks. Section 7.2 outlines the necessary technical background in the different related fields — GIS and graph theory applied to network analysis — while also defining the focus of this study. Section 7.3 describes the methodology used to arrive at optimal microgrid layouts. Section 7.4 discusses the results and compares the performance of different microgrid layouts across pre-defined metrics. Finally, Section 7.5 concludes the discussion on the GIS-based methodologies to determine optimal microgrid layouts.

## 7.1. INTRODUCTION

One of the decisions that need to be taken in microgrid planning based on SHS is the choice of the microgrid layout. However, there is limited knowledge when considering the possible layouts (topologies) for such microgrids, as conventional microgrid topologies are limited to certain standard layouts, like spider, ring, bus, and radial layouts. On the other hand, the real-world spatial spread of the households in a given area might deem a particular standard layout more expensive due to higher cabling costs. It could also be that a different layout altogether might be needed for a specific case. In this chapter, an integrated geographic information system (GIS)-based methodology is proposed that takes into account the ground-level data, uses graph theory concepts to reduce cabling costs, and finally uses an optimization algorithm to strike a balance between cables costs and the operational parameters of the microgrid like line losses and line congestion, suitable to be applied at a pre-electrical design phase of the microgrid planning.

### 7.1.1. LITERATURE REVIEW

#### CONVENTIONAL MICROGRID TOPOLOGY STUDIES

With regards to the conventional microgrid topology studies, the range of topologies explored in the past is limited. Before the diffusion of renewables, the easiest way to provide energy to remote communities was to install centralised generators (such as diesel gensets) to which all households were connected via two possible layouts. First was the spider topology or spider diagram, sometimes also called as the *hub-and-spoke* layout [1], meaning that each household is directly connected to the generator by a dedicated cable segment. Second was the radial topology, sometimes also called the *hub-and-trunk* layout [1], in which multiple branches span from the central generator, reaching each household in a consecutive way along the branch, with the possibility of sub-branches being implemented [2, 3]. These topologies present a major drawback in terms of fault tolerance, since if one of the cable segments is disconnected because of a failure, the households which are connected to that branch will be totally cut out from energy supply and will suffer major power outages, especially in the case of centralized microgrids [4].

In the context of decentralized SHS-based microgrids, however, the fault tolerance of

(a) Spider topology        (b) Radial topology
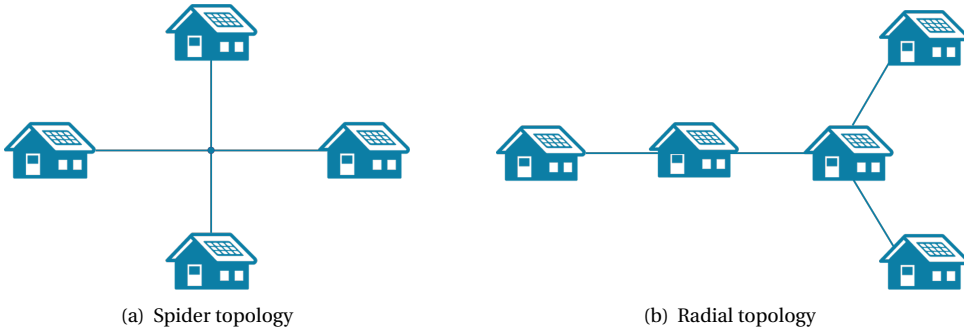
Figure 7.1: Examples of radial topology and spider diagram adapted to the context of decentralized microgrid with SHS.

these layouts can be inherently better than centralized microgrids. Nonetheless, energy sharing can still be impacted by failures. A conceptual illustration for the radial and spider topologies adapted to SHS-based decentralized microgrids can be seen in Figure 7.1. Even though those layouts are typical of centralized generators, they are going to be anyway included into the comparative analysis between decentralized microgrid layouts in this study, as seen later in Section 7.3.

Another kind of topology, which is actually applicable both to centralised and decentralised microgrids, is called the bus topology, which consists of a single (DC) bus to which all households are singularly connected (Figure 7.2(b)). In [2], a comparative analysis of this DC bus layout and the already mentioned centralised radial topology is carried out, highlighting how the distributed bus solution is more easily modularised and scalable, fitting in the framework of a bottom-up approach to electrification.



(a) Ring topology        (b) Bus topology
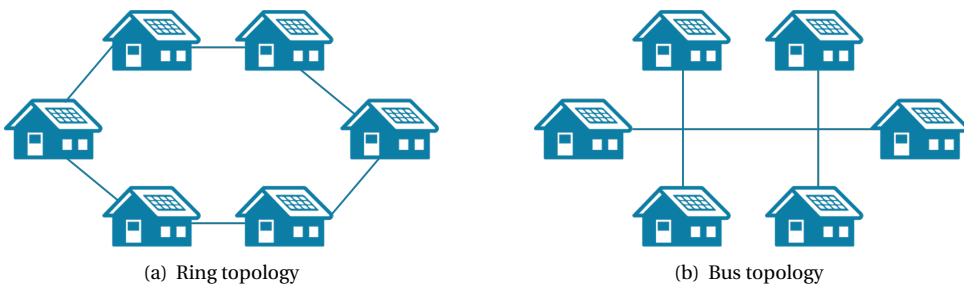
Figure 7.2: Examples of ring and bus topologies adapted to the context of decentralized microgrid with SHS.

Another possible layout option, which is mentioned and described, among others, in [3] and [5], is called the ring topology, consisting of a consecutive connection of all the involved households, forming a closed loop which spans through and around the village/neighbourhood, as depicted in Figure 7.2(a).

The last kind of topology is the meshed grid topology. Meshed grids have the peculiar characteristics of having redundant cable segments, providing alternative paths for energy

exchange. One major advantage of meshed microgrids is an highly increased fault tolerance, since even if one or multiple cable segments fail or are tampered, the alternative paths manage to keep the whole microgrid functioning properly. Another advantage is given by a more even voltage level distribution, which leads to lower fluctuations and differences in voltage between different sections of the grid [3, 6]. The obvious downside of this kind of topology is a more complex layout and higher costs due to more cable length needed to connect households with redundant paths.

### GIS-based studies

There have been a limited number of GIS-based studies in the past related to electrification planning. However, they differ in scope and considerations with respect to the study described in this chapter, as explained in this section.

Most GIS-based studies for electrification planning found in literature are focused on specific geographical areas. For example, a GIS-based decision support tool is discussed specifically for northeast of Brazil in [7], a cost-effective electrification is sought for Kenya based on GIS in [8], a GIS-based Network Planner tool is presented in [9] to compare the electrification options in Ghana, another Network Planner tool-based study is presented for the case of Nigeria in [10], and site selection for micro-hydro power generation systems in the eastern Himalayan region of India is enhanced using GIS in [11]. GIS is also used to perform a cost comparison of technology approaches to improve energy access with case studies for Ethiopia and Nigeria in [12], a fully GIS-based energy access modeling is performed for a case study for Ethiopia in [13], another case study on Ethiopia is considered while using geospatial energy access planning in [14], and another GIS-based case-study on Nigeria for electrification planning is detailed in [15].

In terms of applications, the GIS-based studies reported in literature so far encompass a range of applications within the context of electrification planning. For instance, performance of PV mini-grid systems over large geographical areas is determined using GIS in [16]. In [9], data on electricity demands and costs is combined with population and other socio-economic data while computing demand estimates, with the aim for identifying the most viable electrification alternative amongst grid extension, standalone SHS, and mini-grid. Additionally, the microgrids considered are AC and also diesel-based. Again, least cost electrification is sought in [8] between standalone SHS and grid extension without considering microgrids. Similarly, a least cost model is built in [12] to compare technology costs of electrification through multiple renewable technology-based mini-grids, standalone PV, and grid extension. However, diesel is also considered as one of the supply technologies for both standalone systems and mini-grids. Population density is considered along with costs of grid-based electricity for the case-studies in Nigeria and Ethiopia. The concept of multitier framework (MTF) for measuring energy access is also considered, while the two cost-based parameters considered in [12] are levelized cost of electricity (LCOE) and total costs per household. Both urban and rural areas of Nigeria are considered in the study described in [15], which uses GIS-based data to arrive at LCOE for different electrification options including diesel gensets. A similar analysis is undertaken in [14] for Ethiopia.

A variety of energy technologies is considered including PV, biomass, wind, diesel and hydro in [17], which develops an Open Source Spatial Electrification Toolkit (OnSSET)

using GIS and an integrated electrification model. Different considerations like household density, local renewables and diesel costs, local grid distances, and kWh/household/year for various tiers of the MTF are taken into account in [17], in sub-Saharan Africa. In [7], renewable energy management is the primary goal while using GIS for the semi-arid environments in north-eastern Brazil. Biomass is also considered as an energy source in [7]. Satellite imagery is used in [18] for the purpose of identifying extremely poor villages suitable for unconditional cash transfers for poverty alleviation and siting PV rural microgrids. GIS is used for the purpose of creating energy access projections in [13]. A recent study has also integrated urban energy models within GIS into an open source platform for the optimization of energy systems in cities, which also helps in the optimal allocation of distributed storage in urban energy systems [19].

As seen in this section, while GIS has been used for electrification planning in general, there is a clear research gap in terms of investigating microgrid topologies or layouts using GIS. Furthermore, the microgrids considered in this chapter are decentralized, based on SHS, and are purely DC in nature. Additionally, graph theory-based concepts and spatial geometry are utilized in this study to arrive at the optimal microgrid layouts. In this chapter, using GIS as the first step, a methodology is developed to identify the optimal microgrid layouts for the purpose of off-grid electrification.

### 7.1.2. SCOPE OF THIS STUDY

The work described in this chapter is limited to a pre-electrical design phase study, which can already give insights towards the optimal topology for a decentralized microgrid. The main aim of this work is the generation, analysis and comparison of different microgrid topologies at the scale of an intra-village or community interconnection, using graph theory concepts for gaining insights towards cost considerations as well as some electrical operational parameters like line congestion and redundancy, starting from real ground-level data.

### 7.1.3. CONTRIBUTIONS OF THIS CHAPTER

Following are the main contributions of this chapter.

1. **Incorporation of ground-level data through GIS.** The use of GIS enables the efficient analysis of high resolution ground level geographic data, which reflects the actual physical spread of the households in remote areas.

2. **Graph theory-based analysis.** A graph theory-based analysis at a village or community level offers a more realistic methodology than depending on conventional microgrid layouts that may not be tailored for the specific geographic spread of the households at a given site.

3. **Passive optimization at the design stage.** The methodology proposed in this chapter enables a passive optimization at the design stage between the cabling costs and the operational parameters like line congestion without necessitating an active power flow analysis.

## 7.2. Graph theory

Graph theory is a branch of mathematics that deals with the study of mathematical elements called *graphs*. This section outlines a few basic concepts from graph theory and describes how they can be used in the context of evaluating microgrid topologies.

### 7.2.1. Graph theory: some concepts and definitions

#### Graph

A graph $G = (V, E)$ is a pair of subsets, in which $V$ is a set of $n$ vertices (or nodes) and $E$ is a set of $m$ edges (lines). Each edge $e$ in the set $E$ is an object that connects between them two nodes $i$ and $j$ of the set $V$. An edge is said to be *incident* to the two vertices it connects, while each of the two vertices can be said to be *adjacent* to each other when connected through a common edge.

Edges can also be created by connecting a single vertex to itself; in this case the edge is said to be a *self-loop*. However, given that this study deals with the use of graph theory only in the context of electricity networks and microgrids, such self-loops will not be considered.

#### Edge weights

Edges are usually assigned a weight, an additional parameter for the analysis of the network characteristics. The weight can be any kind of network characteristic depending on the kind of network being considered and the nature and purpose of the analysis. For example, length of each edge in meters can be used a weight for the specific purpose of microgrid topology analysis.

#### (Un)directed graphs

An undirected graph is one where each edge is only defined by an unordered pair of vertices $(i, j)$ it connects, along with its weight. On the other hand, a directed graph, also sometimes called a *Digraph*, is a graph with oriented edges. That is, an edge now has to be additionally defined by its direction. Therefore, in the case of digraphs, the ordered couple of vertices $(i, j)$ will be different from $(j, i)$. Figure 7.3 depicts simple examples of directed and undirected graphs.
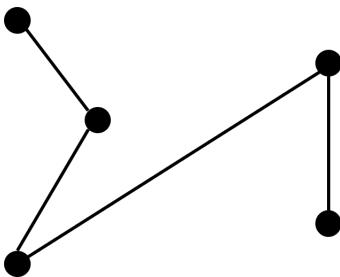


(a)  Undirected graph with 5 vertices and 4 edges.
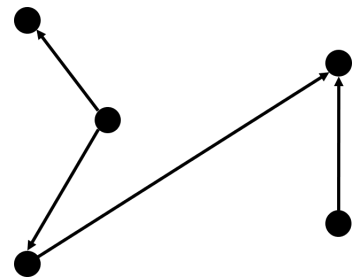
(b)  Directed graph with 5 vertices and 4 directed edges

Figure 7.3: Examples of directed and undirected graphs.

### DEGREE OF CONNECTIVITY

Degree of connectivity of a vertex is defined as the number of edges incident on the vertex. Consequently, a few special vertices can be classified based on their degree of connectivity. For example, *isolated* vertices have a degree of 0 as they are completely disconnected from the rest of the graph; vertices with a degree of connectivity 1 are called *end* vertices as they are the dead-end branches in a graph; vertices in a graph with $n$ edges and having a degree of connectivity of $n - 1$, i.e., connected to every other vertex through a single edge, are called *dominant* or *universal* vertices. An example of a dominant vertex is the central node of the spider diagram considered in Figure 7.1(a).

### PATHS AND (UN)CONNECTED GRAPHS

A *path* is a sequence of edges connecting an ordered sequence of vertices in a graph. A path from vertex $i$ to vertex $j$ is a sequence of edges starting from vertex $i$ and finishing at vertex $j$ going through a finite or infinite number of vertices along the way. Consequently, an edge $(i, j)$ in $E$ can be a possible path from $i$ to $j$, but need not be the only path.

A *connected* graph is one in which there is at least one existing path connecting any pair of vertices $i, j$ in $V$ through any path or a number of edges in $E$. An example illustration can be seen in Figure 7.4(c). On the other hand, if even one pair of vertices in $V$ remains unconnected, then the graph is said to be *unconnected*. By definition, an unconnected graph is devoid of any universal vertices. An example of unconnected graph can be seen in Figure 7.4(b).

Additionally, the concepts of *empty* and *complete* graphs can be introduced. A graph $G = (V, E)$ is said to be an empty graph if the set $E$ is empty. In other words, no edges exist in the graph. Alternatively, it can be said that the degree of connectivity is 0 for all the vertices in $V$. Figure 7.4(a) illustrates an empty graph. Finally, a complete graph is one in which each vertex $i$ in $V$ is connected to every other vertex $j$ through a direct edge in $E$. Therefore, a complete graph is composed of only universal vertices. Figure 7.4(d) illustrates a complete graph. Furthermore, it can be said that the number of edges $m$ in a complete graph is given by Equation 7.1.

$$m = n(n - 1) \text{ for a digraph} \tag{7.1}$$
$$= \frac{n(n - 1)}{2} \text{ for an undirected graph}$$



(a) Empty          (b) Unconnected          (c) Connected          (d) Complete
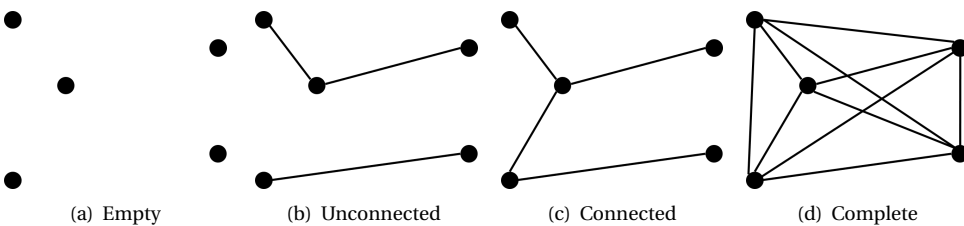
Figure 7.4: Types of graphs for the same set of vertices $V$.

Given that this study focuses on microgrid topologies, the work described here will

focus on connected graphs. In other words, the microgrid is assumed to connect all households in the given settlement.

### Matrix representation

For using graphs in the context of computation, two particular matrix structures can help in representing correlation between nodes or vertices and edges, viz., *adjacency matrix* and *incidence matrix.*

An adjacency matrix $A$ is an $n \times n$ matrix, representing a graph $G$ in terms of adjacency between its vertices, as shown in Equation 7.2.

$$A_{ij} = 0 \forall (i, j) \notin E \text{ i.e., if } i \text{ and } j \text{ are not adjacent} \tag{7.2}$$
$$A_{ij} = 1 \forall (i, j) \in E \text{ i.e., if } i \text{ and } j \text{ are adjacent}$$

Consequently, it can be said that the adjacency matrix for an empty graph will have $A_{ij} = 0 \forall i, j$, while the adjacency matrix for a complete graph will have $A_{ij} = 1 \forall i \neq j$, as the diagonal elements being equal to 1 would represent self-loops.

An incidence matrix $I$ is an $m \times n$ matrix, representing a graph $G$ in terms of the incidence of each edge $e$ in $E$ with each vertex $v$ in $V$, as shown in Equation 7.3 for an undirected graph.

$$I_{ve} = 0 \text{ i.e., if } e \text{ is not incident with } v \tag{7.3}$$
$$I_{ve} = 1 \text{ i.e., if } e \text{ is incident with } v$$

The definition of each edge in the matrix is therefore dependent on the two vertices it connects. For a directed graph, an additional information on direction needs to be present. This is typically done by identifying the start vertex or node with a value of -1 and end node with a value of 1 in each edge column $e$.

### 7.2.2. Trees in graph theory

A *tree* in graph theory can be defined as an acyclic connected undirected graph, or an undirected graph without any loops. In other words, each pair of nodes is connected by means of a single unique path. For any given set of $n$ nodes, a tree is, by definition, composed of $m = n - 1$ edges. A tree is a sub-graph of the given graph $G = (V, E)$, which connects at the same time all the vertices included in a given subset of $V$, using edges included in $E$. If all the vertices in $V$ are connected by a single tree, that tree is then called a *spanning tree*. The concept of trees is very important in the area of network analysis, and is also used in this study. A thorough and exhaustive work on trees in graph theory can be found in [20].

### Minimum spanning tree

The concept of trees can be applied to many practical problems in which the aim is to connect a subset of elements (nodes, vertices, people, houses, etc. depending on the kind of network) using the lowest possible number of relations (edges, lines, connections, etc. depending on the kind of network). These kinds of problems usually have cost minimization as one of the main criteria for connecting the desired elements. Therefore, one of the main geometrical problems addressed in graph theory addressed by mathematicians is a

way to obtain the shortest or least costly spanning tree for a given subset of vertices in $V$ for a graph $G$. Such a sub-graph or tree connecting all the vertices without any cycles with a minimum possible total edge-weight is called a *minimum spanning tree* (MST).
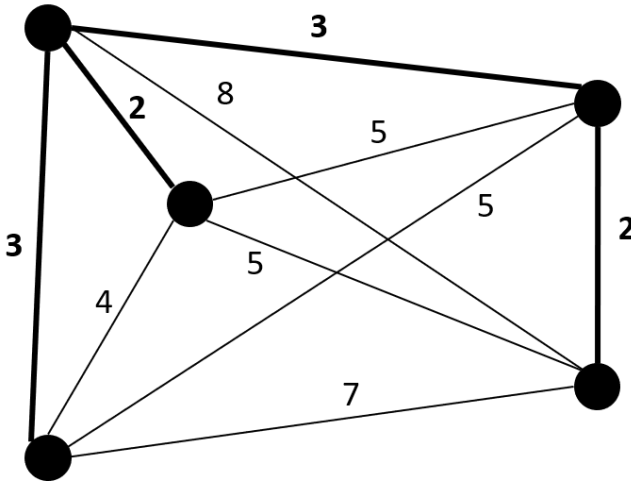


Figure 7.5: Example of a minimum spanning tree (MST) for a weighted graph. The MST as a sub-graph is shown in bold in the otherwise connected graph.

The problem of MST, by definition, is only applied to weighted edges. Figure 7.5 shows an example of an MST for an undirected graph with weighted edges. The MST problem has been discussed in literature for decades, with many algorithms having been developed to solve it already since the 1950s [21], the most known and efficient examples being Kruskal's and Prim's algorithms.

Prim's algorithm, which is also used later to generate the MST layout, utilizes the concept of the *nearest neighbour*, which means the vertex which has the shortest distance (weight) in $G$ from a given vertex or sub-tree. The idea behind Prim's algorithm can be explained as follows [22].

1. Take the starting graph $G = (V, S)$ for the set of vertices $V$, knowing the weight of each single edge contained in $S$.

2. Start creating a tree $T = (V, E)$, $E$ being an empty set of edges.

3. Perform one of the following actions:

    (a) Add to $E$ the edge in $S$ connecting any vertex in $V$ to its nearest neighbour.

    (b) Add to $E$ the edge in $S$ connecting any sub-tree in $T$ to its nearest neighbour.

4. Repeat step 3 until a spanning tree is formed in $T$.

5. The obtained spanning tree $T$ is an MST for the set of vertices $V$ and the set of edges $S$.

This algorithm is particularly useful for Euclidean applications to connect points in a geometrical plane using Euclidean distance as weight. This is because the weights of the potential edges do not necessarily need to be known aforehand as an input to the algorithm as long as the geometrical locations of the points are known, which can be used to calculate the distance between each pair of points.

### 7.2.3. Graph theory applied to network analysis

Myriads of real-world applications exist for graph theory. Some common examples include planning (or maintenance) of road networks, water supply networks, electricity transmission grid, GPS navigation systems, among many others. For the study described in this chapter, graph theory is going to be used as a tool to evaluate, analyze and compare microgrid layouts or topologies. Therefore, the vertices of the graphs would be the single nodes of the microgrid, which in this study are the single households inside a community with SHS that need to be interconnected. The edges of the graph would be the lines (cables) of the microgrid's electrical distribution network that is physically connecting the households.

One major advantage of using these concepts is the great flexibility they offer, making it viable to study different parameters and aspects of microgrids with just minor modifications. As an example, different aspects of the microgrids can be analyzed considering different characteristics of the lines as weight of the edges. For example, using the physical euclidean length of the cables as weight is a good way to analyze and compare cable costs for different layouts, while using cable resistances as weight can be useful for power flow analysis and for losses calculations.

Examples of graph theory applied to electrical network problems are already found in literature with different scopes and purposes. An extensive overview of how electrical networks can be analyzed and represented using graph theory, focusing mainly on the circuit modelling point of view, is given in [23]. Graph theory application to network planning at the microgrid level has been suggested in literature, usually focusing on just one algorithm or one suggested starting topology, without usually making an extensive comparison of different possible solutions [24].

#### Average network length

The most obvious parameter for the comparison and bench-marking of topologies is the network length itself. The *average network length* in this context can then be defined as the distance that needs to be covered with cables per household for each topology. Naturally, for cost considerations, it is desirable to keep the average network length as low as possible. It should be noted that the actual costs of installing a microgrid would include other aspects such as poles, interfacing converters, etc. However, for the purpose of comparing the microgrid layouts with each other, the average network length is deemed to be a sufficient first indicator to give insights on cost comparisons.

Given the least total edge length and therefore the least average network length, the MST will be considered as an additional layout apart from the 4 conventional topologies shown in Figures 7.1 and 7.2 when considering the microgrid topologies in this study.

**AVERAGE SHORTEST PATH LENGTH**

In general, the shortest path problem aims to find the path between two vertices $i$ and $j$ in a weighted graph $G$, which has the lowest possible sum of the weights of the edges included in the path. Many different versions of the problem can be formulated, depending on the graph being directed or undirected and the vertices that are taken into consideration. The simplest version is the single-pair shortest path problem, which considers only one pair of vertices $i$ and $j$, $i$ being the starting point of the path and $j$ the end point of the path. There are many algorithms providing solutions to the shortest path problem, like the Dijkstra algorithm [25] and the Floyd-Warshall algorithm [26]. The all-pairs shortest path length problem � is addressed in these, which is particularly useful for the calculation of the *average shortest path length* of a graph or network by simply averaging the length of all the shortest paths found by the algorithm. As explained later in Section 7.3, the average shortest path length can be used as a representation of some network characteristics, such as redundancy, congestion avoidance and loss reduction. Hence, this parameter is going to be used for microgrid topology comparison and optimization.

## 7.3. METHODOLOGY

In order to arrive at the optimized microgrid topologies, a series of steps is carried out, starting with obtaining real-world geographical inputs from a GIS software.

### 7.3.1. GIS-BASED DATA PROCESSING

The overall GIS-based methodology is depicted in the flowchart shown in Figure 7.6. The output topologies obtained from this GIS-based methodology will then be used in the layout optimization described in Section 7.3.3.
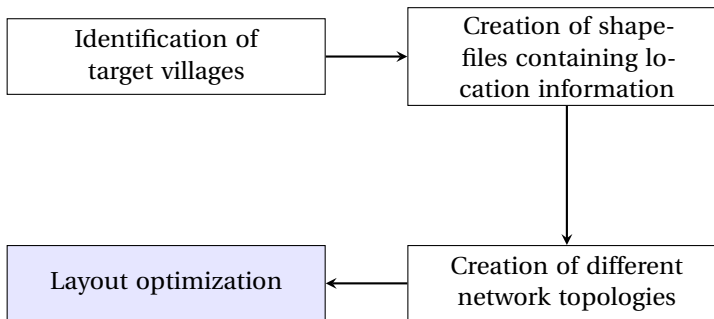


Figure 7.6: Block diagram explaining the overall methodology based on QGIS. The shaded block involving layout optimization is explained in detail in Section 7.3.3 and Figure 7.14.

**QUANTUM GIS (QGIS)**

In general, a Geographic Information System can be defined as any system which has the purpose to collect, analyze, process, represent and communicate spatial and geographic

---

✷ the computation of the shortest paths from one single vertex $i$ to all other vertices in the graph, for all pairs of vertices $(i, j)$ at once.

data. For the purpose of this study, a fully open source GIS software called Quantum GIS (QGIS) was used [27]. QGIS has an interface that provides a visualization window for geographical features, a customized toolbar, a browser panel, a layer panel and a useful built-in Python console, including an internal editor, as shown in Figure 7.7. All the data is stored in layer files, with the format being shapefiles (.shp), which is a composite ensemble of different files storing geometrical features (points, lines or polygons), their geographical location, and a given set of attributes. The version of QGIS used in this study was "QGIS 2.18 las Palmas de Gran Canaria".
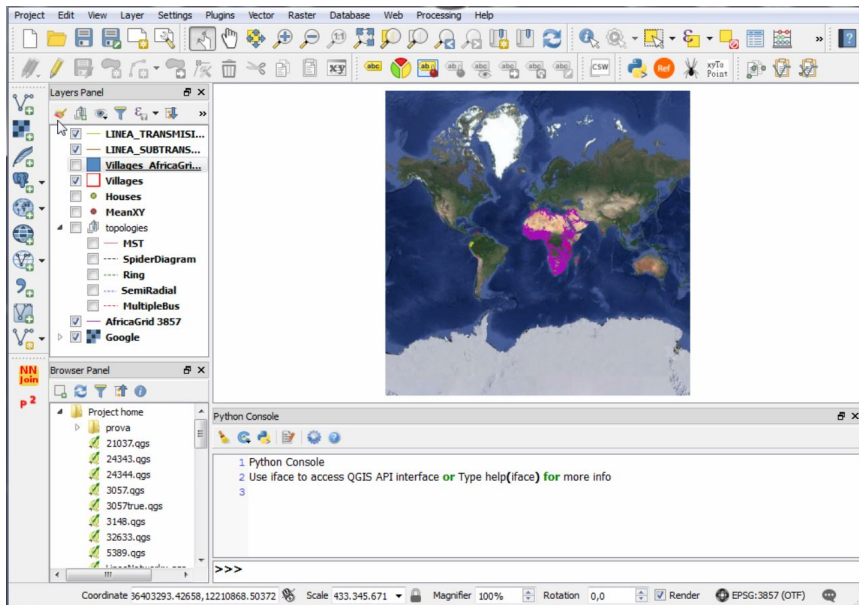


Figure 7.7: Snapshot of the QGIS interface.

### LOCATION SELECTION

The first step using QGIS was the identification of a sample of (remote) locations to be used as case studies, from different (rural) parts of the world. It was decided to look for remote areas in different countries and different environments, to give a varied sample, and to focus mainly on small villages, with a number of households up to around 40. In the process of choosing the smaller villages, it was also chosen to select settlements showing different spatial household distribution patterns for sake of variety and diversity of the sample. Part of the sample was selected starting from available databases for real-world rural electrification projects, while other locations were chosen from specific targeted countries with energy access issues and based on their distance from available infrastructure. For example, the set of Tanzanian villages were retrieved from the Rural Electrification Densification Programme (REDP) database [28]. Similarly, for villages in Bangladesh, an available database on "hard-to-reach" communities was used to pick these locations [29]. This resulted in the selection of 42 locations, spread over 12 different

countries, as shown in Figure 7.8.



Figure 7.8: The selected locations for the case-studies shown on the world map.

The sample locations, as shown in Table 7.1, ranges from 5 to 40 households per location, from a density of around 100 households per km$^2$ to around 5000 households per km$^2$ and from a surface area of around 3000 m$^2$ to around 150000 m$^2$. The countries which were included into the analysis are Tanzania, Gabon, Cameroon, Madagascar, Bangladesh, India, Nepal, Cambodia, Colombia, Peru, Brazil and Iceland. Iceland was included just to show how the methodology can also be applied to isolated areas of developed nations. All the other selected countries at the time of conducting this study had low rural electrification rates and the chosen locations (villages) were disconnected from the main grid.

Table 7.1: Ranges of parameters for the selected locations.

|                              | Min   | Max     |
| ---------------------------- | ----- | ------- |
| Number of Households [hh]    | 5     | 40      |
| Density [hh/km$^2$]          | 93.58 | 5016.03 |
| Area [m$^2$]                 | 2851  | 145324  |

With the villages identified, the next step was to create shapefiles containing information about the locations. Two types of shapefile layers were created:

- Point shapefiles, containing point features representing households of the locations

- Polygon shapefiles, containing the external perimeter of the locations

After having created the shapefiles of the locations, it was possible to start the analysis of the gathered information, using the geographical correlation based on coordinate proximity between the separate shapefiles. Figure 7.9 shows a sample of 3 of the locations with identified households and their external perimeters.



Figure 7.9: Sample of the locations with identified households and external perimeter. From left to right: locations 10, 15, and 26.

Once the two shapefiles and the mentioned attributes had been created, the next step in the QGIS-based analysis was to create different microgrid layouts to connect the households between each other.

### 7.3.2. Microgrid topology creation

Five different kind of microgrid topologies were identified and chosen to be compared in this study, viz: 1. Spider diagram 2. Ring topology 3. Bus topology 4. Radial topology 5. Minimum Spanning Tree (MST).

Before the creation of these topologies for each location, one additional feature had to be identified, viz., the center of the village, which is the point having the minimum average distance from the households. The (x,y) coordinates of this central point were found using Equation 7.4.

$$x_{\text{c}} = \frac{\sum_{k=1}^{hh} x_k}{hh}$$

$$y_{\text{c}} = \frac{\sum_{k=1}^{hh} y_k}{hh}$$

(7.4)

in which $hh$ is the number of households of the given village, $x_{\text{c}}$ and $y_{\text{c}}$ are the coordinates of the center of the village and $x_k$ and $y_k$ are the coordinates of each of the households inside a given village. It must be noted that in this case the same relevance (weight) was assigned to each household. It is possible to multiply each coordinate by a relative weight if, for example, different household power production and energy demands need to be taken into account. These calculations to find the center of the location can be performed easily within QGIS.

### Spider diagram

Starting from the spider diagram in which every single household is connected directly to a central point (in this case the just identified center of the village), a tool from the

QGIS repository called "RT QSpider" can be used. This tool creates a line shapefile layer containing multiple line geometries, taking as inputs starting and ending (x,y) coordinates from a defined input layer. In this case, the starting coordinates are the single household coordinates, and the end coordinates are $x_c$ and $y_c$. It is possible then to join these lines together to form a single poly-line geometry, representing the final spider diagram for each location using `Vector -> Geometry Tools -> Singleparts to Multiparts`.

### RING TOPOLOGY

The ring topology consists of a single line, connecting the households one by one forming a closed loop. In terms of graphs, every node in this network has a degree of connectivity equal to 2. Also, if any of the edges of the network is removed, the network is still a connected graph (Section 7.2.1). Households are, therefore, connected to each other with single lines, which can then be joined together with the same procedure used for the spider diagram.

### BUS TOPOLOGY

Bus topology creation is more complicated. This topology consists of one (or more) straight connection lines (bus lines) running through the village, to which the households are directly connected via a (ideally) perpendicular line. To implement that in QGIS, the bus(es) has to be identified and drawn manually. Then, using a short Python script in the console, it is possible to identify, for each household, the closest point on the bus line and connect, with an additional, perpendicular line, the household to the central bus.

### RADIAL TOPOLOGY

The radial topology uses the household closest to the centre of the village ($x_c$,$y_c$) as a central starting point for the microgrid. If there is not any household sufficiently central, then the centre of the village itself is used as origin of the network. This also means that some of the villages will have a radial network with a number of nodes equal to the number of households, while other villages might have one extra hub node as origin which does not correspond to an actual household, exactly as in the spider diagram. From this origin, the network expands radially towards the most peripheral households. Once each radial branch is created, the following households are either connected to the closest branch, or a new branch is created connecting them directly to the origin, depending on the distance. For bigger villages, sub-branches can also be added.

### MINIMUM SPANNING TREE

Finally, the MST, consisting of the shortest possible combination of edges that leads to a completely connected graph, is identified in a relatively easy manner in the QGIS environment using a plug-in available in the QGIS repository: "ReconstructLine". This useful plug-in accepts as input a set of points, which have to belong to the same shapefile layer, and gives as output a set of single lines connecting one point to the other in a predefined line shapefile layer, so that the resulting overall network is the Minimum Spanning Tree for that specific set of points, using as working principle the Prim's algorithm [22]. The single lines can then be merged into a poly-line representing the whole network using the already mentioned process.
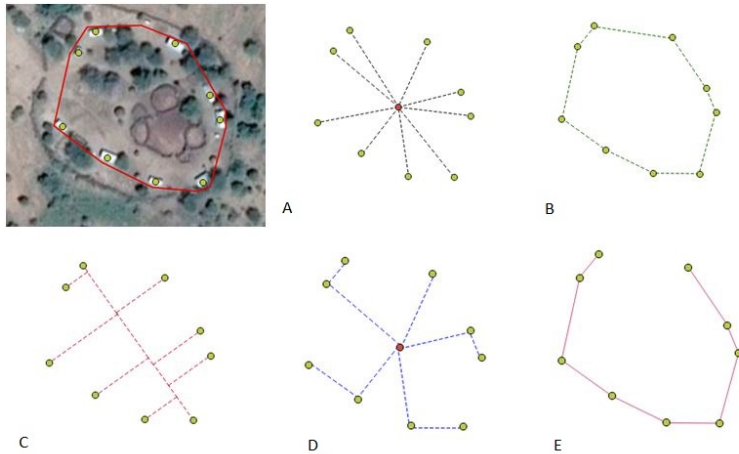
Figure 7.10: Map view and resulting network topologies for location 23. A: Spider Diagram. B: Ring. C: Bus. D: Radial. E: MST.

After the topologies have been created, each of the chosen locations should have five different layouts to connect its households with each other, without any household left disconnected. An example of the graphical visualization of the resulting networks is shown in Figure 7.10 for location 23.

The geometrical length of each of the created network can be easily derived in the attribute field calculator of the line shapefile in QGIS, using the command $length. Spatially correlating each of the network to the original village, it is then possible to collect in one single shapefile, namely the original polygon layer in which all the villages were stored, all the information gathered so far: location number, country, area, perimeter, number of houses, house density and now length of each of the identified topology. It is then trivial to calculate for each village the average needed length of the network, in [m/hh], directly in the attribute table. A summary of all these parameters and characteristics, for the considered sample of villages, is shown extensively in Table 7.2 in Section 7.4.

### 7.3.3. Layout optimization
The topologies created with the methodology described in Section 7.3.2 are going to be utilized in the following steps as the starting topologies for a layout optimization, which is going to be performed using an algorithm written in Python.

#### The rationale behind the optimization
So far, the interconnection costs in the form of network length has been the main parameter of comparison between the topologies. That is why only topologies that are spanning trees have been selected as the initial topologies for comparison. That is, there are no redundant edges in the topologies (except for the ring topology, which has one extra edge closing the ring loop). This ensured a minimization of the network length, within the constraints imposed by each given topology definition.

Nonetheless, cost saving is not the only important aspect while designing a DC microgrid for interconnecting SHS. Additional network lines (added edges), which lead to increased costs, can bring benefits for other aspects of the microgrid operation. Three of those aspects are going to be discussed in the following paragraphs: redundancy, congestion avoidance and losses reduction.

**Redundancy**    Redundancy can be interpreted as safety or reliability of the network in case of damages to single lines. Each spanning tree, on losing even a single edge, becomes separated into two different sub-networks, isolated from each other. This means that potential exchange of energy from one sub-network to the other is not possible anymore. Furthermore, if in one of the sub-networks the energy production and energy reserve is not enough to satisfy the demand of the same sub-network at a given moment, the risk of energy outages and the loss of load probability dramatically increases. With additional edges, increasing the redundancy of the network, additional alternative paths can be found for at least some sub-sections of the network. The most peripheral nodes of the network would always suffer higher risks of isolation then more central, better connected households, but, as more edges are added to the network, the overall risk of isolation of sub-networks is reduced. An example of that can be seen in Figure 7.11.
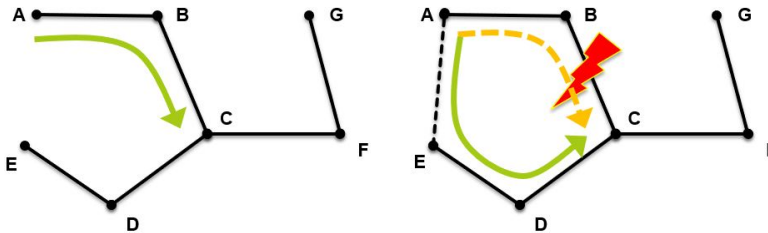


Figure 7.11: Example of increased redundancy for power flow from A to C by addition of edge AE, making the topology resilient to a fault in, say, edge BC.

**Congestion avoidance**    Congestion in one or multiple lines is detrimental for the performance of microgrid networks. If the power flow exceeds the technical limits of a cable, the consequence can be its failure and hence the complete disconnection of the line. Moreover, the power losses in a cable are proportional to the square of the current flowing in it, leading to very high ohmic losses. As in the case of redundancy, adding new edges may offer a second alternative path for power flow from a given household A to a given household B, reducing risks of congestion. An example can be seen in Figure 7.12.

**Line-loss reduction**    The concept of average shortest path length defined in Section 7.2.1 helps in understanding the potential of line loss reduction through the addition of network edges. The shortest path length in a network for a given pair of nodes is the length of the shortest route to connect those two nodes to each other following the edges of the graph. The average shortest path length is simply the average of this distance over all the possible
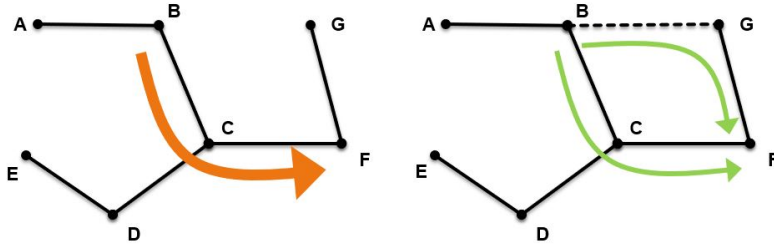
Figure 7.12: Example of congestion avoidance by edge addition. Power flow from B to F can be via C as well as G due to addition of edge BG.

pairs of nodes in the network. As the cable resistance is proportional to the length of the line, the line losses due to power exchange between households increases with increasing average shortest path length. The addition of new edges can create new shortest paths between pair of households, reducing the average shortest path length of the network and potentially the losses in power exchanges. An example of that can be seen in Figure 7.13.
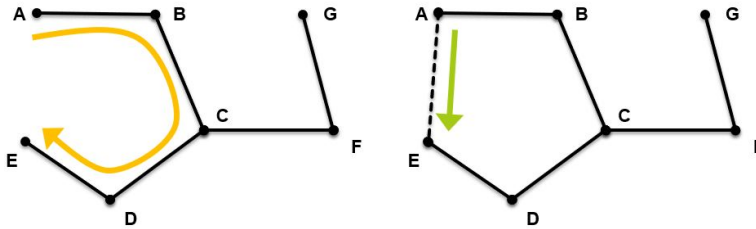


Figure 7.13: Example of decreased shortest path length between A and E by addition of edge AE.

#### OPTIMIZATION

The potential benefits of the addition of redundant edges in these topologies necessitate an optimization that not only aims at minimizing cable lengths and therefore cable costs but also tries to find a trade-off between costs reduction and the said mentioned benefits. It is difficult to quantify these benefits in order to compare them with cable length costs, especially in this first phase of network planning. Nonetheless, in order to compare these benefits, it was decided to use the average shortest path length of the network as a second parameter to optimize, taking it as a general indicator of the level of redundancy, congestion avoidance and losses reduction, as opposed to average network length, which is taken as an indicator of direct cable costs. The proposed target function to be optimized is shown in Equation 7.5.

$$f = \sqrt{\mathtt{wf} \cdot (\bar{l})^2 + (\overline{spl})^2} \tag{7.5}$$

in which $\bar{l}$ is the average network length in [m], $\overline{spl}$ is the average shortest path length of the network in [m] and $\mathtt{wf}$ is a user-defined weight factor. This weight factor is tuned to
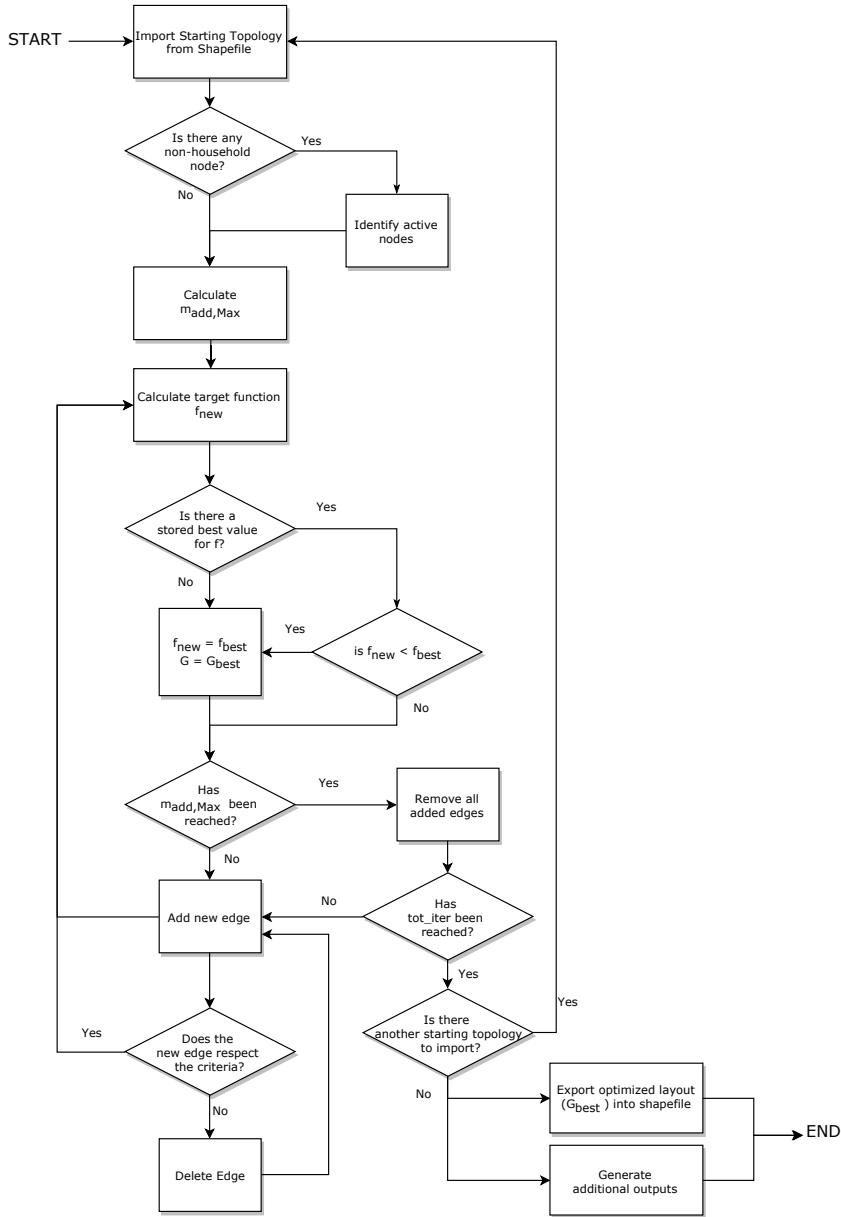
Figure 7.14: Flowchart of the proposed algorithm. A starting network topology is imported in `.shp` format to be processed by the algorithm. Passive nodes are identified, if present. Edge addition iterations are performed until `tot_iter` is reached, re-initialising the edge addition process from the starting topology every $m_{add,Max}$ edges. Each new edge is checked under a set of criteria before being added. A target function is calculated at every iteration and the best overall graph $G_{best}$ is stored and saved as optimized output. Multiple starting topologies can be used to optimize a graph (topology).

prioritize one or the other parameter which is considered more important for each single application and target microgrid site.

In this study, different weight factors were used during the analysis to check the sensitivity of the result to weight factor variations. Before microgrid implementation, a deeper analysis is needed to identify a precise case-specific weight factor to be applied, depending on a combination of technical and socio-economical aspects at the microgrid sites. Examples of such aspects can be availability of materials, expected energy demand, planned size of SHS, risk of tampering, energy security requirements, climate conditions, and many more. In this work, weight factors in the range of 0.1 to 2 are suggested as reasonable values for the optimization algorithm. The way Equation 7.5 is written, higher weight factors will prioritize cable costs over the mentioned benefits, so minimization of the average network length will be more relevant than the minimization of average shortest path length, hence resulting in fewer edges added. On the other hand, lower weight factors will prioritize redundancy, congestion avoidance and losses reduction, minimizing the average shortest path length as much as possible, hence tending to add more edges to the starting topology.

The topologies obtained in Section 7.3.2 are going to be used as starting networks for the addition of new edges, hence forming so called "meshed" microgrids, which can be simply defined as microgrids in which one or more loops can be identified.

### ALGORITHM

To perform this optimization, an algorithm in Python language was written, following the flowchart shown in Figure 7.14. The algorithm takes as inputs one or more of the starting topologies, and it processes it by adding new edges for a user-defined number of iterations, trying to minimize the target function which takes into account both average network length and the average shortest path length. As some starting topologies may have non-household nodes, active (household) nodes are identified first. The maximum number of edges $m_{\text{Max}}$ for a graph $G$ was given by Equation 7.1. If $m_{\text{start}}$ is the number of edges in the starting topology, then the maximum number of edges $m_{\text{add,Max}}$ that must be added to reach a complete graph is given by Equation 7.6, where $n$ is the number of active nodes (households).

$$m_{\text{add,Max}} = \frac{n \cdot (n-1)}{2} - m_{\text{start}} \tag{7.6}$$

As addition of edges till $m_{\text{add,Max}}$ can be computationally intensive, a user-defined input `tot_iter` is provided such that the iteration stops when this value is reached (each iteration is an edge added). Overall, the algorithm needs as input the starting topology shapefile(s), `tot_iter` for each starting topology, and `wf` for the target function. The algorithm outputs the new shapefile of the optimised graph, a spreadsheet of the $\bar{l}$ and $\overline{spl}$ values for all graphs evaluated during the iterations, a scatter graph with those values, and a graphical representation of the network layout. An additionally useful output is a set of `.mat` files containing information on the nodes and edges of the optimised network.

Table 7.2: Attribute table of the locations shapefile, containing the gathered, measured and calculated data on the 42 chosen locations.

| Location | Country | Area [m²] | Perimeter [m] | Houses [hh] | Density [hh/km²] | MST [m] | Spider [m] | Ring [m] | Radial [m] | Bus [m] | MST [m/hh] | Spider [m/hh] | Ring [m/hh] | Radial [m/hh] | Bus [m/hh] |
|---|---|---|---|---|---|---|---|---|---|---|---|---|---|---|---|
| 1 | Colombia | 11043.0 | 678.0 | 14 | 1267.8 | 362.5 | 878.7 | 564.4 | 368.0 | 418.6 | 25.9 | 62.8 | 40.3 | 26.3 | 29.9 |
| 2 | Iceland | 11823.1 | 618.0 | 6 | 507.5 | 304.0 | 410.5 | 468.0 | 309.8 | 348.3 | 50.7 | 68.4 | 78.0 | 51.6 | 58.1 |
| 3 | Iceland | 85486.2 | 1679.5 | 8 | 93.6 | 820.7 | 1720.3 | 1413.4 | 892.2 | 863.9 | 102.6 | 215.0 | 176.7 | 111.5 | 108.0 |
| 4 | Peru | 15914.7 | 747.7 | 16 | 1005.4 | 444.6 | 1176.4 | 692.1 | 456.5 | 546.3 | 27.8 | 73.5 | 43.3 | 28.5 | 34.1 |
| 5 | Peru | 79484.6 | 1270.4 | 40 | 503.2 | 1305.8 | 4403.3 | 1594.0 | 1456.1 | 1962.1 | 32.6 | 110.1 | 39.9 | 36.4 | 49.1 |
| 6 | Colombia | 6406.2 | 598.8 | 10 | 1561.0 | 283.9 | 549.5 | 506.0 | 283.9 | 300.5 | 28.4 | 54.9 | 50.6 | 28.4 | 30.1 |
| 7 | Colombia | 11407.5 | 521.0 | 8 | 701.3 | 300.3 | 520.4 | 437.9 | 324.8 | 319.4 | 37.5 | 65.0 | 54.7 | 40.6 | 39.9 |
| 8 | Colombia | 2851.0 | 225.7 | 5 | 1753.8 | 113.9 | 141.0 | 164.1 | 106.9 | 118.3 | 22.8 | 28.2 | 32.8 | 21.4 | 23.7 |
| 9 | Colombia | 30192.6 | 1059.5 | 12 | 397.4 | 644.7 | 1328.0 | 934.6 | 717.4 | 761.7 | 53.7 | 110.7 | 77.9 | 59.8 | 63.5 |
| 10 | Brazil | 11440.3 | 645.8 | 9 | 786.7 | 309.8 | 723.1 | 524.8 | 326.7 | 416.7 | 34.4 | 80.3 | 58.3 | 36.3 | 46.3 |
| 11 | Brazil | 30608.2 | 1361.9 | 18 | 588.1 | 727.4 | 2806.2 | 1285.6 | 728.8 | 901.5 | 40.4 | 155.9 | 71.4 | 40.5 | 50.1 |
| 12 | Colombia | 7870.6 | 496.4 | 13 | 1651.7 | 281.5 | 546.7 | 414.3 | 296.4 | 398.7 | 21.7 | 42.1 | 31.9 | 22.8 | 30.7 |
| 13 | Tanzania | 24714.9 | 1099.5 | 29 | 1173.4 | 869.4 | 2362.8 | 1154.5 | 943.1 | 1116.5 | 30.0 | 81.5 | 39.8 | 32.5 | 38.5 |
| 14 | Madagascar | 13455.5 | 520.3 | 19 | 1412.1 | 424.7 | 995.2 | 525.9 | 461.5 | 707.9 | 22.4 | 52.4 | 27.7 | 24.3 | 37.3 |
| 15 | Tanzania | 34537.6 | 1391.8 | 16 | 463.3 | 832.9 | 1611.2 | 1250.6 | 861.2 | 923.1 | 52.1 | 100.7 | 78.2 | 53.8 | 57.7 |
| 16 | Tanzania | 18130.1 | 947.4 | 10 | 551.6 | 489.2 | 1242.5 | 805.1 | 522.4 | 547.5 | 48.9 | 124.2 | 80.5 | 52.2 | 54.7 |
| 17 | Tanzania | 17974.1 | 604.9 | 8 | 445.1 | 365.9 | 601.6 | 523.6 | 365.9 | 423.7 | 45.7 | 75.2 | 65.5 | 45.7 | 53.0 |
| 18 | Tanzania | 52032.9 | 1475.2 | 15 | 288.3 | 863.8 | 2501.0 | 1408.4 | 921.4 | 969.4 | 57.6 | 166.7 | 93.9 | 61.4 | 64.6 |
| 19 | Tanzania | 7555.5 | 556.2 | 14 | 1853.0 | 363.7 | 896.5 | 515.2 | 379.9 | 421.5 | 26.0 | 64.0 | 36.8 | 27.1 | 30.1 |
| 20 | Tanzania | 15026.5 | 636.9 | 11 | 732.0 | 357.6 | 771.1 | 566.9 | 370.9 | 521.1 | 32.5 | 70.1 | 51.5 | 33.7 | 47.4 |
| 21 | Tanzania | 8643.9 | 466.5 | 8 | 925.5 | 270.2 | 453.7 | 387.3 | 270.2 | 280.7 | 33.8 | 56.7 | 48.4 | 33.8 | 35.1 |
| 22 | Tanzania | 41539.1 | 1051.6 | 17 | 409.3 | 842.9 | 1650.8 | 1091.1 | 890.0 | 1039.0 | 49.6 | 97.1 | 64.2 | 52.4 | 61.1 |
| 23 | Tanzania | 6608.0 | 301.0 | 9 | 1362.0 | 229.5 | 393.7 | 274.7 | 288.3 | 312.3 | 25.5 | 43.7 | 30.5 | 32.0 | 34.7 |
| 24 | Tanzania | 14606.7 | 645.3 | 14 | 958.5 | 426.8 | 1075.0 | 652.6 | 455.5 | 487.4 | 30.5 | 76.8 | 46.6 | 32.5 | 34.8 |
| 25 | Nepal | 45111.1 | 1680.3 | 38 | 842.4 | 1145.0 | 6159.5 | 1688.5 | 1160.8 | 1415.8 | 30.1 | 162.1 | 44.4 | 30.5 | 37.3 |
| 26 | Tanzania | 25229.2 | 713.2 | 21 | 832.4 | 544.1 | 1553.4 | 687.1 | 572.8 | 586.6 | 25.9 | 74.0 | 32.7 | 27.3 | 27.9 |
| 27 | Cambodia | 145324.1 | 2385.7 | 36 | 247.7 | 1979.4 | 7683.6 | 2458.3 | 2083.2 | 2250.4 | 55.0 | 213.4 | 68.3 | 57.9 | 62.5 |
| 28 | Tanzania | 46461.8 | 1234.6 | 20 | 430.5 | 936.2 | 2520.0 | 1267.4 | 959.3 | 1167.3 | 46.8 | 126.0 | 63.4 | 48.0 | 58.4 |
| 29 | Cambodia | 16860.5 | 784.0 | 23 | 1364.1 | 503.8 | 1897.3 | 693.8 | 510.5 | 790.2 | 21.9 | 82.5 | 30.2 | 22.2 | 34.4 |
| 30 | India | 57058.7 | 1442.2 | 29 | 508.2 | 957.1 | 3961.4 | 1339.0 | 999.9 | 1352.6 | 33.0 | 136.6 | 46.2 | 34.5 | 46.6 |
| 31 | India | 11606.2 | 589.9 | 24 | 2067.9 | 454.2 | 1074.7 | 606.3 | 471.5 | 637.8 | 18.9 | 44.8 | 25.3 | 19.6 | 26.6 |
| 32 | India | 11628.8 | 629.4 | 27 | 2321.8 | 461.0 | 1749.8 | 561.9 | 469.5 | 587.0 | 17.1 | 64.8 | 20.8 | 17.4 | 21.7 |
| 33 | India | 7201.9 | 575.4 | 26 | 3610.2 | 400.7 | 1050.3 | 547.4 | 411.0 | 487.1 | 15.4 | 40.4 | 21.1 | 15.8 | 18.7 |
| 34 | India | 6877.8 | 499.9 | 12 | 1744.7 | 287.5 | 563.6 | 392.6 | 287.5 | 328.8 | 24.0 | 47.0 | 32.7 | 24.0 | 27.4 |
| 35 | India | 5130.6 | 378.7 | 20 | 3898.2 | 284.2 | 653.6 | 384.5 | 293.9 | 334.3 | 14.2 | 32.7 | 19.2 | 14.7 | 16.7 |
| 36 | Bangladesh | 3189.8 | 310.4 | 16 | 5016.0 | 204.5 | 437.7 | 230.2 | 212.6 | 234.0 | 12.8 | 27.4 | 14.4 | 13.3 | 14.6 |
| 37 | Bangladesh | 6808.9 | 370.4 | 20 | 2937.3 | 326.4 | 633.8 | 418.7 | 335.5 | 440.6 | 16.3 | 31.7 | 20.9 | 16.8 | 22.0 |
| 38 | Bangladesh | 3312.7 | 385.9 | 10 | 3018.7 | 173.6 | 367.6 | 251.4 | 173.6 | 206.3 | 17.4 | 36.8 | 25.1 | 17.4 | 20.6 |
| 39 | Bangladesh | 6076.7 | 417.5 | 24 | 3949.5 | 310.1 | 835.3 | 425.2 | 329.3 | 372.6 | 12.9 | 34.8 | 17.7 | 13.7 | 15.5 |
| 40 | India | 42668.7 | 1157.7 | 29 | 679.7 | 990.0 | 3553.5 | 1290.5 | 1034.3 | 1595.5 | 34.1 | 122.5 | 44.5 | 35.7 | 55.0 |
| 41 | Cameroon | 31263.5 | 1026.1 | 31 | 991.6 | 849.1 | 3381.9 | 1016.3 | 878.8 | 1225.0 | 27.4 | 109.1 | 32.8 | 28.3 | 39.5 |
| 42 | Gabon | 4527.3 | 290.1 | 9 | 1988.0 | 198.6 | 289.6 | 237.6 | 198.9 | 207.3 | 22.1 | 32.2 | 26.4 | 22.1 | 23.0 |

7

## 7.4. Results and discussion

### 7.4.1. Topology creation using QGIS

Based on the steps outlined in Section 7.3.2, the 5 different topologies were created for each of the 42 locations. A summary of all the parameters for each of the 5 topologies for every location is tabulated in Table 7.2. This is the basis for the comparison of different topologies in terms of costs and for the identification of trends useful for evaluating the optimal design of microgrid topologies.

The household density in the selected locations show a strong correlation with the average network length needed per household to completely connect them into a microgrid. Understandably, the more clustered the households are, the smaller the distance between them. This trend is confirmed by the measured length of all the 5 topologies as shown in Figure 7.15, where the single results for each village and each topology are shown together with topology-specific trend lines. The average lengths range from a minimum value of up to 14 m/hh for MST topology in really clustered villages, up to a maximum of around 215 m/hh for a spider topology in really sparse villages. It is clear, then, how the feasibility of microgrid is highly affected by the household density and the household distribution of each village location.
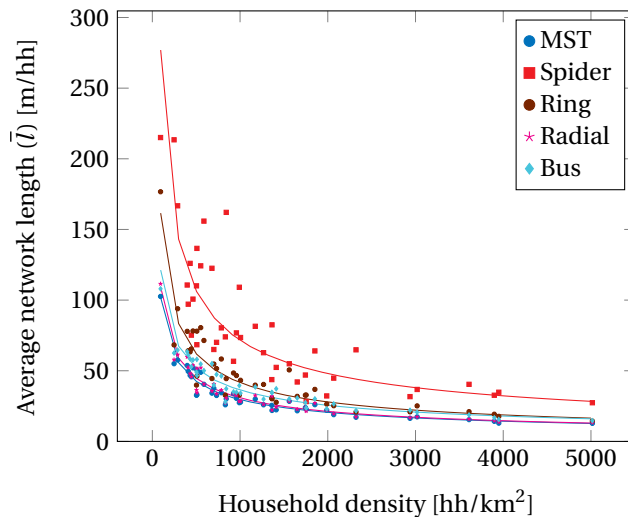


Figure 7.15: Scatter plot showing the variation in average network length $\bar{l}$ for the different topologies over the house densities along with corresponding trendlines.

In terms of general trend, the topologies described can be ranked in the following order, from the best to the worst in terms of average network length:
MST < Radial Topology < Bus Topology < Ring Topology < Spider Diagram.

However, it must be noted that this ranking and the ratios between different topologies is not the same for each of the identified villages. In fact, it is dependent on various factors, such as the number of houses, the shape of the village and, most importantly, the geometrical distribution of the households inside the village, which can make one

topology more convenient for specific cases. Some interesting examples of specific villages are the following, which are also shown in Figure 7.16.

- Location 7, which has a clear, long shape, is symmetrically distributed on the sides of a straight road. It does not have any household near the center of the village, and is more suitable for a bus topology (108 m) than for a radial topology (111 m), as seen in Figure 7.16(a).

- Location 23 has a very peculiar circular layout for household distribution. In this small village, a ring topology (30.5 m) is slightly more convenient than a radial topology with the origin in the center of the village (32 m), as seen in Figure 7.16(b).

- Location 8 is the smallest village of the sample. Its shape and the scattered distribution of the houses make in this case a Radial topology (21 m) with the origin (a fictitious node) in the centre of the village even more convenient than an MST (23 m), as seen in Figure 7.16(c).

These are just some of the cases that could be analyzed singularly, but it already gives a hint of how the optimal layout topology is highly case-specific. Nonetheless, it is hoped that the methodology proposed in this chapter can help in identifying the optimal layout in such cases.



(a) red = Bus, blue = Radial

(b) red = Ring, blue = Radial
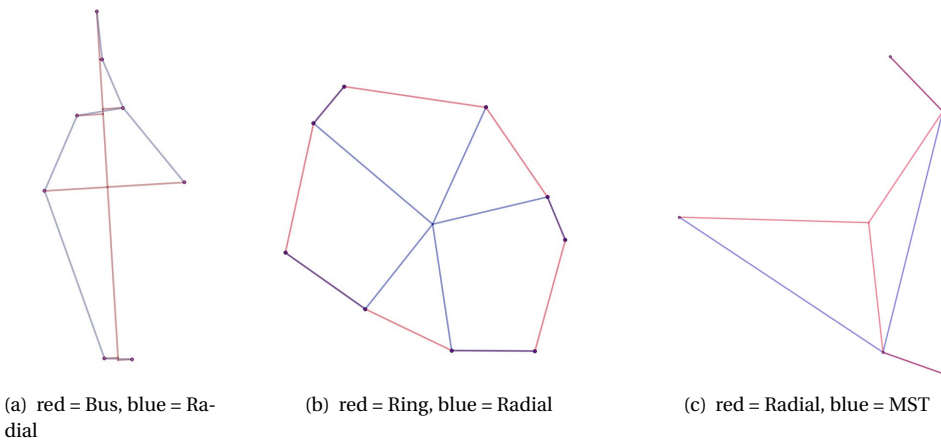
(c) red = Radial, blue = MST

Figure 7.16: Specific cases of topology comparison: (a) Location 7 (b) Location 23 (c) Location 8

In general, however, it can be said that the greater the number of houses, the worse the performance of spider topology. This can be easily explained geometrically as each household gets connected directly to the centre of the village, creating a number of "branches" which are inefficiently close to each other. Thus, in 40 out of 42 cases in the location set, the spider diagram is the least convenient topology. Hence, this particular layout should be avoided for decentralized microgrid planning. The only exceptions where a spider topology might still make sense would be a fully centralized generation or for centralized public loads in decentralized microgrids.

### 7.4.2. Layout optimization

The algorithm described in Section 7.3.3 has been applied to a limited number of villages chosen among the 42. For most of the examined villages, the algorithm was run separately for each different starting topology, obtaining topology-specific optimized meshed grids as well as overall best solutions. For other villages, especially with higher number of houses, the algorithm was run starting only from some of the potential starting topologies, which were considered more suitable, for computational reasons. The smallest village of the sample set is first considered, which has only 5 households, making it easier to see how the algorithm works and how the different weight factors used influence the outcome of the optimization. The values of $\overline{spl}$ and $\overline{l}$ for all the potential network layouts are shown in the scatter graph in Figure 7.17, resulting as an output of the algorithm using all five different starting topologies. The bigger points with different colours on the top-left corner of the graph are representing the starting networks.
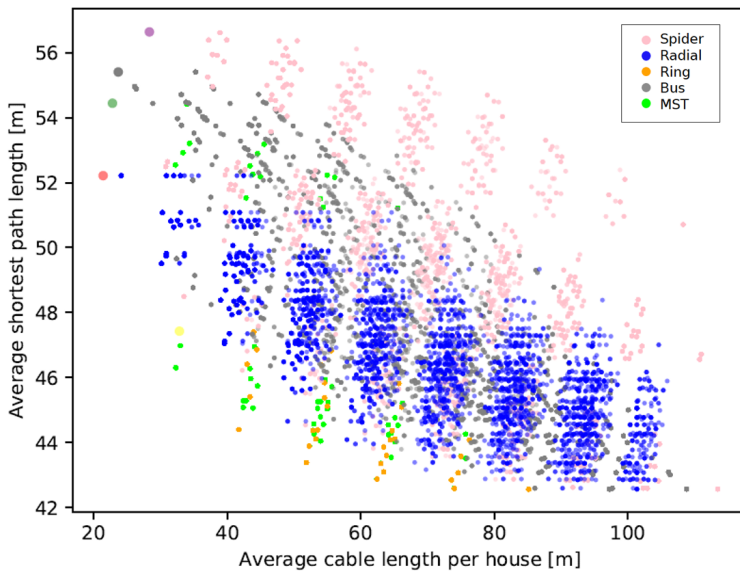


Figure 7.17: Average network length and average shortest path length of network layouts generated and tested by the algorithm for location 8. Different colours represent different starting topologies.

It can be seen that as more edges are added, thus increasing the average cable length, the average shortest path length decreases, as expected, until it reaches a minimum threshold. This threshold is reached when the network has become a complete graph, having then the maximum possible average cable length and the minimum average shortest path length, since every pair of nodes is directly connected via an edge. It is important to notice that the complete form of the network changes according to the starting topology, for example, because of non-household nodes and bus lines, hence changing the maximum average cable length, but not the minimum average shortest path length, which is always reached with spanning trees. This explains why in Figure 7.17 the complete graph starting from the spider topology (the farthest on the right pink dot) is

not the same as the complete graph starting from the bus topology (the farthest on the right grey dot). It is also interesting to see how the spider diagram, which was the least convenient topology in terms of pure cable length (Figure 7.15), is also performing worse than the other layouts in terms of average shortest path length, reinforcing the statement about its inadequacy as topology choice for decentralized microgrids.
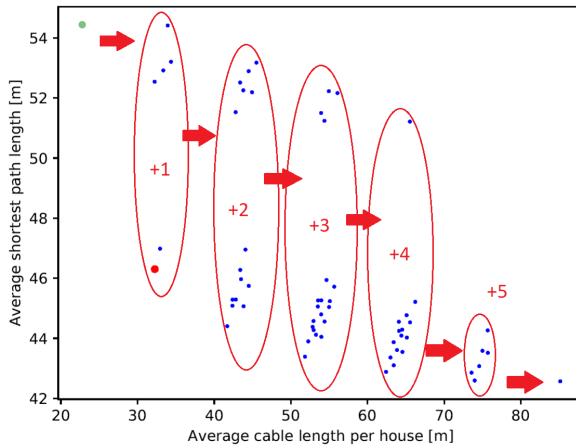


Figure 7.18: Average network length and average shortest path length of network layouts for location 8, starting from MST topology. The green dot indicates the starting network, while the red dot indicates the optimal solution, found after one edge addition while using a weight factor of 0.3.

The scatter graph resulting from running the algorithm with only the MST as starting topology is shown in Figure 7.18, which shows how the addition of each edge leads to a gradual change in the parameters, from the starting graph to the complete graph. It is also possible to graphically see six "stages" of solutions, each representing one consecutive edge addition. As the number of nodes increases, the computational complexity increases as well, leading to scatter graphs which are less clear and distinct compared to the simplest case, but the trends can still be identified. As an example, in Figure 7.19 the scatter graph resulting from running the algorithm for location 12, which has thirteen households, is shown.

#### INFLUENCE OF WEIGHT FACTOR AND STARTING TOPOLOGY

Going back to location 8, the algorithm was implemented using different weight factors in the range between 0.1 and 2. As expected, this leads to different optimized layouts, especially in terms of number of added edges. The lower the weight factor, the lower importance of network length and the more edges were added to the initial network in order to reach the optimized topology, as shown in Figure 7.20. It can be seen that for such a small village, it can happen that no edges are added at all for some topologies at high weight factors, because the benefit would be considered too small to justify the addition of a single edge, hence the optimized layout ends up being the starting topology
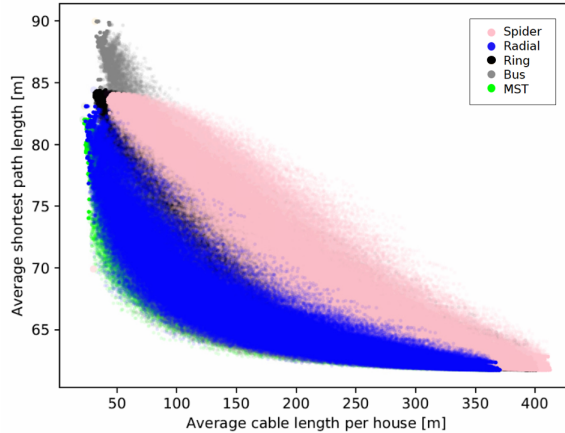
Figure 7.19: Average network length and average shortest path length of network layouts for location 12, which has 13 households. Different colours depict different starting topologies.
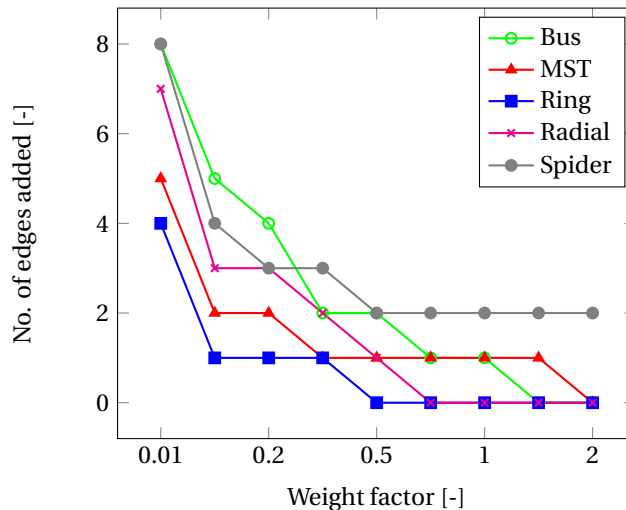


Figure 7.20: Edges added to reach the optimized layout for village 8 with different weight factors and starting topologies.

itself. That is for example the case for a weight factor of 2, in which 4 out of 5 starting topologies do not require any edge addition.

Apart from the single starting topologies, the influence of the weight factor can also be seen in the final optimized layouts. In Figure 7.21, the final layout for location 8 is shown for different weight factors. The weight factor 0.01 is willingly exaggerated on the side of deprioritization of cable length and it was purely chosen to emphasize the edge addition. It can be seen how the layout changes with the weight factor, and also how different weight factors can lead to different starting topologies to be optimal. As an

(a) `wf = 2`    (b) `wf = 0.3`    (c) `wf = 0.1`    (d) `wf = 0.01`

Figure 7.21: Global optimized layouts for location 8 with different weight factors.

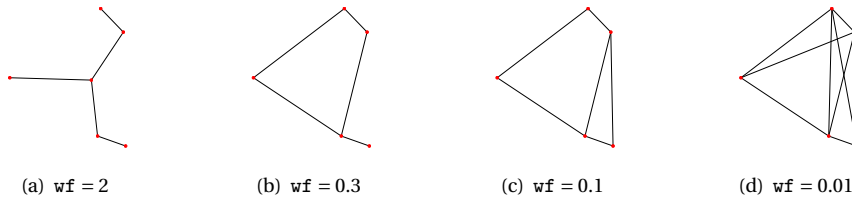example, while for a weight factor of 2 the radial topology was a better starting topology, for a weight factor of 0.3 an MST was optimal. It must be also noted that in some cases the optimal layout can also be reached by starting with different topologies. For example, the optimal layouts for weight factors 0.1 and 0.01 could be reached both starting from a ring topology and from an MST topology.

In Figure 7.22, the optimized layouts of village 8 are shown for different starting topologies. It was chosen to show the topology-specific results for a weight factor of 0.3 because all the results had at least one edge added to the starting network. The partial optimized layouts were then compared to each other to find the global optimal, which in this particular case resulted to be the one obtained from a MST starting topology.



(a) Original spread    (b) MST    (c) Radial
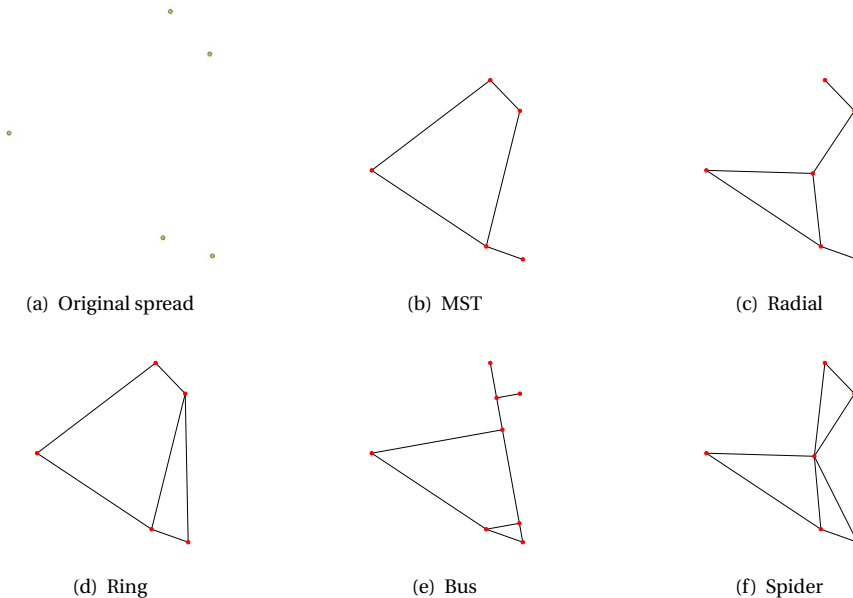
(d) Ring    (e) Bus    (f) Spider

Figure 7.22: Optimised layouts for location 8 with weight factor 0.3 and different starting topologies.

From these observations, it can be said that lower weight factors lead to the an increased addition of edges to reach the optimal layout independent of the starting topology.

It is also noticed that the edges that are more likely to be added to reach an optimal layout are usually short edges that close new loops into the network or cut through already existing loops. As mentioned in Section 7.3.3, the idea of assigning a weight factor is a user choice and dependent on the specific requirements from the microgrid at the target site. Even though the weight factor has a bearing on the final optimized layout, the general applicability of the proposed methodology in this study still stands.

## 7.5. CONCLUSIONS

This chapter presented a GIS-based methodology to evaluate and compare optimal topologies for decentralized microgrids. The main benefits of the method are the incorporation of ground-level data through GIS and a spatial geometry-based analysis using graph theory, which enable a passive optimization process at the design stage. The proposed methodology allows not only for a comparison between various candidate microgrid topologies in terms of network lengths (costs) but also an optimization between cabling costs and potential operational parameters like line congestion and line losses. This is done through an algorithm that minimizes a target function comprising average network length and average shortest path length. In general, denser target locations led to lower average network lengths, while graph theory-based layout (MST) outperformed conventional topologies like ring, spider, bus in terms of average network length. It was seen that each location requires case-specific considerations, and case-specific conditions play a vital role in the application of this methodology. The user-defined weight factor can be a useful parameter to tweak while using the proposed methodology.In conclusion, combined use of GIS and graph theory can be powerful in planning of rural electrification projects, and classical superimposed microgrid layouts can be outperformed by layouts obtained from such an integrated methodology.

### 7.5.1. RECOMMENDATIONS AND FUTURE WORK

The optimization can be made computationally faster through smarter edge addition. The use of weight factors can be better correlated with active power flow analysis that takes into account the various supply and demand attributes for the microgrid. The weight factors can also be made a function of the wire gauge chosen.

## REFERENCES

[1]  H. Louie, *Off-Grid Electrical Systems in Developing Countries*. Springer, 2018.

[2]  A. Werth, N. Kitamura, I. Matsumoto, and K. Tanaka, "Evaluation of centralized and distributed microgrid topologies and comparison to open energy systems (oes)," in *2015 IEEE 15th International Conference on Environment and Electrical Engineering (EEEIC)*, pp. 492–497, June 2015.

[3] F. Islam, K. Prakash, K. Mamun, A. Lallu, and H. R. Pota, "Aromatic network: a novel structure for power distribution system," *IEEE Access*, vol. 5, pp. 25236–25257, 2017.

[4] D. Burmester, R. Rayudu, W. Seah, and D. Akinyele, "A review of nanogrid topologies and technologies," *Renewable and Sustainable Energy Reviews*, vol. 67, pp. 760–775, 2017.

[5] T. Dragičević, X. Lu, J. C. Vasquez, and J. M. Guerrero, "Dc microgrids — part ii: A review of power architectures, applications, and standardization issues," *IEEE transactions on power electronics*, vol. 31, no. 5, pp. 3528–3549, 2015.

[6] K. Prakash, A. Lallu, F. Islam, and K. Mamun, "Review of power system distribution network architecture," in *2016 3rd Asia-Pacific World Congress on Computer Science and Engineering (APWC on CSE)*, pp. 124–130, IEEE, 2016.

[7] C. Tíba, A. L. B. Candeias, N. Fraidenraich, E. d. S. Barbosa, P. B. de Carvalho Neto, and J. B. de Melo Filho, "A gis-based decision support tool for renewable energy management and planning in semi-arid rural environments of northeast of brazil," *Renewable Energy*, vol. 35, no. 12, pp. 2921–2932, 2010.

[8] M. Zeyringer, S. Pachauri, E. Schmid, J. Schmidt, E. Worrell, and U. B. Morawetz, "Energy for Sustainable Development Analyzing grid extension and stand-alone photovoltaic systems for the cost-effective electri fi cation of Kenya," *Energy for Sustainable Development*, vol. 25, pp. 75–86, 2015.

[9] F. Kemausuor, E. Adkins, I. Adu-Poku, A. Brew-Hammond, and V. Modi, "Electrification planning using network planner tool: The case of ghana," *Energy for Sustainable Development*, vol. 19, pp. 92–101, 2014.

[10] S. Ohiare, "Expanding electricity access to all in nigeria: a spatial planning and cost analysis," *Energy, Sustainability and Society*, vol. 5, no. 1, p. 8, 2015.

[11] S. Choudhury, A. Parida, R. M. Pant, and S. Chatterjee, "Gis augmented computational intelligence technique for rural cluster electrification through prioritized site selection of micro-hydro power generation system," *Renewable Energy*, vol. 142, pp. 487–496, 2019.

[12] F. F. Nerini, O. Broad, D. Mentis, M. Welsch, M. Bazilian, and M. Howells, "A cost comparison of technology approaches for improving access to electricity services," *Energy*, vol. 95, pp. 255–265, 2016.

[13] F. Dalla Longa, T. Strikkers, T. Kober, and B. van der Zwaan, "Advancing energy access modelling with geographic information system data," *Environmental Modeling & Assessment*, vol. 23, no. 6, pp. 627–637, 2018.

[14] D. Mentis, M. Andersson, M. Howells, H. Rogner, S. Siyal, O. Broad, A. Korkovelos, and M. Bazilian, "The benefits of geospatial planning in energy access–a case study on ethiopia," *Applied Geography*, vol. 72, pp. 1–13, 2016.

**7**

[15] D. Mentis, M. Welsch, F. Fuso Nerini, O. Broad, M. Howells, M. Bazilian, and H. Rogner, "A GIS-based approach for electrification planning-A case study on Nigeria," *Energy for Sustainable Development*, vol. 29, pp. 142–150, 2015.

[16] T. Huld, M. Moner-Girona, and A. Kriston, "Geospatial analysis of photovoltaic mini-grid system performance," *Energies*, vol. 10, no. 2, pp. 1–21, 2017.

[17] D. Mentis, M. Howells, H. Rogner, A. Korkovelos, C. Arderne, E. Zepeda, S. Siyal, C. Taliotis, M. Bazilian, A. de Roo, *et al.*, "Lighting the world: the first application of an open source, spatial electrification tool (onsset) on sub-saharan africa," *Environmental Research Letters*, vol. 12, no. 8, p. 085003, 2017.

[18] K. R. Varshney, G. H. Chen, B. Abelson, K. Nowocin, V. Sakhrani, L. Xu, and B. L. Spatocco, "Targeting Villages for Rural Development Using Satellite Image Analysis," *Big Data*, vol. 3, no. 1, pp. 41–53, 2015.

[19] A. Alhamwi, W. Medjroubi, T. Vogt, and C. Agert, "Development of a gis-based platform for the allocation and optimisation of distributed storage in urban energy systems," *Applied Energy*, vol. 251, p. 113360, 2019.

[20] M. Brazil and M. Zachariasen, "Optimal interconnection trees in the plane," *Algorithms and Combinatorics*, vol. 29, 2015.

[21] R. L. Graham and P. Hell, "On the history of the minimum spanning tree problem," *Annals of the History of Computing*, vol. 7, no. 1, pp. 43–57, 1985.

[22] R. C. Prim, "Shortest connection networks and some generalizations," *The Bell System Technical Journal*, vol. 36, no. 6, pp. 1389–1401, 1957.

[23] F. Dörfler, J. W. Simpson-Porco, and F. Bullo, "Electrical networks and algebraic graph theory: Models, properties, and applications," *Proceedings of the IEEE*, vol. 106, no. 5, pp. 977–1005, 2018.

[24] S. Nolan, S. Strachan, P. Rakhra, and D. Frame, "Optimized network planning of mini-grids for the rural electrification of developing countries," in *2017 IEEE PES PowerAfrica*, pp. 489–494, IEEE, 2017.

[25] E. W. Dijkstra, "A note on two problems in connexion with graphs," *Numerische Mathematik*, vol. 1, pp. 269–271, 1959.

[26] R. W. Floyd, "Algorithm 97: shortest path," *Communications of the ACM*, vol. 5, no. 6, p. 345, 1962.

[27] Quantum GIS, "(software) qgis ver 2.18 las palmas de gran canaria," 2017.

[28] ArcGIS Map Repository, "Rural electrification densification programme." Accessed: 2018-06-01.

[29] ArcGIS Map Repository, "Hard to reach unions in bangladesh." Accessed: 2018-06-01.

# 8

## CONCLUSION

*Everything that has a beginning has an end*

The Oracle

### 8.1. GENERAL CONCLUSIONS

The research work presented in this dissertation was founded on the idea of contributing towards achieving universal electrification. The existing electrification pathways were critically analyzed, and the shortcomings of solar home systems, centralized microgrids, and grid extension were discussed. SHS can effectively achieve only lower tiers of electrification, viz., up to tier 2 and 3, while centralized microgrids and central grid extension suffer from high (techno-economic) thresholds to reach the necessary scale. Research gaps were identified from a technological point of view, necessitating the work done on adaptable load profile construction as a starting point for off-grid system design. Load profiles were constructed comprising dedicated off-grid super-efficient DC appliances for each of the five tiers of the multi-tier framework (MTF) for measuring household electricity access. Batteries in SHS were another focus of this dissertation, and a battery lifetime estimation methodology was introduced based on dynamic capacity fading. The proposed lifetime estimation model yielded state of health (SOH) estimations within less than 3% of the estimate obtained from an empirically derived model of Lithium-Iron Phosphate (LiFePO$_4$) battery over the battery lifetime simulation period. The intricate interdependencies between SHS parameters led to a detailed system sizing effort taking into account battery lifetime, excess PV generation, and system power availability for different tiers of electrification. Optimal SHS sizes for each tier of the MTF were obtained, which clearly showed the inadequacy of SHS to meet higher tiers (especially tier 5) of electrification. A bottom-up, decentralized, modularly expandable and scalable microgrid architecture was proposed based on interconnected SHS; a related case-study showed that more than 40% energy storage sizing gains are achievable for a tier 5 level electricity demand in the interconnected SHS-based microgrid when compared to standalone SHS.

Finally, a Geographic Information System (GIS)-based methodology was proposed that can identify optimal microgrid layouts while utilizing real-world ground-level data and concepts from graph theory as applied to network analysis. Case studies of 42 remote locations for SHS-based microgrids showed that graph theory-based minimum spanning tree (MST) achieved least network lengths when compared to conventional microgrid topologies like bus, spider, and radial topology for most cases. The described integrated methodology using GIS and graph theory can be applied on a case-specific basis to plan rural electrification projects, especially when going from SHS to a bottom-up microgrid.

## 8.2. CONTRIBUTIONS

Following are the main contributions of this PhD dissertation.

1. A bottom-up stochastic load profile construction tool that is fully scalable and adaptable to different user groups.

2. A battery lifetime estimation methodology that accounts for dynamic capacity fading of the battery

3. A methodology to optimize the standalone SHS size for various levels of electrification, taking into account battery lifetime while maintaining adequate levels of power supply.

4. An SHS architecture that is modular and scalable for both individual SHS expansion and microgrid expansion.

5. Quantification of the benefits of moving from standalone SHS to sharing energy in an interconnected SHS-based microgrid in terms of battery storage size.

6. A Geographic Information System (GIS)-based, customizable, and region-specific methodology to identify optimal microgrid topologies based on interconnected SHS.

## 8.3. TOPICAL CONCLUSIONS

The key findings that answer the thematic research questions (from Section 1.3.3) are discussed in this section.

### 8.3.1. ELECTRIFICATION PATHWAYS
**OVERVIEW OF PRESENT ELECTRIFICATION PATHWAYS FOR UNIVERSAL ELECTRIFICATION**
*Limitations of the present electrification pathways*
   The three different electrification pathways, viz., grid extension, centralized microgrids, and standalone solar-based solutions like pico-solar products and SHS, were critically compared on their relative merits and demerits. While standalone solar-based solutions like pico-solar and SHS can provide on-demand electrification, they lack the necessary power levels in their present form to cater to tiers 4 and 5 levels of electricity demand. Grid extension can easily supply the higher tiers in terms of power level but is far from an on-demand solution to the electrification of remote areas. To a lesser

extent, centralized microgrids also necessitate a minimum population density and demand threshold to justify investments. For climbing up the electrification ladder, an SHS-based decentralized microgrid is proposed that could potentially reach higher tiers of electrification without the disadvantages of grid extension and centralized microgrids.

### 8.3.2. SHS

#### LOAD PROFILES
*Constructing load profiles for the various levels of (off-grid) electrification*

A stochastic load profile construction methodology was presented in Chapter 3 to quantify the energy needs for the various tiers of the multi-tier framework in the form of load profiles. The loads were entirely composed of dedicated, off-grid, and in some cases the so-called super-efficient, appliances. A method for incorporating the coincidence factor was introduced, which can help with peak estimation for the load profile. The load profile estimation methodology is dependent on the sanctity of the appliance level inputs, which can be enhanced with dedicated field interviews/surveys or even on-line field data. The load profiles resulting from this work were used as inputs for the rest of the dissertation.

#### BATTERIES IN SHS
*Estimating battery lifetime for an SHS application*

An improved methodology for estimating the battery lifetime was discussed in Chapter 4 without needing to model the electrochemical processes within the battery or requiring dedicated experiments. Four different battery technologies were compared, viz., Lead-Acid (LA)-gel, LA-flooded, Nickel-Cadmium (NiCd), LiFePO$_4$ for a given SHS tier 3 application, with LiFePO$_4$ showing the best results with the highest estimated lifetime of 16.7 years. Comparison of this proposed dynamic model with an experimentally derived empirical model of LiFePO$_4$ battery yielded very close results, with the SOH values over time being within less than 3% of each other. The methodology outlined in this chapter can potentially help SHS designers in estimating battery lifetimes at the SHS design stage. The battery lifetime estimation was also used in Chapter 5 for the optimal sizing of SHS.

#### SYSTEM SIZING
*Optimizing SHS size considering battery size, system power availability, excess PV generation, and battery lifetime*

Optimal sizing is a crucial exercise in off-grid design as it prevents oversizing or undersizing of SHS, which can lead to high system costs or inadequate power availability, respectively. The study described in Chapter 5 detailed the optimal sizing of SHS for every tier of the multi-tier framework for household electricity access. A genetic algorithm-based multi-objective optimization was performed, which gave insights on the delicate interdependencies of the various system metrics like loss of load probability, excess energy, and battery lifetime on the SHS sizing. Optimal system sizes for each tier of the MTF were presented, and the implications of these system sizes were discussed from the perspective of state-of-the-art SHS. It was evident that meeting tier 5 level demand was untenable through the usage of SHS alone. The performance of the optimal standalone SHS sizes on the system metrics as found in Chapter 5 was used as a baseline for comparing the benefits of going from standalone SHS to SHS-based microgrid.

**8**

### 8.3.3. SHS-BASED DC MICROGRID

**BENEFITS OF AN SHS-BASED DC MICROGRID**

*Quantifying the benefits on the battery storage sizing and power availability when going from standalone SHS to SHS-based microgrids*

A modularly expandable and scalable DC microgrid architecture was proposed in Chapter 6 as a logical next step for SHS-based electrification. Meeting the energy demand of higher tiers like tier 4 and tier 5 is shown to be possible with this approach of bottom-up, interconnected SHS-based microgrid as opposed to standalone SHS. On modeling the energy sharing between the SHS, it was shown that battery sizing gains of more than 40% and 30% could be achieved with interconnectivity at tier 5 and tier 4 levels, respectively, as compared to standalone SHS to meet the same loss of load probability threshold. These gains are poised to increase further depending on the demand diversity of the load profiles, which tends to increase with increasing microgrid size.

**OPTIMAL MICROGRID TOPOLOGIES**

*Finding the optimal microgrid topology for interconnection of SHS considering the spatial spread of the households*

A GIS-based methodology was presented in Chapter 7 to evaluate and compare optimal topologies for decentralized microgrids. The main benefits of the method are the incorporation of real-world ground-level data through GIS and spatial geometry-based analysis using graph theory. The proposed methodology allows not only for a comparison between various candidate microgrid topologies in terms of network lengths (costs) but also an optimization between cabling costs and operational parameters like line congestion and line losses. The selected locations in the case-studies were seen to require a dedicated and case-specific consideration. Graph theory-based layout (minimum spanning tree) outperformed conventional topologies like ring, spider, bus in terms of average network length. This work underlined the utility of the combined use of GIS and graph theory to arrive at optimal microgrid layouts for rural electrification planning.

## 8.4. RECOMMENDATIONS AND FUTURE WORK

At the time of writing this dissertation chapter, the total population without electricity access had fallen below 1 billion for the first time since 1990 to 840 million⩔. It is still a tall task to electrify the 840 million by 2030. The research conducted in this PhD project, primarily focused on achieving universal electricity access, can be further enhanced through the following recommendations.

### 8.4.1. SHS

**LOAD PROFILES**

The load profile estimation methodology explained in Chapter 3 can tremendously gain from field research on load consumption. While the load profile construction can be tailored for different target user groups, a back and forth may be needed with the on-field usage patterns. This is even more important when considering seasonal patterns or local socio-cultural behaviours. Comparison of the stochastic load profiles should be made

---

⩔IEA, IRENA, UNSD, WB, WHO (2019), Tracking SDG 7: The Energy Progress Report 2019, Washington DC

with field data, especially for higher tiers of electrification, as and when such data is available.

The deterministic nature of the final load profiles used for the later system analysis also affects the battery lifetimes and corresponding system sizes. While this does not change the applicability of the underlying methodologies covered in this dissertation, it is should be noted that based on the context and site-specific analysis, the actual sizing of the SHS components and microgrid might differ from that arrived at in the chapters.

### SHS BATTERIES

The work described in the dissertation concerning SHS battery can further benefit from field data on on-line SOH monitoring. This can be used to empirically update the lifetime estimation methodology proposed in Chapter 4 at the SHS design stage. Additionally, more field data from SHS batteries would also help replicate the exact usage conditions for battery capacity fading tests in the lab. Hybrid batteries could also be considered to cater to different C-rate requirements, especially for tiers 4 and 5. Autonomous battery integrated DC appliances can also be explored to enable a modular growth up the energy ladder, especially up to tier 3 level electrification. Battery management systems (BMS) can be improved upon to accommodate additional capabilities like enabling power-sharing between interconnected SHS.

In the analysis considered in this dissertation, the end of life for batteries was considered at 80% state of health as it is usually specified by battery manufacturers. However, for low C-rate applications like SHS, this limit could be pushed lower, paving the way for the use of second-life batteries handed down from other applications like electric vehicles. This would need a dedicated investigation on the battery health of second-life batteries for SHS applications.

## 8.4.2. SHS-BASED MICROGRIDS

### BOTTOM-UP DC MICROGRID ARCHITECTURE

The dual voltage microgrid architecture suggested in this dissertation leaves several channels open for further research. Having a 350 V DC bus requires additional work on safety and protection. There were no standards for remote rural DC microgrids available at the time of writing this dissertation. Voltage set-points for the decentralized control described in Appendix C can benefit from available benchmarks. Having readily available standards for the plug-and-play type of (DC) microgrid deployment can also greatly increase the implementation and adoption levels of decentralized (DC) microgrids. The non-availability of DC microgrid standards for rural electrification for above 100 V, coupled with slow proliferation of high power DC appliances for productive usage will keep solar-AC systems very much in competition in the foreseeable future. Also, further research is needed to compare the topologies obtained through the GIS study in Chapter 7 in terms of experimental implementation.

### ALGORITHMS FOR ENERGY EXCHANGE

Research into smart algorithms is needed for energy exchanges in such remote rural DC microgrids. The algorithms should enable the decentralized control and expansion of such microgrids, while also maintaining the levels of robustness needed in the microgrid

for deployment and adoption in low-resource settings. Additionally, the algorithms should facilitate energy exchange while minimizing line congestion in the microgrid. Finally, monetization of energy exchange for such a network should be explored, so that positive cash-flows can arise in such community microgrids, thereby lessening the burden on OPEX expenditures for maintenance and upkeep of the microgrid infrastructure.

### 8.4.3. Multidisciplinary research

Finally, the technical research conducted in this project and presented in this dissertation is only part of the story when it comes to the larger target of universal electrification. Although not within the scope of this dissertation, there are several other areas of research that need to be undertaken to make significant strides towards universal electrification. For instance, innovative business models are needed to make the SHS-based technological solutions accessible and affordable to the most energy-deprived communities. Context-specific user research needs to take place, especially when productive use of energy needs to be taken into account. Additionally, policies need to be updated and adapted to accommodate as well as aid the rapid rise of SHS with their batteries and DC appliances. Policies will also be instrumental for supporting the growth of DC microgrids that can utilize existing SHS as well as be ready for eventual grid expansion.

Thus, to fully assess the feasibility of such an SHS-based scalable off-grid electrification vision towards universal electrification, a broader multi-disciplinary approach is needed that includes fitting business models, socio-cultural aspects of contexts where the microgrid is to be deployed, and effective policies that stimulate technology adoption.

**8**

*Each day we go to our work in the hope of discovering — in the hope that some one, no matter who, may find a solution of one of the pending great problems, and each succeeding day we return to our task with renewed ardor; and even if we are unsuccessful, our work has not been in vain, for in these strivings, in these efforts, we have found hours of untold pleasure, and we have directed our energies to the benefit of mankind.*

Nikola Tesla

# Appendix A: Constructing Equivalent Electrical Circuit Models of Battery Cells for SHS Applications

## A.1. Introduction

In this study, two battery technologies commonly used in SHS were explored: the valve regulated lead–acid (VRLA) battery and the LiFePO$_4$ (LFP) battery. Lead–acid is the cheapest technology in the market in comparison with the other common battery technologies [3]. In particular, the valve regulated type of lead–acid battery is sealed, which reduces the risk of liquid leaking when compared to flooded lead–acid battery. Moreover, VRLA battery is entirely maintenance free [4]. In the case of LFP battery, it has surged as a predominant technology due to its appropriate chemical and thermal stability together with its high energy capacity [5]. Additionally, LFP batteries have experienced a reduction in price that is expected to continue [6].

### A.1.1. Selecting the Battery Model

Depending on the application, accuracy, complexity, compatibility and universality, there are several technical methods to approach an expected battery model. Generally, there are three levels of battery models according to the degree of physical insight, viz., white box (e.g., electrochemical/physical model), grey box (e.g., equivalent electrical circuit model) and black box (e.g., artificial neural network model) [7].

The equivalent electrical circuit model (EECM) presents a good balance of computational time, precision, and complexity. As the EECM models the battery with only electrical components, they are highly compatible with other electrical models, which make them easy to implement with battery management systems and in other electrical engineering applications. Moreover, the construction of EECM does not have a very comprehensive co-relation with electrochemical processes inside the battery. As a result, there is no limitation on distinct battery types when modelling the battery by EECMs. Hence, the electrical equivalent circuit model (EECM) is selected in this study.

---

### A.1.2. IMPORTANCE OF LOW CURRENT BATTERY MODELS FOR SHS

Battery modelling is essential in SHS design, as they help to elucidate the relationship between power required by a predefined load and the operational conditions in which the batteries are used. Particularly, in SHS, the C-rates (related to the rate at which a battery is charged or discharged) are usually lower than 0.5 C, with the lowest C-rate being 1/120 C to 1/100 C [8, 9].However, the existing battery cell level models do not focus on low C-rates; instead, they normally study a wide range of C-rates with high sampling resolution. For example, C-rates of 0.1 C, 0.5 C, 1 C, 2 C, 3 C, 4 C, 7 C, and 9 C have been proposed in [10], while other authors have explored C-rates of 0.04 C, 0.1 C, 1 C, 2 C, 3 C, 5 C, and 10 C [11], and 0.1 C, 0.5 C, 1 C, 2 C, 3 C, and 4 C [12]. Therefore, the applicability of these models in wide C-rate ranges does not necessarily validate their suitability for SHS.

Consequently, we focus on the low battery C-rates reflecting typical SHS applications. To obtain an accurate battery model which suitable for low C-rate applications, experiments with narrower C-rate range but with high sample resolutions are proposed. The applicable C-rate range of this model is 0.05 C–0.5 C with the sample resolution of 0.05 C–0.1 C.

### A.1.3. CONTRIBUTIONS

The work described in this appendix chapter contributes to the current state-of-the-art by

- developing an accurate battery cell level model especial for a low currents, as the case in SHS;

- proposing a common modelling methodology based on electrical circuit model applicable to both VRLA and LFP batteries; and

- improving the current electrical circuit models for VRLA battery including

  - a non-linear relation between $V_{OC}$ and SOC;
  - a $2^{nd}$ order RC circuit-based EECM model using a Thevenin approach;
  - considering the parasitic branch of the EECM in terms of SOC and C-rate-based Coulombic efficiency.

## A.2. BACKGROUND

### A.2.1. BATTERY PARAMETERS

*State of the Charge (SOC)*: SOC is usually defined as the proportion of the maximum possible electric charge that is present inside a rechargeable battery [13]. It is calculated as the ratio between the difference of the battery capacity and the net electric charge discharged from a battery since the last full state of charge. The SOC can be expressed by Equation A.1.

$$SOC = \frac{Q_t - Q_e}{Q_t} = \frac{Q_r}{Q_t} \tag{A.1}$$

$$Q_e = \int_0^t I_m d\tau \tag{A.2}$$

$$I_{\text{m}} = I_{\text{batt}} - I_{\text{p}} \tag{A.3}$$

where $Q_{\text{t}}$ is the temperature dependent actual capacity, $Q_{\text{e}}$ is the capacity that be extracted from the battery starting from its full state, and $Q_{\text{r}}$ is the capacity that remaining in the battery. $I_{\text{m}}$ is the main branch current, which is the result of the load current applied to the battery minus the current consumed in side-reactions ($I_{\text{p}}$). $I_{\text{m}}$ is positive if the battery is discharging and $I_{\text{m}}$ is negative if the battery is charging.

*Electromotive force (emf)*: The electromotive force of a cell is the algebraic sum of the potential difference of two half cells, which is the chemical potential of redox reactions happening on these two electrodes [14].

*Open circuit voltage (OCV, or $V_{\text{OC}}$) and cte-OCV*: The open circuit voltage (OCV) is the potential difference across its terminals when there is no current flow in or out of a reversible cell [15]. If the battery rests enough time (depending on the battery technology) with no current flow, the OCV can be called Close-to-Equilibrium open circuit voltage (cte-OCV) [16]. This value can be regarded as the estimated emf value.

*Current rate (C-rate)*: The current rate, which is also called $C$-rate, is defined as the ratio of magnitude of charge/discharge current in Amperes to the nominal capacity of the battery in Ampere-hour. The C-rate represents the speed of charge/discharge, and it can be calculated using Equation A.4 [17].

$$C - rate = \frac{I_{\text{batt}}}{Q_{\text{n}}} \tag{A.4}$$

where $I_{\text{batt}}$ is the current applied on the battery in the unit of ampere (A), and $Q_{\text{n}}$ is the nominal battery capacity in the unit of ampere hour (Ah).

### A.2.2. Construction of the Dynamic Battery Model

A good battery model should be capable of predicting both the battery storage capability information and the voltage response to the load. An equivalent electrical circuit model (EECM) can describe both characteristics. In some cases, modelling the side reactions is required in terms of battery losses, which is also possible to be realized with the EECM.

As shown in Figure A.1, there are three main parts in the EECM to model the different features of the battery. First part is the storage circuit. Three parameters should be modelled in this sub-circuit: the battery capacity (which is the charge storage ability), the amount of charge is left in the battery (SOC), and the open circuit voltage $V_{\text{OC}}$.

The second part is the voltage response circuit, which focuses on the internal structure of the battery. This makes it possible to imitate the electrical response of the battery under different loads. In this study, a Thevenin model is applied, and it consists of a resistance in series with RC pairs.

The last part is the parasitic branch, which is used to model the side reactions that induce loss of charge in the battery. There are many ways to model these battery losses. For example, Figure A.1 shows the parasitic branch in the form of a resistance ($R_{\text{p}}$). For both battery technologies, the basic construction of EECM is applicable, as shown in Figure A.1.
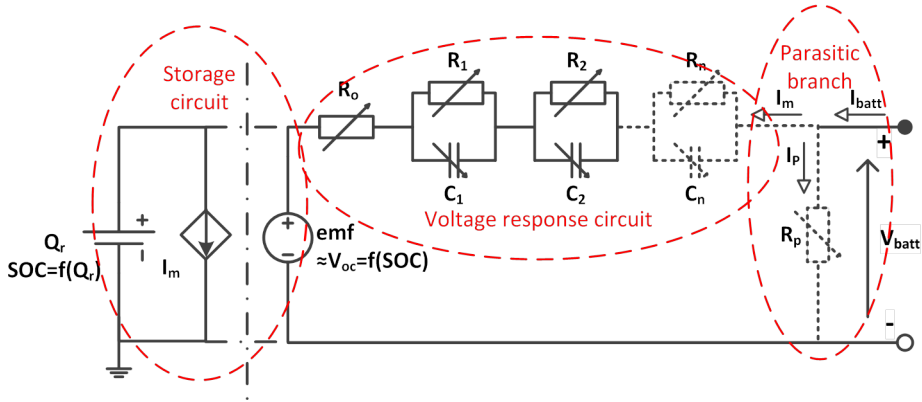
Figure A.1: Schematic of the overall EECM construction.

### A.2.3. STORAGE CIRCUIT

As discussed in Section A.2.1, the cte-OCV can be regarded as the emf value. As the emf values are SOC dependent, the cte-OCV can be used as a SOC indicator. In this study, the SOC value is selected as the independent variable, while the coulomb counting method is used to determine the SOC. The SOC can be expressed by Equation A.1.

### A.2.4. ELECTRICAL RESPONSE CIRCUIT

There is a deviation of voltage from the equilibrium state, also called polarization, whenever the battery is loaded. Conversely, the voltage recovers back towards the equilibrium state whenever the load is disconnected. Hence, a voltage relaxation phenomenon is observable in a no-load interval (also called rest interval) when the battery is operating. The battery internal impedance can be potentially extracted from this voltage relaxation.

The non-load rest interval during a discharge stage is shown in Figure 2(b). The voltage response can be divided into two parts, viz., an instantaneous voltage jump right after the load is paused, followed by a gradual increase of the voltage towards the cte-OCV. Those two voltage responses are correlated with two electrical parts: the ohmic resistance $R_o$, and the resistance/capacitance pairs ($R_1C_1$, $R_2C_2$), as introduced in the construction of EECM model in Figure A.1.

Generally, there is an expected time window for each of the voltage response. An EECM containing two RC-pairs is assumed. It is suggested that, within a five seconds time-window, the voltage boost ($V_o$) right after the load disconnection is induced by the ohmic resistance $R_o$ [18]. The time window for the rest of the gradual voltage increase caused by the RC pairs is called the time constant. The time constant reflects the rate of change of voltage; if the voltage changes faster, the time constant is smaller [19]. The increase in voltage right after the immediate voltage increase is the "short-term voltage response". This short time interval ($\tau_1$) is expected to be around 10 seconds, and this voltage increase ($V_1$) is related to the first RC-pair, which is the $R_1$, $C_1$ in Figure 2(b) [20]. The following increase in voltage ($V_2$) is then treated as the long-term voltage response after a long time interval ($\tau_2$), which corresponds to the second RC-pair ($R_2$, $C_2$), as shown

(a) The electrical circuit elements
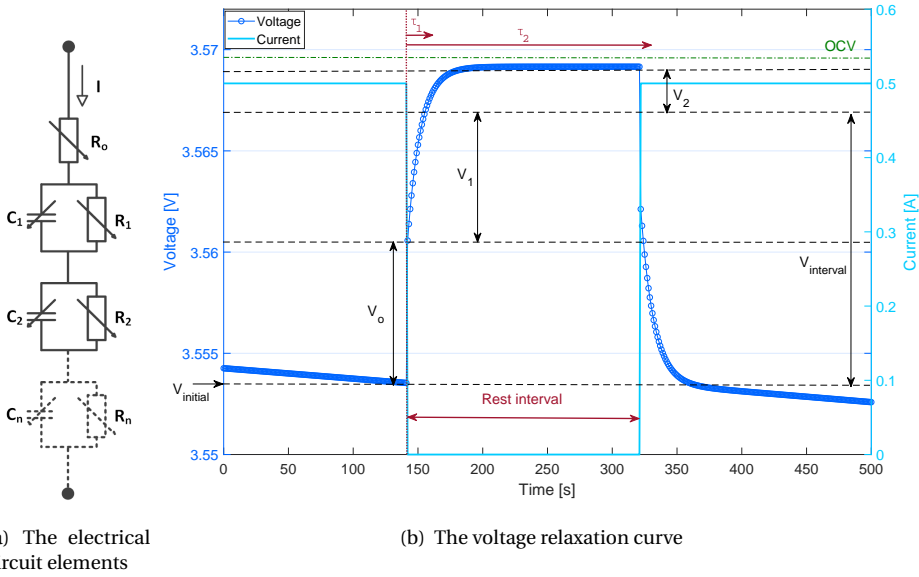
(b) The voltage relaxation curve

Figure A.2: An example of voltage relaxation during rest interval in discharge with corresponding circuit elements.

in Figure 2(b). It is possible to increase the number of RC-pairs and divide the voltage relaxation into more parts, with which the accuracy of the model is improved, such as the $R_n$, $C_n$ in Figure 2(b). Many authors suggest to model the lead–acid battery with first order RC circuit. However, for Li-ion batteries, all three orders of RC circuit model are commonly seen [21, 12, 22, 23, 24]. Eventually, the relaxation voltage will reach cte-OCV if the rest interval is long enough. However, it is necessary to strive an optimum balance between accuracy and complexity. Therefore, the study described in this chapter has considered two RC pairs.

Curve fitting method was applied on each of the voltage relaxation results. The recognition of each part of the voltage and the corresponding time constant was done by *nonlinear least squares curve fit* in Matlab [20]. The distinct voltage and time constant values were then fitted into the RC circuit complete response equations to obtain the values of electrical elements in the model. The equations are listed below as Equations A.5 to A.9.

$$V_{\text{interval}} = V_1(1 - e^{\frac{-t}{\tau_1}}) + V_2(1 - e^{\frac{-t}{\tau_2}}) + V_0 \tag{A.5}$$

$$V_{\text{OC}} = V_{\text{initial}} + V_0 + V_1 \mid_{t\to\infty} + V_2 \mid_{t\to\infty} \tag{A.6}$$

$$R_0 = \frac{V_0}{I} \tag{A.7}$$

$$R_k = \frac{V_k}{I} \tag{A.8}$$

$$C_k = \frac{\tau_k}{R_k} \tag{A.9}$$

where k=1, 2, 3, ..., n.

## A.2.5. PARASITIC REACTION CIRCUIT

The electrical components interpreted in the previous subsections describe the behaviour of the battery based on its main reactions. During operation, not all the battery energy is involved in its main (charging/discharging) reactions; there are unwanted side reactions responsible for loss of useful energy. Therefore, additional elements are needed to model a parasitic branch considering the side reactions.

Especially when charging a lead–acid battery, significant losses can occur, which has a huge impact on the battery dynamic behaviour. This is particularly true when the battery is at a high SOC (>95%). Therefore, the charge loss of VRLA during the charging stage is considered as the most dominant loss mechanism. This loss is mainly due to gassing and oxygen recombination, but the transient gassing phenomenon can be quite complex and unpredictable especially for VRLA batteries [25].

There are different methods to model the parasitic branch. Some models use a self-discharge conductance to represent the side reactions, where the conductance is the function of battery voltage, or side reaction related voltage and the temperature [21, 22]. Some other models represent the side reaction by means of gassing current, as the function of water decomposition voltage and the temperature, instead of modelling the side branch circuit [26].

In this study, an equation is derived from the one proposed in [27]. This method is based on the principle that the losses incurred in the parasitic branch can be viewed as the Coulombic inefficiency of the battery. Therefore, this method models the parasitic branch in the form of the Coulombic efficiency as a function of SOC and the battery current, as shown in Equation A.10.

$$\eta_c = 1 - exp\left(\frac{b}{a \times \frac{I_{\text{test}}}{I_{\text{ref}}} + c} \times (SOC - 1)\right) \tag{A.10}$$

where $I_{\text{ref}}$ is the reference current, and $I_{\text{test}}$ is the test current. $a$, $b$, and $c$ are the experimentally derived empirical constants. It must be noted that, as the current terms in Equation A.10 occur in the form of a ratio, the Coulombic efficiency can be considered as a function of C-rate as well.

## A.3. METHODS AND EXPERIMENT

### A.3.1. CHOICE OF OPERATIONAL VARIABLES

For both battery technologies, each of the internal impedances is known to be, to some extent, influenced by the SOC, the temperature, and the current [28]. To obtain a proper dynamic battery model, a battery should ideally be tested with all three variables. However, the influence of operating temperature was not investigated in this study. All experiments were performed in a laboratory with the temperature controlled in the range of 20–22 °C. Therefore, all experiments can be considered as under constant room temperature conditions. SOC and current (in the form of C-rate) were the main operational variables considered in this study.

### A.3.2. OVERALL METHODOLOGY

The EECM model is assumed as shown in Figure A.1, with two RC pairs. The choice of two RC pairs is justified in Section A.4. For the task of fully constructing the EECM model for both VRLA and LFP batteries, the following methodology was followed involving experiments, data analysis, and model verification.

1. **Experimentation.** Series of experiments were performed to extract the parameters of each electrical element pertaining to every sub-circuit.

   (a) *Storage circuit.* The cte-OCV measurement method was performed.

   (b) *Voltage response circuit.* Voltage relaxation (also called step response) method was used.

   (c) *Parasitic branch.* The differential recharge efficiency measurement method was used.

   These measurements were applied on each featured SOC and with selected current rate, as further described in Table A.1.

2. **Parameter extraction.** The parameters of each component in the EEMC were extracted and analyzed based on the experiments. The values of those parameters were then summarized into equations, and those equations can represent each of the electrical element in the electrical circuit.

3. **EECM construction and model verification.** All parts of the electrical elements were put together to construct the full EECM. Finally, the constructed EECM of each battery was simulated and compared with the experimental results.

### A.3.3. EQUIPMENT AND MATERIALS

In this study, the battery tester used is MACCOR® Series 4000 Automated Test System [29]. The batteries selected for tests are Cyclon® AGM D single cell and A123systems® ANR26650M1B, and both of the battery cells have 2.5 Ah capacity [30, 31].

Table A.1: Specification and summarized charge/discharge method for both battery technologies.

| Battery Brand | A123systems® APR26650M1B | Cyclon® AGM D Single Cell | | | | | | |
|---|---|---|---|---|---|---|---|---|
| **Battery capacity** | 2.5 Ah | 2.5 Ah | | | | | | |
| **Nominal voltage** | 3.3 V | 2 V | | | | | | |
| **End of charge** | CC-CV: 3.6V until I ≤ 0.01C | CC-CV: 2.5V until I ≤ 0.002C | | | | | | |
| | | Depending on C-rate and EODV: | | | | | | |
| **End of discharge** | CC-CV: 2.5V until I ≤ 0.01C | C-rate | 0.05 | 0.1 | 0.2 | 0.4 | 1 | 2 | >5 |
| | | EODV | 1.75 | 1.7 | 1.67 | 1.65 | 1.6 | 1.55 | 1.5 |

The basic charge and discharge methods applied in this study are constant current (CC) method and constant current–constant voltage (CC-CV) method. The CC method involves charging or discharging the battery with a constant current until the battery voltage reaches a specific value. The specified voltage to stop the discharging process is called the end of discharge voltage (EODV). The CC-CV method involves first charging/discharging the battery with constant current until the battery voltage reaches the pre-set value, and

then switch to constant voltage stage, which involves charging/discharging the battery with a constant voltage.

The in-detailed charge and discharge method of each battery technology is summarized in Table A.1. This follows the recommendations and best practices outlined in the data sheets and previous articles [30, 31, 32, 20].

### A.3.4. STORAGE CIRCUIT

The purpose of this set of experiments is to obtain the relation between the cte-OCV and the SOC. Therefore, the cte-OCV should be measured at different SOC values, and the battery is fully discharged before the measurement. During the experiments, the battery was monotonically charged to full and then discharged to empty, with both procedures being executed in steps of 5% SOC. Coulomb-counting method was used to approach the designated SOC demarcation. After each step, the battery was rested for a constant time to reach the close-to-equilibrium state, at which point the voltage was measured and noted as the cte-OCV value. The C-rate was 0.2, while the rest time was 3 h for VRLA battery and 4 h for LFP battery. Three battery cells were tested to get a result with better accuracy.

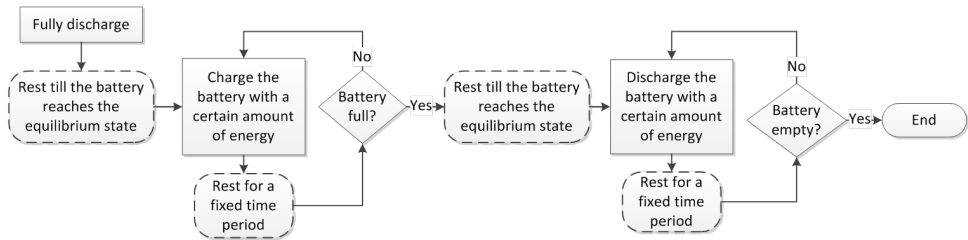The experimental procedure is illustrated in the flowchart shown in Figure A.3.



Figure A.3: Test procedure of cte-OCV-SOC measurement and the Internal impedance circuit measurement.

### A.3.5. VOLTAGE RESPONSE CIRCUIT

The electrical elements in the model were tested while the battery underwent eight different C-rates at different SOC levels. The test procedure esd similar to the cte-OCV test, as shown in Figure A.3, with the only difference being the amount of energy being charged/discharged in each step, and the resting time interval. In this test, the step size of charge/discharge was 0.15 Ah, and the relaxation time between each step was 3 min for both battery technologies. The resting time between charge/discharge was 1 h for both battery technologies.

The C-rates tested were: 0.05 C, 0.1 C, 0.15 C, 0.2 C, 0.25 C, 0.3 C, 0.4 C, and 0.5 C.

### A.3.6. PARASITIC BRANCH

A simplified measurement was applied to estimate the Coulombic efficiency in this study. The Coulombic efficiency was approximately measured and calculated from the integral recharge efficiency. The test procedure is outlined as follows.

1. Fully charge and discharge the battery to measure the initial battery capacity and the overall Coulombic efficiency.

2. Discharge the battery to a specific SOC value (x%) and note down the discharged capacity $Q_d$.

3. Fully recharge the battery and record the recharged capacity $Q_c$.

4. Calculate the recharge efficiency $Q_d/Q_c$ assuming it is the averaged integral recharge efficiency at the mean SOC between x% and 100%.

5. Go back to Step 2 and repeat the steps until enough data points are obtained.

6. Test the whole procedure under different C-rates.

One thing should be noted: after each charge/discharge step, the battery needed to rest until reaching its equilibrium state, for 1 h in this case.

Then, the averaged integral recharge efficiency was fitted to Equation A.10 to get the roughly estimated Coulombic efficiency as a function of SOC and C-rates.

The experimental settings are summarised in Table A.2.

Table A.2: Experimental setting for Coulombic efficiency measurement for VRLA battery.

|  | **High SOC** | **Low SOC** |
|---|---|---|
| **SOC value** | 90% to 99%; 1% steps | 10% to 90%; 10% steps |
| **C-rate** | 0.1 C, 0.2 C, 0.3 C, 0.4 C | 0.1 C, 0.2 C, 0.3 C, 0.4 C |

### A.3.7. EECM Construction

After achieving all the required values of the electrical elements, the battery model can be constructed according to the EECM as shown in Figure A.4.

It must be noted that the parasitic resistance $R_p$ shown in Figure A.4 is not an actual circuit element in the EECM but only a notional lossy element that signifies side-reaction. In the proposed model in this study, the VRLA losses are actually quantified through the Coulombic efficiency, as shown in Equation A.10.

The SOC of the battery can be represented by Equation A.1, while the main branch current $I_m$ is calculated through Equation A.11. The Coulombic efficiency $\eta_c$ is obtained from Equation A.10.

$$I_m = \eta_c \times I_{batt} \tag{A.11}$$

The dynamic battery voltage of each part of the circuit can be calculated by using the achieved electrical elements through simple circuit analysis, as shown in Section A.2.4. The battery voltage is shown in Equation A.12.

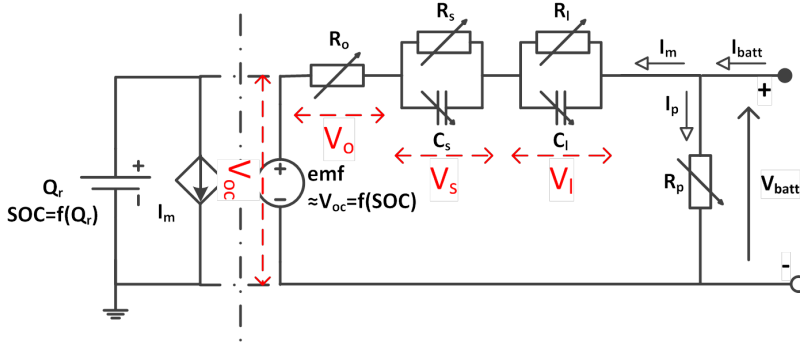$$V_{batt} = V_{OC} \pm V_o \pm V_s \pm V_l \tag{A.12}$$

Figure A.4: The construction of the EECM. The subscripts s and l stand for short and long time duration respectively with respect to voltage relaxation ($\tau_1$, $\tau_2$ in Figure 2(b)).

where $V_{\text{batt}}$ is the battery voltage and the $\pm$ sign in Equation A.12 is dependent on the current direction, i.e., + implies charging and $-$ implies discharging the battery.

## A.4. RESULTS AND DISCUSSION

### A.4.1. EXPERIMENTAL RESULTS

#### CTE-OCV AS A FUNCTION OF SOC

The cte-OCV and SOC are correlated; as the SOC increases, the cte-OCV also rises. Although many papers and manufacturers' datasheets suggest that the cte-OCV of VRLA versus SOC shows a linear relation [33, 34], our study found that a rational curve fit is better than a linear fit. This new fit is especially relevant when the battery is at low SOC, as plotted in Figure A.5. Hence, the empirical-based rational Equation A.13 was proposed and employed instead of a linear relationship.

$$V_{\text{OC}} = \frac{0.2428 \times SOC^2 + 1.935 \times SOC + 0.09876}{SOC + 0.05336} \tag{A.13}$$

In the case of LFP battery (Figure A.6), there is a sudden increase in $V_{\text{OC}}$ when the SOC is close to 100%; similarly, the $V_{\text{OC}}$ drops when the SOC is almost 0%. The cte-OCV and SOC behaviour can be perfectly fitted into a double exponential curve [35]. This has been verified by this study, as shown in Figure A.6, where the hysteresis phenomenon between the $V_{\text{OC}}$ values when charging or discharging is depicted. This hysteresis phenomenon was modelled in the electrical response circuit instead of $V_{\text{OC}}$-SOC equation for both batteries.

The fitted cte-OCV-SOC result of LFP battery is written in Equation A.14.

$$V_{\text{OC}} = 3.307 \times e^{\frac{-0.004117}{SOC+0.01772}} + e^{138.7(SOC-1.013)} + 0.05098 \times SOC \tag{A.14}$$

#### INTERNAL IMPEDANCE

To choose an optimised EECM structure, the fitting comparison from first to third orders of RC circuits are plotted in Figure 7(a) and 7(b). These two figures show one sample
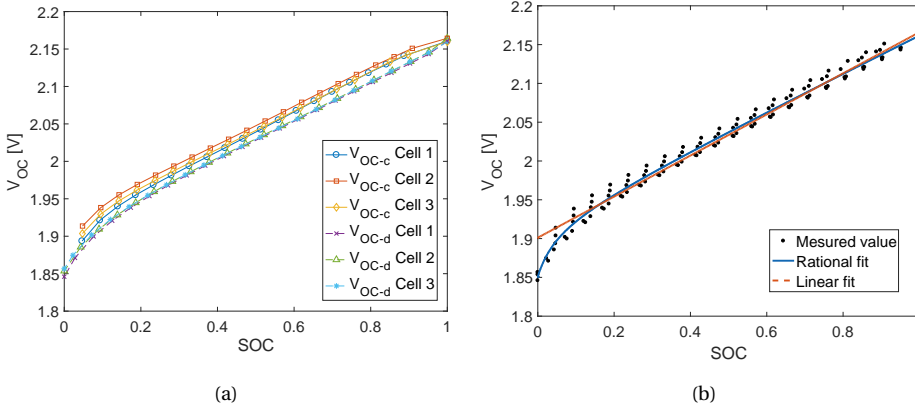
Figure A.5: Measured open circuit voltage versus SOC of VRLA battery: (**a**) $V_{OC}$ measured during charge and discharge separately; and (**b**) the measured data points and the fitted curves.

of voltage increase during the relaxation time and the fitting result with three different orders of RC circuits for both battery technologies.

From these curves, it can be concluded that the second order RC circuits have sufficient accuracy for both battery technologies. In addition, modelling the battery with a higher order of RC circuit requires more parameters. Thus, the second order RC circuits were selected for modelling both battery technologies owing to their lower complexity but sufficient accuracy.

The measured and fitted results of electrical elements in EECMs of LFP and VRLA batteries are shown in Figures A.8–A.11, where $R_o$ is the ohmic resistance; $R_s$, $C_s$ are the values of RC pair representing the voltage relaxation in the short time-window ($\tau_1$ in Figure 2(b)); $R_l$, $C_l$ are the values of RC pair used to represent the voltage relaxation in the long time-window ($\tau_2$ in Figure 2(b)).

In Figures A.8 and A.9, some features of VRLA batteries can be inferred with respect to the internal impedance circuit elements, as listed below.

1.   All the electrical elements show a strong dependency on SOC.

2.   All the elements also show an inverse trend versus SOC in charge stage and discharge stage.

3.   In terms of current dependency, elements during charge and discharge stages have diverse behaviours. While charging, only $R_l$ and $C_l$ values show a clear operational current dependence. While discharging, all the elements except $R_o$ are evidently influenced by the operational current.

Therefore, the $R_l$ and $C_l$ in discharge stage and all the elements in charge stage were modelled as the function of operational current. The detailed equations are listed as below:
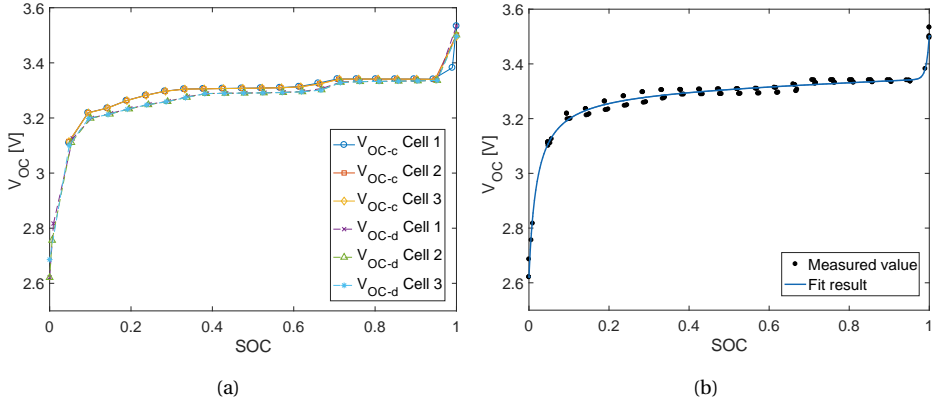
Figure A.6: Measured open circuit voltage versus SOC of LFP battery: (**a**) the hysteresis of $V_{OC}$ when charge and discharge the battery separately; (**b**) the measured data points and the fitted curve.

## CHARGE

$$R_{o\_VAc} = 0.03782 \cdot e^{1.301 \cdot SOC} + 4.226e - 6 \cdot e^{12.64 \cdot SOC} \tag{A.15}$$

$$R_{s\_VAc} = 4.246e - 13 \cdot e^{29.05 \cdot SOC} + 0.03787 \cdot e^{1.467 \cdot SOC} \tag{A.16}$$

$$C_{s\_VAc} = -2666 \cdot SOC^4 + 4113 \cdot SOC^3 - 1558 \cdot SOC^2 - 112.6 \cdot SOC + 229.3 \tag{A.17}$$

$$\begin{aligned} R_{l\_VAc} = &(4.952 \cdot SOC^4 - 7.819 \cdot SOC^3 + 4.168 \cdot SOC^2 - 0.8406 \cdot SOC + 0.1783) \\ &\times \left(9.8198e - 4 \cdot e^{-48.992 \cdot (C_r - 0.2)} + 0.67172 \cdot e^{-5.6015 \cdot (C_r - 0.2)} + 0.3273\right) \\ &\times \left(-2.191 \cdot SOC^3 + 2.62 \cdot SOC^2 - 1.006 \cdot SOC + 1.12\right) \end{aligned} \tag{A.18}$$

$$\begin{aligned} C_{l\_VAc} = &\left[-8768 \cdot (SOC - 1)^3 - 1.961e4 \cdot (SOC - 1)^2 - 1.512e4 \cdot (SOC - 1)\right] \\ &\times \left[11.66 \cdot (C_r - 0.2)^3 - 4.366 \cdot (C_r - 0.2)^2 + 2.43 \cdot (C_r - 0.2) + 1\right] \end{aligned} \tag{A.19}$$

## DISCHARGE

$$\begin{aligned} R_{o\_VAd} = &\frac{0.01226 \cdot SOC^3 + 0.007354 \cdot SOC^2 + 0.02339 \cdot SOC + 0.003575}{SOC + 0.03138} \\ &\times \left[-78.342 \cdot (C_r - 0.2)^4 + 25 \cdot (C_r - 0.2)^3 + 4.6032 \cdot (C_r - 0.2)^2 - 2.1016 \cdot (C_r - 0.2) + 1\right] \\ &\times \left(0.4411 \cdot e^{-16.19 \cdot SOC} + 0.9853 \cdot e^{0.01733 \cdot SOC}\right) \end{aligned} \tag{A.20}$$
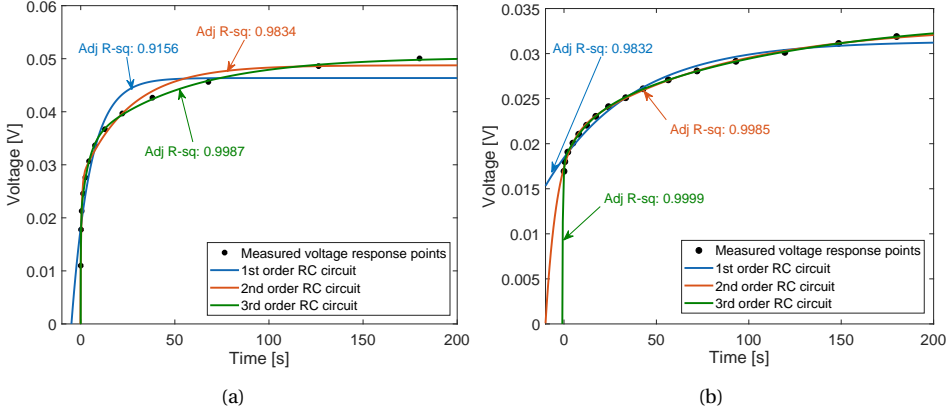
Figure A.7: Comparison of accuracy with modelling battery into different orders of RC circuits: (**a**) VRLA battery; (**b**) LFP battery.

$$R_{\text{s\_VAd}} = \frac{0.01341 \cdot SOC^3 + 5.996e - 4 \cdot SOC^2 + 0.02 \cdot SOC + 6.888e - 4}{SOC + 0.01043}$$
$$\times \left[ \left(6.6819e2 \cdot e^{-0.0011936 \cdot (C_r - 0.2)} + 0.15861 \cdot e^{-14.305 \cdot (C_r - 0.2)} - 667.3473\right) \right.$$
$$\left. \times 1.003 \cdot e^{0.01652 \cdot SOC} + 0.3767 \cdot e^{-20.89 \cdot SOC} \right] \tag{A.21}$$

$$C_{\text{s\_VAd}} = \left(-1116 \cdot SOC^4 + 2320 \cdot SOC^3 - 1640 \cdot SOC^2 + 458.5 \cdot SOC + 49.67\right)$$
$$\times \left[ \left(-3.3295 \cdot (C_r - 0.2)^2 + 2.7116 \cdot (C_r - 0.2) + 1\right) \times \left(0.9504 \cdot e^{0.0464 \cdot SOC} + 0.3536 \cdot e^{-609.2 \cdot SOC}\right) \right] \tag{A.22}$$

$$R_{\text{l\_VAd}} = \frac{0.1373 \cdot SOC^4 - 0.1344 \cdot SOC^3 + 0.04953 \cdot SOC^2 + 0.01366 \cdot SOC + 0.003415}{SOC + 0.01673}$$
$$\times \left[ \left(0.13707 \cdot e^{-16.624 \cdot (C_r - 0.2)} - 1.021 \cdot e^{0.91595 \cdot (C_r - 0.2)} + 1.8839\right) \right.$$
$$\left. \times 0.9371 \cdot e^{0.05663 \cdot SOC} + 0.421 \cdot e^{-13.09 \cdot SOC} \right] \tag{A.23}$$

$$C_{\text{l\_VAd}} = \left(-6879 \cdot SOC^4 + 1.73e4 \cdot SOC^3 - 1.877e4 \cdot SOC^2 + 8425 \cdot SOC + 492.4\right)$$
$$\times \left[3.8298 \cdot (C_r - 0.2) + 1\right] \times \left(0.5753 \cdot e^{-674 \cdot SOC} + 0.8458 \cdot e^{0.2202 \cdot SOC}\right) \tag{A.24}$$

From the results in Figure A.10 and A.11, some conclusions for LFP batteries can be drawn:
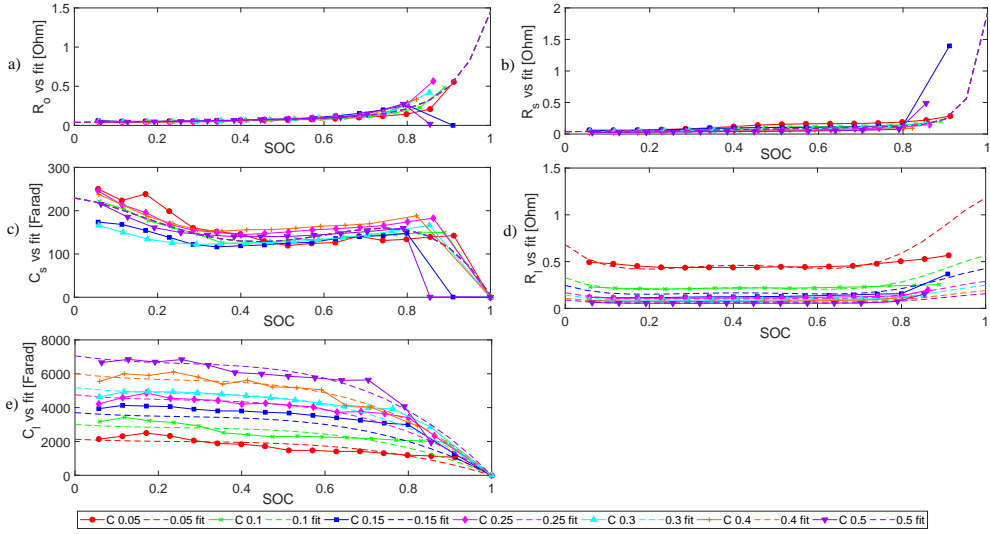
Figure A.8: The values of RC elements and their fitted results: VRLA batteries during charge.

1.  Except for $R_o$, all other electrical elements show a strong dependency on SOC.

2.  All electrical elements exhibit an inverse behaviour versus SOC in charge and discharge.

3.  The operational current influences $R_s$, $R_l$ and $C_l$ in both charge and discharge processes.

Therefore, all the elements could be expressed as the function of SOC for better accuracy, even though Ro does not vary too much with different SOC values. Elements $R_s$, $R_l$ and $C_l$ were modelled as the function of both SOC and C-rate.

In these two figures, it can be observed that the fitting of all the electrical elements for battery model construction has a high accuracy. The equations of all these electrical elements for LFP battery are listed below.

## CHARGE

$$R_{o\_LPc} = 0.0334 \cdot SOC^4 - 0.06141 \cdot SOC^3 + 0.03985 \cdot SOC^2 - 0.01104 \cdot SOC + 0.04918 \quad \text{(A.25)}$$

$$\begin{aligned} R_{s\_LPc} = & \left(0.01036 \cdot e^{0.295 \cdot SOC} + 3.829e-6 \cdot e^{8.363 \cdot SOC}\right) \\ & \times \left(0.2304 \cdot C_r^2 - 0.775 \cdot C_r + 1.1458\right) \times \left(-0.2068 \cdot SOC^2 + 0.1532 \cdot SOC + 1.011\right) \end{aligned}$$
(A.26)

$$C_{s\_LPc} = 1451 \cdot e^{-0.3283 \cdot SOC} - 9.562e-8 \cdot e^{22.43 \cdot SOC} \quad \text{(A.27)}$$
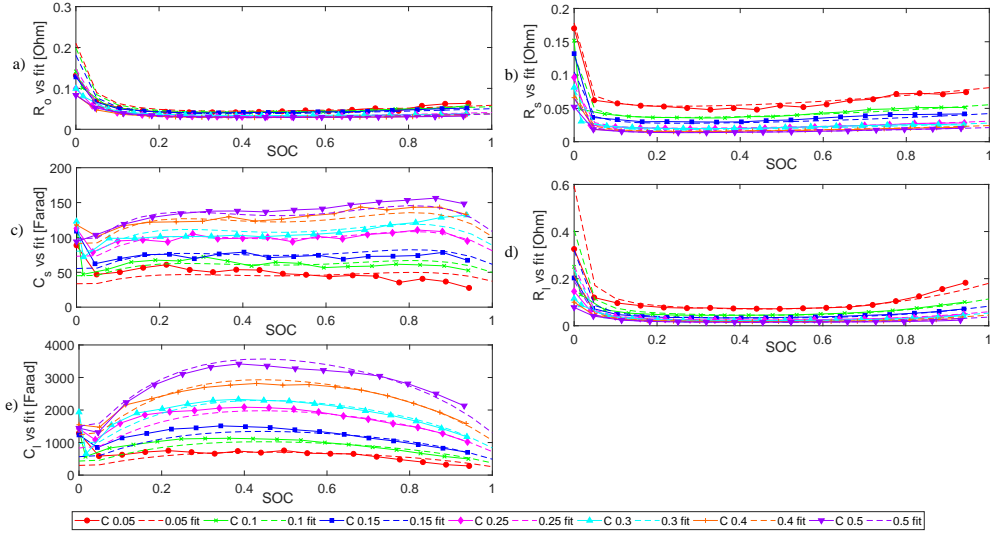
Figure A.9: The values of RC elements and their fitted results: VRLA batteries during discharge.

$$R_{l\_LPc} = [0.9515 + 0.05887 \cdot cos(xw) - 0.06694 \cdot sin(xw) - 0.01243 \cdot cos(2xw)$$
$$- 0.04918 \cdot sin(2xw) - 0.02577 \cdot cos(3xw) - 0.01927 \cdot sin(3xw)]$$
$$\times \left(7.677 \cdot e^{-28.9 \cdot C_r} + 1.7054 \cdot e^{-2.789 \cdot C_r}\right) \times (-0.1976 \cdot SOC + 1.169)$$
$$x = SOC; w = 4.494 \tag{A.28}$$

$$C_{l\_LPc} = [1.672e4 + 7346 \cdot cos(xw) + 6107 \cdot sin(xw) + 3910 \cdot cos(2xw)$$
$$+ 859.6 \cdot sin(2xw) + 1356 \cdot cos(3xw) - 4264 \cdot sin(3xw)]$$
$$\times \left(-1.272 \cdot C_r^2 + 2.346 \cdot C_r + 0.5817\right) \times \left(-0.08145 \cdot SOC^2 + 0.06667 \cdot SOC + 0.9769\right)$$
$$x = SOC; w = 4.76 \tag{A.29}$$

### DISCHARGE

$$R_{o\_LPd} = 0.04153 \cdot SOC^4 - 0.09593 \cdot SOC^3 + 0.07794 \cdot SOC^2 - 0.0273 \cdot SOC + 0.05125 \tag{A.30}$$

$$R_{s\_LPd} = \left(-0.0325 \cdot SOC^3 + 0.06854 \cdot SOC^2 - 0.04985 \cdot SOC + 0.02432\right)$$
$$\times \left(1.084 \cdot e^{-0.534 \cdot C_r} + 0.4643 \cdot e^{-14.45 \cdot C_r}\right) \times \left(0.03161 \cdot SOC^2 - 0.07195 \cdot SOC + 1.032\right)$$
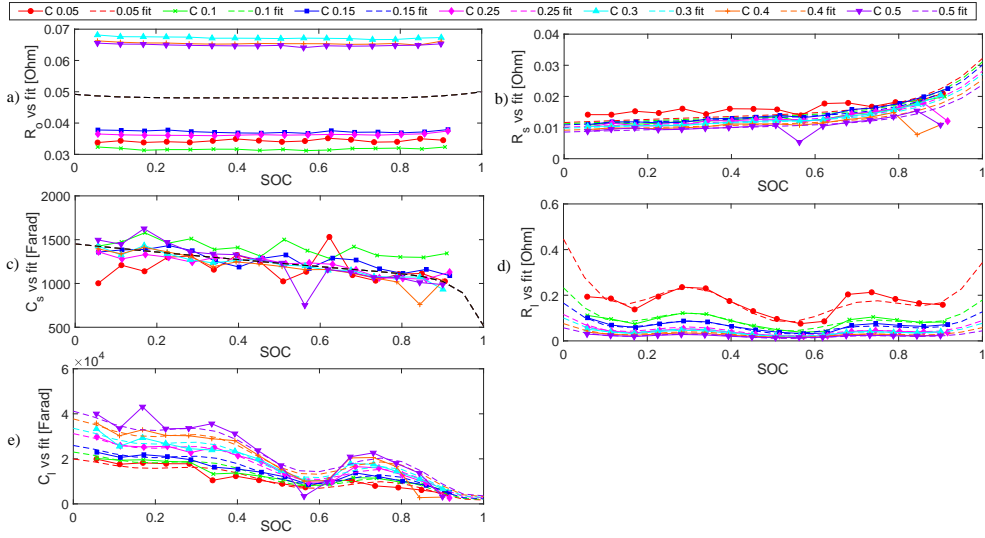$$\tag{A.31}$$

Figure A.10: The values of RC elements and their fitted results: LFP batteries during charge.

$$C_{s\_LPd} = 909 \cdot e^{0.4785 \cdot SOC} - 764.6 \cdot e^{-7.692 \cdot SOC} \tag{A.32}$$

$$
\begin{aligned}
R_{l\_LPd} = &(219.3 \cdot SOC^8 - 1031 \cdot SOC^7 + 1986 \cdot SOC^6 - 2021 \cdot SOC^5 \\
&+ 1167 \cdot SOC^4 - 381 \cdot SOC^3 + 65.8 \cdot SOC^2 - 5.111 \cdot SOC + 0.1754) \\
&\times \left(1.307 \cdot e^{-1.872 \cdot C_r} + 6.3160 \cdot e^{-20.67 \cdot C_r}\right) \times (0.04198 \cdot SOC + 0.9656)
\end{aligned} \tag{A.33}
$$

$$
\begin{aligned}
C_{l\_LPd} = &(1.22e4 - 2988 \cdot cos(xw) - 2455 \cdot sin(xw) - 1326 \cdot cos(2xw) \\
&- 3567 \cdot sin(2xw) - 5139 \cdot cos(3xw) - 1171 \cdot sin(3xw)) \\
&\times \left(-2.322 \cdot C_r^2 + 2.473 \cdot C_r + 0.5983\right) \\
&x = SOC; w = 5.522
\end{aligned} \tag{A.34}
$$

## COULOMBIC EFFICIENCY

The measured and fitted Coulombic efficiency result of VRLA battery is plotted in Figure A.12.

The Coulombic efficiency is expected to decrease when current increases. However, the efficiency measured with 0.2C is higher than that measured with 0.1 C, and the result measured with 0.4 C is larger than the one measured with 0.3 C. This is because 0.1 C and 0.3 C measurements were operated on the same battery, while a different battery was tested with 0.2 C and 0.4 C. The differences between batteries may lead to
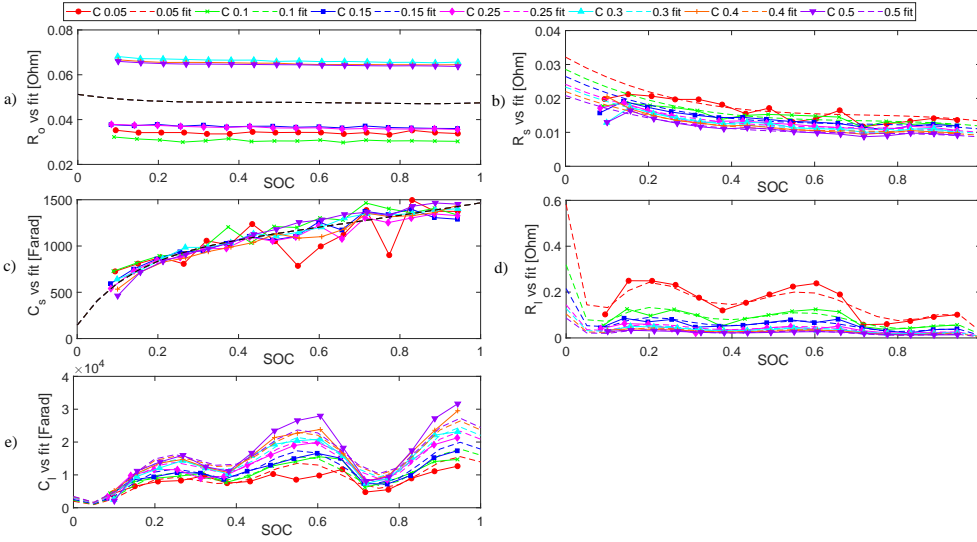
Figure A.11: The values of RC elements and their fitted results: LFP batteries during discharge.

this consequence. Nevertheless, the Coulombic efficiency tested with higher C-rate is lower than one tested with lower C-rate for the same battery. Therefore, the Coulombic efficiency is fitted into the modified Equation A.10, which was introduced in Section A.3.6. The result is shown in Equation A.35.

$$\eta_{\mathrm{c}} = 0.977 \left[ 1 - e^{\frac{5.466}{5.569e-3\frac{C_{\mathrm{r}}}{0.2}+0.03745} \times (SOC-1)} \right] \tag{A.35}$$

where $C_{\mathrm{r}}$ is the C-rate.

## A.4.2. Simulation and Validation

In this section, the simulation results and the experimental data are compared. The comparison of measured voltage and simulated voltage for both battery technologies are plotted in Figures A.13 and A.14.

As stated in Section A.2.2, there are three essential features that should be reflected in the model: the storage feature, the voltage response and the parasitic side reaction. In this study, the SOC is the independent variable, and the voltage response is the main feature being modelled. The Coulombic efficiency is included in the storage circuit as well as the voltage response circuit. Hence, the voltage is selected to evaluate the accuracy of the model. To quantify the model accuracy, all the modelled and measured voltage values are calculated and evaluated using Equation A.36. Then, for each battery, there is an averaged error value achieved among the whole charge/discharge process.

$$\text{error} = \frac{V_{\mathrm{sim}} - V_{\mathrm{exp}}}{V_{\mathrm{exp}}} \times 100 \tag{A.36}$$
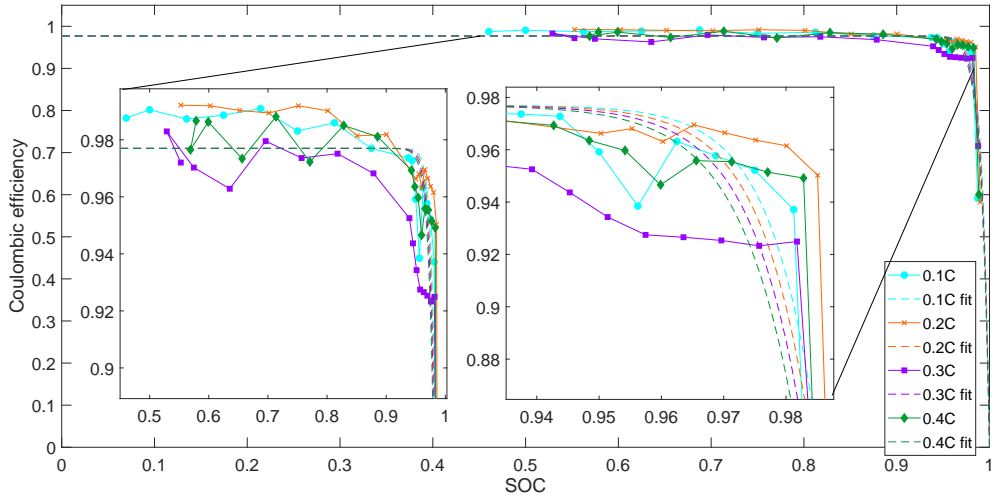
Figure A.12: Measured Coulombic efficiency of VRLA battery with SOC and with different C-rate.

where $V_{sim}$ is the simulated voltage and $V_{exp}$ is the measured voltage.

The constant voltage (CV) charging stages were omitted from the calculation because, in the real measurement, the pause steps are accomplished by the tester, and it depends on the natural battery features. This step counting outcome accomplished by the tester in CV stage is unable to be repeated with the simulation. How it works is reflected in Figures A.13 and A.14. For example, the comparison results of VRLA batteries is shown in Figure A.13. The discrepancy in this figure between the experimental and the simulation results (e.g., 600–1000, 250–700 and 150–650 min in Figure A.13a–c, respectively) are due to the step counting method difference. Therefore, the CV stages for both battery technologies are eliminated.

The comparison results of VRLA batteries are in Figure A.13. The simulated voltage curve increases slower than the measured one during the last charging stage before the battery reaches the CV stage, which is, e.g., around 600 min in Figure A.13a. This slower increase trend of voltage is due to the modelled Coulombic efficiency loss. This can be attributed to the fact that the number of measured Coulombic efficiency data points when the SOC > 98% are insufficient. The fitted Coulombic efficiency result then cannot model the VRLA battery behaviour accurately when it reaches the high SOC stage, especially when the SOC higher than 98%.

For VRLA batteries, the maximum averaged error among all eight different C-rates is 1.7664%, while discounting the CV charging stage. The Coulombic efficiency fitting results might be one of the reason causing the error here.

Figure A.14 shows the comparison results of LFP batteries. For LFP batteries, the maximum averaged error among all different C-rates, which is eight batteries in total, is 1.6708%. The discrepancy of the wedges shaped charge/discharge steps is mainly due to the differences in ohmic resistance. The error from ohmic resistance counts at least 0.5%.

The dynamic models of both battery technologies are therefore considered accurate.
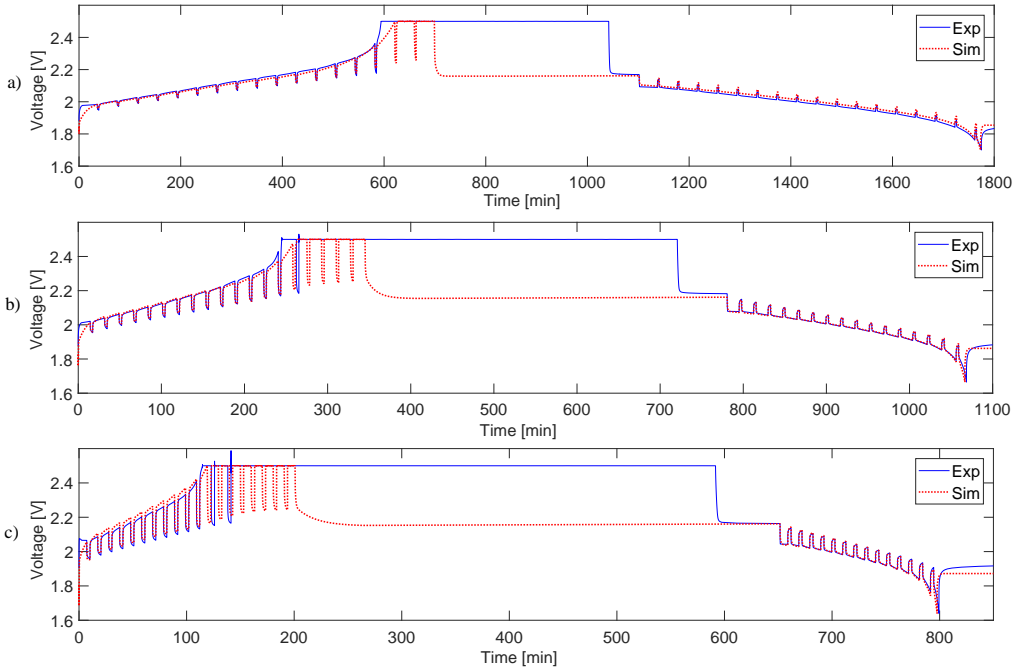
Figure A.13: Comparison of experimental result and simulation result-VRLA battery.: (**a**) test with 0.1 C; (**b**) test with 0.25 C; and (**c**) test with 0.5 C.

## RECOMMENDATIONS

Firstly, it is recommended to identify and develop a more accurate methodology to measure the Coulombic efficiency. The methodology presented in this chapter is sufficient over most of the SOC range, except beyond 98%, where the achievable SOC granularity of the method is lower than desirable. Even though more accurate industrial test methods for Coulombic efficiency measurement are mostly chemical-based, it is still worthwhile developing a simple method with sufficient accuracy over the entire operational SOC range, especially for electrical models. Secondly, the batteries' dynamic behaviour was modelled only when the batteries were new. The dynamic performance evolution through ageing is currently ignored. This is proposed to be improved in the future work. Thirdly, the impact of temperature needs to studied as an independent and controllable variable. Finally, this EECM is proposed to be applied in actual SHS use-cases by using battery charging and discharging profiles from SHS applications.

## A.5. CONCLUSIONS

In this study, two battery technologies (VRLA and LFP) were chosen for experimentally determining the dynamic behaviour of the battery, with the eventual goal of constructing an EECM model. The constructed model works well throughout the C-rate range from 0.05 C to 0.5 C, with an error lower than 2% for both LFP and VRLA batteries. The chosen
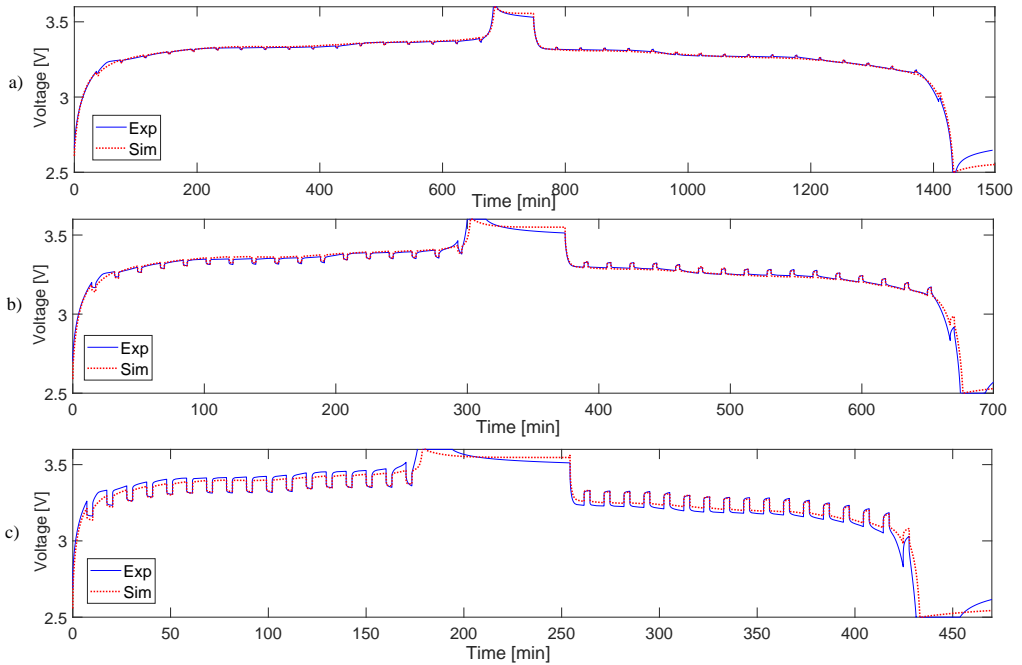
Figure A.14: Comparison of experimental result and simulation result-LFP battery: (**a**) test with 0.1 C; (**b**) test with 0.25 C; and (**c**) test with 0.5 C.

C-rate range gave a better granularity for the intended application of SHS. The non-linear relation between SOC and $V_{OC}$, the use of 2nd order RC circuit in EECM, and the quantification of the parasitic branch of VRLA cells in the form of SOC and C-rate-based Coulombic efficiency $\eta_c$ were identified as methodological contributions for modelling the dynamic behaviour of VRLA batteries. Additionally, the model developed in this work is at the cell level, which is fully scalable to battery pack level. The proposed model can be used by SHS designers for understanding application-specific battery behaviour in the context of system design and analysis.

## REFERENCES

[1] IEA, *Energy Access Outlook 2017 - From Poverty to Prosperity*. Organization for Economic Cooperation and Development, International Energy Agency, 1 ed., 2017.

[2] N. Narayan, T. Papakosta, V. Vega-Garita, Z. Qin, J. Popovic-Gerber, P. Bauer, and M. Zeman, "Estimating battery lifetimes in solar home system design using a practical modelling methodology," *Applied Energy*, vol. 228, pp. 1629 – 1639, 2018.

[3] J. Leadbetter and L. G. Swan, "Selection of battery technology to support grid-integrated renewable electricity," *Journal of Power Sources*, vol. 216, pp. 376–386, 2012.

[4] P. Moseley and D. Rand, "Chapter 1 - the valve-regulated battery — a paradigm shift in lead-acid technology," in *Valve-Regulated Lead-Acid Batteries* (D. Rand, J. Garche, P. Moseley, and C. Parker, eds.), pp. 1 – 14, Amsterdam: Elsevier, 2004.

[5] N. S. Hudak, "4 - nanostructured electrode materials for lithium-ion batteries," in *Lithium-Ion Batteries* (G. Pistoia, ed.), pp. 57 – 82, Amsterdam: Elsevier, 2014.

[6] B. Nykvist and M. Nilsson, "Rapidly falling costs of battery packs for electric vehicles," *Nature Climate Change*, vol. 5, no. April, pp. 329—-332, 2015.

[7] C. Zhang, K. Li, S. McLoone, and Z. Yang, "Battery modelling methods for electric vehicles - A review," *2014 European Control Conference, ECC 2014*, pp. 2673–2678, 2014.

[8] P. Mohanty and M. Gujar, *PV Component Selection for Off-Grid Applications*, pp. 85–106. Cham: Springer International Publishing, 2016.

[9] D. G. für Sonnenenergie. London: Earthscan, english ed., 2005.

[10] A. Stroe, D. Stroe, M. Swierczynski, R. Teodorescu, and S. K. Kær, "Lithium-ion battery dynamic model for wide range of operating conditions," in *2017 International Conference on Optimization of Electrical and Electronic Equipment (OPTIM) 2017 Intl Aegean Conference on Electrical Machines and Power Electronics (ACEMP)*, pp. 660–666, May 2017.

[11] B. Y. Liaw, G. Nagasubramanian, R. G. Jungst, and D. H. Doughty, "Modeling of lithium ion cells—a simple equivalent-circuit model approach," *Solid State Ionics*, vol. 175, no. 1, pp. 835 – 839, 2004. Fourteenth International Conference on Solid State Ionics.

[12] S. Tian, M. Hong, and M. Ouyang, "An experimental study and nonlinear modeling of discharge I-V behavior of valve-regulated lead-acid batteries," *IEEE Transactions on Energy Conversion*, vol. 24, no. 2, pp. 452–458, 2009.

[13] *Introduction*, pp. 1–9. Dordrecht: Springer Netherlands, 2008.

[14] T. Crompton, "1 - introduction to battery technology," in *Battery Reference Book* (T. Crompton, ed.), pp. 1 – 64, Oxford: Newnes, third edition ed., 2000.

[15] C. A. Vincent, "2 - theoretical background," in *Modern Batteries (Second Edition)* (C. Vincent and B. Scrosati, eds.), pp. 18 – 64, Oxford: Butterworth-Heinemann, second edition ed., 1997.

[16] M. Dubarry, V. Svoboda, R. Hwu, and B. Yann Liaw, "Incremental Capacity Analysis and Close-to-Equilibrium OCV Measurements to Quantify Capacity Fade in Commercial Rechargeable Lithium Batteries," *Electrochemical and Solid-State Letters*, vol. 9, no. 10, pp. A454–A457, 2006.

[17] M. Root, *The TAB Battery Book An In-Depth Guide to Construction, Design, and Use.* McGraw-Hill Companies, 2010.

[18] D. Doerffel, *Testing and Characterisation of Large High-Energy Lithium-Ion Batteries for Electric and Hybrid Electric Vehicles*. PhD thesis, 2007.

[19] W. Waag, S. Käbitz, and D. U. Sauer, "Experimental investigation of the lithium-ion battery impedance characteristic at various conditions and aging states and its influence on the application," *Applied Energy*, vol. 102, pp. 885–897, 2013.

[20] L. Lam, P. Bauer, and E. Kelder, "A practical circuit-based model for Li-ion battery cells in electric vehicle applications," in *Telecommunications Energy Conference (INTELEC), 2011 IEEE 33rd International*, pp. 1–9, IEEE, 2011.

[21] C.-J. Zhan, X. Wu, S. Kromlidis, V. Ramachandaramurthy, M. Barnes, N. Jenkins, and A. Ruddell, "Two electrical models of the lead–acid battery used in a dynamic voltage restorer," *IEE Proceedings - Generation, Transmission and Distribution*, vol. 150, no. 2, p. 175, 2003.

[22] M. Ceraolo, "New Dynamical Models of Lead – Acid Batteries," *IEEE Transactions on Power Systems*, vol. 15, no. 4, pp. 1184–1190, 2000.

[23] X. Hu, S. Li, and H. Peng, "A comparative study of equivalent circuit models for Li-ion batteries," *Journal of Power Sources*, vol. 198, pp. 359–367, 2012.

[24] S. Panchal, J. Mcgrory, J. Kong, R. Fraser, M. Fowler, I. Dincer, and M. Agelin-Chaab, "Cycling degradation testing and analysis of a lifepo4 battery at actual conditions," *International Journal of Energy Research*, vol. 41, no. 15, pp. 2565–2575, 2017.

[25] W. E. M. Jones and D. O. Feder, "Behavior of vrla cells on long term float. ii. the effects of temperature, voltage and catalysis on gas evolution and consequent water loss," in *Proceedings of Intelec'96 - International Telecommunications Energy Conference*, pp. 358–366, Oct 1996.

[26] S. Buller, *Impedance-based simulation models for energy storage devices in advanced automotive power systems*. Phd thesis, RWTH Aachen University, 2003.

[27] R. Kaushik and I. G. Mawston, "Coulombic efficiency of lead/acid batteries, particularly in remote-area power-supply (RAPS) systems," *Journal of Power Sources*, vol. 35, no. 4, pp. 377–383, 1991.

[28] D. Andre, M. Meiler, K. Steiner, C. Wimmer, T. Soczka-Guth, and D. U. Sauer, "Characterization of high-power lithium-ion batteries by electrochemical impedance spectroscopy. I. Experimental investigation," *Journal of Power Sources*, vol. 196, no. 12, pp. 5334–5341, 2011.

[29] MACCOR, "Series 4000 Automated Test System," pp. 1–4.

[30] Enersys, "Application Manual of CYCLON AGM single cell," no. December, 2008.

[31] A123 Systems, "Nanophosphate High Power Lithium Ion Cell ANR26650M1-B," pp. 2–3, 2012.

[32] J. H. Yan, H. Y. Chen, W. S. Li, C. I. Wang, and Q. Y. Zhan, "A study on quick charging method for small VRLA batteries," *Journal of Power Sources*, vol. 158, no. 2 SPEC. ISS., pp. 1047–1053, 2006.

[33] J. H. Aylor, A. Thieme, and B. W. Johnson, "A Battery State-of-Charge Indicator for Electric Wheelchairs," *IEEE Transactions on Industrial Electronics*, vol. 39, no. 5, pp. 398–409, 1992.

[34] S. P. S. Pang, J. Farrell, J. D. J. Du, and M. Barth, "Battery state-of-charge estimation," *Proceedings of the 2001 American Control Conference. (Cat. No.01CH37148)*, vol. 2, pp. 1644–1649, 2001.

[35] Y. Hu, S. Yurkovich, Y. Guezennec, and B. J. Yurkovich, "Electro-thermal battery model identification for automotive applications," *Journal of Power Sources*, vol. 196, no. 1, pp. 449–457, 2011.

# APPENDIX B: EVALUATING THE IMPACT OF TEMPERATURE ON SOLAR HOME SYSTEMS

## B.1. INTRODUCTION

As price is a key sensitive parameter especially for rural off-grid markets, any degradation in performance or lifetime of SHS will adversely impact the overall system costs. In most of the rural off-grid areas that are un(der)-electrified, the ambient temperatures are often much higher than the standard testing conditions (STC) temperature of 25°C. Therefore, the work described in this appendix chapter investigates the impact of temperature on the performance and lifetime of SHS. This study answers the following questions in the context of rural electrification:

1. What is the performance-degradation in SHS energy yield due to temperature?

2. What is the impact of temperature on the lifetime-degradation of (a lead-acid) battery in SHS?

## B.2. BACKGROUND

The block diagram of a typical SHS has been seen in Chapter 1 in Figure 1.7. We focus on PV and battery within the scope of this study. While the temperature impact on PV and battery are quantitatively analyzed, the temperature impact on the power electronics is also qualitatively commented upon in brief.

### B.2.1. PHYSICAL EFFECTS OF TEMPERATURE ON SHS COMPONENTS

Temperature is a key parameter that influences both performance (efficiency) as well as the lifetime of SHS components, especially for implementations in off-grid areas experiencing high ambient temperatures. A brief technological background on the physical effects of temperature on SHS is given below.

#### INFLUENCE OF TEMPERATURE ON PV MODULE

At the device level, the temperature has two contradictory effects on a solar cell. On the one hand, an increase in temperature decreases the bandgap and consequently the

---

open circuit voltage ($V_{OC}$) of the solar cell [1, 2]. On the other hand, having a positive temperature coefficient of short circuit current ($I_{SC}$), an increase in temperature causes an increase in the $I_{SC}$. For the same input irradiance level, the loss in voltage is the dominating effect, eventually leading to a decrease in the output power [1, 2].

In terms of lifetime, crystalline silicon (c-Si) modules, the most commonly used PV technology in SHS, have been reported to experience a lifetime-degradation rate of around 0.5-0.9%/year range, including the degradation due to higher temperatures in hot and humid climates [3]. The temperature-induced lifetime-degradation of PV modules is as such not explored in this study.

### INFLUENCE OF TEMPERATURE ON BATTERY

Temperature can have a very short-term positive influence on the battery performance. This is because depending on the state of health (SOH) of the battery, the increase in electrolyte temperature can lead to a heightened chemical activity for the forward reaction. If the efficiency is purely looked upon as the ratio between energy taken out to the energy put into the battery, higher efficiency can be temporarily attained as compared to the case without any temperature increase [4].

However, an increase in temperature can be severely detrimental to the lifetime of the battery. It can lead to accelerated failure mechanisms due to grid corrosion and water loss for evaporation or hydrogen evolution at the negative plates of a lead-acid battery [5].

### INFLUENCE OF TEMPERATURE ON POWER ELECTRONICS

Power electronics present in SHS in the form of converters generally comprise of switches and passive elements. In terms of performance, the largest impact of temperature is on switch conduction losses due to an increase in the on-resistance ($R_{DS_{ON}}$). In terms of passives, the filter capacitor value is hardly affected by temperature, while its Equivalent Series Resistance (ESR) decreases with increase in temperature, leading to a reduction in its impedance[6]. With rising temperatures, the ferrite cores generally exhibit marginally decreasing losses until around 80-90°C, after which the losses increase [7].

In terms of lifetime, the degradation in life-cycles is usually denoted as a function of the thermal stress cycles that the power electronic component undergoes. Very high temperatures can lead to the copper and tin at the solder joints forming a brittle alloy, thus often making the solder joints the weakest link in the reliability of the power electronics in use. In any case, for the currently rated power levels in SHS (sub 200 W), the state-of-the-art power converters are expected to last at least 20 years.

## B.2.2. SCOPE OF THIS STUDY

The temperature impact on SHS components can be broadly classified as either performance-degrading (drop in efficiency or energy yield) or lifetime-degrading (drop in life-cycles). Based on the relative impact of the type of degradation, the work described in this chapter focuses on quantifying the performance-degradation of PV modules and lifetime-degradation of the battery in SHS.

The physical effects of temperature outlined in Section B.2.1 vary in degree between the kind of technology being used. Based on the application space of rural electrification, the chosen technologies for this study are crystalline silicon for the PV module, and valve-

regulated lead-acid (VRLA) lead-acid gel for the battery, as these were the most popular technologies being used by SHS providers at the time of conducting this study.

Additionally, while past studies have individually looked into the temperature impact on PV [3, 1], battery [5], there is a lack of a comprehensive work on temperature impact on SHS in the context of rural electrification and particular application use-case for a given load profile and battery usage. This work described here aims to create fresh insights in this direction.

## B.3. METHODOLOGY

The methodology consists of simulating models for quantifying the performance and lifetime-degradation of SHS components. Inputs to the simulation and the models used are described below.

### B.3.1. INPUTS TO THE SHS SIMULATION

The system level simulation was run over a period of 1 year corresponding to the availability of meteorological data with 1-minute resolution.

#### METEOROLOGICAL DATA

The meteorological data was obtained from the Meteonorm software and consisted of PV irradiance, wind speed, and ambient temperature with 1 min resolution [8]. The sun position data was obtained using the sun position algorithm from Sandia National Labs [9]. As ground level meteorological data for an off-grid rural location could not be found, the choice of location was considered to be Ahmedabad in India (23.03°N, 72.58°E), a city that also receives a very high amount of irradiance (around 5.5 equivalent sun hours per day) and experiences very high temperatures of around 40°C. This is considered as a good representative choice for investigating the temperature impact on SHS.

#### LOAD PROFILE

Given the recent proliferation of efficient off-grid DC appliances, only DC loads were considered to be used in the load profile [10, 11, 12]. The load profile was selected from a study by the authors [13], which detailed the construction of stochastic load profiles to map the energy consumption for the various tiers of the multi-tier framework for measuring electricity access. A tier 3 household electricity need was assumed for this study. Consequently, a tier 3 load profile was used as an input to the SHS simulation.

#### PV MODULE

The selected PV module is Jinko Solar JKM265P. Given the rating of 265 Wp, 1 PV module is sufficient to cover the average daily energy needs. To satisfy the load completely, however, an appropriately sized battery storage will be needed, which is discussed in Section B.3.3. The main module characteristics have been tabulated in Table B.1.

#### BATTERY

A VRLA battery was chosen for the simulation. The datasheet provided in [14] was vital to perform the analysis of temperature impact on lifetime-degradation, as described later in Section B.3.4.

Table B.1: Main parameters of PV module Jinko Solar JKM265P.

| Parameters | Value |
|---|---|
| Power $P_{mpp}$ (Wp) | 265 |
| Area $A_M$ (m$^2$) | 1.6368 |
| $V_{OC}$ (V) | 38.6 |
| $I_{SC}$ (A) | 9.03 |
| $V_{mpp}$ (V) | 31.4 |
| $I_{mpp}$ (A) | 8.44 |
| $k$ (%/°C) | -0.41 |
| NOCT (°C) | 45 |
| $\eta_{stc}$ (%) | 16.19 |

### B.3.2. ESTIMATING PV YIELD

Estimating the PV yield while accounting for the thermal losses comprises multiple steps, as described below.

#### PLANE OF ARRAY (POA) IRRADIANCE

First, the optimal module orientation is evaluated by examining the effect of various module orientations, i.e., tilts and azimuths, by calculating the POA irradiance at each orientation. The orientation maximizing the annual POA irradiation is chosen as the optimal one. The 3 different components of irradiance, Direct Normal Irradiance (DNI), Diffused Horizontal Irradiance (DHI), and Global Horizontal Irradiance (GHI), which are obtained from the Meteonorm database, contribute differently at different module orientations. These are taken into account using the following equations, which help calculate the irradiance components, viz., direct, diffused, and albedo radiation incident on the POA [2]:

$$\cos\theta = \sin(E_s)\cos\phi + \cos(E_s)\sin\phi\cos(A_m - A_s) \tag{B.1}$$

$$G_{direct} = DNI\cos\theta \tag{B.2}$$

$$G_{diffused} = DHI\left(\frac{1+\cos\phi}{2}\right) \tag{B.3}$$

$$G_{albedo} = GHI\left(\frac{1-\cos\phi}{2}\right) \times \alpha \tag{B.4}$$

Where: $E_s$: Elevation of the sun, $A_s$: Azimuth of the sun, $A_m$: Azimuth of the module, $\phi$: Module tilt, $\theta$: Angle between DNI and the normal to the POA, $\alpha$: albedo of the landscape (assumed 0.15). Finally, the POA irradiance is calculated as shown in Equation B.5.

$$G_{POA} = G_{direct} + G_{diffused} + G_{albedo} \tag{B.5}$$

#### PV MODULE TEMPERATURE

As the meteorological data only gives ambient temperature, the module temperature needs to be then correctly estimated. Three different PV module temperature estimation

models from the literature were used in this study. These are the nominal operating cell temperature (NOCT) model, Duffie-Beckman (DB) model, and the fluid-dynamics (FD) model. Note that the cell temperature is assumed to be the same as the PV module temperature when referring to the quantity $T_M$ in these models.

### NOCT MODEL

This is a simplified steady-state model with NOCT of the PV module as a reference point. As the NOCT for a typical c-Si module is around 40-45 °C, the module temperature is always greater than the ambient temperature for a positive value of POA. The governing equation is as follows [2].

$$T_M = T_{amb} + \frac{T_{NOCT} - 20\,°C}{800} \times G_{POA} \tag{B.6}$$

Where $T_M$ is the module temperature, $T_{amb}$ is the ambient temperature, $T_{NOCT}$ is the NOCT of the PV module, which is test-measured at 800 W/m$^2$ and 20 °C. However, the NOCT model fails to take into account several other parameters.

### DUFFIE-BECKMAN

The Duffie-Beckman (DB) model takes into account additional parameters, viz., wind speed, cell efficiency, transmittance, and absorptivity [15].

$$T_M = T_{amb} + \frac{T_{NOCT} - 20\,°C}{800} \times G_{POA} \left( \frac{9.5}{5.7 + 3.8 \times w} \right) \left( 1 - \frac{\eta_{cell}}{T \times a} \right) \tag{B.7}$$

Where $w$ is the windspeed, $\eta_{cell}$ is the cell efficiency, $T$ is the transmittance of the module front, and $a$ is the absorptivity of the module.

### FLUID-DYNAMIC MODEL

Both NOCT and DB models fail to take into account the location dependent diverse meteorological conditions [2]. The fluid-dynamic (FD) model, based on a detailed thermal energy balance between a tilted module and its surroundings, overcomes the drawbacks of both DB and NOCT models. The governing equation is stated in Equation B.8 [2]. A detailed derivation is present in [16].

$$T_M = \frac{aG_{POA} + h_c T_a + h_{r,sky} T_{sky} + h_{r,gr} T_{gr}}{h_c + h_{r,sky} + h_{r,gr}} \tag{B.8}$$

Where $aG_{POA}$ is the heat received from the sun; $h_c$ is the convective heat transfer coefficient between the module and the surroundings; $h_{r,sky}$ and $h_{r,gr}$ are the linearized coefficients of radiative heat exchange between the upper part of the module and the sky, and the back of the module and the ground, respectively [2]; $T_a$, $T_{sky}$, and $T_{gr}$ are temperatures of the surroundings, sky, and ground respectively.

### DYNAMIC EFFICIENCY AND PV POWER

As the output of the PV module varies based on meteorological conditions like irradiance, temperature, and wind speed, the instantaneous efficiency is dynamic and can be very different from the STC efficiency. To evaluate the dynamic efficiency and PV power,

first the PV output power at 25 °C is calculated as a function of irradiance as shown in Equations B.9 through B.12 [2].

$$V_{OC}(25\,^{\circ}C, G_{POA}) = V_{OC}(STC) + \frac{nk_BT}{q} ln\left(\frac{G_{POA}}{G_{STC}}\right) \tag{B.9}$$

$$I_{SC}(25\,^{\circ}C, G_{POA}) = I_{SC}(STC)\frac{G_{POA}}{G_{STC}} \tag{B.10}$$

$$P_{mpp}(25\,^{\circ}C, G_{POA}) = FF \times V_{OC}I_{SC}(25\,^{\circ}C, G_{POA}) \tag{B.11}$$

$$\eta(25\,^{\circ}C, G_{POA}) = \frac{P_{mpp}(25\,^{\circ}C, G_{POA})}{G_{POA} \times A_M} \tag{B.12}$$

Where $k_B$ and $q$ are the universal Boltzmann constant and charge constant respectively, n is the ideality factor (usually $\approx 1.5$ for c-Si [2]), and FF is the fill factor. Now the temperature effect can be added to the $P_{mpp}$ by using the temperature coefficient of power (the $k$ value) the manufacturer states in the PV datasheet (Table B.1), giving the dynamic PV output power as shown in Equation B.13.

$$P_{mpp_{dyn}} = P_{mpp}(25\,^{\circ}C, G_{POA}) + kP_{mpp}(STC)(T_M - 25\,^{\circ}C) \tag{B.13}$$

Finally, the dynamic efficiency can be calculated as

$$\eta_{dyn} = \frac{P_{mpp_{dyn}}}{G_{POA} \times A_M} \tag{B.14}$$

### EVALUATING PV PERFORMANCE

With the dynamic PV output and efficiency known, the PV performance can be quantified based on 3 metrics, viz. DC yield, corrected efficiency, and the Module Ideality Factor (MIF). The DC yield is simply the integrated PV output power over the period of 1 year (Equation B.15). The corrected efficiency is defined in Equation B.16.

$$E_{DC}^{Y} = \int_{t=0}^{1year} P_{mpp_{dyn}} dt \tag{B.15}$$

$$\eta_{corr} = \frac{E_{DC}^{Y}}{\int_{t=0}^{1year} G_{POA} \times A_M dt} \tag{B.16}$$

### MODULE IDEALITY FACTOR (MIF)

Module Ideality Factor is defined as an indicator of the proportion of expected PV yield actually available after accounting for the thermally induced losses for a given PV module[17]. MIF is a module dependent parameter that is different for every module depending on the impact of temperature on the performance of the module. For an ideal PV module with no thermally induced losses, the MIF=1.

$$MIF = \frac{E_{DC}^{Y}}{\int_{t=0}^{1year} G_{POA} \times A_M \times \eta_{stc} dt} \tag{B.17}$$

### B.3.3. Battery sizing

Based on the corrected PV output yield after accounting for thermal losses, and the load profile described in Section B.3.1, an appropriate battery size is chosen such that the load profile is satisfied at least a certain percent of the times in terms of the LLP, as seen in Section B.4.2.

### B.3.4. Assessing temperature impact on battery lifetime

The battery lifetime was estimated based on a non-empirical method including the influence of temperature in 3 main steps, as described below.

#### Manufacturer's information

The battery manufacturer often provides cycle-life curves as a function of 2 distinct stress-factors, viz. depth of discharge (DOD) and temperature, as seen previously in Chapter 4 (Figure 4.3). Look-up functions are created based on these curves, and the cycle-life curves for the intermediate temperatures are interpolated using linear interpolation. Thus, any given temperature and DOD can be mapped to a particular cycle-life that the battery would enjoy at those stress factor levels.

#### Battery usage from SHS simulation

With the corrected PV output and the evaluated battery size (Section B.3.3), an SHS simulation based on energy balance is run on MATLAB. A constant battery efficiency of 90% and power converter efficiency of 95% are assumed during operation. The simulation helps in understanding exactly the kind of cycling the battery undergoes in a year, which is used then in conjunction with the manufacturer's data as follows.

#### Battery lifetime estimation including temperature

Firstly, the micro-cycles of the battery are extracted from the SHS simulation based on the current zero-crossings (ZCs), as explained in detail in Chapter 4. The overall average DOD ($\overline{DOD}$) is calculated as shown in Equation B.18, where $\overline{DOD_i}$ and $E_{\mathrm{thr}_i}$ are the average DOD and energy throughput values for every micro-cycle respectively [10].

$$\overline{DOD} = \frac{\sum\limits_{i=1}^{N} \overline{DOD_i}.E_{\mathrm{thr}_i}}{\sum\limits_{i=1}^{N} E_{\mathrm{thr}_i}} \tag{B.18}$$

The mean temperature ($\overline{T}$) is similarly calculated for the active periods of the battery, as shown in Equation B.19. $\overline{T_{\mathrm{ambient}_i}}$ is the mean ambient temperature for the particular micro-cycle, while $t_i$ is the duration of the micro-cycles.

$$\overline{T} = \frac{\sum\limits_{i=1}^{N} \overline{T_{\mathrm{ambient}_i}}.t_i}{\sum\limits_{i=1}^{N} t_i} \tag{B.19}$$

Then, the cycle-life number $n$ is obtained from the look-up functions described in Section B.3.4. Equation B.20 is then used to calculate the battery lifetime ($L$) in years [10], where $E_{\mathrm{nom}}$ is the nominal battery energy capacity in Wh.

$$L = n \times \overline{DOD} \times \frac{2 \times E_{\mathrm{nom}}}{\sum\limits_{i=1}^{N} E_{\mathrm{thr}_i}} \tag{B.20}$$

For comparison, the lifetime is estimated by keeping the ambient temperature constant at 25 °C and considering ambient temperature fluctuations along with 2 scaled temperature fluctuation profiles, as shown in Section B.4.2.

## B.4. RESULTS AND DISCUSSION

### B.4.1. PV RESULTS

#### POA IRRADIANCE AND PV ORIENTATION

Following the steps described in Section B.3.2, an optimal orientation of 26° tilt and 232° azimuth (due North) were obtained, which maximized the POA irradiation from 5.34 equivalent sun hours (ESH) per day (flat orientation) to 7.03 ESH per day for an optimal orientation. This optimal orientation was assumed for the rest of the PV analysis and the SHS simulation.

#### MODULE TEMPERATURE ESTIMATION

Based on the methodology for temperature estimation explained in Section B.3.2, the module temperature was estimated using 3 different models from the literature. The estimated module temperatures are shown in Figure B.1 for a representative day (day #95) of the year when the irradiance is the highest.
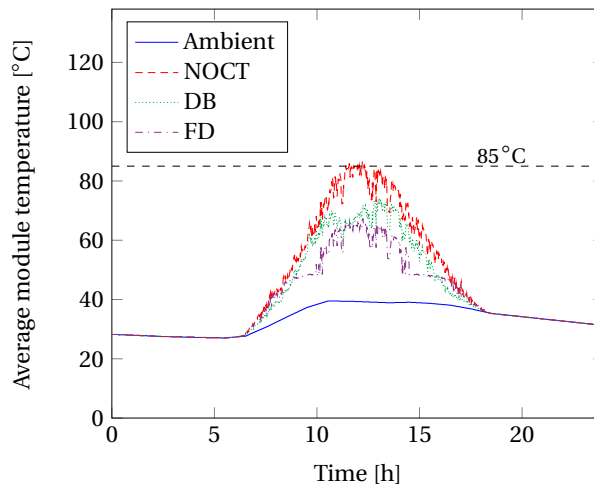


Figure B.1: Estimated module temperatures for different models used, along with the ambient temperature for day #95. The dashed line represents the maximum operating temperature of the PV module.

The NOCT model is constantly pessimistic in estimating the module temperature, resulting in the highest temperature estimates of all the models. It can be seen that for the chosen day with the highest irradiance, the DB model estimates a relatively higher module temperature compared to the FD model. However, for the 1-year long simulation, the average temperature estimated by the DB model is marginally lower than that by the FD model.

Additionally, the maximum module temperature estimated by the NOCT model is 86.7 °C, which is higher than the operational temperature limit of 85 °C of the PV module. Additionally, the NOCT model is very simplistically linear. Therefore, the NOCT model is deemed inadequate to be applied under high irradiance conditions. On the other hand, the DB and FD models are found to be similarly applicable for the given meteorological conditions. Nonetheless, this close agreement of DB and FD model cannot be generalized to other meteorological conditions. The battery sizing and SHS simulation were implemented using the PV temperatures as estimated by the FD model.
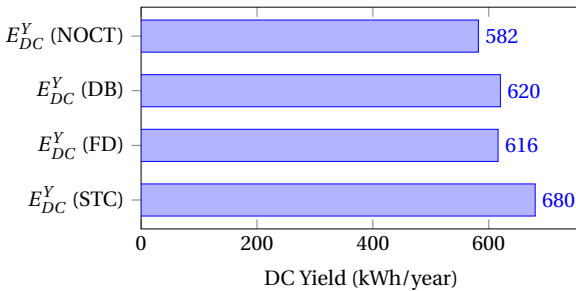


Figure B.2: Annual PV yield evaluated under different predictions of module temperatures, including STC.

## PV PERFORMANCE

With the module temperature evaluated through the different temperature models, the dynamic PV output was calculated as shown in Section B.3.2. Consequently, the metrics defined in Section B.3.2 were evaluated. The comparison of PV yields is shown in Figure B.2. The yield when the module temperature predicted by the NOCT model is the most pessimistic, while the DB and FD cases show similar yields. However, it must be noted that dynamically, DB and FD models lead to different module temperatures, as was seen in Figure B.1. The corrected efficiency and the MIF as the outcome of various module

Table B.2: Corrected efficiency and MIF values under different module temperature estimations vis-a-vis the STC case.

| Metric | STC | NOCT | DB | FD |
|---|---|---|---|---|
| $\eta_{\text{corr}}$ (%) | 16.19 | 13.85 | 14.77 | 14.67 |
| MIF (-) | 1 | 0.856 | 0.912 | 0.906 |

temperature estimation models are tabulated in Table B.2. Again, the values for the case
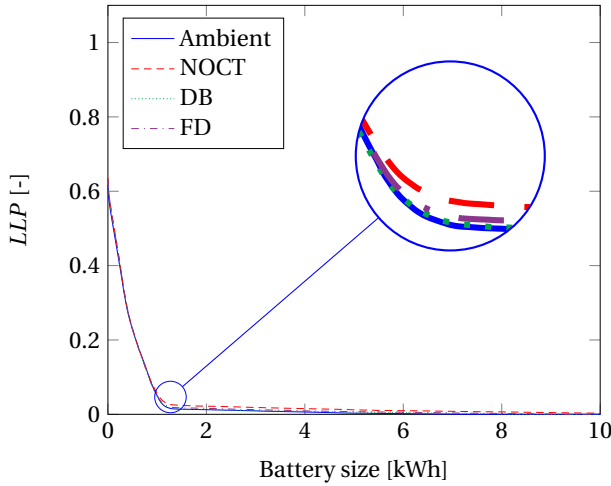
Figure B.3: *LLP* variation based on SHS simulations for various storage sizes and PV outputs due to different temperature estimation models.

of DB and FD models-based temperature estimations are quite close. However, this is liable to change based on a different location with different meteorological conditions. The most remarkable inference is that thermally induced losses can account for 10% losses in the DC yield in such a tropical climate.

### B.4.2. BATTERY RESULTS

#### BATTERY SIZING

Based on the LLP optimization methodology described in Section B.3.3, the *LLP* was evaluated for various storage sizes assuming the PV outputs due to the different temperature estimation models, as shown in Figure B.3. Except for the case with NOCT-based PV output estimation, the rest of the cases largely show a similar LLP profile with varying battery sizes (magnified section in Figure B.3), meaning that the thermally induced losses, while reducing the PV yield, did not significantly alter the battery sizing for the given scenario. It is an economically optimal choice to select the battery around the knee point of the curve. This corresponds to an *LLP* of 1.8% and a battery size of 1.44 kWh assuming a corrected PV output as estimated by the FD model.

#### BATTERY USAGE AND LIFETIME

Based on the selected storage size, an SHS energy balance based model was simulated. The ZCs method described in Section B.3.4 provided a $\overline{DOD}$ of 0.3253. Using Equation B.20, the lifetime was calculated for a constant temperature of 25 °C, and 3 different cases, viz. with fluctuating ambient temperatures and 2 different scaling factors to the ambient temperatures (1.2 and 1.5). Each of them results in a different usage mean temperature. The lifetime results are shown in Table B.3, where SF is the scaling factor applied to the ambient temperature profile.

Including the variability in temperature profiles leads to a 2.6 to 33% drop in the

Table B.3: Impact of temperature on estimated battery lifetime.

|  | T=25°C | ambient | SF = 1.2 | SF = 1.5 |
|---|---|---|---|---|
| $\overline{T}$ (°C) | 25 | 26.4 | 31.6 | 39.5 |
| $L$ (years) | 7.8 | 7.6 | 6.6 | 5.2 |

estimated battery lifetime. The lifetime estimation methodology explained here considers only the active period of battery operation. Depending on the battery usage for the specific load profile and PV output, the lifetime estimation is liable to change. Nonetheless, the temperature impact on battery lifetime is quantified for the given location and load profile. Most importantly, the methodology described here can be applied to any location and load profile to size the SHS and determine the battery usage while estimating the temperature impact on PV performance and battery lifetime.

### RECOMMENDATIONS

It must be noted that the temperature scaling factor used in the study for examining the impact of temperature on the battery is not a true reflection of the range of temperature fluctuations experienced by the battery on a daily basis. The study can be expanded through the addition of detailed temperature profiles, and further validating the models through temperature controlled experiments on battery behaviours.

## B.5. CONCLUSION

The modeling methodology described in this appendix chapter was used to quantitatively analyze the impact of temperature on the performance of the PV module and lifetime of a lead-acid battery in SHS for a given location and load profile. Three different mathematical models were used to estimate the PV module temperature. The NOCT model was deemed inadequate to estimate module temperature with very high POA irradiance values, which is a common occurrence in the tropical latitudes. The PV yield can drop to almost 10% due to thermally induced losses. Although thermally induced losses reduce the PV yield, they are found to have minimal impact on the battery sizing for the considered load profile. The optimal LLP-based battery sizing methodology was used to arrive at a battery size of 1.44 kWh. A non-empirical lifetime estimation methodology was used to evaluate the battery lifetime. Temperature variations during the active battery periods are shown to lead to a 2.6 to a maximum of 33% drop in battery lifetime as compared to the standard condition of 25°C. In conclusion, this chapter presented a methodology to estimate the thermally induced losses in an SHS for rural electrification, which can be further used to size the SHS accordingly.

### REFERENCES

[1] A. Q. Jakhrani, A. K. Othman, A. R. H. Rigitand, and S. R. Samo, "Comparison of solar photovoltaic module temperature models," *World Applied Sciences Journal*, vol. 14, no. SPL ISS 3, pp. 1–8, 2011.

[2] K. Jäger, O. Isabella, A. H. Smets, R. Van Swaaij, and M. Zeman, *Solar Energy: The physics and engineering of photovoltaic conversion, technologies and systems*. UIT Cambridge, 2016.

[3] D. C. Jordan, S. R. Kurtz, K. VanSant, and J. Newmiller, "Compendium of photovoltaic degradation rates," *Progress in Photovoltaics: Research and Applications*, vol. 24, no. 7, pp. 978–989, 2016. PIP-15-244.R1.

[4] J. Yang, C. Hu, H. Wang, K. Yang, J. B. Liu, and H. Yan, "Review on the research of failure modes and mechanism for lead-acid batteries," *International Journal of Energy Research*, vol. 41, no. 3, pp. 336–352, 2017.

[5] P. Ruetschi, "Aging mechanisms and service life of lead-acid batteries," *Journal of Power Sources*, vol. 127, no. 1-2, pp. 33–44, 2004.

[6] "Aluminum electrolytic capacitors - general technical information," 2016.

[7] "Material specification for ferrite core - 3c95 data sheet," 2015.

[8] Meteotest, "Meteonorm ver 7.1," 2014.

[9] S. PVPMC, "Photovoltaic performance modeling collaborative," 2014.

[10] N. Narayan, T. Papakosta, V. Vega-Garita, J. Popovic-Gerber, P. Bauer, and M. Zeman, "A simple methodology for estimating battery lifetimes in solar home system design," in *2017 IEEE AFRICON*, pp. 1195–1201, Sep 2017.

[11] H. Olk and J. Mundt, "Photovoltaics for Productive Use Applications. A catalogue of DC-Appliances," *Deutsche Gesellschaft für Internationale Zusammenarbeit (GIZ) GmbH*, 2016.

[12] Global LEAP, "The State of the Off-Grid Appliance Market," *Tech. Rep.*, 2016.

[13] N. Narayan, Z. Qin, J. Popovic-Gerber, J.-C. Diehl, P. Bauer, and M. Zeman, "Stochastic load profile construction for the multi-tier framework for household electricity access using off-grid dc appliances," *Energy Efficiency*, Nov 2018.

[14] "Installation , commissioning and operating instructions for valve-regulated stationary lead-acid batteries - solar battery data sheet," 2015.

[15] J. A. Duffie and W. A. Beckman, *Solar Engineering of Thermal Processes Solar Engineering*. Hoboken, New Jersey: John Wiley & Sons, 4th ed., 2013.

[16] M. K. Fuentes, "A Simplified Thermal Model for Flat-Plate Photovoltaic Arrays," tech. rep., Sandia National Labs., Albuquerque, NM (USA), 1987.

[17] N. Narayan, "Solar charging station for light electric vehicles: A design and feasibility study," Master's thesis, Delft University of Technology, 2013.

# APPENDIX C: DECENTRALIZED CONTROL-SCHEME FOR DC-INTERCONNECTED SOLAR HOME SYSTEMS FOR RURAL ELECTRIFICATION

## C.1. INTRODUCTION

To enable higher power levels of electricity access in an economically viable way, energy sharing between these individual SHS through interconnectivity is a logical progression, as also detailed in Chapter 6. A rural dc microgrid comprising SHS has been proposed in literature before [1, 2]. However, existing rural dc microgrid studies mainly focus on one voltage level, e.g. 12 V [3]. The SHS interconnectivity must be implemented at a higher voltage level in order to reduce the conduction losses and cable costs. Existing control schemes do not take into account such multi-voltage dc microgrids.

Additionally, in such an interconnected network of SHS, the battery usage needs to be appropriately controlled. Since the microgrid formation is assumed to be bottom-up, the control scheme for energy sharing in the microgrid should also be decentralized.

In this appendix chapter, the state of charge (SOC) balancing in such an interconnected SHS-based dc microgrid is addressed. In particular, the adaptive droop-based SOC control is extended for multiple voltage levels in a dc microgrid without any means of active communication. This is achieved through the creation of a voltage dead-band, SOC-based droop resistances, and the use of voltage ratios in dc-dc converters.

The existing state of charge (SOC)-based droop controllers for microgrids do not take into account multiple voltage levels. E.g., droop control at 48 V is considered in [4, 5], while passive droop control for a 12 V SHS-based microgrid is studied in [6]. State of charge (SOC)-based adaptive droop control for distributed storage units in a microgrid with one voltage bus is presented in [7], which aims to balance the battery SOC across the microgrid. However, in an SHS-based microgrid as presented in our study, SOC balancing between the batteries is not the primary objective.

In this chapter, for a decentralized rural dc microgrid comprising individual solar home systems (SHS) with multiple voltage levels, viz., 48 V and 350 V, a decentralized
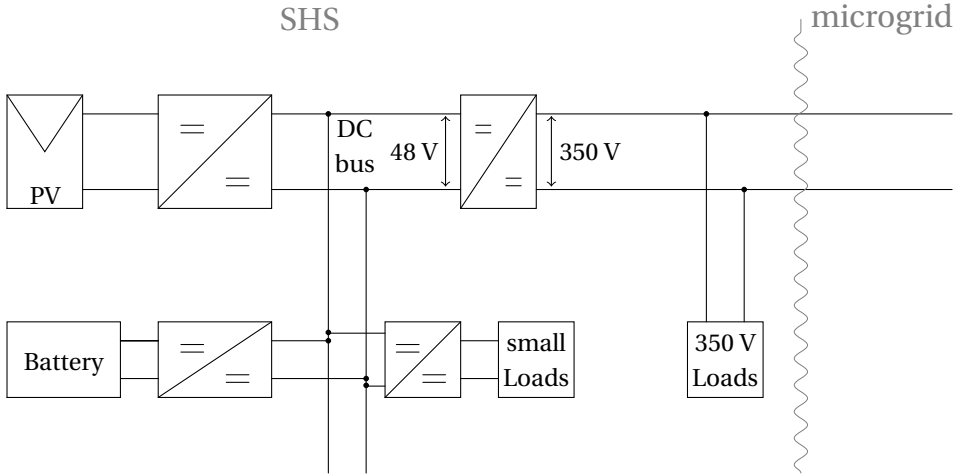
Figure C.1: SHS-based dc microgrid architecture showing the small intra-SHS loads being operated at 48 V, and high power loads being operated at 350 V. Each SHS component is connected to the 48 V bus via a dc–dc converter.

control scheme to enable power sharing between the SHS is proposed. This control scheme should not only facilitate power exchange but also allow for SOC balancing while preventing unnecessary (dis)charging of batteries. The proposed approach presents a novel way to share the power between SHS without the need for communication between them. The SOC-based adaptive droop control enables different rates of charging and discharging the batteries based on the dynamic SOC levels. The proposed microgrid converter control scheme passively conveys voltage-based information between the different voltage levels both inside the SHS and outside, within the microgrid. The proposed control scheme also prevents charging of batteries with energy from other batteries in the microgrid.

### C.1.1. CHAPTER LAYOUT

This appendix chapter is organized into five sections. Section C.1 introduces this work, while Section C.2 presents the microgrid case-study. Section C.3 details the adaptive SOC-based droop control, and Section C.4 discusses the simulation results of a heterogeneous microgrid with 5 households using the proposed decentralized control scheme. Finally, Section C.5 concludes this work while listing the future work and recommendations.

## C.2. MICROGRID CASE-STUDY

### C.2.1. SHS-BASED MICROGRID

Figure C.1 presents the dual-voltage SHS-based microgrid. Small intra-household loads are connected to the 48 V bus via the load converter. Higher power loads can be connected to the 350 V bus. All the SHS components, viz., PV, battery, and load, have a dedicated converter that helps in implementing the decentralized droop control. Apart from power

conversion, the 48 V–350 V dc–dc converter also performs the crucial task of enabling controlled power sharing between the SHS in the meshed microgrid, as discussed in Section C.3.5.

### C.2.2. SCENARIO FOR MICROGRID SIMULATION

A total of 5 interconnected households with SHS were considered, as shown in Figure C.2. It should be noted that only SHS 1 was considered to be having a high power load on the 350 V network.
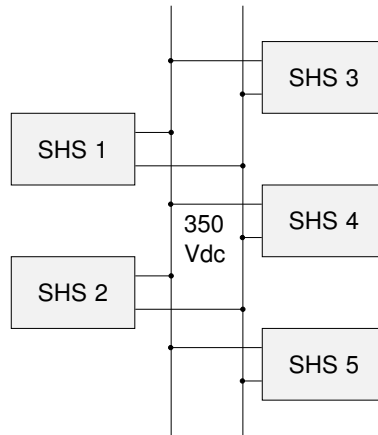


Figure C.2: Microgrid with 5 SHS interconnected on the 350 V line. Note that only SHS 1 has loads connected directly on the 350 V line. All the SHS have smaller loads on the 48 V line within the household.

### C.2.3. INPUT DATA TO THE MICROGRID MODEL

Load data has a resolution of 1-minute and is based on a previous work by the authors [8]. The PV generation data is modeled based on the irradiance data from the Meteonorm tool for a tropical location that experiences on an average 5 equivalent sun hours per day [9]. The meteorological data resolution is also 1-minute. Each SHS is rated at 400 Wp with a battery storage of 72 Ah at 48 V. The intra-SHS load profiles (loads on the 48 V bus) considered for each house were with slight variations, i.e., SHS 1 to SHS 5 were considered with a mix of high, low, and medium profiles, as defined in [8].

## C.3. CONTROL OF INTERCONNECTED SHS BATTERIES

### C.3.1. THE NEED FOR DEDICATED BATTERY CONTROL

When interconnecting solar home systems, multiple batteries will also be connected. If batteries with identical battery chemistry and similar state of health are used, it may be possible to interconnect them directly, i.e., without the dedicated battery converter shown in Figure C.1. However, this comes with several challenges. Care has to be taken to equalize the voltages otherwise very high balancing currents would flow, causing unnecessary battery cycling. Additionally, very high short-circuit currents can occur

with many batteries connected in parallel. In this case, it is not possible to control the charge of individual batteries. Moreover, it can be challenging to add more storage to the system as batteries may not match or have a different degradation and therefore different characteristics.

Connecting batteries with dedicated converters can remove these challenges. Each battery can then be controlled independently. Different battery chemistries could be combined, and systems can be expanded. This additional flexibility has to be balanced against some drawbacks such as additional converter cost and power conversion losses of these converters.
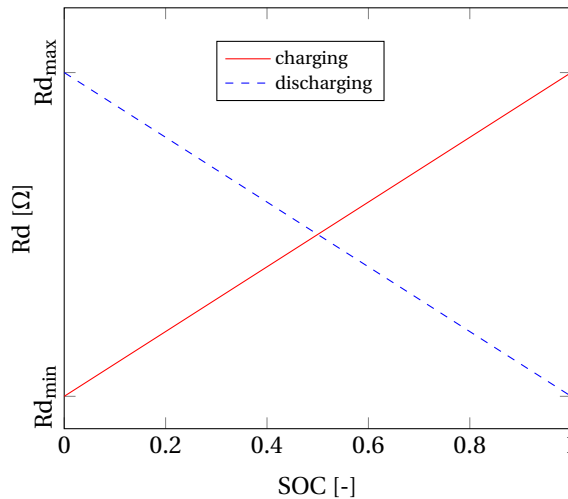
## C.3.2. BATTERY CONVERTER



Figure C.3: Concept illustration depicting SOC-dependent droop resistance Rd.

Assuming that each battery has its own converter, the question arises, how they should be controlled. In general, it is desired to balance the state of charge (SOC) of the different batteries. However, specific objectives might justify a deviation from this usually accepted norm. E.g., in case of backup power for important application, a battery may be desired to be maintained at as high an SOC as possible.

The general approach in this chapter is to use only local voltage information for the control. The basic principle will be to use some sort of adaptive droop control to implement the various conditions that may appear. In general, the battery converter could be controlled with droop control on the microgrid side (48 V bus), providing more current to the microgrid the lower the bus voltage goes and charging with higher power the higher the bus voltage is.

Several considerations should be taken into account. In general, one undesirable operation would be the charging of one battery by discharging another battery in the microgrid. This creates additional losses, especially if power could also otherwise be taken directly from the charged battery at a later stage. Ideally, this would be taken care

of if all the droop curves cross the voltage axis at the same voltage. However, in practice, measurement precision can lead to undesired behavior. Therefore, a dead-band is added to make sure that all batteries stop charging before the first battery starts discharging and vice versa.

In order to have a state of charge (SOC) of the batteries-based droop control in the microgrid, the voltage droop slope is being adjusted based on the SOC. The charging and discharging battery currents can therefore be in proportion to the battery SOC. This concept is illustrated in Figure C.3. If a battery with a lower SOC is charging, the droop slope has to be less steep in order to increase the charging current compared to a battery with a higher SOC. For discharging, it is the other way around: the battery with the lower state of charge has to have a steeper droop slope in order to discharge slower than a fuller battery. Additionally, when a battery is full or empty the power has to be curtailed. Figure C.4 shows the various voltage/current droop profiles depending on the SOC of batteries.
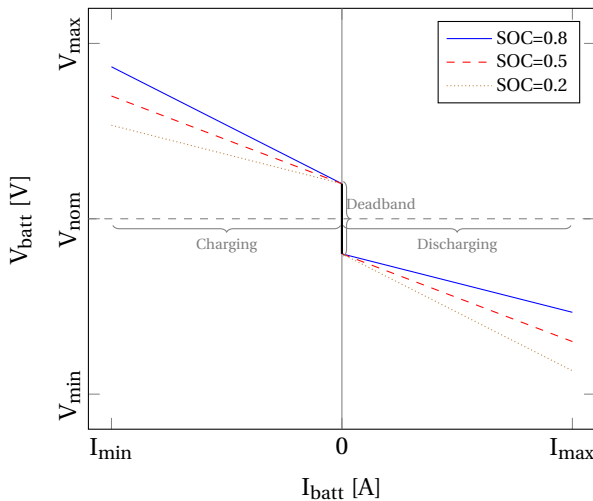


Figure C.4: V-I diagram of the battery converter depicting the different droop slopes based on the SOC and the introduced deadband.

Voltage drop in lines will result in some disturbance on the control. This results in batteries closer to a load to see a lower voltage and contribute more power than other batteries that are further away. On the other hand, batteries that are closer to a source will charge faster because they perceive a higher voltage. Qualitatively, however, this has a positive impact on reducing the line losses in the microgrid. If the dead-band is chosen too small, it could happen that some batteries close to a source are charging while others closer to the load are discharging at the same time. This can be prevented by choosing the dead-band large enough, such that it covers the maximum resistive voltage drop expected in the microgrid. However, this may not always be desirable as it will force the discharging voltages to be significantly lower, thus requiring more current and more line losses for the same load power.
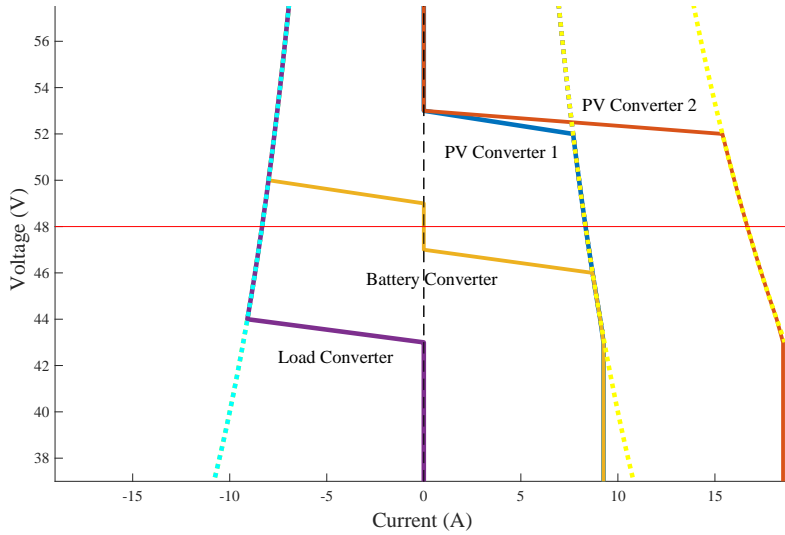
Figure C.5: Illustration for the various converter operating modes for the PV, battery and load converter. The linear parts of the I–V plot refer to the droop mode, while the curved parts are the constant power mode.

### C.3.3. PV CONVERTER

PV is connected to the dc microgrid by a dc/dc converter, as seen in Figure C.1. Under normal operation, it will perform maximum power point tracking (MPPT). However, if the voltage in the microgrid rises too high, then the PV output power has to be curtailed. This can be achieved by adding a voltage droop on the PV output. The voltage droop should only start at a voltage set point where all the batteries in the microgrid are already charging at full power.

### C.3.4. LOAD CONVERTER

The load converters usually just provide power to the loads as required while performing voltage regulation if necessary. However, in case of insufficient power supply in the microgrid, the load has to be shed. This can be realized through a voltage-based hysteresis, but if the load is controllable, it would be preferable to implement a droop to slowly reduce the power depending on the power availability. In a simple form, this demand response should happen if the voltage is so low that all the batteries in the microgrid are already providing maximal power.

The operation modes of the PV, battery, and load converters within the SHS have been captured in an I–V plot in Figure C.5. A voltage deadband between 47 and 49 V can be seen for the battery converter. The linear parts of the plot pertain to the droop mode, while the curved parts refer to the constant power operation. As seen in Figure C.5, the load converter does not instantaneously go from constant power mode to load shedding but instead undergoes a droop mode to gradually reduce the power. Two PV converters can be seen in Figure C.5, which depict the capability of this control scheme to employ different PV converters rated at different powers with different setpoints for the droop

mode and the constant power mode. This demonstrates the utility of the proposed decentralized control scheme in making use of differently rated resources within the SHS-based microgrid in a decentralized manner.

### C.3.5. Principle of control for the 48–350 V converter

The control scheme discussed in Section C.3 will work for the small 48 V DC nanogrid within the SHS. To interconnect multiple SHS and form a dc microgrid, higher voltages are necessary to reduce the line losses and consequently, the cable cost. This can be achieved by adding a dc–dc converter at each SHS, as also seen in Figure C.1, which ensures the SHS operating within the household at 48 V is connected to the 350 V network. The control of this dc–dc converter should facilitate the battery balancing without any communication.

The principle of operation is based on the voltage ratio $k$ between the high voltage and low voltage side and the nominal voltage ratio $k_n$. The higher the voltage ratio $k$ compared to the nominal ratio $k_n$, the more power is flowing from high voltage to the low voltage side, i.e., the SHS is taking power from the microgrid. This can be the case to either fulfill the high-power loads of the SHS, or the small power loads or simply charge the battery with excess power available in the rest of the microgrid. If the voltage ratio is equal to the nominal ratio ($k = k_n$), there is no power exchange between the SHS and the microgrid. Finally, if the voltage ratio is lower than the nominal ratio ($k < k_n$), power is flowing from the low voltage to the high voltage side. The converter current is proportional to $k - k_n$.

## C.4. Simulation results

The decentralized control scheme explained in Section C.3 and Section C.3.5 was implemented on Simulink for the microgrid case-study described in Section C.2. For the 5 households, the power exchange was simulated over a single day, highlighting different modes of operation. The simulation results are presented in Figure C.6–Figure C.12. The current flow for each SHS component, viz., PV, battery, and load, within each household SHS is shown in Figure C.6–Figure C.10.
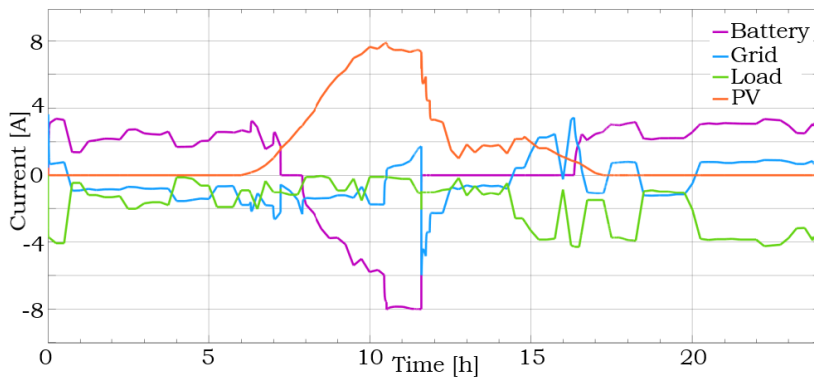


Figure C.6: Current flow in the PV, battery, load and the 48 V bus for SHS 1 over a day.

The "Grid" current marked in these figures refers to the current flowing in the 48 V dc bus. A positive grid current implies the local SHS at the 48 V bus side seeking power from the microgrid side. A positive battery current implies discharging, while a negative battery current implies charging of the battery. The PV and load only exhibit positive and negative currents corresponding to the source and load nature of their behaviour, respectively. Note that the load currents in Figure C.6–Figure C.10 only refer to the lower power loads connected on the 48 V bus for each SHS. The high power load connected on the 350 V line is seen in Figure C.12.
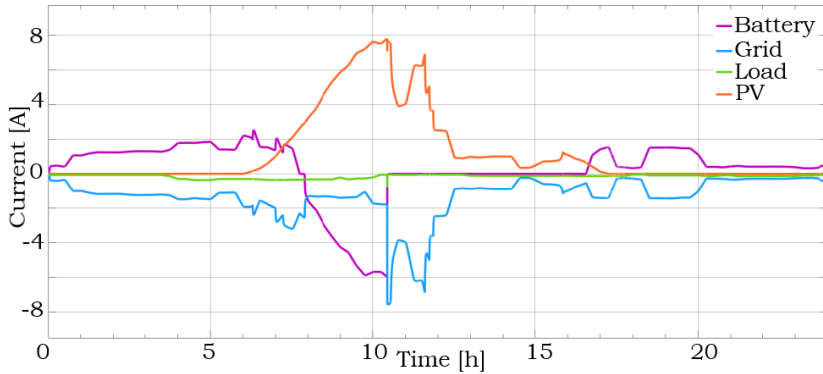


Figure C.7: Current flow in the PV, battery, load and the 48 V bus for SHS 2 over a day.

As described in Section C.2, only household SHS 1 is considered to be having high power loads attached to the 350 V line in the case study. In the pre-dawn hours, the high power load in SHS 1 needs to be fulfilled. As seen in Figure C.6–Figure C.12, batteries from SHS 2 and SHS 5 contribute more power compared to the rest of the interconnected SHS batteries owing to their higher initial SOC levels. The amount of transferred power also depends on the SOC-based droop control from the local battery converter, as described in Section C.3.
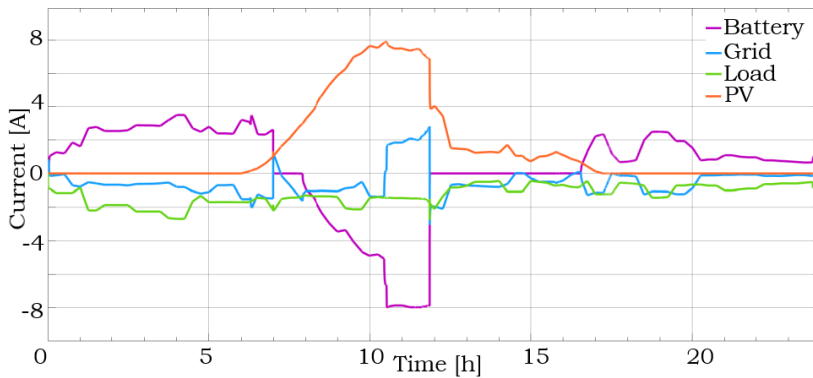


Figure C.8: Current flow in the PV, battery, load and the 48 V bus for SHS 3 over a day.

The location of the installed high power load is not necessarily a bottleneck for the interconnected SHS-based microgrid. As long as the microgrid voltage level is sufficient enough with respect to the individual voltage set points so that the local SHS components keep producing more power, the interconnection concept can be used to exchange power within the microgrid.
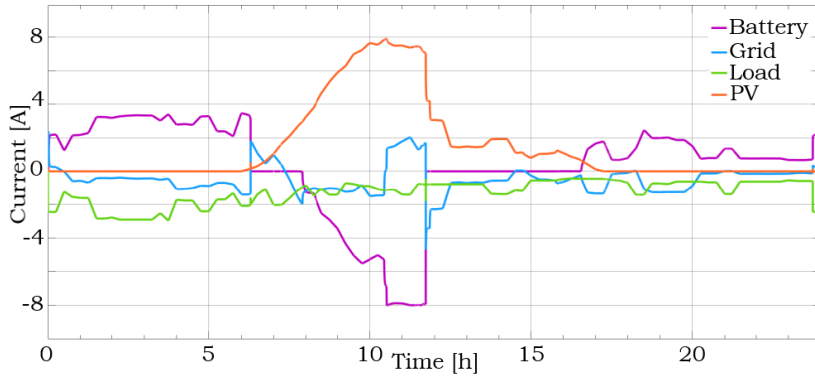


Figure C.9: Current flow in the PV, battery, load and the 48 V bus for SHS 4 over a day.

The other benefit of excess power sharing can be immediately seen around 10:30 AM in the simulation, when batteries of SHS 2 and SHS 5 are already at 100% SOC and the local load demand in SHS 2 and SHS 5 is relatively low. Interestingly, the PV converter does not curtail the power production in SHS 2 and SHS 5 immediately. Instead, the excess power is first used to charge the other batteries at full power (close to 8 A) so that all the SHS batteries reach 100% SOC first. Only after that does the PV curtailment kick in at the local SHS PV converter.
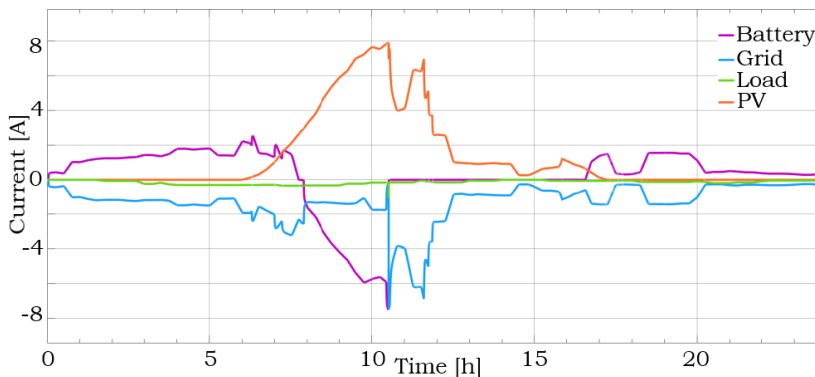


Figure C.10: Current flow in the PV, battery, load and the 48 V bus for SHS 5 over a day.

Similarly, around 3:30 PM, the load demand in SHS 1 is higher than the local PV production, the excess power from the PV in other SHS is utilized. This is possible as the local loads in other SHS are lower than the local PV production. Thanks to this mode of

operation, the local batteries are kept untouched as long as the load demand within the microgrid can be already utilized by the excess PV. This is where the battery deadband comes in handy to prevent unnecessary local battery discharge. The stored battery energy can, therefore, be used at a later stage after sunset.
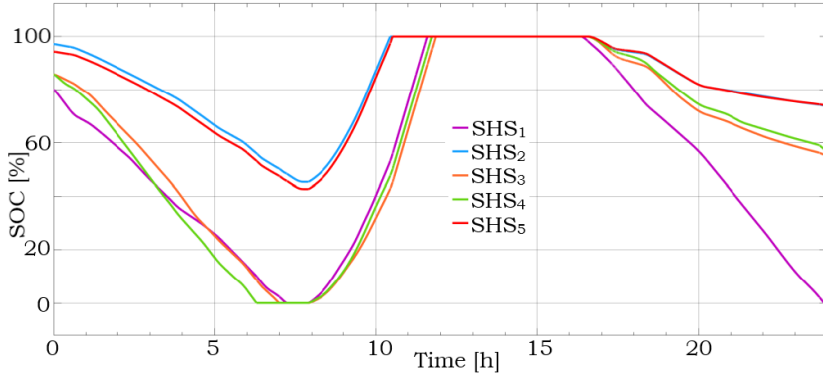


Figure C.11: SOC for all the 5 interconnected SHS batteries within the microgrid over a day.
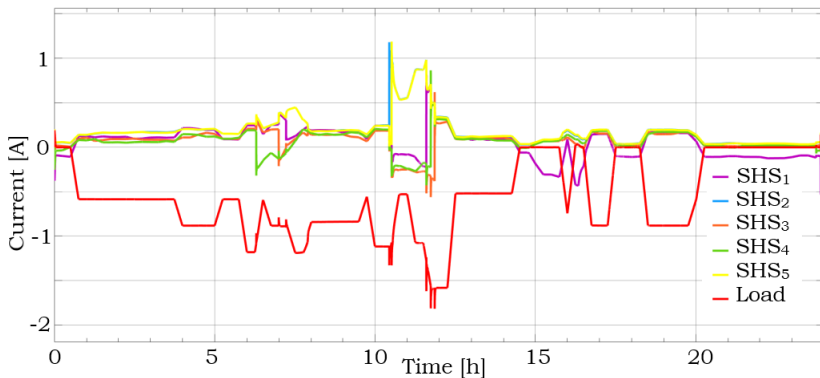


Figure C.12: Line currents in the 350 V line for each SHS over a day. The high power load connected on the 350 V line is also shown in red.

## C.5. CONCLUSIONS

This chapter proposed the concept of a decentralized control scheme that can enable power sharing between solar home systems in a rural dc microgrid. Moreover, the advantages of a communication-less, SOC-based adaptive droop control were presented. Introducing a deadband in the battery converter's droop characteristics helped prevent unnecessary cycling of the battery. Additionally, having the droop resistances adaptive to the battery SOC levels ensures that a discharging battery experiences higher C-rates while at higher SOC levels and lower C-rates at lower SOC levels. Moreover, the power

exchange modeled in the SHS-based microgrid demonstrates how the excess PV power can be shared instead of curtailing when otherwise in standalone mode.

## RECOMMENDATIONS AND FUTURE WORK

The work described in this chapter was limited to modeling and simulation of a microgrid with 5 independent but interconnected SHS. The model should be scaled up to larger microgrid sizes while increasing the number of PV generation and load variation scenarios. Additionally, the decentralized control scheme can be implemented on hardware to experimentally validate the SOC-based adaptive droop.

## REFERENCES

[1] S. Groh, D. Philipp, B. E. Lasch, and H. Kirchhoff, "Swarm electrification-suggesting a paradigm change through building microgrids bottom-up," in *Developments in Renewable Energy Technology (ICDRET), 2014 3rd International Conference on the.* IEEE, 2014, pp. 1–2.

[2] N. Narayan, A. Chamseddine, V. Vega-Garita, Z. Qin, J. Popovic-Gerber, P. Bauer, and M. Zeman, "Exploring the boundaries of solar home systems (shs) for off-grid electrification: Optimal shs sizing for the multi-tier framework for household electricity access," *Applied Energy*, vol. 240, pp. 907 – 917, 2019. [Online]. Available: http://www.sciencedirect.com/science/article/pii/S0306261919303502

[3] S. Groh, D. Philipp, B. E. Lasch, and H. Kirchhoff, "Swarm electrification: Investigating a paradigm shift through the building of microgrids bottom-up," in *Decentralized Solutions for Developing Economies.* Springer, 2015, pp. 3–22.

[4] N. L. Diaz, T. Dragičević, J. C. Vasquez, and J. M. Guerrero, "Intelligent distributed generation and storage units for dc microgrids - a new concept on cooperative control without communications beyond droop control," *IEEE Transactions on Smart Grid*, vol. 5, no. 5, pp. 2476–2485, 2014.

[5] M. Nasir, Z. Jin, H. A. Khan, N. A. Zaffar, J. C. Vasquez, and J. M. Guerrero, "A decentralized control architecture applied to dc nanogrid clusters for rural electrification in developing regions," *IEEE Transactions on Power Electronics*, vol. 34, no. 2, pp. 1773–1785, 2019.

[6] H. Kirchhoff, M. Schmid, P. Adelmann, and K. Strunz, "Passive droop control in a decentralized 12v dc energy access microgrid with lead acid batteries," in *Micro Perspectives for Decentralized Energy Supply: Proceedings of the International Conference (2015, Bangalore).* Universitätsverlag der TU Berlin, 2015, p. 61.

[7] X. Lu, K. Sun, J. M. Guerrero, J. C. Vasquez, and L. Huang, "State-of-charge balance using adaptive droop control for distributed energy storage systems in dc microgrid applications," *IEEE Transactions on Industrial electronics*, vol. 61, no. 6, pp. 2804–2815, 2014.

[8] T. D. Heeten, N. Narayan, J. C. Diehl, J. Verschelling, S. Silvester, J. Popovic-Gerber, P. Bauer, and M. Zeman, "Understanding the present and the future electricity needs: Consequences for design of future solar home systems for off-grid rural electrification," in *2017 International Conference on the Domestic Use of Energy (DUE)*, April 2017, pp. 8–15.

[9] Meteotest, "(software) meteonorm ver 7.1," 2014.

# LIST OF PUBLICATIONS

## JOURNAL ARTICLES
### Related to the PhD

11. **N. Narayan**, Z. Qin, J. Popovic-Gerber, J. C. Diehl, P. Bauer, and M. Zeman. Stochastic load profile construction for the multi-tier framework for household electricity access using off-grid DC appliances, *Energy Efficiency*, In Topical Collection of Journal Energy Efficiency on Off-grid Appliances and Smart Controls for Energy Access, Springer 2018. **(Ch 3)**

10. **N. Narayan**, T. Papakosta, V. Vega-Garita, Z. Qin, J. Popovic-Gerber, P. Bauer, and M. Zeman. Estimating battery lifetimes in Solar Home System design using a practical modelling methodology, *Applied Energy*, Volume 228, 2018, Pages 1629-1639, ISSN 0306-2619. **(Ch 4)**

9. **N. Narayan**, A. Chamseddine, V. Vega-Garita, Z. Qin, J. Popovic-Gerber, P. Bauer, and M. Zeman. Exploring the boundaries of Solar Home Systems (SHS) for off-grid electrification: Optimal SHS sizing for the multi-tier framework for household electricity access. *Applied Energy*, 240, 2019, Pages 907-917. **(Ch 5)**

8. **N. Narayan**, A. Chamseddine, V. Vega-Garita, Z. Qin, J. Popovic-Gerber, P. Bauer, and M. Zeman. Quantifying the Benefits of a Solar Home System-Based DC Microgrid for Rural Electrification. *Energies*, 2019, 12(5), 938. **(Ch 6)**

7. Y. Yu, **N. Narayan**, V. Vega-Garita, J. Popovic-Gerber, Z. Qin, M. Wagemaker, P. Bauer, and M. Zeman. Constructing Accurate Equivalent Electrical Circuit Models of Lithium Iron Phosphate and Lead–Acid Battery Cells for Solar Home System Applications. *Energies*, 2018, 11(9), 2305. **(Appendix A)**

6. **N. Narayan**, M. Tagliapietra, Z. Qin, J. Popovic-Gerber, P. Bauer, and M. Zeman. Optimal microgrid layout using Geographic Information System and graph theory concepts, submitted. **(Ch 7)**

5. **N. Narayan**, V. Vega-Garita, Z. Qin, J. Popovic-Gerber, P. Bauer, and M. Zeman. The long road to universal electrification: A critical look at present pathways and challenges, submitted. **(Ch 2)**

### Collaborations

4. V. Vega-Garita, L. Ramirez-Elizondo, **N. Narayan**, and P. Bauer. Integrating a photovoltaic storage system in one device: A critical review. *Progress in Photovoltaics: Research and Applications*, 2019, 27(4), 346-370.

3. A. Shekhar, V. K. Kumaravel, S. Klerks, S. de Wit, P. Venugopal, **N. Narayan**, P. Bauer, O. Isabella, and M. Zeman, "Harvesting Roadway Solar Energy—Performance of the Installed Infrastructure Integrated PV Bike Path," in *IEEE Journal of Photovoltaics*, 2018, vol. 8, no. 4, pp. 1066-1073.

2. V. Vega-Garita, M.F. Sofyan, **N. Narayan**, L. Ramirez-Elizondo, and P. Bauer. Energy Management System for the Photovoltaic Battery Integrated Module. *Energies*, 2018, 11, 3371.

1. V. Vega-Garita, A. Hanif, **N. Narayan**, L. Ramirez-Elizondo, & P. Bauer. Selecting a suitable battery technology for the photovoltaic battery integrated module. *Journal of Power Sources*, 2019, 438, 227011.

## CONFERENCE PROCEEDINGS
### Related to the PhD

11. **N. Narayan**, V. Vega-Garita, Z. Qin, J. Popovic-Gerber, P. Bauer and M. Zeman, "A modeling methodology to evaluate the impact of temperature on Solar Home Systems for rural electrification," 2018 IEEE International Energy Conference (ENERGYCON), Limassol, Cyprus, 2018, pp. 1-6. **(Appendix B)**

10. *(Outstanding Paper Award)* **N. Narayan**, T. Papakosta, V. Vega-Garita, J. Popovic-Gerber, P. Bauer and M. Zeman, "*A simple methodology for estimating battery lifetimes in Solar Home System design,*" 2017 IEEE AFRICON, Cape Town, 2017, pp. 1195-1201. **(Ch 4)**

9. **N. Narayan**, B. O-Malik, L. Mackay, Z. Qin, J. Popovic-Gerber, P. Bauer and M. Zeman, "*Decentralized Control-Scheme for DC-Interconnected Solar Home Systems for Rural Electrification,*" 2019 IEEE International Conference on DC Microgrids (ICDCM), Matsue, Japan, 2019, pp. 1-6. **(Appendix C)**

8. **N. Narayan**, Z. Qin, J. Popovic-Gerber, P. Bauer and M. Zeman, "*Evaluating the techno-economic feasibility of battery technologies in the context of Solar Home Systems*" *European Conference on Power Electronics and Applications (IEEE EPE ECCE Europe)*, Riga, 2018.

7. T. den Heeten, **N. Narayan**, J. C. Diehl, J. Verschelling, S. Silvester, J. Popovic-Gerber, P. Bauer and M. Zeman, "Understanding the present and the future electricity needs: Consequences for design of future Solar Home Systems for off-grid rural electrification," *2017 International Conference on the Domestic Use of Energy (DUE)*, Cape Town, 2017, pp. 8-15. **(Partly Ch 2)**

6. **N. Narayan**, J. Popovic, J. C. Diehl, S. Silvester, P. Bauer and M. Zeman, "Developing for developing nations: Exploring an affordable solar home system design," *2016 IEEE Global Humanitarian Technology Conference (GHTC)*, Seattle, WA, 2016, pp. 474-480.

### Collaborations

5. V. Vega-Garita, D. De Lucia, **N. Narayan**, L. Ramirez-Elizondo and P. Bauer, "PV-battery integrated module as a solution for off-grid applications in the developing world," 2018 IEEE International Energy Conference (ENERGYCON), Limassol, Cyprus, 2018, pp. 1-6.

4. I. Sulaeman, V. Vega-Garita, G. R. C. Mouli, **N. Narayan**, L. Ramirez-Elizondo and P. Bauer, "Comparison of PV-battery architectures for residential applications," *2016 IEEE International Energy Conference (ENERGYCON)*, Leuven, 2016, pp. 1-7.

3. V. Vega-Garita, S. Garg, **N. Narayan**, L. Ramirez-Elizondo, P. Bauer, "Testing a PV-battery Integrated Module Prototype", 2018 World Conference on Photovoltaic Energy Conversion (WCPEC-7)

2. **N. Narayan**, J. Popovic, P. Bauer, A. Smets, M. Zeman, "A critical review of PV system design rules for optimizing energy yield and space utilization", 2016 European Photovoltaic Solar Energy Conference (32nd EUPVSEC)

1. L. Locatelli, **N. Narayan**, A. Battaglia, A. Canino, C. Gerardi, O. Isabella, M. Zeman, "Correcting temperature-dependent efficiency model for commercial double junction thin film silicon modules", 2015, European Photovoltaic Solar Energy Conference (31st EUPVSEC)

# ACKNOWLEDGEMENTS

People always warned me how a PhD project could finish the joy in one's life. Instead, I was fortunate to experience the joy of finishing the PhD. Of course, several people have been a part of this journey, and I shall acknowledge them here in a rather haphazard order. In case you don't find your name or contribution here, please understand that a byproduct (amongst many others) of my PhD thesis is a fuzzy memory. Please know that in my heart of hearts and a grateful yet forgetful mind, your contribution holds a special place and that recollecting your name the night before this book was sent to the printers proved unsuccessful. You know who you are, and a big thanks to you.

Firstly, I'd thank my promotors prof. Pavol Bauer and prof. Miro Zeman for giving me the opportunity to pursue my PhD on such a fulfilling problem statement. I thank Pavol for giving me the benefit of the doubt and showing immense patience with my results, and also for the timely nudges that brought me the much-needed perspective within my PhD project. I thank Miro for the brief yet fruitful interactions throughout the PhD, always being positive and supportive of my work.

Thanks to Dr. Zian Qin, my daily supervisor, for always being ready to have a discussion. Zian, though you moved to Delft while I was halfway through the PhD project, you immediately came on board and understood and accepted the challenges such a unique PhD project posed. Sorry for thoroughly exploiting your open-door policy, or assuming that you had one in the first place while you perhaps didn't.

Thanks to Dr. Jelena Popovic, my daily supervisor for the first year and a half. You continued to provide invaluable feedback and kept me up to date with the ground reality of SHS scaling difficulties. Thank you for initiating the project and choosing me to work on it. Hope I was able to do some justice to the initial problem statement you had in mind. I'm very glad that you are continuing to battle the EA problem on academic as well as entrepreneurial fronts. Here's hoping that we can make some dents with technology in this shape-shifting EA monster.

Frans Pansier, it was always a pleasure to converse. I could discuss my project at any level of abstraction with you, and you always understood and appreciated the complexity and challenges of the project in all its glory. Thank you for sharing your treasure chests of knowledge with me.

Thanks also to my mentor Prof. Inald Lagendijk for the limited but helpful interactions in my first year. Thanks to my doctoral defense committee members, Prof. Peter Lund, Prof. Arno Smets, Dr. Roland Valckenborg, and Dr. J. C. Diehl for agreeing to be part of the committee. I appreciate the timely feedback and constructive discussions on my thesis manuscript.

I benefited from interactions with SHS companies during this project. Thanks to Bernard and Thomas from SolarWorks! for always being enthusiastic about discussing various aspects related to this dynamic sector. Thanks to Jeroen Verschelling from Kam-Works for collaborating with us through an MSc thesis project in Cambodia. I'm grateful

to Ashley from BBOXX for an insightful discussion in the formative months of my PhD, and also to Iwona and Chris for helping me whenever I reached out to them. Also thanks to Hannes Kirchhoff and Neel Tamhane from ME-SolShare, Rob de Jeu and Marcel van Heist from Rural Spark, and Vinay Jaju from ONergy for early discussions.

Thanks to TU Delft Global for their fellowship that supported this PhD. Nick, Jennifer, Esther, Annelies, Friso and team were helpful when both the initiative and my project were at a fledgling stage. The Delft Global community at large has been very helpful throughout my project. Especially in the student projects of JC, there are plenty of valuable insights that have been useful more than once.

To go through the PhD and come out relatively sane, it's important to have the right set of people around you. Especially in the formative phase of a PhD, the influence of peers in a research group can have the impact of a dynamite — both destructive and constructive, but without the fortune of the explosives industry and the legacy of an annual international award. And before this metaphor blows up in my face, I shall continue. Tsegay, thanks for your practical tips during coffee conversations. Laurens, hopefully, we can still collaborate in some form or the other; good luck with all the challenges and (dc) opportunities. Soumya, wouldn't want to make fun of you here, would be quite the *suicide*, despite the anecdotes in my *arsenal*. We should play chess again sometime. Udai, it was always nice to have discussions on a range of topics. Nils, my lunch hunger has been conditioned over time to trigger with your 'lunch' pings. Conveniently, your pings for football also get me hungry for food. I blame it on the WhatsApp group named after a meal. Pavel, starting with the APE lab supervision back in 2016, I've always enjoyed discussing a variety of topics with you from arts to history, including (Except!) the Mongols.

Ibra, thanks for being the only other nut to splurge on good coffee while on a PhD stipend. Always wondered if your proclivity to dish out GIFs has anything to do with your singing aspirations (keyword: Tenor). Lucia, thanks for never making me feel like we had a wall between our offices — always heard you loud and clear. Between the notes you hit in your conversation and Ibra in his singing, you've got some unique voice signatures coming out of that office. Faisal, thanks for reminding me how much I missed playing tennis. No thanks though for the furious yet graceful backhands that I could never return. Do keep that poet in you alive too! Marco, I hope by the time you're done with your PhD you'd be less traumatized by pineapples on pizzas. Francesca and Wenli, (wireless) power to you guys! Mladen, never thought you'd start a trend with the man-purse, but you found a follower in Aditya. Aditya, props to you for always mixing serious scientific work with your monkey business. Thanks to Ilija, Tianzhu, Jiayang, Piao, Thiago, *Guillmero*, Luis, Laura, Wiljan, Babak, Djurre, Farshid, Alessandro, Dhanashree, Mohamad, Armando, Jianning, Fabio — because interaction during coffee, cake, and even group meetings helped.

In terms of the office room, Tim was the first glimpse into a focused PhD researcher balancing family and his PhD. I realized a year later that it wasn't an exception but the norm in the 'cursed' family-room office of LB 3.680. Gautham, I've known you since we came here for our MSc. Thanks for all the discussions, plants, and delicious food (the edible sort of plants) we had in the office, as well as helping out with all the smart tips and advice to navigate through the everyday PhD/administrative hurdles. Victor -

Man, thanks for being an inspiration throughout my PhD. After seeing you juggle PhD, life, wife, and son, I really had no room for complaints. I'll never forget your pearls of wisdom and secret to a happy life ;) I'll always cherish our chess discussions, and the helpful *crapohccino* breaks. Yunhe, thanks for (briefly) being part of the office. When I say the office benefited from your presence, I mean it, including the walls and the ceiling — you've definitely left your Mark. I am glad you found humans to practice martial arts against at the sports center.

Thanks to Minos, VGP, Dong, Martin, Milos, and others who graduated during my early PhD years — you guys made me reaffirm this journey has an end. Special thanks to Joris, Bart, and Harrie for helping out in the lab. I'll remember the brief time spent in the group by Juan Pablo, Na Li, Shubhangi, Andreas, Yufei, Jintao. Thanks also to the secretaries Sharmila, Ellen, Ilona for helping out with any queries. Sharmila, special thanks for restocking the cookies in your office from time to time. For the new researchers who just joined the group, and for the many about to, I wish you the best.

Had the good fortune of working with several MSc students during the thesis. I learnt a lot, both technically and culturally while working with them. Mentoring students was also an exercise in introspection. I accomplished more in the thesis while working with them than I could ever have had by myself. Natalie, Yunhe and Thekla were the first students. Gaurav and Thomas joined from TPM and IDE, with fieldworks in India and Cambodia respectively. I co-supervised Bryan, Wenrui, and Yunizar with other PhD researchers. The last set of students were Naveen, Ali, Michele, and Luca. You all made a difference to my PhD journey. Thank you all for wanting to pursue your MSc theses with me.

To my Delft Global fellows, thanks for supporting me. In you, I found a community also trying to balance the technological V social dimensions of your projects. Roos, I wish I had your abilities to just figure things out so easily. Thanks for our support-group coffees and good luck with your final lap, almost there! Michel and Mitasha (M&M), you guys inspire me to no end. Michel, I am glad I got you back onto coffee; here's to many more. Dominik, must catch up on those Vietnam stories. Juan Carlo, great project — Keep it flowing and pump it up! Saqr, Henry, keep the energy high. Pieter, really like your happy-go-lucky attitude with which you *seas* the day, work or otherwise. Stay current, and keep it floating! Anteneh, Rachel, you guys are doing phenomenal work together. Yask, you've built a very fulfilling project for yourself, brick by brick. Tope, you are an inspiration; good luck with your company and your re-search. Juan, high five and a thumbs up to your PhD project; one day I'd love to play rock, paper, scissors with your prototype (and win). Camille, Petra, Merel, Christine, Mona, Hendrik — keep up the great work. And the new fellows: Monica, David, Daniel, welcome and good luck!

JC, thanks for always helping out with your extended network and infectious enthusiasm. I do hope you will add Energy back onto your plate apart from Health. Abhigyan, we should continue our discussions — technology alone is not going to help in SDG 7. Astrid, thank you for understanding my story so well and producing those beautiful illustrations.

Since July 2019, I've also found another warm work environment in 5.29 (extra warm in those summer days). Claire, thanks for always being so understanding and supportive; I'll try my best to keep short updates during coffee breaks actually within 10 mins. Roel, thanks for letting me digress during all the bilas, and also telling me what bilas were in the first place. Cheers to Danielle for always switching languages just for me in the office.

Sophie, you had me on day 1 when you said I could share your stash of goodies — bet you didn't figure back then you'd also be sharing an annoying amount of daily puns. Thanks for keeping the office 'not too old'. On that note, Petra, welcome to the team.

For all the LaTex troubles and MATLAB tips, I cannot thank the unsung heroes of Stack Exchange enough. My love-hate relationship with LaTex would have ended a long time ago if it weren't for you guys. Also, a shout-out to Coffee Star and Brandmeester in Delft (and the pico-baristo at home) for breaking me free of the Stockholm syndrome I'd otherwise developed towards the *crapohccino* machines.

For my home away from home, cheers to the Beachhouse, and the beachboys — the other family. Chris(-Helena-Emilian), Manu(-Katrin), Philipp(-Steffi-Johanne), Louis(-Stef-Walden) — how quickly the family has grown — thanks for starting gen-1 of the beachhouse. Akshay, Danny, Paula(-Mike), and later Marija, Jo, I will forever cherish the endless food, chai, board games, armchair philosophizing, geeking out, homophones, horizontal skyscrapers, foiling robberies, ninja mom adventures, YT education, and of course, buxfer emails 🦇. And the old cartel friends who still managed to stay in touch despite the geographies — Sutji(-Peii-Clara-Cederic), Hugo(-Rene), Catherin(-Daniel-Vera), Yuan(-Yifan). Special shout out to the colony friends and their better halves, some of who are halfway across the world now — I am so fortunate to have those childhood bonds still running strong. To my NITC corridor friends, after a bit of a hiatus, I was glad to be back in touch with you guys.

Also experienced the joy of celebrating my wedding during the PhD in 2016, both in India and in NL. The band of friends who made it all the way to India and were braver than me in trying all the food — props to you guys. That Great Indian Wedding was an unforgettable experience. I've also been fortunate to have made great friends here over the years. Ashish (*le bro*), Riddhi-Varun, Amreen-Harmen, Jefta-Jo-Ty-Dy, Gunjan-Shreyas, Ying Zi, Rishabh, Romy, Annalena-Suzanne, Akshara, Aakarsh, Esther-Vincent, Elvira-Berend, Sheng, JK, Luc-Marie-Nour, Mo-Johnny, Laura, Gintare, Anna, Leila, Delaram-Dena, and the list goes on. And the friends from the verre oosten — Nestor, Una, Jelena and Mark — here's to more cats, babies and bears, and as always, looking forward to seeing everyone next (will be on my Judgment Day I suppose). Also, special thanks for the Dutch translation! Cheers to my Findian friends Arun & Amrita; from webcomics to chess, we have managed to stay in touch all these years, impressively without any IMs.

To team Harbour View — mumzie, poppy, and aafy, thank you for always making me feel so loved and pampered, and part of an epic adventure whenever we are traveling together. Can't wait for the next adventures and bezzique sessions. Mumzie, I've enjoyed all our conversations from history and religion to the latest in your scientific research. Poppy, I always admire your energy and spirit; I wish I could be even half as active. Aafy daffy, my munchkin, love you for always taking the right (my) side in all the board game arguments. Better come back soon!

To team UK — bro, masi, siddu, loved my family time there when I could just laze around. We badly need to increase the channel crossings. Thank you for always looking out for me, bro. Knowing you had my back gave me the fortitude to always soldier on. To masi - I may not say this often enough, but thank you for being the silent prime mover of the team in the background. Sid, you are growing up too fast; come here soon so

---

🦇 Some stories could not make this official list as the narration of events is still disputed

we can keep track. Can't wait to play chess with you. Love you guys. To pati, who has unconditionally loved me since I was a child, and still worries that I'll catch a cold in the rain. I'll forever cherish the memories with you and thatha. And mathe, you and appa never made me second-guess my decisions and supported me despite how hard it got for you. I've never really had it tough in life, not because life has been easy, but because you guys were the real heroes always fighting the battles in the background, making life seem easy. Love you, and thank you for always being there.

And finally, to Sanaa 🦇, words won't do justice to your contribution in me accomplishing this PhD. While that could have been an excellent excuse not to write anything more, I shall still endeavour. You've been with me through this every step of the way. You've been the rock — not the kind that traps someone between itself and a hard place — that I could always count on. For all the evenings I worked late, the movies we missed, the outings I couldn't join, the weekends I couldn't chill with you, thank you for always understanding. For all the times you did put your foot down wanting me to take a break, I am actually grateful (that the foot came down for my benefit). And you know how much I love challenges, that's why you always planned our holidays right around my deadlines. Some of my fondest memories in these years are from the weekend getaways and the travels. Oh, and thank you for also losing a few games every now and then just to make me feel good amid all my work deadlines (*cough*), just like you forgive me every time you are wrong. But seriously, thank you for making this happen with me. You know this couldn't have been possible for me without you. I wouldn't want it any other way.

---

🦇Because I know you will read this, I shall stick to facts and only facts

# ABOUT THE AUTHOR

Nishant was born in the *tiny* town of Dombivli in the outskirts of Mumbai, India in 1986. He grew up in the unusually calm and scenic part of Mumbai called Anushakti Nagar, finishing higher secondary schooling in 2004 from Atomic Energy Junior College. He obtained his bachelor's degree in Electronics and Communication Engineering in 2008 from National Institute of Technology Calicut, India. He then worked for 3 years in the semiconductor industry at Texas Instruments India at the Bangalore R&D centre as a Hardware Digital Design Engineer.

Making up his mind to switch from semiconductors to renewable energies, he moved to the Netherlands in 2011 to pursue a Master's degree in Sustainable Energy Technology. He successfully obtained his MSc in 2013, specializing in solar energy and storage, fully realizing the irony that solar PV energy is founded on semiconductors. From 2013 to 2015, he worked on various research and education projects related to PV system design, massive open online course (MOOCs) development, PV Lab, smart grids, and wireless power transfer in the Photovoltaic Materials and Devices (PVMD) and DC Systems, Energy Conversion and Storage (DCES) groups within the Electrical Sustainable Energy Department (ESE) of TU Delft, respectively.

In July 2015, he received a fellowship from TU Delft | Global Initiative to pursue a PhD in the DCES group on solar home systems for improving electricity access — a topic both technologically and personally close to his heart. Until June 2019, he worked on his PhD in the multi-faceted problem space of energy access, focusing on solar home systems, battery storage, and decentralized DC microgrids. In the last few years, he has met many inspiring people devoted to the cause of the UN SDGs, especially SDG 7 ('Ensure access to affordable, reliable, sustainable and modern energy for all'). Through the work and interactions during his PhD, he is surer than ever that the key to solving urgent global issues lies in multi- and trans-disciplinary efforts. From July 2019, he has been developing the Energy Access Program of TU Delft | Global Initiative. He is currently building a research roadmap to bring together researchers and experts cross-cutting different expertise as well as local partners in un(der-)electrified regions for co-solving the multilateral issues surrounding SDG 7.